Structural Engineering Report No. 150

BEHAVIOUR OF TRANSVERSELY LOADED CONTINUOUS STEEL - CONCRETE COMPOSITE PLATES

By

STEPHEN J. KENNEDY
and
J. J. CHENG

July, 1987

118. *Effective Lengths of Laterally Unsupported Steel Beams* by C.D. Schmitke and D.J.L. Kennedy, October 1984.

119. *Flexural and Shear Behaviour of Large Diameter Steel Tubes* by R.W. Bailey and G.L. Kulak, November 1984.

120. *Concrete Masonry Prism Response due to Loads Parallel and Perpendicular to Bed Joints* by R. Lee, J. Longworth and J. Warwaruk.

121. *Standardized Flexible End Plate Connections for Steel Beams* by G.J. Kriviak and D.J.L. Kennedy, December 1984.

122. *The Effects of Restrained Shrinkage on Concrete Slabs* by K.S.S. Tam and A. Scanlon, December 1984.

123. *Prestressed Concrete Beams with Large Rectangular Web Openings* by T. do M.J. Alves and A. Scanlon, December 1984.

124. *Tests on Eccentrically Loaded Fillet Welds* by G.L. Kulak and P.A. Timler, December 1984.

125. *Analysis of Field Measured Deflections Scotia Place Office Tower* by A. Scanlon and E. Ho, December 1984.

126. *Ultimate Behaviour of Continuous Deep Reinforced Concrete Beams* by D.R. Ricketts and J.G. MacGregor, January 1985.

127. *The Interaction of Masonry Veneer and Steel Studs in Curtain Wall Construction* by W.M. McGinley, J. Warwaruk, J. Longworth and M. Hatzinikolas, May 1985.

128. *Evaluation of Existing Bridge Structure by Nondestructive Test Methods* by L. Mikhailovsky and A. Scanlon, May 1985.

129. *Finite Element Modelling of Buried Structures* by D.K. Playdon and S.H. Simmonds, October 1985.

130. *Behaviour and Ultimate Strength of Transversely Loaded Continuous Steel Plates* by K.P. Ratzlaff and D.J.L. Kennedy, November 1985.

131. *Inelastic Lateral Buckling of Steel Beam-Columns* by P.E. Cuk, M.A. Bradford and N.S. Trahair, December 1985.

132. *Design Strengths of Steel Beam-Columns* by N.S. Trahair, December 1985.

133. *Behaviour of Fillet Welds as a Function of the Angle of Loading* by G.S. Miazga and D.J.L. Kennedy, March 1986.

134. *Inelastic Seismic Response of Precast Concrete Large Panel Coupled Shear Wall Systems* by M.R. Kianoush and A. Scanlon, March 1986.

135. *Finite Element Prediction of Bin Loads* by A.H. Askari and A.E. Elwi, June 1986.

136. *Shear Behavior of Large Diameter Fabricated Steel Cylinders* by J. Mok and A.E. Elwi, June 1986.

137. *Local Buckling Rules for Structural Steel Members* by S. Bild and G.L. Kulak, May 1986.

138. *Finite Element Prediction of Reinforced Concrete Behavior* by S. Balakrishnan and D.W. Murray, July 1986.

139. *Behavior and Strength of Masonry Wall/Slab Joints* bu T.M. Olatunji and J. Warwaruk, July 1986.

140. *Bayesian Analysis of In-Situ Test Data for Estimating the Compressive Strength of Concrete in Existing Structures* by G.J. Kriviak and A. Scanlon, July 1986.

141. *Shear-Moment Transfer in Slab-Column Connections* by S.D.B. Alexander and S.H. Simmonds, July 1986.

142. *Minimum Thickness Requirements for Deflection Control of Two-Way Slab Systems* by D.P. Thompson and A. Scanlon, November 1986.

143. *Shrinkage and Flexural Tests of Two Full-Scale Composite Trusses* by A. Brattland and D.J.L. Kennedy, December 1986.

144. *Combined Flexure and Torsion of I-Shaped Steel Beams* by R.G. Driver and D.J.L. Kennedy, March 1987.

145. *Cyclic and Static Behaviour of Thin Panel Steel Plate Shear Walls* by E.W. Tromposch and G.L. Kulak, April 1987.

146. *Postbuckling Behavior of Thin Steel Cylinders Under Transverse Shear* by V.G. Roman and A.E. Elwi, May 1987.

147. *Incipient Flow in Silos - A Numerical Approach* by R.J. Link and A.E. Elwi, May 1987.

148. *Design of Web-Flange Beam or Girder Splices* by D. Green and G.L. Kulak, May 1987.

149. *Spreadsheet Solution of Elastic Plate Bending Problems* by G.E. Small and S.H. Simmonds, July 1987.

150. *Behaviour of Transversely Loaded Continuous Steel-Concrete Composite Plates* by S.J. Kennedy and J.J. Cheng, July 1987.

STRUCTURAL ENGINEERING REPORT 150

BEHAVIOUR OF TRANSVERSELY LOADED CONTINUOUS STEEL-CONCRETE COMPOSITE PLATES

by

STEPHEN J. KENNEDY
J.J. CHENG

Department of Civil Engineering
University of Alberta
Edmonton, Alberta

July 1987

ABSTRACT

It is apparent from a review of the literature and current research related to the design of "ice-resisting walls" for offshore structures, that there is a need for more efficient designs of these structural elements. The objective of this study was to examine an alternate structural element which is simple in detail and utilizes the capacity of the section.

An experimental and analytical program was undertaken to determine the strength and behaviour of steel-concrete composite sandwich plates, without mechanical shear interconnectors, subjected to transverse loads. The simple details of this element make design and construction easy.

A series of six continuous composite plate elements, with a centre span of 3050 mm, were tested with a four point load system. The composite members were continuous over supporting bulkheads and were axially restrained. The primary variables investigated were steel plate thickness, which varied from 3.18 to 6.35 mm, and section depth which gave span to depth ratios from 15 to 25. Three regions of behaviour of the members were observed; flexural, flexural membrane and membrane. The capacity of the element was not limited to its flexural capacity. The average maximum centre span deflection at failure exceeded one-sixth of the span.

Analyses presented include the development of:

1. a model to describe the flexural behaviour of composite sandwich plates without mechanical shear

interconnection;

2. a model to describe the membrane behaviour of steel plates of finite width and flexible boundaries;
3. a failure criterion to describe rupture of the steel plates at the supports.

The results predicted by the models are in good agreement with the test results.

The models allow the design engineer to proportion the section to achieve the required flexural and membrane behaviour, and to determine the structure's energy absorption capacity. Simplicity of design and construction, ductility and high strength make this structural element a viable alternative for use as an ice-resisting wall in offshore structures.

ACKNOWLEDGEMENTS

This report is a copy of a doctoral thesis of the same title submitted by Stephen J. Kennedy in August 1987. Dr. J.J. Cheng supervised the preparation of this thesis. The efforts of the supervisory committee are also acknowledged.

Funding for this study was provided by the Central Research Fund of the University of Alberta, the office of the Dean of Engineering, the Department of Civil Engineering, and grants from the Natural Sciences and Engineering Research Council of Canada provided to Dr. D.J.L. Kennedy and Dr. J.J. Cheng.

The assistance and cooperation of the technical staff of the I.F. Morrison Structural Laboratory, Technical Services, Civil Engineering Machine and Electronics Shop, all at the University of Alberta, is acknowledged.

A special gratitude of thanks goes to friends and colleagues who all put in a great deal of work, time, energy, and personal interest into the completion of this project; Dr. D.J.L. Kennedy, Dr. D.W. Murray, Dr. F. Otto, Tom Casey, Giovanni Di Pietro, Clark Bicknell, Kurt Ratzlaff, Jose Napoleao, Scott Alexander and Richard Bailey.

The support, time, and the personal interest that Karen Baker put in for the preparation and the completion of this thesis are gratefully acknowledged.

Table of Contents

List of Tables

List of Figures

LIST OF SYMBOLS

A = Coefficient to describe a stress-strain curve

A_f = Area of the steel plate after failure, mm^2

A_o = Original area of the steel plate, mm^2

a = x-component of the rigid body displacement, mm

B = Coefficient to describe a stress-strain curve

b = $a(\sin\theta/\cos\theta)$, mm

C = Coefficient to describe a stress-strain curve

C_1 = Net horizontal force from compression strut 1, kN

C_2 = Net horizontal force from compression strut 2, KN

CS_1 = Force in compression strut 1, kN

CS_2 = Force in compression strut 2, kN

c = $a(\cos\theta/\sin\theta)$, mm

D = Coefficient to describe a stress-strain curve

d = Diameter of concrete cylinder, mm; Section depth, mm

d_c = Depth of concrete core, mm

E = Coefficient to describe a stress-strain curve

E_c = Modulus of elasticity for concrete, MPa

E_{st} = Strain hardening modulus of steel, MPa

F = Coefficient to describe a stress-strain curve; Frictional force; Net horizontal force from compression struts 1 and 2, kN

f_c = Uniaxial compressive stress of concrete expressed as a function of strain, MPa

f_t = Split cylinder strength, MPa

f'_c = Uniaxial compressive strength of concrete, MPa

f_r = Modulus of rupture of concrete, MPa

G = Coefficient to describe a stress-strain curve

G_k = Confinement characteristic, MPa/mm

H = Horizontal force at midspan, membrane solution, kN

h = Plate thickness, mm

k_1 = Bulkhead flexural stiffness, kN/mm

k_2 = Adjacent span axial stiffness, kN/mm

k_3 = Axial stiffness of the high strength load rods, kN/mm

k_4 = Load transfer plate flexural stiffness, kN/mm

k_5 = Horizontal reaction frame stiffness, kN/mm

LVDT = Linear Variable Differential Transformer

L = Clear span length of test plate, mm

L_h = Length of the horizontal strut beween the inner most load point and centre span, mm

L_1 = Length of compression strut 1, mm

L_2 = Length of compression strut 2, mm

l = Length of concrete cylinder; Length of clear span, mm

l_{oc} = Original gauge length, concrete

l_{os} = Original gauge length, steel

M_p = Fully plastic moment per unit length, kN m/m

N = Normal force, kN

P = Applied point load, kN; Normal force, kN

P_f = Friction force, kN

P_{h1} = Horizontal component of the force in compression strut 1, kN

P_{h2} = Horizontal component of the force in compression strut 2, kN

P_n = Normal component of the applied point load, kN

P_t = Tangential component of the applied point load, kN

p = One-half the applied point load, kN

q = Uniform load per unit area, MPa

q_c = Critical value of uniform load = $16M_p/L^2$, MPa

S = Membrane force, kN

T_b = Force in the bottom plate at centre span, kN

T_{bh} = Horizontal component of the force in the bottom plate at the support, kN

T_{bv} = Vertical component of the force in the bottom plate at the support, kN

T_f = Pretension force in the steel plates, kN

T_t = Force in the top plate at centre span, kN

T_{th} = Horizontal component of the force in the top plate at the support, kN

T_{tv} = Vertical component of the force in the top plate at the support, kN

t = Age of concrete, days

t_b = Bottom steel plate thickness, mm

t_f = Thickness of the steel plate after failure, mm

t_o = Original thickness of the steel plate, mm

t_t = Top steel plate thickness, mm

U = Ultimate stress for uniaxial stress

V = Net vertical force from compression struts 1 and 2, kN

W = The energy of local plastic distortion per unit volume

w = Steel plate width, mm

w_f = Width of the steel plate after failure, mm

w_{max} = Midspan deflection, mm

w_o = Original width of the steel plate, mm

$\bar{x}$ = Mean value

Y = Ultimate force at the critical section

z = Bearing length, mm

a = $-\nu/(1-\nu)$

a_1 = Angle of compression strut 1 with the horizontal, rad

a_2 = Angle of compression strut 1 with the horizontal, rad

β = $1-\nu+\nu^2$

γ = Octahedral shearing strain, mm/mm

δ = Dilatation associated with the volume change that occurs during elastic straining; Displacement, mm

Δ_e = Elongation or shortening of concrete over a given gauge length

Δ_{int} = Internal deformation, mm

Δ_s = Change in length of steel over a given gauge length

ϵ = Strain, mm/mm

ϵ_{cx} = Longitudinal in-plane strain in the concrete at a distance 'x' from a point of zero slip

ϵ_f = Engineering strain at fracture, mm/mm

ϵ_ℓ = True longitudinal strain in the steel plate, mm/mm

ϵ_o = Strain at the maximum compressive strength, f'_c, mm/mm

ϵ_{st} = Strain hardening strain, mm/mm

ϵ_{sx} = Longitudinal in-plane strain in the steel at a distance 'x' from a point of zero slip, mm/mm

ϵ_t = True through-thickness strain in the steel plate, mm/mm

ϵ_u = Strain at the ultimate tensile strain, σ_u, mm/mm

ϵ_x = Maximum principal strain, mm/mm; Strain in the 'x' direction

ϵ_{xus} = Strain in the 'x' direction for a state of uniaxial stress, mm/mm

ϵ_{xps} = Strain in the 'x' direction for a state of plane strain, mm/mm

ϵ_w = True strain across the width of the steel plate, mm/mm

ϵ_y = Yield strain, mm/mm; Strain in the 'y' direction

ϵ_z = Strain in the 'z' direction

ϵ_1 = Principal strain

ϵ_2 = Principal strain

ϵ_3 = Principal strain

ρ = Reinforcement ratio

θ = Angle of rotation, rad; Angle of the critical element with respect to the horizontal

μ = Coefficient of friction,

μs = Microstrain

ν = Elastic value for Poisson's Ratio

ν_p = Inelastic value for Poisson's Ratio

σ = Stress, MPa; Standard deviation

σ_p = Proportional limit, MPa

σ_{sy} = Static yield stress, MPa

σ_u = Ultimate tensile strength, MPa

σ_x = Normal Stress in the 'x' direction, MPa

σ_{xus} = Stress in the 'x' direction for a state of uniaxial stress, MPa

σ_{xps} = Stress in the 'x' direction for a state of plane stress, MPa

σ_y = Normal stress in the 'y' direction, MPa

$\sigma_{y\ell}$ = Lower yield stress, MPa

σ_z = Normal stress in the 'z' direction, MPa

σ_{yu} = Upper yield stress, MPa

σ_1 = Longitudinal stress, MPa; Principal stress, MPa

σ_2 = Transverse stress, MPa; Principal stress, MPa

σ_3 = Principal stress, MPa

τ_{oct} = Octahedral shear stress, MPa

ω_x = Local slip, mm

1. INTRODUCTION

1.1 General

One of the problems faced by engineers and naval architects from Canada and other northern regions is how to design reasonable and reliable offshore structures in hostile environments, such as the Canadian Beaufort Sea. The problem of design exists because:

1. these structures do not fit into the normal realm of engineered structures, such as a highway bridge or an office building;
2. many of the design equations in current standards are not applicable;
3. the environmental loads are not well defined;
4. the equivalent static loads are estimated to be several orders of magnitude greater than typical engineering loads;
5. the type of load is uncommon;
6. the material and structural behaviour characteristics are not well known for cold temperatures, varying strain rates, and energy absorption;
7. the element of risk is large.

Because of these problems exploration structures have been designed typically using conventional structural systems and are constructed of either large heavily reinforced concrete sections or thick stiffened flat steel plates.

In an effort to find cost effective solutions for the construction of these structures, composite steel-concrete sandwich plate construction was proposed by Matsuishi et al. (1977). A schematic diagram of a typical offshore structure, with steel-concrete sandwich plates as the exterior walls, is shown in Figure 1.1. The composite plate consists of two steel plates, acting as a shell, with a concrete core and is supported by internal bulkheads. This form of construction has several distinct advantages over the other forms of construction. These are: (i) economy of material (fewer stiffeners are required than for steel plates), (ii) simple construction details, (iii) simplified design, (iv) improved load carrying characteristics, especially with respect to local impact.

1.2 Objectives

The objectives of this experimental and analytical study are:

1. to develop mathematical models which describe the strength and behaviour of a steel-concrete composite plates, without mechanical shear interconnectors, when subject to transverse loads;
2. to verify these models experimentally;
3. to determine the shear deformation response of the steel plate concrete interface;
4. to establish the relationship for sliding friction between steel and concrete for varying normal loads;

5. to examine the effects of end restraint and the problems of implementing such restraint;
6. to propose a design methodology consistent with limit states philosophy for this structural element;
7. to outline areas of future work.

1.3 Scope

Steel-concrete sandwich ancillary specimens and plate elements were constructed and tested at room temperature under laboratory conditions. These test specimens were constructed from mild steel plate and with concrete purchased from a local batch plant.

Ancillary tests were conducted to obtain material properties and to establish local behavioural characteristics.

Six steel-concete composite plate elements, with a centre span of 3050 mm, were tested with a four point load system. The composite members were continuous over supporting bulkheads and were axially restrained. Modified bulkhead details were used as supports.

Two basic geometric properties were varied; the nominal steel plate thickness (3.18, 4.76 and 6.35 mm), and the section depth to give span to depth ratios of 15, 20 and 25. As well, one plate element consisting of two 6.35 mm thick plates lying one on top of the other without concrete infill was tested. This test provided a basis with which the behaviour of the composite tests could be compared. In all

cases the loads were quasi-static and short term.

The test results were analysed and compared to mathematical models of the flexural and membrane behaviour. An ultimate strength interaction equation was developed to give the rupture load of the composite plate. Within the limitations of the tests conducted, a design methodology is presented.

1.4 Outline

A review of existing literature on composite sandwich plate behaviour and steel plate membrane behaviour is presented chronologically in Chapter 2.

The objectives of the experimental program and the method by which they were achieved are outlined in Chapter 3. The purpose, number and type of tests, the construction, the instrumentation, and the experimental method are described in detail.

Material properties and load deformation behaviour of the steel and concrete are defined in Chapter 4. The transformation model, which converts longitudinal stress-strain curves of a conventional uniaxial coupon test to an equivalent one for plane strain, and the corresponding transformed stress-strain curves are also presented in this chapter.

The test results and analysis of the steel-concrete interface tests are presented in Chapter 5.

The test results for the composite and steel plate tests presented in Chapter 6 include:

1. general load deflection behaviour and failure modes;
2. crack patterns;
3. steel and concrete strain distributions;
4. slip distributions;
5. restraint measurements - vertical, in-plane and lateral;
6. plate dimensions.

Flexural and membrane models to describe the load deflection behaviour of composite sandwich plates without mechanical shear interconnection are developed in Chapter 7 and compared with the test results. Parametric studies conducted using these models are also presented. The development of an ultimate strength interaction equation, based on the state of stress at the critical section and on an extension of the von Mises-Huber-Hencky yield criterion to ultimate, is presented and compared to the test data.

Chapter 8 describes the application of this type of structural element to the design of offshore structures.

A summary, conclusions and recommendations, and a brief discussion of possible future work are presented in Chapter 9.

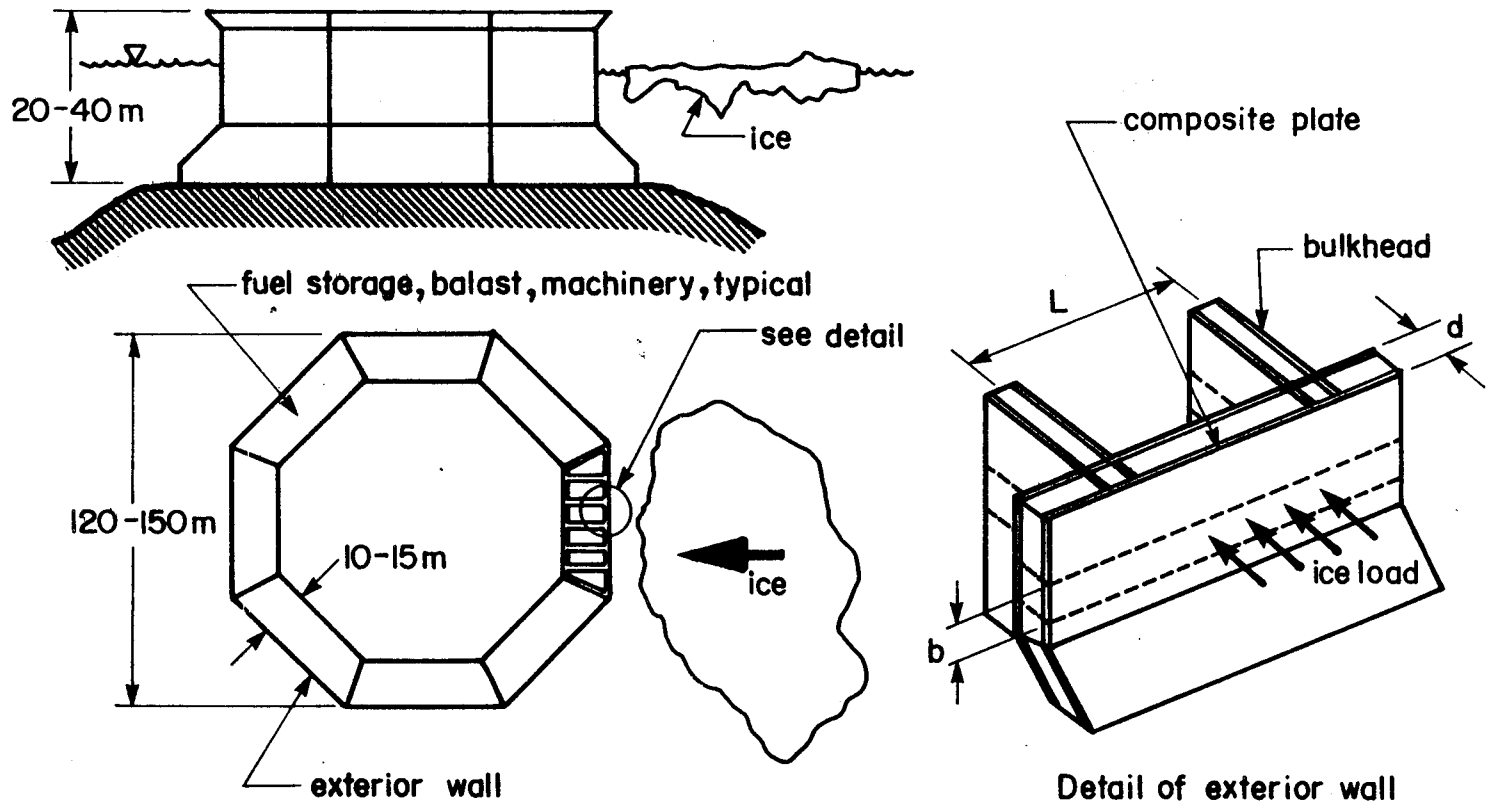

Figure 1.1 TYPICAL OFFSHORE CAISSON STRUCTURE WITH STEEL CONCRETE SANDWICH PLATES

2. LITERATURE REVIEW

2.1 General

A review of the literature relating to the design of "ice-resisting walls" for offshore structures in the Arctic and elsewhere shows that there is a need for more efficient designs for these structural elements, especially for production structures. The design of ice-resisting walls should:

1. be based on an appropriate design philosophy;
2. draw upon past experience so that economy of design and good performance characteristics can be achieved by combining the most favourable behavioural characteristics of various types of construction.

Drucker (1957), in a paper on plastic analysis as applied to naval architecture, discusses the criteria for deciding when a limit load in bending or string load (membrane behaviour) should be applied in design. He concluded that, for the design against a rare catastrophe, a string load or combined bending and string load seemed appropriate, even for moderately deep beams. This concept is supported by Hughes and Gerwick. Hughes (1983) comments that in some special design applications, such as for icebreakers and for protection against blast or collision, where extreme loads occur, significant deformation should be allowed. Gerwick (1984) considers the possibility of applying a two level design philosophy for the design of offshore

structures, which parallels the philosophy of earthquake design. The first level considers that an elastic response is required of the structure for normal design level events and the second considers rare events (extreme overload from ice or collision) for which local damage is permitted, as long as it does not lead to progressive collapse. Based on Drucker's conclusions, the first level of design could be associated with beam behaviour and the second with some combination of beam and membrane behaviour or membrane behaviour.

Based on past experience, evaluations and surveys of the design and performance of offshore structures and icebreakers in the Arctic, Chiu (1981), Croasdale (1983), Bruce and Roggensack (1984), among others, have concluded that:

1. local damage can be tolerated without loss of overall structural integrity;
2. the allowance of an "acceptable" amount of plastic deformation in the plating panels between frames for icebreakers will realize significant savings;
3. increased stiffener spacing, or complete elimination, could result in 40 to 50% reduction in weight of an all steel offshore caisson type structure, with corresponding economy. It was suggested that this could be achieved by introducing a double hull without stiffeners, but with concrete between the hull plates;
4. composite plate construction has distinct advantages

over other forms of construction, such as, (i) simple construction details, (ii) improved thermal resistant properties and (iii) favourable local load carrying characteristics.

Literature pertaining to both the behaviour of composite sandwich elements, and steel plate elements was reviewed, and summaries are presented in Sections 2.2 and 2.3, respectively. Salient points are summarized in Section 2.4.

2.2 Behaviour of Composite Sandwich Beam and/or Plate Elements

The behaviour of composite sandwich beams or plate elements is generally described as being either flexural or tied arch. Flexural behaviour is associated with relatively flexible elements in which an adequate description of the internal forces can be made using beam theory. Generally, the composite element exhibits a number of evenly distributed flexural cracks under load and fails as a result of either a compression failure of the concrete at midspan or yielding of the bottom plate. Tied arch behaviour is associated with a significantly more rigid element in which an adequate description of the internal forces can be made using truss like elements and the compression field theory. Cracking of the concrete is generally limited and failure defined by a compression failure of the concrete in one of the diagonal struts located in the region of maximum shear.

2.2.1 Matsuishi, Nishimaki, Takeshita, Iwata, Suhara (1977)

2.2.1.1 Experimental Program

Number of Tests: 18
L/d Range: 2.9 to 5.6
Scale: not specified
Type of Load: static; one or two concentrated loads
Type of Element: simply supported beam
Parameters: (1) type, arrangement and number of shear connectors
(2) diaphragms
(3) plate thicknesses
Types of Failure: yielding of the tension plate followed by crushing of the concrete at midspan or buckling of the compression plate
Behaviour: flexural, tied arch

2.2.1.2 Summary

The test specimens were designed, proportioned and tested to investigate bending, shear and combined bending and shear behaviour. The ultimate strength of the members was determined from equations based on equilibrium and material capacities of the beam cross-section at the critical midspan section. The mean test to predicted ratio was 0.97 with a coefficient of variation of 0.120. The two simplified methods proposed to determine the ultimate strength are by beam theory and by truss theory.

2.2.2 Matsuishi, Nishimaki, Takeshita, Suhara (1978)

2.2.2.1 Summary

A method of nonlinear analysis using the finite element method was developed to describe the behaviour of the beams tested by Matsuishi et al. (1977). Forms of nonlinear behaviour included:

1. cracking of the concrete under tension;
2. plastification of the concrete under compression;
3. plastification of the steel (yielding and/or buckling);
4. gap formation between the steel plate and the concrete.

The finite element analysis yielded results that were in good agreement with the test results, with respect to load deflection curves, crack patterns and failure loads. Including both the flexural and axial stiffness of the steel plate in the analysis leads to a poor correlation between the analysis and the test results. Modelling the steel as bar elements, with axial stiffness only, gave results which were in reasonable agreement with the tests.

2.2.3 Matsuishi, Nishimaki, Iwata, Suhara (1980)

2.2.3.1 Experimental Program

Number of Tests: 21
L/d: 5.6
Scale: not specified
Type of Load: dynamic, sinusoidal, 0.2 to 0.4 Hz, four different load sequences, one concentrated load
Type of Element: simply supported beam
Parameters: (1) type, arrangement and number of shear connectors
(2) diaphragms
(3) plate thicknesses
(4) load sequence
Types of Failure: (1) fatigue crack at the weld joint between the tension plate and the diaphragm
(2) buckling of the compression plate or yielding of the tension plate followed by crushing of the concrete
Behaviour: flexural, tied arch

2.2.3.2 Summary

The major contributor to nonlinear behaviour, concrete cracking, occurred on the first cycle of load. Subsequently, the residual deformations were negligible, even after 10^5 cycles. There were no fatigue failures of the concrete in the compression zone. In general the load carrying capacity of the element did not decrease. Fatigue failure of steel details may cause a premature failure of the composite element.

2.2.4 Abam Consulting Engineers (1985)

2.2.4.1 Experimental Program

Number of Tests: 34
L/d Range: 3.3 to 6
Scale: 1/4 to 1/3
Type of Load: static, 1 to 5 concentrated loads on the test span, single concentrated load on the adjacent cantilever span
Types of Elements: (1) simply supported beams with cantilevers
(2) three span continuous beams
(3) slabs
Parameters: (1) concrete density
(2) concrete strength
(3) concrete confinement
(4) shear connection
(5) stiffeners
(6) bearing details
(7) specimen temperature
Types of Failure: not specified
Behaviour: flexural, tied arch

Due to the confidential nature of this work, the details and description of the test results and analysis are not available.

2.2.5 Hattori, Ishihama, Yamamoto, Matsuishi, Iwata (1985)

2.2.5.1 Experimental Program

Number of Tests: 4
L/d: 2.84
Scale: 1/3
Type of Load: static; one concentrated load on each span
Type of Element: two span simply supported continuous beam
Parameters: (1) longitudinal stiffeners welded to the outside of the bottom plate , or an equivalent amount of steel plate
(2) thermal fatigue, freeze-thaw cycles
Types of Failure: yielding of the bottom plate
Behaviour: tied arch

2.2.5.2 Summary

Although the mechanical properties of the concrete deteriorated slightly with an increasing number of freeze-thaw cycles, the limited data indicated that there was no appreciable effect on the ultimate strength of the elements. This was due to the fact that the strength of the element was governed by the yield strength of the plates as opposed to the compressive resistance of the concrete strut. A nonlinear finite element analysis modelled the elastic plastic behaviour. A simplified model, idealizing the element as a truss structure, gave a reasonable estimate of the ultimate load.

2.2.6 Akiyama, Koseki, Taira, Sasaki (1986)

2.2.6.1 Experimental Program

Number of Tests: 9
L/d Range: 3 to 10
Scale: not specified
Type of Load: static, concentrated load at midspan
Type of Element: simply supported beam

Parameters: (1) shear span to depth ratio
(2) steel ratio
(3) reinforcing method against shear
Types of Failure: (1) yielding of the tensile steel plate for ρ = 0.5% and 0.9%
(2) degradation of the concrete for ρ = 1.68% and 2.24% followed by a brittle fracture
Behaviour: flexural, tied arch

2.2.6.2 Summary

The strength of the sandwich beam element was estimated with good accuracy by applying the ultimate strength method for reinforced concrete members.

2.2.7 Nojiri, Koseki (1986)

2.2.7.1 Experimental Program

Number of Tests: 24
L/d Range: 2 to 5
Scale: 1/3
Type of Load: static, concentrated load at midspan
Type of Elements: (1) 14 one span beams
(2) 10 two span beams
Parameters: (1) shear span to depth ratio, a/d
(2) steel index, $\rho f_y/f'_c$
(3) type and quantity of shear reinforcement
Types of Failures: (1) yield of the bottom plate and ultimately crushing of the diagonal concrete strut at the lower end
(2) one specimen, with a steel ratio, ρ = 4%, failed by crushing of the compressive strut prior to the steel plate yielding
Behaviour: tied arch

2.2.7.2 Summary

A method for estimating the ultimate capacity is outlined for members with and without shear reinforcement. The method suggests that the capacity of the composite section be limited to the lesser of the flexural capacity as

governed by yield of the steel plates and the shear capacity as governed by Niwa's equation (1984) for members without web reinforcement or by the ACI (1983) shear equations for members with web reinforcement. Based on this method, the mean value for the test to predicted ratio was 1.03 with a coefficient of variation of 0.09. The theory of reinforced concrete has been suggested as a simplified design method to determine the strength of the composite sandwich element.

2.2.8 Ozawa, Tanaka, Ueda (1986)

2.2.8.1 Experimental Program

Number of Tests: 4
L/d: 10.1
Scale: 1/3
Type of Load: static, two concentrated loads at third points
Type of Element: simply supported beam
Parameters: (1) flange thickness
(2) steel web thickness
Types of Failures: (1) yielding of the tensile steel, buckling of the compression steel followed by crushing of the concrete in the constant moment region
(2) crushing of the concrete in a compression strut in the shear span, followed by yielding of tensile steel in the constant moment region and buckling of the compression steel in the shear span
Behaviour: flexural, tied arch

2.2.8.2 Summary

The shearing force is carried by the steel web and by tied arch action. The model proposed to determine the ultimate capacity of the member, which assumes that the steel web yields and the concrete struts crushes, gives

excellent test to predicted values. A reduction factor of 0.7 for the compressive strength of the concrete in the strut has been incorporated in the analysis to account for the reduced strength due to cracking.

2.2.9 Shioya, Matsumoto, Okada, Ota (1986)

2.2.9.1 Experimental Program

Number of Tests: 17 (12 flexural tests and 5 shear tests)
L/d: 2.9, 11.1
Scale: 1/3 to 1/2
Type of Load: static, two concentrated loads at 1/3 and 1/4 points, one concentrated load in each adjacent cantilever span
Types of Elements: (1) simply supported beams
(2) simply supported beams with cantilevers
Parameters: inner stiffener configurations, height, spacing and direction
Types of Failure: (1) elastic or plastic buckling of the compression steel followed by flexural compressive failure of the concrete
(2) shear compression failure of the diagonal compression strut (concrete)
Behaviour: flexural, tied arch

2.2.9.2 Summary

The flexural capacity of a slender beam element is predicted with reasonable accuracy using traditional reinforced concrete analysis and by treating the composite section as a doubly reinforced concrete section. The "shear" capacity for specimens with L/d equal to three were accurately predicted using Niwa's equation. The shear capacity of two specimens with L-shaped stiffeners was less than their counterparts with a lattice of flat bar stiffeners due to slip at the steel-concrete interface. The

composite models had 5 to 20 times the energy absorption capability of comparable reinforced concrete sections.

2.2.10 Centre for Frontier Engineering Research (1987)

2.2.10.1 Experimental Program

Number of Tests: 19 (16 beam tests and 3 slab tests)
L/d: 4, 5, 6
Scale: 1/4 to 1/3
Type of Load: static, single concentrated load to series of six point loads approximating an uniformly distributed load; concentrated loads in each adjacent cantilever span
Types of Elements: (1) simply supported beams with cantilevers
(2) three span continuous plate and/or beam
Parameters: (1) span to depth ratio
(2) plate thicknesses
(3) type of load
(4) number, size and location of diaphragms
(5) support configuration
(6) concrete strength
(7) internal shear reinforcement, studs and and reinforcing bars
(8) width
Types of Failures: (1) flexural failure, yielding and fracture of the bottom plate of one test specimen
(2) "shear" failure, degradation and crushing of the compressive concrete strut
(3) punch through failure of two slabs loaded with a single concentrated load
Behaviour: flexural, truss (tied arch), punching shear

2.2.10.2 Summary

With the exception of one beam which failed in flexure, the others, all being over-reinforced, behaved like tied arches. Typically, the centre span deflections, prior to the shear compression failure of the first compression strut were 1/100 of the span. Post-failure ductility was observed

in all cases. Due to the rigid nature of the concrete blocks, much of the apparent ductility of the specimen resulted from large local deformations. In one specimen these deformations forced a failure at the weld between a diaphragm and the load plate. Increased strength and stiffness were achieved through additional diaphragms.

Slab type specimens exhibited extremely stiff behaviour. In all cases the load was applied over a small area, with a diameter of 200 mm, at midspan. The deformation and failure were localized. A punching failure occurred, indenting and eventually shearing the top plate, forming a shear cone in the concrete core and loading the bottom plate as a membrane with the tension tie diaphragms resisting a large part of the transverse load. In one case the bottom plate fractured along the diaphragms at the weld. Subsequent to the loss in section, the specimen failed in shear compression, as did the beams.

It is stated that the compression field theory could be used to predict the ultimate strength of the beam elements. The ultimate load for each beam element has been determined using Niwa's empirical equation (1984) and Nielson and Braestrup's (1978) upper bound plasticity solution. The mean test to predicted values for these are 1.06 and 0.93 with coefficients of variation of 0.14 and 0.10 respectively. An empirical equation which calculates the shear capacity of the concrete between discrete shear reinforcement provided by the diaphragm plates is presented.

Because of the difficulty in predicting a shear compression failure in the concrete, finite element models using a nonlinear analysis have been used with limited success in predicting the load deflection behaviour.

2.2.11 O'Flynn (1987)

2.2.11.1 Experimental Program

Number of Test: 17
L/d: 4,5,6
Scale: 1/3
Type of Load: static, two concentrated loads or a series of 6 point loads approximating an uniformly distributed load; concentrated loads in each adjacent cantilever span
Type of Element: simply supported beam with cantilevers
Parameters: (1) concrete strength
(2) type of concrete, plain or steel fibre reinforced concrete
(3) lateral confinement of the concrete over the support
(4) support type
(5) type of load
(6) support diaphragms
(7) type, arrangement and number of shear connectors
Types of Failure: (1) crushing of the concrete near the support, with or without a fan type crack pattern, or in one case a horizontal crack along the top of the studs at the support. In 3 specimens this was followed by strain hardening of the support plate or rupture of the support plate or by large centre span deflections
(2) overall crushing of the concrete
(3) crushed concrete at mid-depth
(4) yielding and strain hardening of tension steel, large deformations
Behaviour: flexural, tied arch

2.2.11.2 Summary

This work is primarily an experimental investigation into the behaviour of over-reinforced steel-concrete

composite sandwich plates, where the failure is defined as a loss of load carrying capacity of the concrete core. Conclusions are:

1. the type of shear connector has no apparent effect on the ultimate strength of the element;
2. inappropriately spaced stiffeners for the supporting bulkheads may initiate a local degeneration of the concrete core at the support which may ultimately lead to a reduction in the load carrying capacity;
3. diaphragm plates located at the support have no apparent effect on the ultimate strength;
4. shear connectors on the support plate (with the exception of those anchoring the compression struts) have no apparent effect on the ultimate strength;
5. the ultimate strength increases as a function of the square root of f'_c;
6. steel fibre reinforced concrete increases the ductility of the concrete.

The internal forces for a uniformly loaded specimen could be assessed accurately using compression field theory and a fan type stress field. This was not true for the specimen subjected to a patch or concentrated load. In all cases the ultimate strength was predicted with some accuracy.

A failure criterion for the concrete in composite plates has been developed. It is similar in philosophy to the transverse strain criterion currently suggested in the

general method of CAN3 A23.3 M-84 (1984) but proposes the use of a confinement characteristic, G_K, in place of the transverse strain at the failure location. This criterion was developed for specimens with concrete strengths between 40 and 70 MPa. It also assumes that the concrete fails before the support plate yields. Using this criterion the ultimate strength was accurately predicted.

O'Flynn gives guidelines for the design of composite ice-resisting walls and again cautions about the effect of inappropriately spaced stiffeners on the bulkhead:

1. use Nelson stud connectors for both plates with the appropriate number located in the support region of the support plate;
2. use diaphragm plates at support regions.

2.3 Behaviour of Steel Beams and/or Plate Elements

A detailed review of the analytical and/or experimental work of Timoshenko (1940), Clarkson (1956), Young (1959), Hooke and Rawlings (1969), Hooke (1970) and Kennedy and Hafez (1984) is given in Ratzlaff (1985).

In general, the analytical models presented by these authors consider both the elastic and inelastic performance of transversely loaded, rigidly clamped plates of various aspect ratios. Additional analytical studies were done to determine the effect of boundary movements, which reflect practical boundary conditions found in grillages in typical naval structures, on the behaviour of these plates. Although

it was recognized that, through membrane action, these plates have the capacity to carry substantially more load than that given by the flexural collapse load, the failure was defined by a serviceability criterion in the form of permanent set, as opposed to a strength criterion. To verify the analytical work, a total of twenty-three plates, loaded by hydraulic pressure (only one to failure), and nine beams under a four point load system, were tested by Clarkson (1956), Young (1959), and Hooke and Rawlings (1969). Aspect ratios, slenderness ratios L/d, and boundary conditions were varied.

Additional work of McDermott et al. (1974) and Ratzlaff and Kennedy (1985; 1986) is reviewed in the next two sections.

2.3.1 McDermott, Kline, Jones, Manier, Chiang (1974)

2.3.1.1 Experimental Program

Number of Tests: 10
L/d: 151.5
Scale: 1/5
Type of Load: static; 1 to 6 concentrated load points located at various locations along the length
Type of Elements: flat or stiffened plate strips, continuous over two simple supports; in-plane restraint in the long direction
Parameters: (1) flat or stiffened plate
(2) number, type (25.4 mm radius or 90 degrees sharp edge) and location of load points
Types of Failure: rupture of the plate either at the support or around the load point
Behaviour: flexural, flexural membrane, membrane

2.3.1.2 Summary

A plastic analysis procedure for the structural design of steel plates for collision resistance is presented. The energy lost during the collision is equated to the plastic energy absorbed by the distortion of the ship. The mathematical model assumed for analysing the structural behaviour of the struck ship incorporates three mechanisms for producing plastic deformations:

1. longitudinal plastic buckling of the stiffened hull plating;
2. plastic membrane tension in the stiffened hull plating;
3. yielding or buckling of the web framing (transverse bulkheads).

The anchorage required for the development of the longitudinal membrane tension is provided by the remainder of the ship. Energy solutions are described in detail for the bending phase, membrane tension phase and the web frame buckling or yielding phase. The analysis was extended so that it can be applied to a double hulled ship as well as a single hulled ship and to account for both right angle and oblique angle collisions.

The following conclusions were drawn from the analysis:

1. for strikes adjacent to the bulkheads, an insignificant amount of energy is absorbed in the stiffened shell before rupture occurs;
2. the plastic energy absorbed in the hull during the membrane tension phase is approximately 0.69 to 0.94

times the total plastic energy absorbed by the structure, depending upon the structural configuration. The hull bending plastic energy is insignificant by comparison;

3. the plastic energy absorbed is maximized by maximizing the number of units distorting in membrane tension, the elongation of each unit, the extent of damage and the tensile strength and ductility of the steel plate;
4. plastic energy absorption is maximized in double skin construction where the transverse bulkheads connect the two hulls;
5. the total energy absorbed is sensitive to the value of the maximum tensile strain that the hull plating can sustain.

Based on the test data, the authors present an analytical model to describe the load deflection curve of the stiffened plate and, in great detail, a mathematical model relating bend angle to a maximum strain. Two failure criterion for rupture are described, one for maximum membrane strain, and one for maximum bending and tensile strain. A summary of strains and plastic energy at rupture for the test specimens is given.

2.3.2 Ratzlaff and Kennedy (1985, 1986)

2.3.2.1 Experimental Program Description

Number of Tests: 2
L/d: 103
Scale: not specified

Type of Load: static, hydraulic pressure
Type of Element: plate with an aspect ratio of 3
Parameters: two identical tests
Type of Failure: shearing of plate along the long edge close to midlength
Behaviour: flexural, flexural membrane, membrane

2.3.2.2 Summary (1985)

A review of analytical and/or experimental work related to the behaviour of transversely loaded plates is presented. In light of the given test data, a probable domain for the elastic inelastic behaviour of steel plates was defined from the solution of six different behaviour extremes, where the smallest upper bound and the largest lower bound solution for a particular deflection define the boundaries. The solution is limited to transversely loaded plates with an infinite aspect ratio, no strain hardening of the plate material and perfectly rigid boundaries. The domain is illustrated in Figure 2.1 and the solutions defined as follows:

1. curve F, elastic plastic flexural behaviour only (lower bound);
2. curve M_e, elastic membrane solution (lower bound);
3. curve M_i, inelastic membrane solution (lower bound);
4. curve E, Timoshenko's elastic solution for flexural behaviour with membrane forces included (upper bound);
5. curve Y, Hafez and Kennedy's fully yielded flexural membrane (upper bound);
6. curve N, inelastic membrane solution, ν_p, plastic value of Poisson's ratio, 0.5 (upper bound).

It was postulated that the actual behaviour would be flexural at first, with some influence due to the development of membrane forces, Curve E, then some combination of flexural behaviour (diminishing influence) and membrane behaviour (increasing influence) curve R, and finally pure membrane behaviour at point B. Due to the change in Poisson's ratio from the elastic to the plastic, value the curve would eventually tend toward Curve N from Curve M_i.

A nonlinear finite element analysis of a transversely loaded plate yielded results that were in reasonable agreement with the postulated behaviour. The analysis was also substantiated by available test results as shown in Figure 2.1.

2.3.2.3 Summary (1986)

The paper presents a discussion on the behaviour of rectangular steel plates, clamped on all four edges, subjected to uniform transverse load or a fluid pressure.

Three regions of behaviour were identified and modelled mathematically:

1. elastic flexural membrane;
2. inelastic flexural membrane;
3. inelastic membrane.

A finite element analysis was compared with the results of two small scale model tests and was found to be in reasonable agreement. The plate was modelled for plane strain conditions and the solution incorporated an inelastic

Poisson's ratio response and a linearized stress-strain curve for the plate material.

Two failure criteria based on edge effects, one related to maximum tensile straining due to bending and membrane action and the other to shear loading, were presented. The test to predicted ratio based on the shear limit criterion was 0.97 for the failure load and 1.08 for the corresponding deflection obtained from the inelastic membrane analysis.

A discussion was presented on the implications of using this structural element in the design of offshore structures in the Arctic.

2.4 Summary

During the last ten years, 161 composite sandwich beam elements and six one-way composite sandwich slab elements, with a large number of different test parameters and L/d ratios between 2.9 and 11.1, have been tested as simply supported one or two span continuous structures under a variety of different load patterns. The behaviour has been dominated by flexure or by tied arch action with failures initiated by yielding of the bottom (support) plate in tension; or by buckling of the compression plate coupled with a compression failure of the concrete; or by a compression failure of a concrete strut in the tied arch. No attempts have been made to incorporate the in-plane restraint provided to the element by the rest of the structure. Therefore, the membrane action of the plates, the

ductility and the post-flexural failure behaviour did not play a role. A limited number of tests have been conducted by Matsuishi et al. (1980) on the dynamic response of these elements.

Ultimate loads, as defined by the failures, were predicted with reasonable accuracy using traditional reinforced concrete analysis or by the compression field theory as outlined in CAN3 A23.3 M84 (1984). Several empirical equations have been presented for the calculation of shear strength. Nonlinear finite element analyses have been used successfully only for specimens which fail by yielding of the bottom plate.

The majority of the experimental and analytical work reported in Section 2.3 deals with the post-flexural behaviour of steel plates. In total, 25 steel plates of various aspect and slenderness ratios were tested under hydraulic pressure (only three of them to failure). Nineteen plate strips with in-plane restraint provided and with varying boundary conditions and load patterns were also tested.

The consensus amongst the researchers is that the steel plates or strips exhibited great ductility and post-flexural "failure" strength due to the membrane action of the plates. The best treatment for the prediction of the large deflection behaviour is given by Ratzlaff and Kennedy (1985; 1986). McDermott et al. (1974) present a plastic analysis procedure for the design of steel plates for collision

resistance. Both Ratzlaff and Kennedy (1985; 1986) and McDermott et al. (1974) present failure criteria for the rupture of these plates.

This literature review serves as the basis from which the study and development of flexible composite plate elements can be established. The element conceived for this study incorporates the attributes of both the flexural behaviour of the composite section and the membrane behaviour of the steel plates. The element simply consists of two steel plates and a concrete core. The composite plate elements are without mechanical interconnection and welded sections so that the fundamental behaviour may be determined.

In retrospect, it is ironic that engineers readily accept the use of cables in structures as such bridges and guyed towers, but not the use of plates that behave as cables.

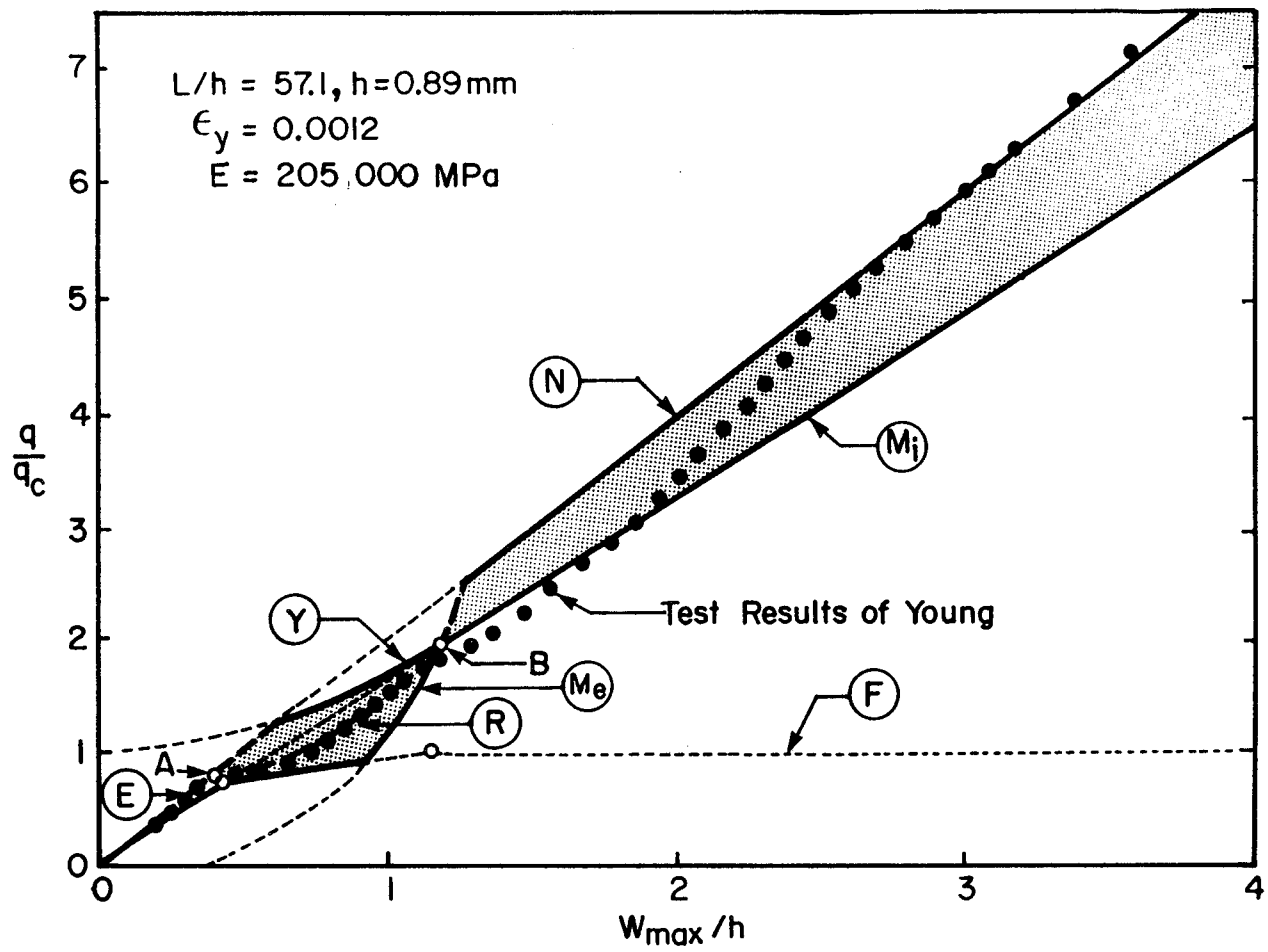

Figure 2.1 TEST RESULTS OF YOUNG (1959) AND BEHAVIOURAL DOMAIN (Ratzlaff and Kennedy 1985)

3. EXPERIMENTAL PROGRAM

3.1 General

The experimental program was designed to:

1. obtain the data necessary to describe the strength and behaviour of steel-concrete sandwich plates without mechanical shear interconnection, when subjected to transverse loads;
2. obtain measurements of boundary forces and movements;
3. obtain data to compliment analytical models, such as the coefficient of friction between steel and concrete under varying normal loads, and basic material and geometric properties.

A series of six one-span continuous composite plate elements with a span of 3050 mm (centre to centre distance between supporting bulkheads) were tested with a four point load system as shown in Figure 3.1. The specimens were continuous over the supporting bulkheads and axially restrained. One specimen consisting of two steel plates one on top of the other without concrete infill was also tested. This test provided a basis with which the behaviour of the composite tests could be compared. Two basic geometric properties were varied to determine their influence on the flexural and membrane behaviour, and on the ultimate strength. Nominal steel plate thicknesses were varied from 3.18 mm to 6.35 mm and the section depth was varied to give span to depth ratios, L/d, from 15 to 25.

Ancillary tests included calibration tests of the load and vertical restraint rods, the horizontal restraint frame columns, the lateral confinement device rods; steel-concrete interface tests; tension coupons; biaxial stressed plane strain cylinder tests; concrete cylinders and concrete prisms.

3.2 Composite Plate Tests

3.2.1 General

The central part of the experimental program was designed to examine both the strength and behaviour of steel-concrete composite plates, with no mechanical shear interconnection, when subjected to transverse loads and the influence of boundary conditions, in-plane restraint and support details, on the load deformation response of the plate element. Six composite plates with varying section depths and plate thicknesses as given in Table 3.1 were tested. The plates were modelled as continuous elements and tested under four point loads as shown in Figure 3.1. Because the composite plate element is a segment of a much larger structure, the boundary conditions, bulkheads and external horizontal reaction frame were designed and interconnected with the plate to provide an equivalent response of the surrounding structure to the plate element under load. Vertical restraint on either side of the test span was provided to approximate that of a continuous

structure. The overall dimensions of the test specimen are given in Figure 3.1.

Test specimens are designated in Table 3.1 as either STEEL (two steel plates with no interconnection), or, as for example C121T6 (C-composite, 121-composite section depth in millimeters, T6-approximate plate thickness in millimeters). For all tests, the length of the test span is the clear distance between supports and is 2850 millimeters.

3.2.2 Test Specimens

The steel plates for fabrication of the test specimens was prepared and delivered to the structures laboratory by Empire Iron Works Ltd., Edmonton. Fabrication of the test specimens took place over a period of three months included the following steps:

1. the plate material was identified and marked;
2. coupon and shear test specimen material was flame cut from the plate material, identified and marked;
3. the original dimensions, plate thickness, width and length were measured and recorded;
4. gauge locations, centre-span, load points, bulkhead locations were located and scribed on the steel;
5. strain gauges were installed on the inside surfaces of the plates for the plate elements and the lead wires attached. Aluminum capsules were epoxied over the gauges and the lead wires arranged and extended. The capsules were painted to prevent an alkali reaction between the

alkali in the concrete and the aluminum. The capsule, as shown in Figure 3.2, protects the strain gauge from the concrete and because of the accordian like arrangement of lead wires within the capsule, up to ±6 mm of relative movement between the concrete core and the steel plate can take place without shearing the leads or the strain gauge;

6. U-shaped inserts for the composite plate over the bulkhead were welded (the inserts provided continuity between the top steel plate of the composite plate element and the side plates of the bulkhead (see detail in Figure 3.6));
7. bulkheads were welded and prepared in four stages as shown in Figure 3.3;
8. gauges were installed and encapsulated on the inside surfaces of the bulkheads;
9. connecting plates were welded to the top and bottom steel plates at a distance of 100 mm from each end to form a long rectangular box;
10. gauge locations and resistances were mapped;
11. forms were built;
12. the steel plates, bulkheads, shear test specimens, modulus of rupture plate elements and cylinders were prepared for casting of concrete. U-shaped inserts for the composite plate were inserted at the prescribed locations. Strain gauge lead wires were fixed in place and protected with tape;

13. with the specimens on their sides, concrete was cast via a hopper and vibrated with pencil vibrators. Subsequently the surface was trowelled smooth;
14. the specimens were removed from the forms and the steel brushed clean;
15. gauges were installed on the outside of the composite plates and the bulkheads; Strain gauge locations and resistances were mapped.
16. specimens were stored;

3.2.3 Test Set-Up

The test set-up consisted of a series of hydraulic jacks, temporary support frames, knife edge roller assemblies, yokes, load and vertical restraint rods, an external horizontal restraint frame, stiffened plate girder, electronic and mechanical instrumentation, a data acquisition system, bulkheads, lateral confinement devices, and the test plate. Figure 3.4 shows schematically a side elevation and a cross section of a composite plate in the test apparatus. For clarity the instrumentation and lateral confinement devices have not been included.

3.2.3.1 Loading Apparatus

Vertical loads were applied to the composite (or steel) plate by a series of load apparatuses, each consisting of a hydraulic jack, yokes, load rods, and a knife-edge-roller assembly as shown in Figure 3.4. The jacks, in compression against the underside of the strong floor, react against a

yoke putting the load rods in tension. The load is transferred from the load rods through another yoke to two knife-edge-roller assemblies and then to the test plate. The load system allows the test plate to move freely relative to the load apparatus with the horizontal location of the load remaining fixed and the direction vertical. Each knife-edge-roller assembly, as shown in Figure 3.5, was designed to carry a 1000 kN load with translation and rotation capacities of ±60 mm and 0.524 radians respectively. The load rods were instrumented to act as load cells.

3.2.3.2 Bulkhead Supports

Each plate element spanned across two identical short columns. These built-up sections, as shown in Figure 3.6, represented bulkhead supports. The supports were designed to behave elastically under maximum load so that they could be readily used as load cells. The leading edge of the bearing plate, next to the central plate element, was rounded to lessen the effect of local stress concentrations which could possibly cause a premature failure of the composite plate.

To establish rotational rigidity at the bulkhead support a tie down was also provided, as shown in Figure 3.6. This mechanism established moment equilibrium over the bulkhead support making the composite plate-bulkhead system a continuous structure.

3.2.3.3 Horizontal Restraint Frame

The horizontal restraint frame lay in the same horizontal plane as the test plate specimen, and provided the in-plane restraint necessary for the development of membrane action. The axial restraint provided was directly related to the horizontal stiffness of the surrounding structure. The frame consisted of two very stiff built-up end beams separated by two HSS 304.8 x 304.8 x 12.7 columns 5400 mm long. This frame was supported vertically by roller assemblies which were located on top of four stub columns. The length of the stub columns was adjustable vertically, so that the centroid of the frame could be placed in the same plane as the centroid of undeformed plate elements of different section depths. A schematic diagram of the frame is given in Figure 3.7. The frame provided restraint of up to 5 000 kN with an axial shortening of approximately 6 mm. The horizontal HSS compression members were instrumented to act as load cells.

3.2.3.4 Vertical Restraint Apparatus

The composite plate element was restrained against vertical movement about midway between the horizontal restraint frame and the bulkhead supports, with the result that the rotations over the bulkhead were negligible, and the vertical and rotational alignment of the plate element with the horizontal restraint frame was ensured. The load system used to provide the restraint was similar in design to the one used for loading as shown in Figure 3.4. Load

rods were instrumented to determine the loads generated by the passive restraint.

3.2.3.5 Lateral Confinement Devices

Segmental external passive clamps were used to provide transverse in-plane restraint against expansion to the concrete along the length of the composite plate as shown in Figure 3.8. The segmental clamps allowed the composite plate to deform without increasing the flexural or in-plane stiffness. Each segment consisted of a stiff contact load distribution plate, HSS load transfer pieces and calibrated load rods as shown in Figure 3.9. The segments were supported on wooden blocks resting on the top of the plate specimens. The stiff contact load distribution plates bore against a series of Teflon pads which were epoxied to the side faces of the concrete core. This arrangement allowed the concrete to move in the plane and along the length of the plate with minimal restraint (no greater than the passive nominal force developed times the coefficient of friction of Teflon on steel) from the lateral confinement device. The devices were proportioned so that up to 25 MPa of pressure could be developed (on the exposed concrete surface) at 70% of the yield strength of the load measuring rods.

3.2.3.6 Instrumentation and Measurement

Applied loads, reactions, steel and concrete strains, rotations, displacements and slip between the steel plate

and the concrete core were measured throughout the duration of each test. The locations of the measurements made on the reaction frame, bulkheads and composite plates (deflections, steel strains, concrete strains and slip measurements) are shown in Figures 3.10, 3.11, 3.12 and 3.13. The type of measurement, instrumentation used, sensitivity, location, purpose and frequency of measurements are described in Tables 3.2 and 3.3.

Additional measurements made to corroborate deflection data and other information during the test include crack widths, locations, directions, lengths and growth; changes in the depth of section; relative displacements of the steel plates with respect to the concrete core; and rotations and final plate dimensions.

3.2.4 Assembly of Test Apparatus

The assembly of the test apparatus and preparation for each plate element test consisted of the following steps:

1. the vertical elevation of the horizontal restraint frame was fixed;
2. bulkheads supports were aligned, placed and grouted into place and bolted to the stiffened plate girder;
3. the horizontal restraint frame was aligned horizontally;
4. load transfer plates were lifted into position;
5. the test plate was lifted into position;
6. proper gap widths for welding the steel plates to the load transfer plates were established;

7. the test plate was bolted to the bulkhead supports through the tensile force mechanism;
8. the load transfer plates were welded to the steel plates;
9. the strain gauges were connected to the lead wires and the lead wires routed;
10. the Teflon pads were epoxied to the concrete surface;
11. the lateral confinement devices were placed in position and the cables from the load cells were routed and connected to the data acquisition system;
12. the load and vertical restraint apparatuses were lifted into place; These were suspended a few millimeters above the test plate;
13. the load alignment frame was lifted and bolted into place;
14. the load alignment rods were threaded into place;
15. the frames to support the LVDT's were attached to the load alignment frame and to the distributing plate element;
16. LVDT's were connected and the cores located to provide the maximum linear range;
17. the necessary computer files were created and the initial data were recorded;
18. the power supply voltages were adjusted to specified values;
19. strain gauge channels were balanced and all the gauges were calibrated;

20. all electronic channels were tested to ensure that proper connections had been made;
21. initial observations and measurements were made and recorded;
22. photos of the undeformed structure were taken.

3.2.5 Test Procedure

3.2.5.1 Load Application

Load was applied to the test plate through the load and vertical reaction apparatuses as described in section 3.2.3.1 and 3.2.3.4. A pneumatically activated hydraulic system with a reservoir, control console, control valves, and a control manifold was used to supply pressure to the jacks. The valves and manifold allow different pressures to be applied for four sets of jacks. The sets of jacks, selected from those available in the laboratory, included:

1. 3 - 50T vertical restraint jacks at the north end;
2. 2 - 60T vertical restraint jacks at the south end;
3. 2 - 200T vertical applied load jacks;
4. 2 - 500T vertical applied load jacks.

The pressure in the corresponding load jacks was adjusted to maintain equal loads at each of the four load points. The pressure, and hence load, for the vertical restraint jacks was adjusted to maintain vertical alignment of the overhanging portion of the test plate in a horizontal position. In all tests the load was applied to the plate element incrementally and monotonically to failure.

3.2.5.2 Load Sequence

The initial load sequence is different from the failure load sequence. The initial load sequence consisted of the following steps:

1. initial readings at zero load;
2. tightening of load transfer plates to the horizontal restraint frame. (This provided a measure of the in-plane forces developed due to welding.) Tightening the tensile load transfer mechanism to make the test plate and the supports continuous;
3. applying the dead load of the load apparatuses:
    1) vertical restraint, north end, 50T jacks;
    2) vertical restraint, south end, 60T jacks;
    3) 200T jack, north end;
    4) 200T jack, south end;
    5) 500T jack, north end;
    6) 500T jack, south end.
4. aligning the yokes below strong floor and extending the jack pistons to make contact;
5. removing temporary banding straps on the composite specimens.

For the failure load sequence increments of load or deformation were applied to the test plate as determined by the load deformation curve. At a deflection of about 300 mm, nuts on the load rods were tightened against the underside of the strong floor so that the 200T and 500T jacks could be fully retracted while maintaining the load on the test

plate. The yokes were then repositioned and aligned and the jack pistons extended. Loading continued as before with an additional 300 mm of stroke available from each of the jacks.

After each load step the valves for the hydraulic system were closed to maintain the load. Some relaxation occurred in the system. For extended interruptions, such as overnight breaks, nuts on the load rods were tightened against the underside of the strong floor to ensure that the load was maintained.

3.2.5.3 Observations and Recording of Data

After each load step electronic and manual readings were recorded and a visual inspection carried out. The latter included:

1. scanning of all LVDT channels to observe the location of the cores and resetting the same when the voltages approached the limits of the linear range;
2. checking deflection of the overhangs of the test plate. Adjustments were made as necessary through the vertical restraint load apparatuses;
3. checking the formation of cracks in both the concrete and steel;
4. determining the displacement of the structure with respect to the load points;
5. aligning the load apparatuses. Adjustments were made as necessary;
6. checking cables and connections to ensure that they were

still attached;

7. checking yielding, yield pattern and progression of yielding in the steel plates;
8. measuring gross displacements of the test plate to corroborate LVDT displacement measurements;
9. and as well observing any
    1) decrease in thickness or width of the steel plates
    2) changes in section depth
    3) relative movement of the steel plate and the concrete core
    4) rotations over the support.

Supporting evidence from observations was measured and recorded. Photographs were taken periodically of the deflected shape and crack pattern and of any physical phenomena which were of interest.

Measurements of concrete strains and slip were taken at the load corresponding to initiation of the compression failure at midspan.

3.3 Ancillary Tests

3.3.1 Calibration

3.3.1.1 Load and Vertical Restraint Rods

Eight 5800 mm long and four 5400 mm long 50.8 mm diameter high strength steel rods were used to transfer load from the jacks to knife-edge-roller assemblies, and hence to

the test specimen as shown in Figure 3.4. These rods, made of AISI 4140 steel, were hardened and tempered to increase the strength and the range of linear behaviour. The mill certificate gave the elastic limit and tensile strength of these rods as 759 MPa and 943 MPa, respectively. Each rod, referred to subsequently as a load or a vertical restraint rod, was instrumented to act as a load cell and calibrated in tension over the expected range of load by loading in the 6700 kN MTS testing machine as follows:

1. load in 100 kN increments to 1000 kN recording both the load and load cell output;
2. unload, take zero readings and zero the load cell;
3. load in 50 kN increments to 950 kN recording data;
4. Repeat steps 2 and 3 until satisfactory repeatability is achieved.

The linear range, repeatability and sensitivity of each rod as a load cell was determined.

3.3.1.2 Compression Members of Horizontal Restraint Frame

Two HSS, 304.8 x 304.8 x 12.7, 5400 mm long members were used as compression members in a frame which provided the horizontal restraint necessary to develop the membrane strength of the steel plates in the test specimen as shown in Figure 3.7. By instrumenting both columns with eight electrical resistant strain gauges, two on each face located at mid-length, they became load cells. The columns were calibrated under uniaxial compression in the 6700 kN testing machine, following procedures similar to those for the load

and restraint rods, but, up to a maximum load of 2200 kN with load increments of 100 kN.

3.3.1.3 Lateral Confinement Device Rods

Thirty-four 1050 mm long, 38.1 mm diameter mild steel rods, part of a series of segmental clamping devices, were used to restrain the concrete transversely during the test as shown in Figure 3.9. These rods were instrumented to act as load cells, and were calibrated in tension in the Baldwin testing machine following procedures similar to those previously described.

3.3.2 Steel-Concrete Interface Friction Tests

3.3.2.1 General

The steel-concrete interface tests were designed to determine:

1. the shear deformation (slip) response of the steel-concrete interface under varying normal loads and different plate thicknesses and roughnesses, and
2. the static and dynamic coefficient of sliding friction for steel on concrete when concrete is cast against the steel.

For this series of tests a steel plate was sheared across a concrete surface while the two were subjected to a constant normal load. A schematic diagram of the test set-up is shown in Figure 3.14. The normal load was applied by a 6700 kN MTS testing machine through a steel roller plate test assembly

which allowed the steel plate to move freely under load, while a horizontal jack displaced the load frame and slid the steel plate across the concrete block. The frictional force for the roller assembly had previously been determined experimentally and was found to be negligible in comparison with the frictional forces transmitted across the interface between the steel plate and the concrete block.

In the first series of tests, consisting of five test specimens of similar geometry and one steel plate thickness, the slips were measured on fresh or virgin surfaces not previously subjected to friction forces. Five different normal loads of 0.2 N, 0.4 N, 0.6 N, 0.8 N and 1.0 N, where N is the normal load required to fracture the steel plate, were used.

Subsequently, in the second series of tests slip measurements were made for a series of increasing normal loads on plates of 3.18, 4.76, 6.35 and 25.4 mm thickness. For the first normal load on each plate, the "virgin" response was obtained.

It is recognized that, in these tests, the steel plates, the concrete and the interface were relatively flat whereas, in the main tests of the composite plates, the members would be bent. The effect of the bending coupled with the membrane forces is seen primarily to increase the normal force between the steel and the concrete.

3.3.2.2 Interface Test Specimens

To prepare the interface specimens:

1. the plate material was identified, marked and measured;
2. three strain gauges were installed on the friction surface of the steel and encapsulated, as shown in Figure 3.15, at prescribed locations;
3. forms were constructed and the concrete cast, against the steel plate, at the same time as the composite plate elements;
4. transition plates were welded to each test plate;
5. two additional strain gauges were installed one on the top and one on the bottom side of the plate 50 mm in front of the concrete block;
6. the test specimen was located and aligned in the test set-up and welded to the horizontal load frame.

3.3.2.3 Test Set-Up

The test set-up as shown in Figure 3.14 consisted of the test specimen, the hydraulic jack, the horizontal load frame, the 1334 kN (300 kip) load cell, the test roller plate assembly, the 6700 kN MTS testing machine, the electronic instrumentation including LVDT's to measure displacements, a data acquisition system, and the reaction supports. The instrumentation is shown in Figure 3.15. The vertical and horizontal forces were determined from the 6700 kN MTS testing machine and the 1334 kN (300 kip) load cell, respectively. The internal force distribution along the steel plate was determined from the measured strains knowing

the stress-strain characteristics of the steel. The slip along the length of the plate was determined from the measured displacements.

3.3.2.4 Test Procedure

The procedure to test each specimen was:

1. after alignment, welding and instrumentation hook-up, initial readings were recorded;
2. a constant normal load was applied;
3. the horizontal load was increased until slip occurred;
4. horizontal loading was continued to establish the dynamic friction coefficient;
5. LVDT'S were reset as necessary;
6. measurements were made and data recorded at appropriate intervals as determined by the horizontal load displacement curve;
7. photographic and written records were kept.

3.3.3 Steel Strength

3.3.3.1 Tension Coupons

For each of the four different steel plates used in these experiments, five coupons from both the longitudinal and transverse directions were tested to determine the uniaxial stress-strain characteristics. The coupons were taken from the parent plate as described in Section 3.2.2. The coupons were cut and milled following ASTM E8-85a (1985) recommendations using a gauge length of 200 mm and a width

of 38.1 mm.

The cross-sectional areas of the reduced area of the coupons were determined from eleven measurements of the reduced width and thickness made along the length prior to testing. Pairs of strain gauges, mounted on both faces of each coupon, allowed the average longitudinal and transverse strains to be measured for strains between 2 and 15 percent as loads were obtained from the testing machines. Large strains were measured both by using an extensometer with a 25.4 mm gauge length and with dividers and a scale over a 200 mm gauge length. The tension coupons were tested in accordance with ASTM E8-85a (1985) in either the 880 kN Baldwin or the 1000 kN MTS testing machine.

3.3.3.2 Plane Strain Uniaxial Stress Comparison Tests

Based on measurements of the original and final dimensions of the steel plates used for the composite plate tests, it was apparent that these plates were subjected to a stress state lying somewhere between uniaxial stress and plane strain. The plane strain stress state is defined as the state of stress in which σ_y, τ_{yz} and τ_{zx} are zero. The strain in the z-direction is zero. The x, y and z directions are taken to be along the length, through the thickness and across the width of the plate, respectively. To determine the internal forces from the strain data, both uniaxial stress and plane strain stress-strain characteristics along the x-direction (maximum principal stress direction) were required. Because of the complexity of performing a plane

strain test on the available plate, a test series was developed to give a semi-empirical transformation model to transform uniaxial stress-strain relationships to plain strain conditions and also to establish the experimental data by which an analytical model could be calibrated.

This series of tests was comprised of three standard tension coupon tests, one cylindrical specimen tested in axial tension (a state of uniaxial stress) and two cylindrical specimens tested under a state of plane strain (when loaded axially and subjected simultaneously to internal pressure). All specimens were taken from the same piece of seamless 1026 steel tube.

The standard coupons were prepared and tested in accordance with ASTM E8-85a (1985).

The geometric properties of the three identical cylindrical test specimens were determined prior to testing. A typical specimen and its instrumentation are shown in Figure 3.16. For the plane strain specimens, the transverse (circumferential) strain at mid-thickness of the reduced wall thickness was maintained at or near zero by adjusting the internal hydraulic pressure for each increment of axial load. These increments were made sufficiently small to ensure that control could be maintained and plastic strain reversals did not occur.

3.3.4 Concrete Strength

Two batches of concrete were used for the test specimens. Compressive and tensile strength tests were conducted to determine the parameters necessary to define the stress-strain curve for uniaxial behaviour as a function of time. The concrete was 51 to 81, and 98 to 111 days old when the plate elements and shear specimens were tested.

3.3.4.1 Uniaxial Compression Tests

Twenty cylinders from batch 1 and twenty-five from batch 2 were tested in accordance with CSA A23.2-9C-M77(1977) to determine the modulus of elasticity, the maximum compressive strength and the stress-strain characteristics in uniaxial compression. The cylinders were cast in cardboard molds, covered with polyethylene, and cured in the laboratory along with the other test specimens. Tests were carried out at ages from 7 to 83 days.

3.3.4.2 Split Cylinder Tensile Tests

Five cylinders from batch no. 2 were tested in accordance with CSA A23.2-13C-M77(1977) to determine the splitting tensile strength. The concrete was 44 to 79 days old when tested.

3.3.4.3 Modulus of Rupture

Six standard 152.4 x 152.4 x 914.4 mm beams were tested in accordance with CSA A23.2-8C-M77(1977) to determine the modulus of rupture. The concrete was 28 to 83 days old when tested.

Table 3.1 GEOMETRIC PROPERTIES OF PLATE ELEMENTS

TEST SPECIMEN	WIDTH w, mm	PLATE THICKNESS		CONCRETE DEPTH, d_c mm	SECTION DEPTH, d mm	L/d
		TOP, t_t, mm	BOTTOM, t_b, mm			
STEEL	500.3	6.96	6.90	-	13.86	205.6
C121T6	500.6	6.86	6.82	109	122.7	23.2
C152T6	500.0	6.70	6.83	140	153.5	18.6
C152T4	500.7	4.87	4.87	143	152.6	18.7
C152T3	500.6	3.13	3.15	146	152.3	18.7
C203T6	500.5	6.77	6.91	191	204.2	14.0

Notes: 1. Test specimen identification; Steel - two steel plates, no interconnection; Composite, i.e. C121T6, C - composite, 121-approximate section depth in mm, T6 - approximate plate thickness in mm.
2. Span length is the clear distance between supports, L=2850 mm.

Table 3.2 RESTRAINED PLATE TESTS - TYPE OF MEASUREMENT AND INSTRUMENTATION

INSTRUMENTATION	LOCATION / DESCRIPTION	PURPOSE	FREQUENCY OF MEASUREMENTS
	Applied Loads		
Electrical Resistance Gauges	Four strain gauges arranged in a full bridge configuration form a load cell to measure axial load. One group of gauges is located on each of the eight loading rods. Refer to Figure 3.4.	Gives the applied load.	Discrete readings taken at the end of each load or deformation increment.
	Vertical Restraint		
Electrical Resistance Gauges	Four gauges arranged arranged in a full bridge configuration form a load cell to measure axial load. One group of gauges is located on each of the four vertical restraint rods. Refer to Figure 3.4.	Gives the vertical restraint from which the internal moments over the supports can be determined.	Discrete readings taken at the end of each load or deformation increment.

Table 3.2 con't

INSTRUMENTATION	LOCATION / DESCRIPTION	PURPOSE	FREQUENCY OF MEASUREMENTS
	Horizontal Restraint - External Frame		
Electrical Resistance Gauges	Eight gauges located midway along the length on each of the two horizontal restraint members of the external frame to measure: (1) the average axial strain, (2) bending strains. Refer to Figure 3.7.	Used to determine (1) the axial restraint provided to the plate element specimen, (2) the bending induced into the frame from the test specimen.	Discrete readings taken at the end of each load or deformation increment.
	Supports - Bulkhead Details		
Electrical Resistance Gauges	A series of gauges located at three levels on each support. Refer to Figure Figure 3.12.	Used to determine the reactions and internal force distributions along the length of the support.	Discrete readings taken at the end of each load or deformation increment.

Table 3.2 con't

INSTRUMENTATION	LOCATION / DESCRIPTION	PURPOSE	FREQUENCY OF MEASUREMENTS
		Steel Strains	
Electrical Resistance Gauges	At a series of locations along the length of the beam, on the top and bottom plates, strain gauges were installed on the outside and inside faces from which longitudinal and/or transverse strains were measured. Refer to Figure 3.11.	Provides a steel strain distribution across the section from which the load carried by the steel at that section may be determined.	Discrete readings taken at the end of each load or deformation increment.
		Concrete Strains	
Mechanical Extensometer	A pair of measurements on one side of the beam, about the neutral axis, were made at a series of locations along the length as shown in Figure 3.13.	Provides a concrete strain distribution across the section from which the load carried by the the concrete at that location may be determined.	One set of readings was taken to correspond with the initiation of the compression failure in the concrete at midspan.

Table 3.2 con't

INSTRUMENTATION	LOCATION / DESCRIPTION	PURPOSE	FREQUENCY OF MEASUREMENTS
		Slip	
Mechanical Extensometer	Location and gauge lengths are as shown in Figure 3.13.	Provides a measure of the relative movement of the steel plates with respect to the concrete core.	One set of readings was taken to correspond with the initiation of the compression failure in the concrete at midspan.
		Deflected Shape	
LVDT's[1]	A series of LVDT's are located along the length of the beam and the bulkhead supports as shown in Figure 3.10	Used to monitor the load deflection response of the structural element under load.	Discrete Readings taken at the end of each load or deformation increment.
	Movement and Deformation of the Horizontal Restraint Frame		
Dial Gauges	One dial gauge located at each of the four columns supporting the horizontal frame. Refer to Figure 3.4.	Used to monitor the horizontal movement and deformation of the horizontal restraint frame.	Discrete readings taken at the end of each load or deformation increment.

Note: 1. LVDT = Linear Variable Differential Transformer.

Table 3.3 RESTRAINED PLATE TESTS - MEASUREMENT, RANGE, ACCURACY

MEASUREMENT	INSTRUMENT	RANGE		ACCURACY, %
		OPERATING	SPECIFIED	and/or smallest Division
Applied loads	Full bridge Calibrated load cell	0 - 500 kN	0 - 950 kN	±0.06 kN
Vertical Restraint	Full bridge Calibrated load cell	0 - 100 kN	0 - 950 kN	±0.03 kN
Horizontal Restraint Frame	8-1/4 bridge strain gauges per column calibrated load cell	0 - 1300 kN	0 - 2200 kN	±0.02 kN
Steel Strains	Normal G.F. = 2.11	0 - 20 000 μs	20 000 μs	±1.0 μs
	High Elongation G.F.=2.055	0 - 40 000 μs	200 000 μs	±0.5 μs

Table 3.3 - Con't

MEASUREMENT	INSTRUMENT	RANGE		ACCURACY, %
		OPERATING	SPECIFIED	and/or smallest Division
Concrete Strains, Steel Strains and Slip	Mechanical Extensometer gauge length			
	100 mm	0 - 20 000 μs ±7.5 mm	150 000 - 300 000 μs ±7.5 mm	±65 μs ±0.001 mm
	200 mm	0 - 10 000 μs ±12.5 mm	125 000 - 250 000 μs ±12.5 mm	±40 μs ±0.001 mm
Deflected Shape	LVDT's			
	±0.1"	±0.1"	±0.1 "	0.0002
	±0.5"	±0.5 "	±0.5 "	0.001
	±1.0"	±1.0 "	±1.0 "	0.002
	±2.0"	±2.0 "	±2.0 "	0.004 "
	±3.0"	±3.0 "	±3.0 "	0.006 "
	10.0"	10.0 "	10.0 "	0.02 "
Horizontal Restraint Frame Movement and Deformation	Mercer Dial Gauge	±0.25"	±0.25"	0.0001"

Notes: 1. LVDT's and dial gauges were reset to keep the instrument with the specified range.
2. Any steel strains exceeding the specified range or of a suspect nature were ignored.

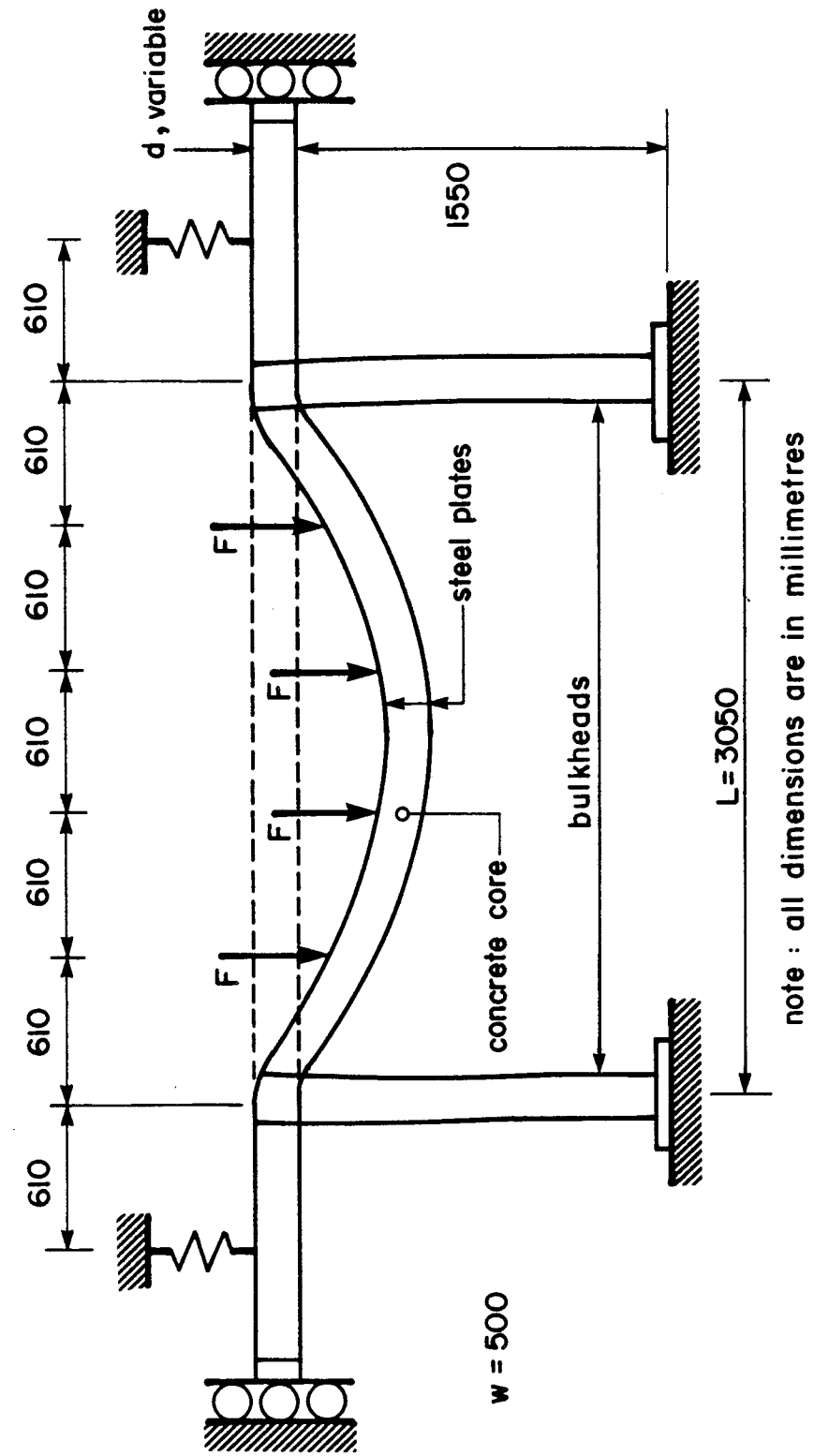

Figure 3.1 SCHEMATIC DIAGRAM OF THE EXPERIMENTAL MODEL FOR THE COMPOSITE PLATE TESTS

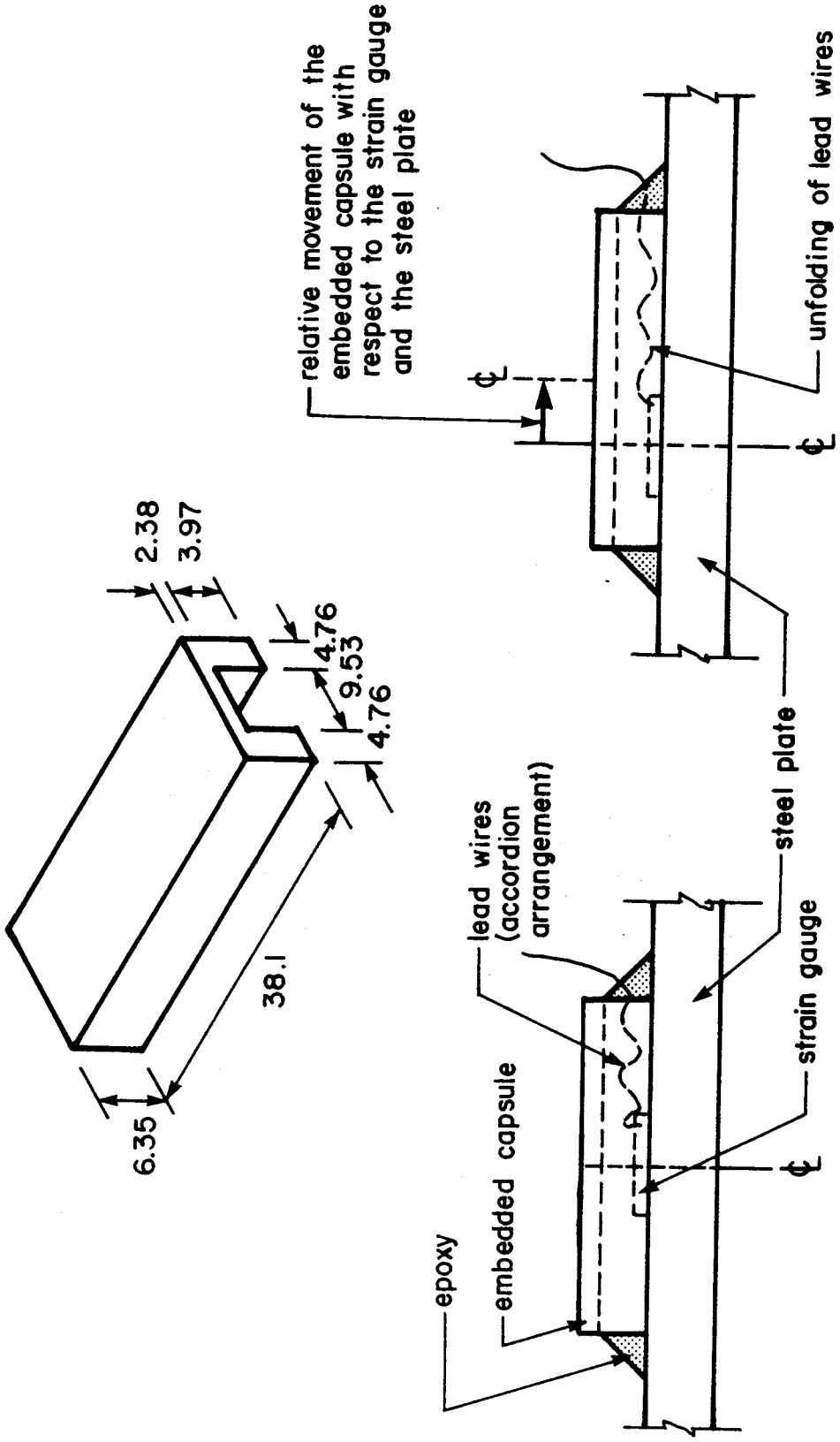

Figure 3.2 ENCAPSULATED GAUGE CONFIGURATION

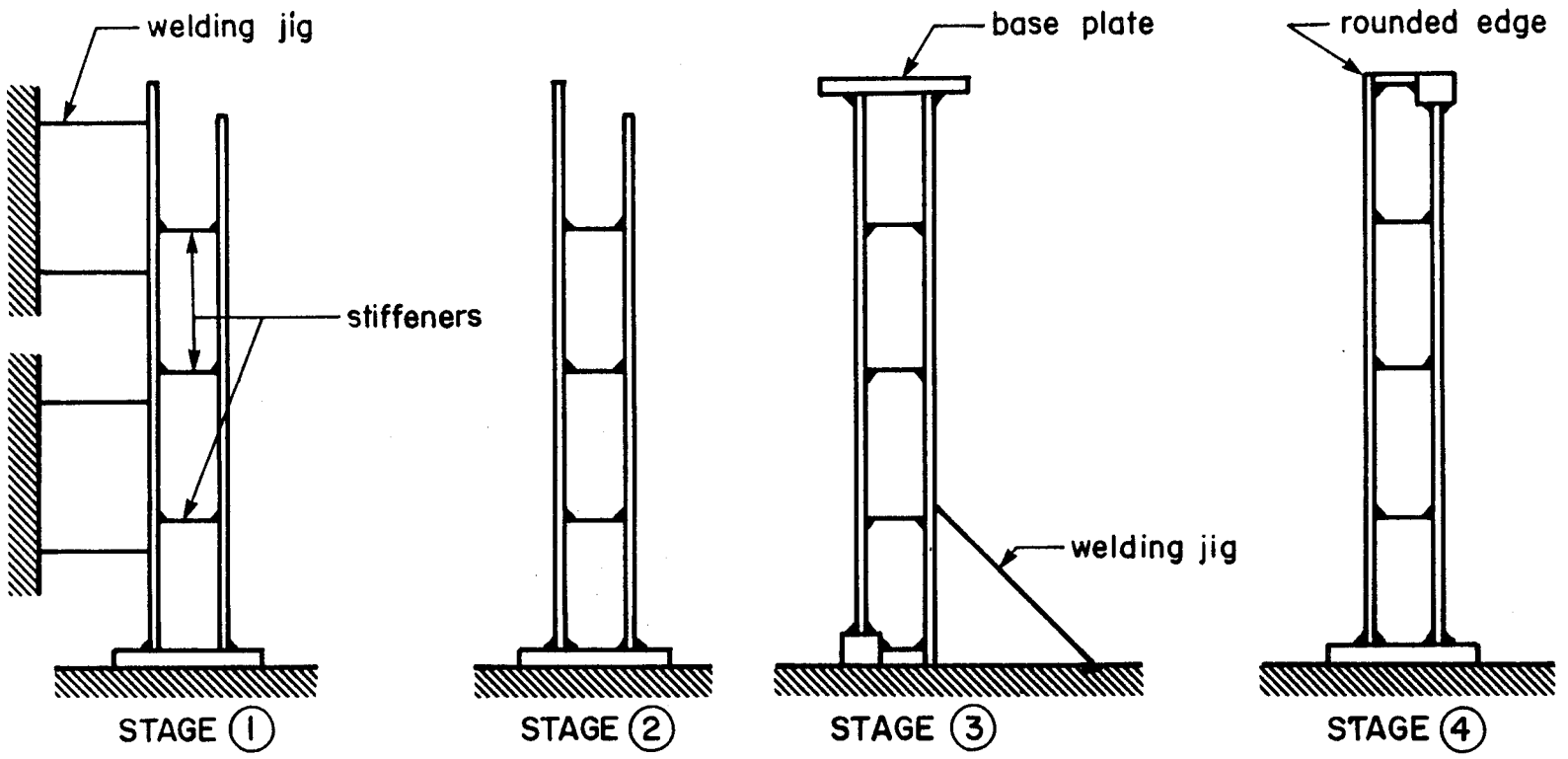

Figure 3.3 BULKHEAD CONSTRUCTION SEQUENCE

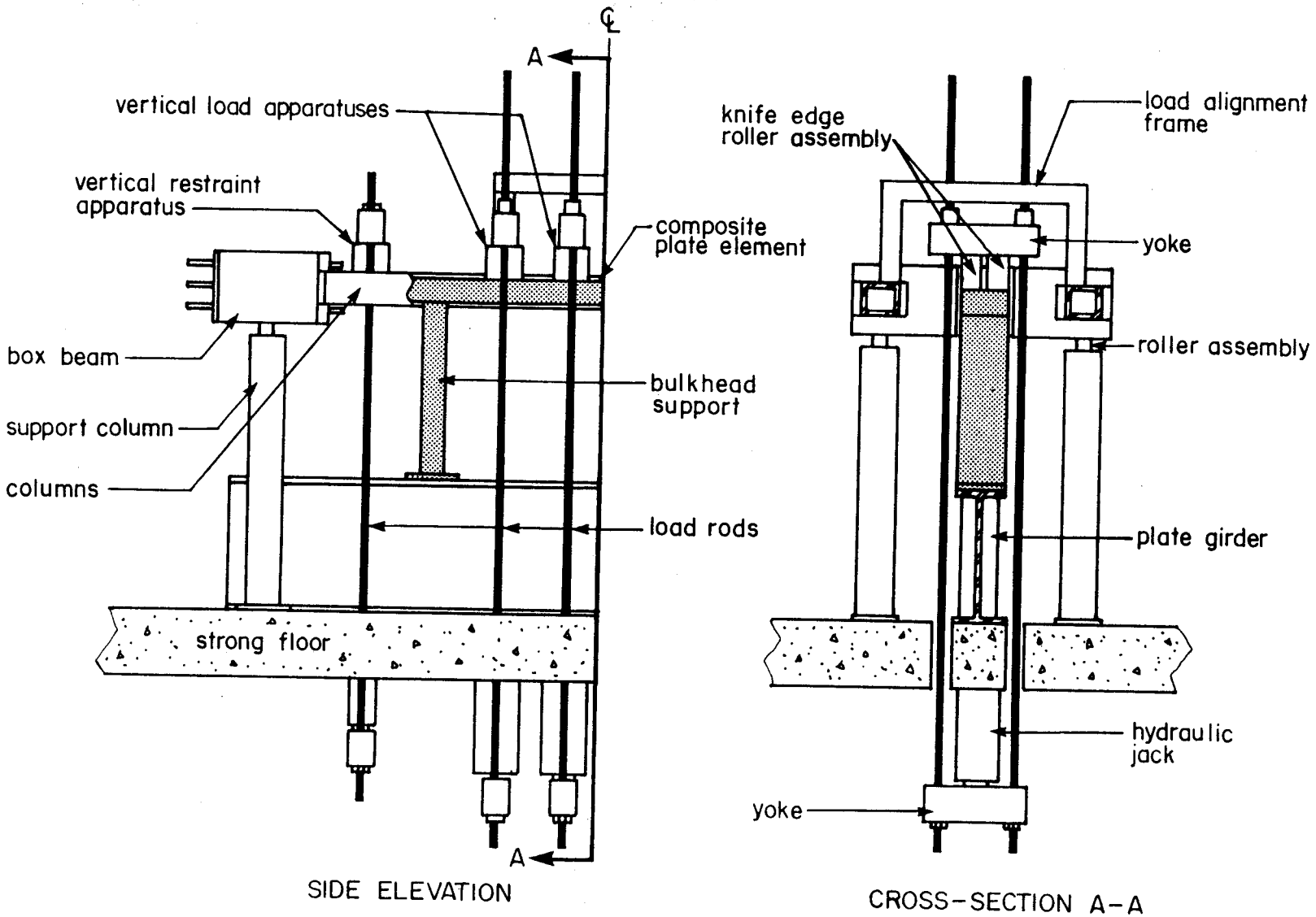

Figure 3.4 SCHEMATIC DIAGRAM OF TEST SET-UP, COMPOSITE PLATE TEST

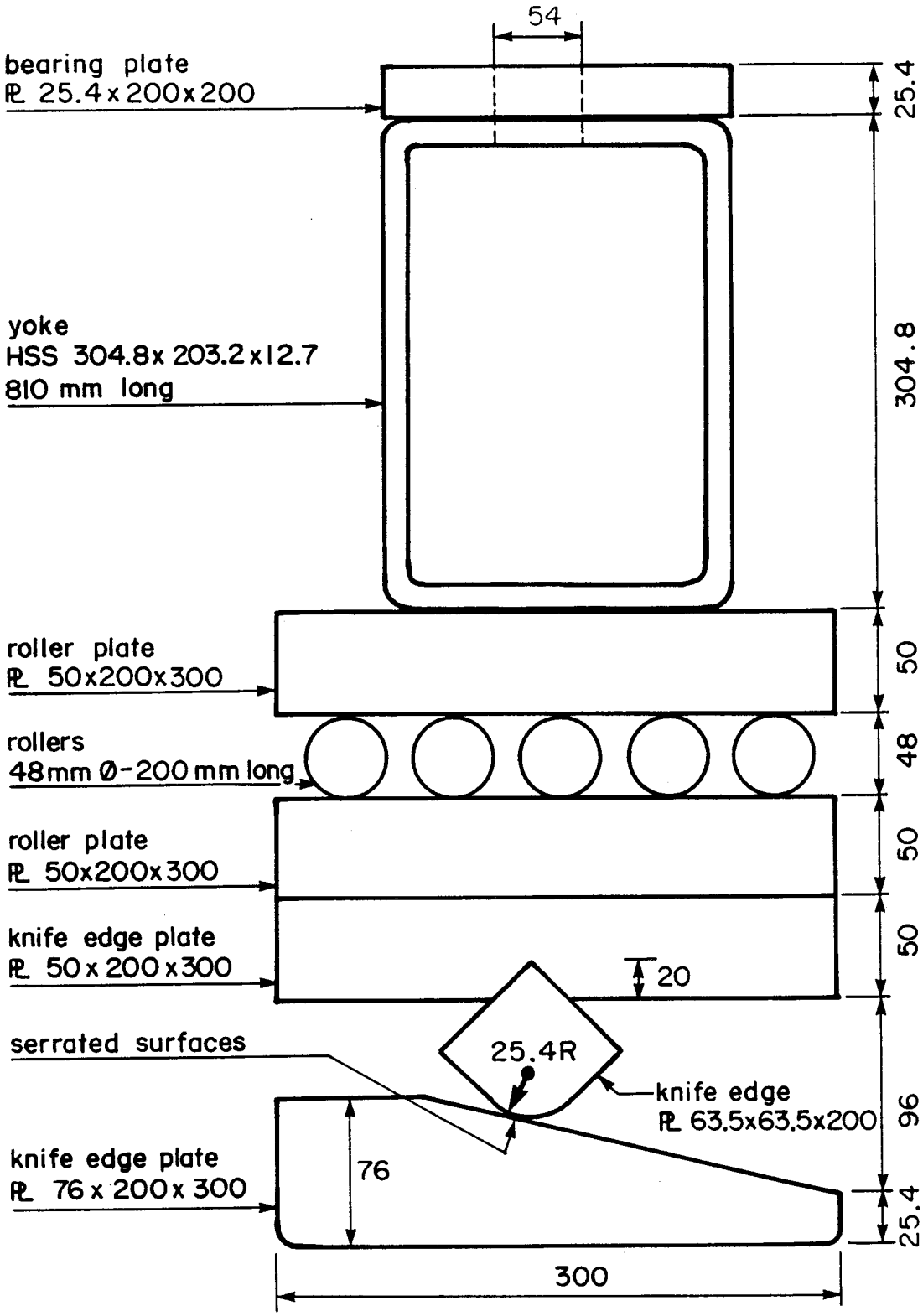

Figure 3.5 KNIFE EDGE ROLLER ASSEMBLY

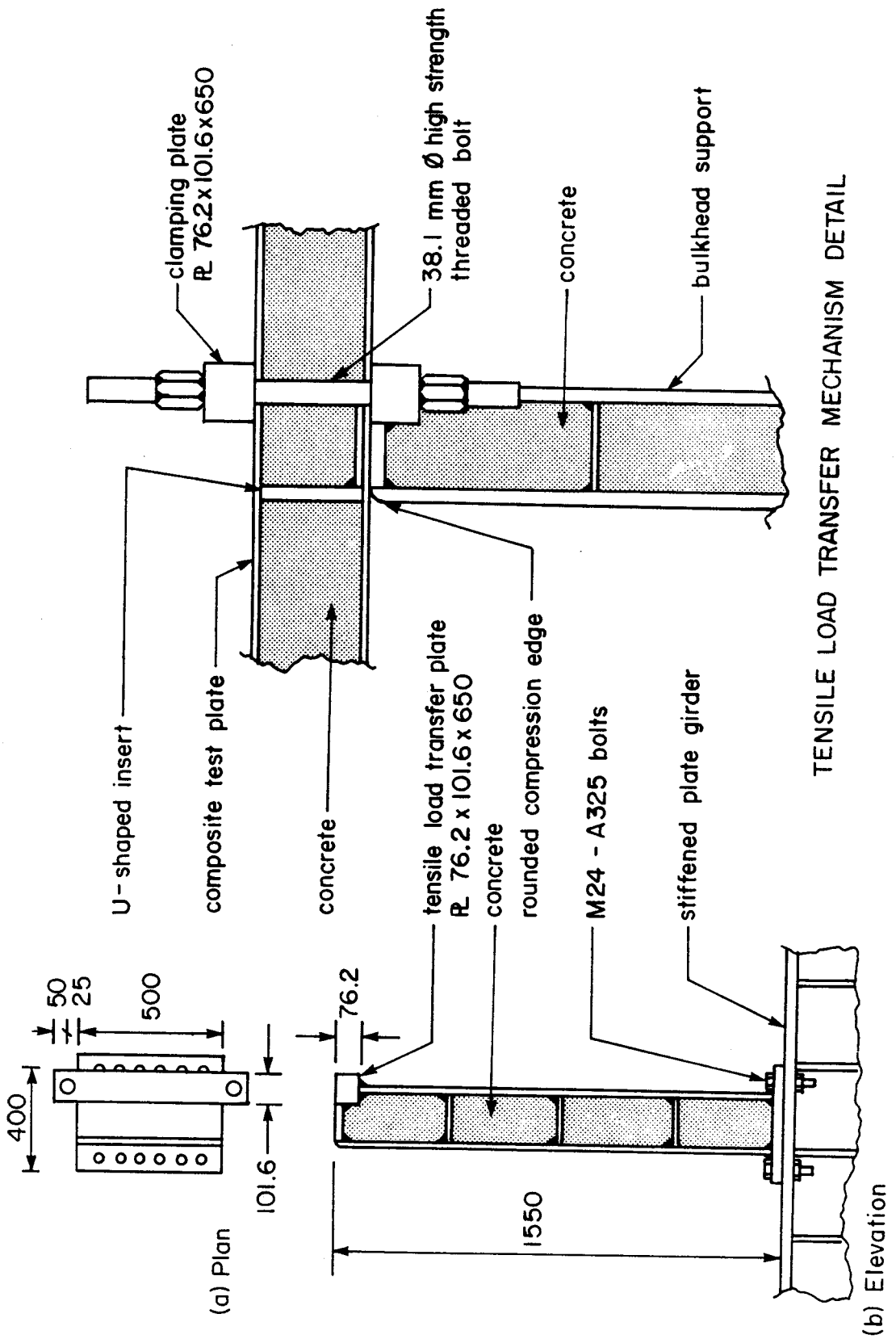

Figure 3.6 BULKHEAD SUPPORT SYSTEM

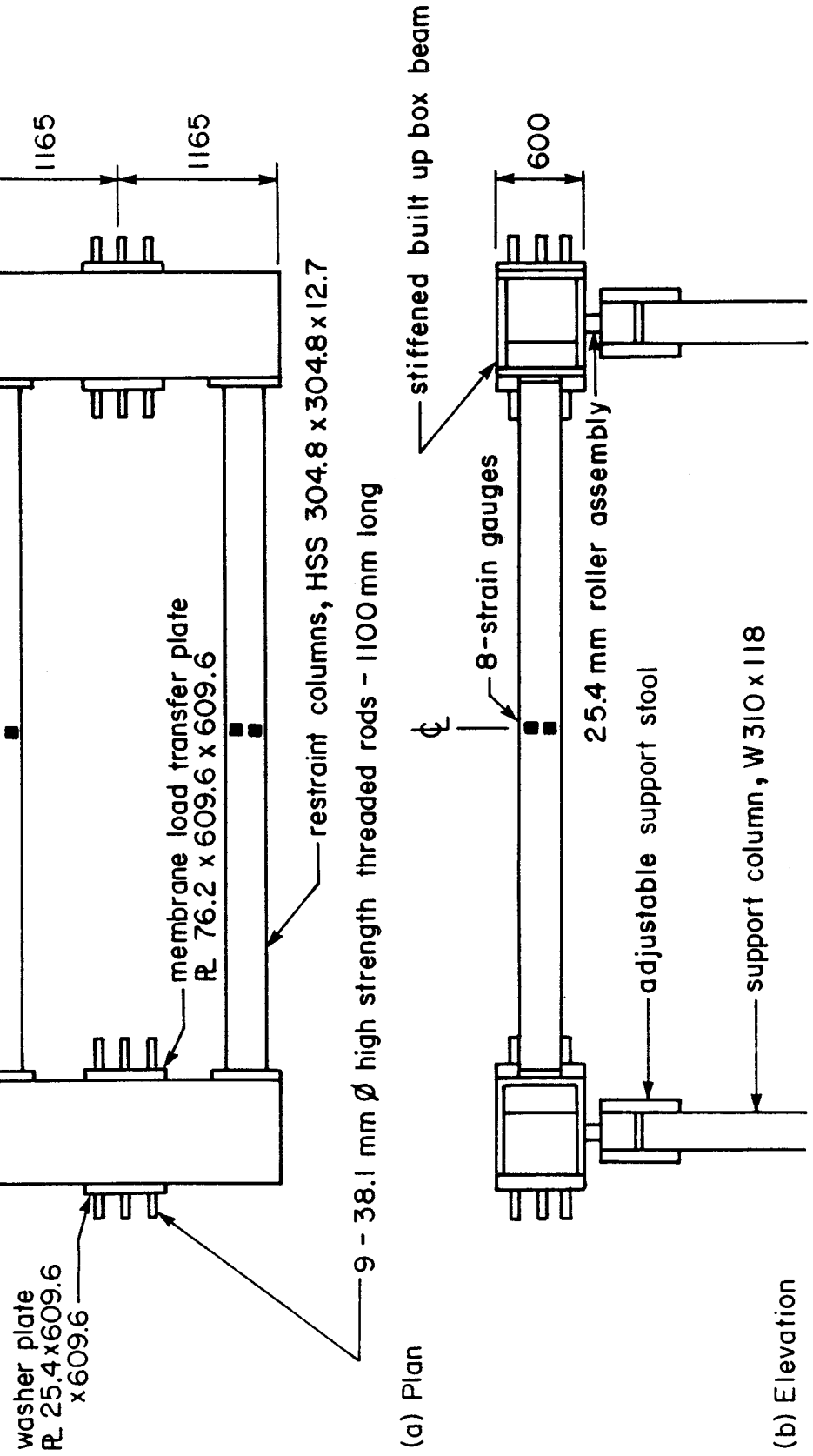

Figure 3.7 HORIZONTAL RESTRAINT FRAME

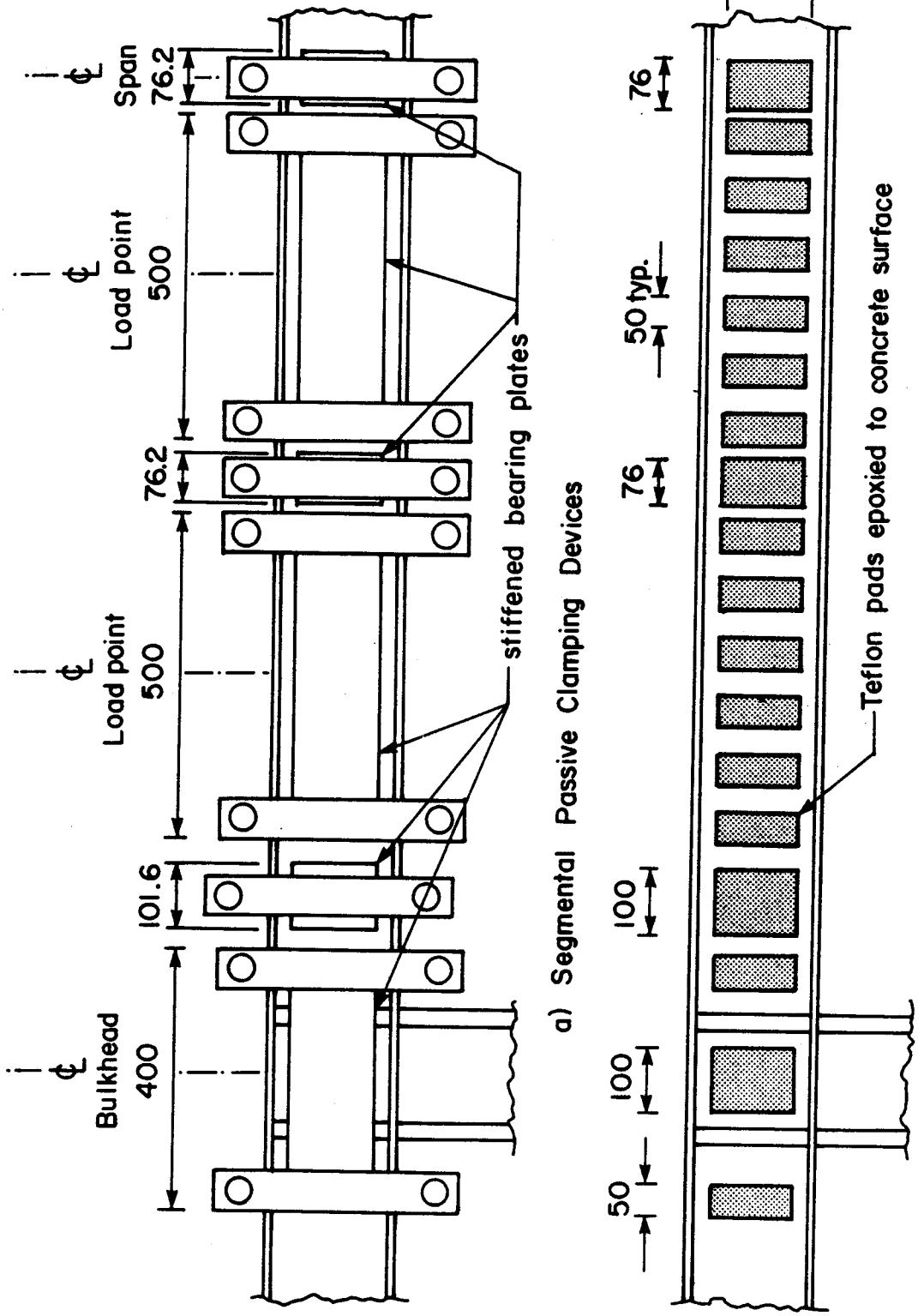

Figure 3.8 LATERAL CONFINEMENT SYSTEM

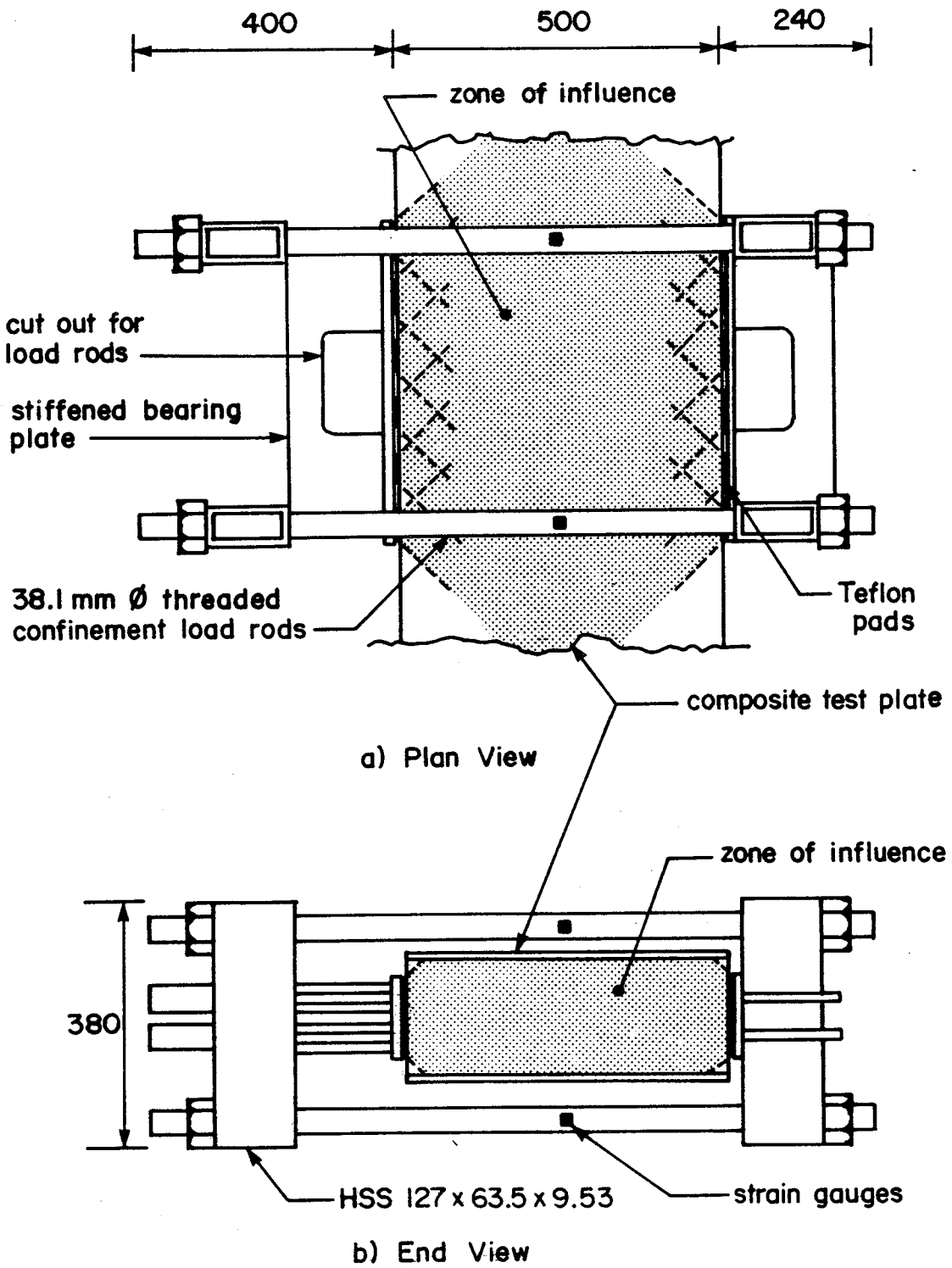

Figure 3.9 LATERAL CONFINEMENT SEGMENT

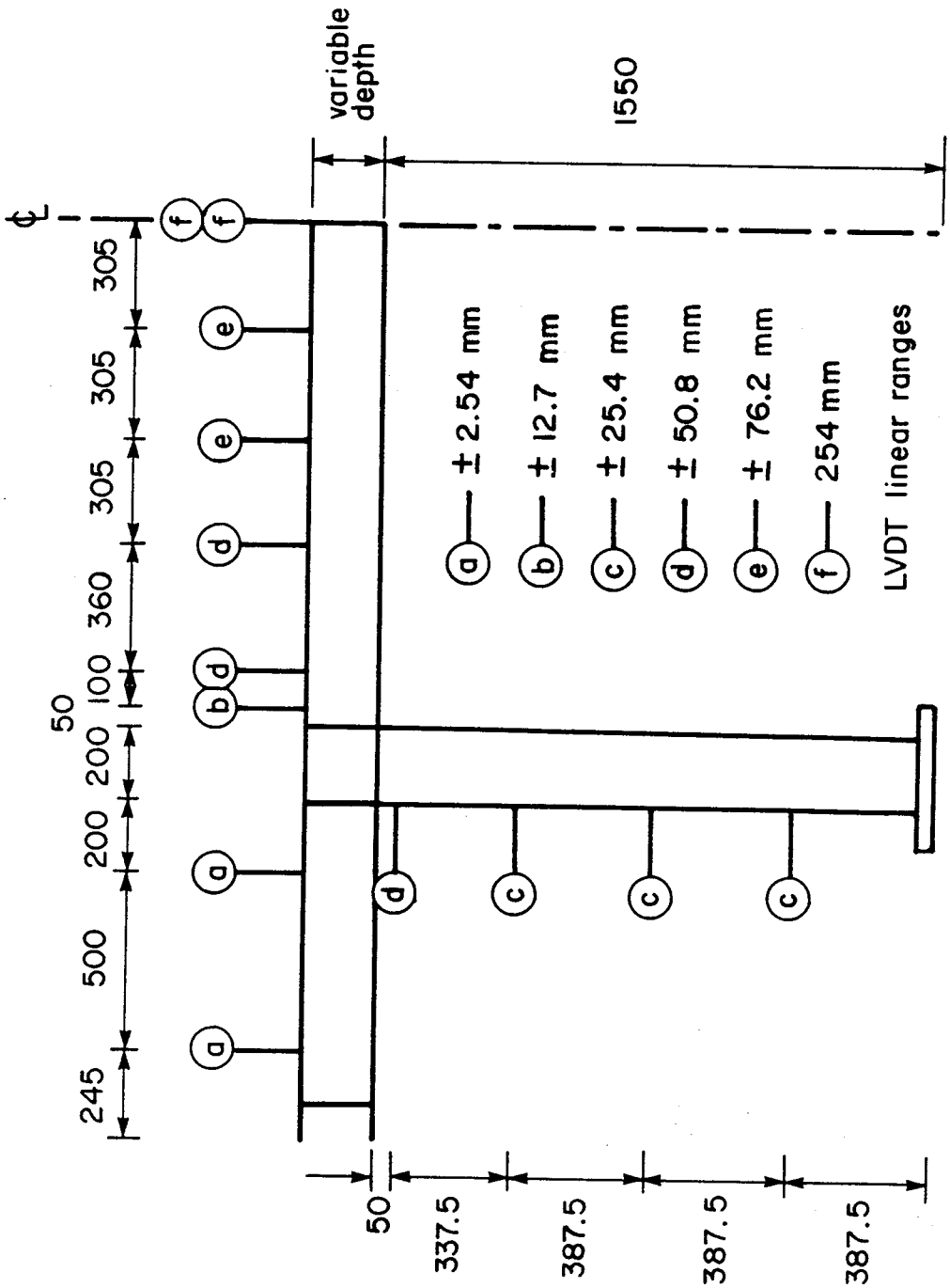

Figure 3.10 INSTRUMENTATION - LVDT'S TO MEASURE DEFLECTIONS

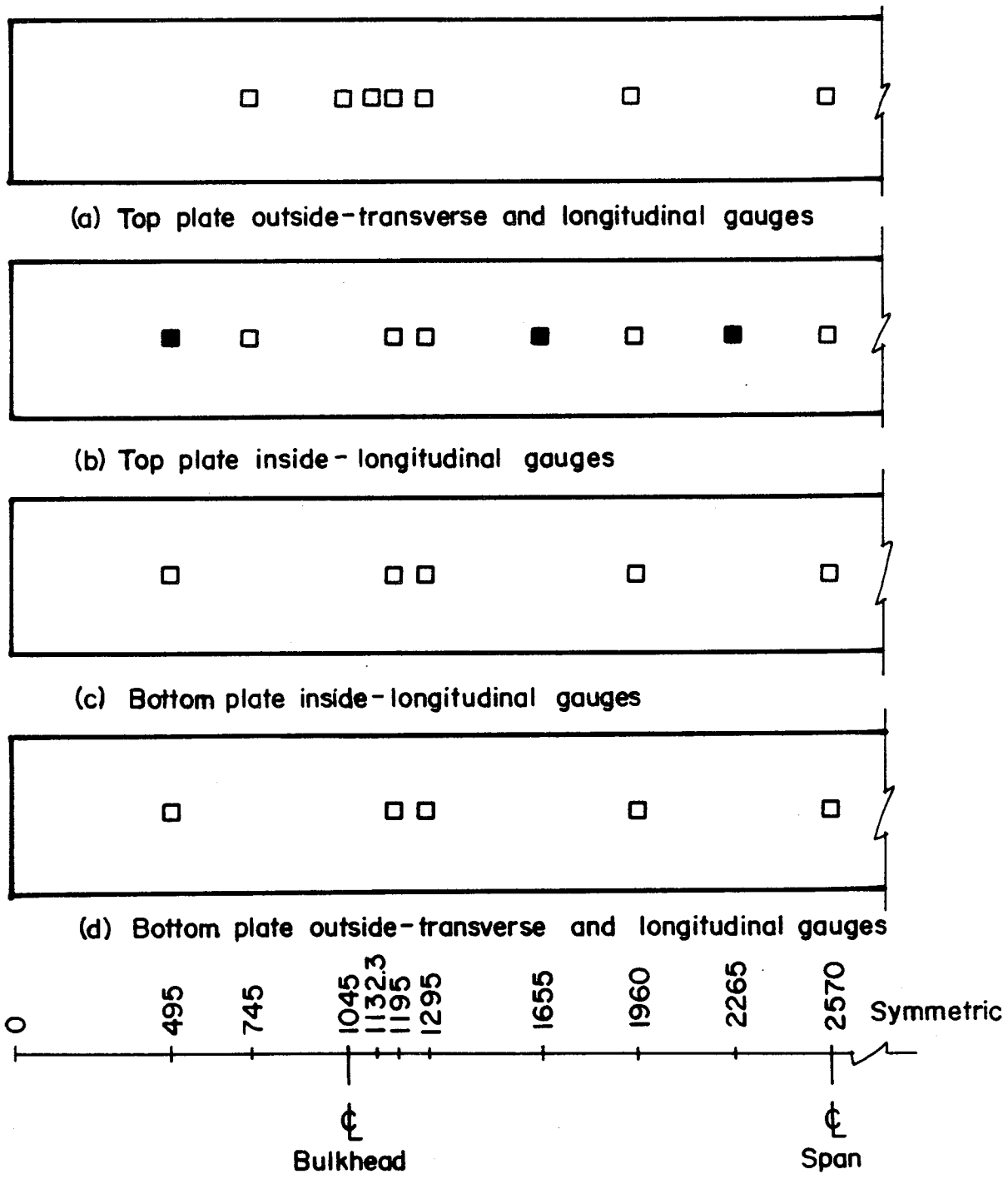

Notes 1. All dimensions are in mm.

2. □ Gauges located on both halves of the plate element

■ Gauges located on one half of the plate element

Figure 3.11 INSTRUMENTATION - STEEL STRAINS, PLATES

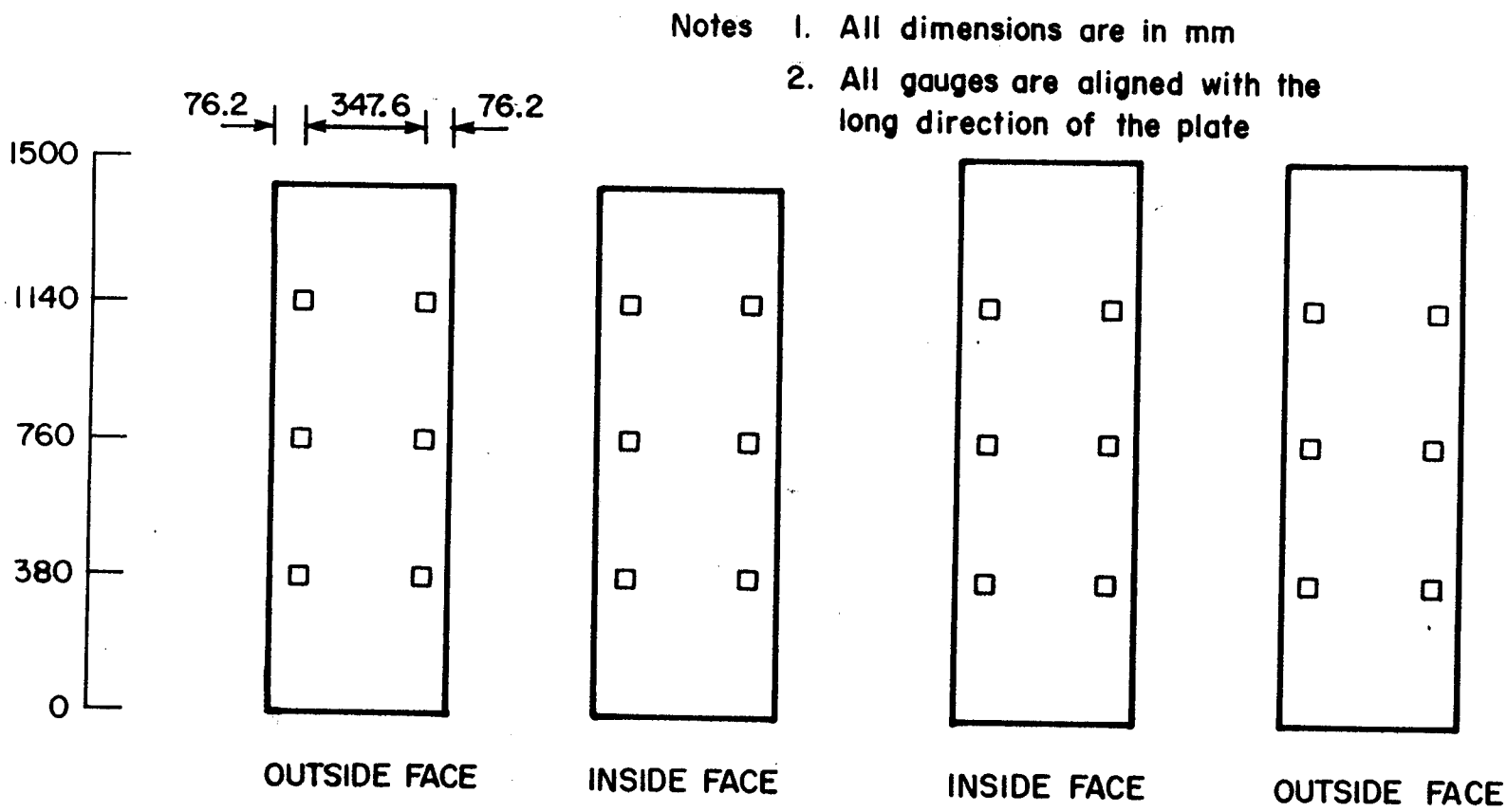

Figure 3.12 INSTRUMENTATION - STEEL STRAINS, BULKHEADS

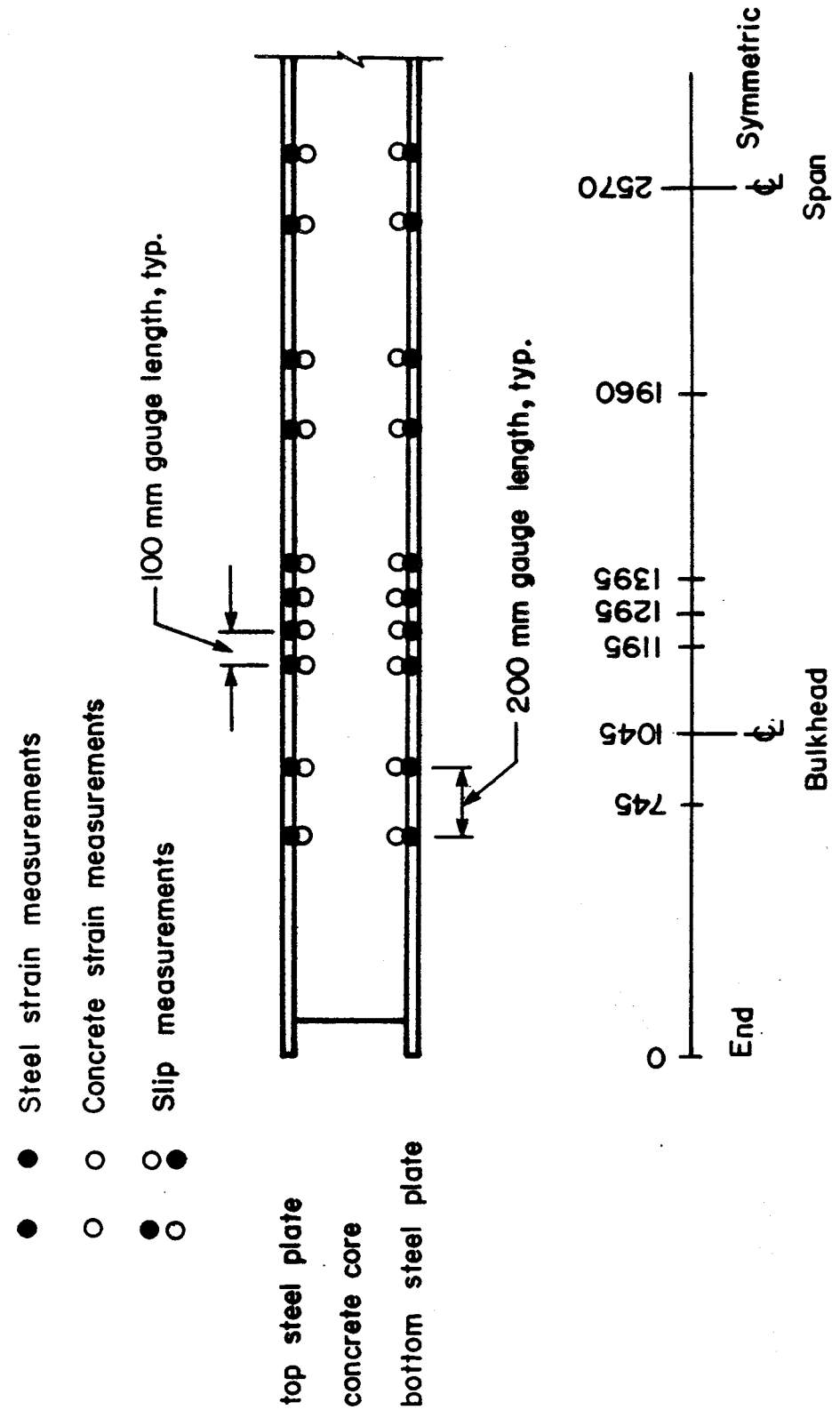

Figure 3.13 INSTRUMENTATION - CONCRETE STRAINS AND SLIP MEASUREMENTS

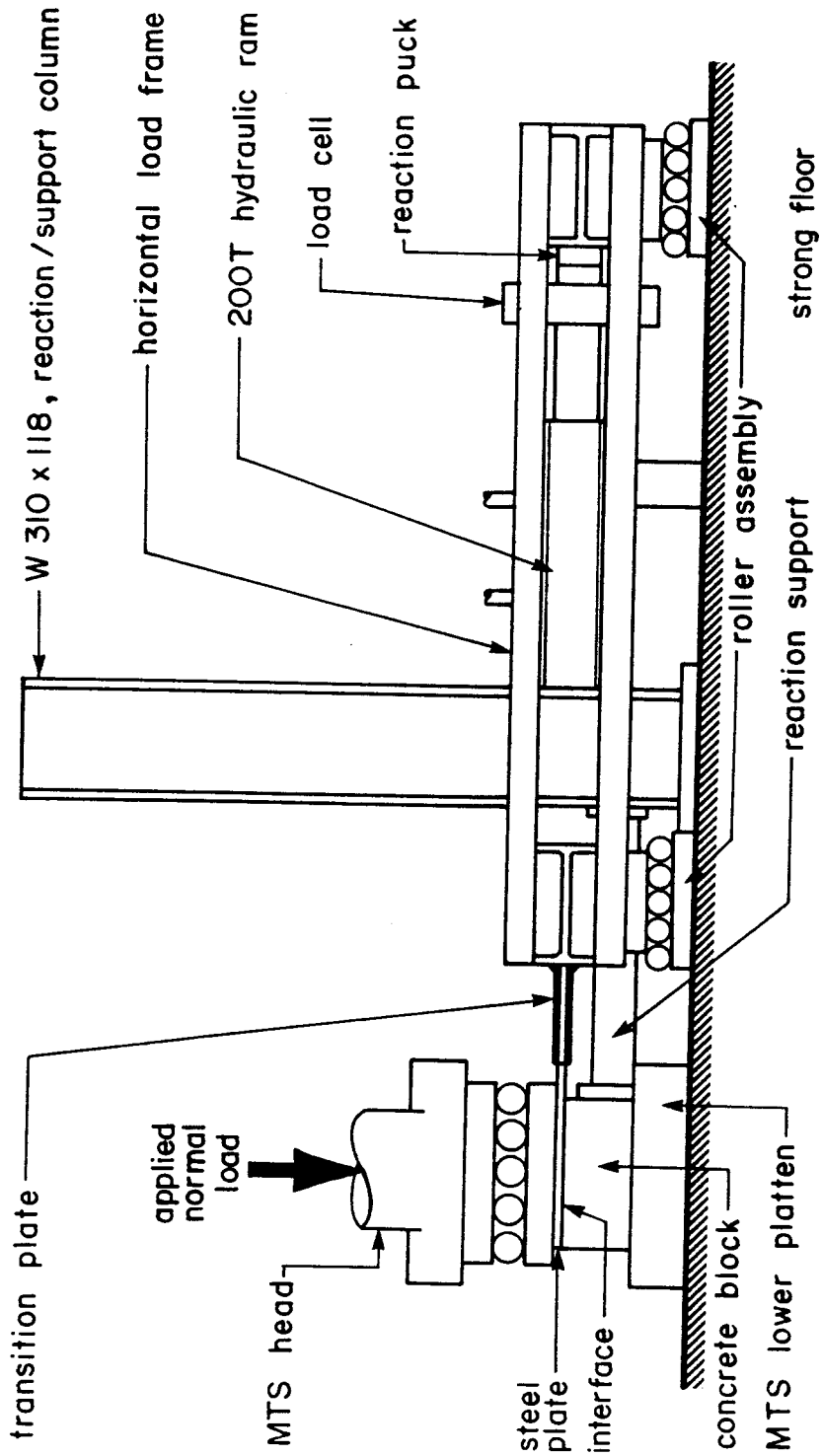

Figure 3.14 SCHEMATIC DIAGRAM OF TEST SET-UP FOR STEEL CONCRETE INTERFACE TEST

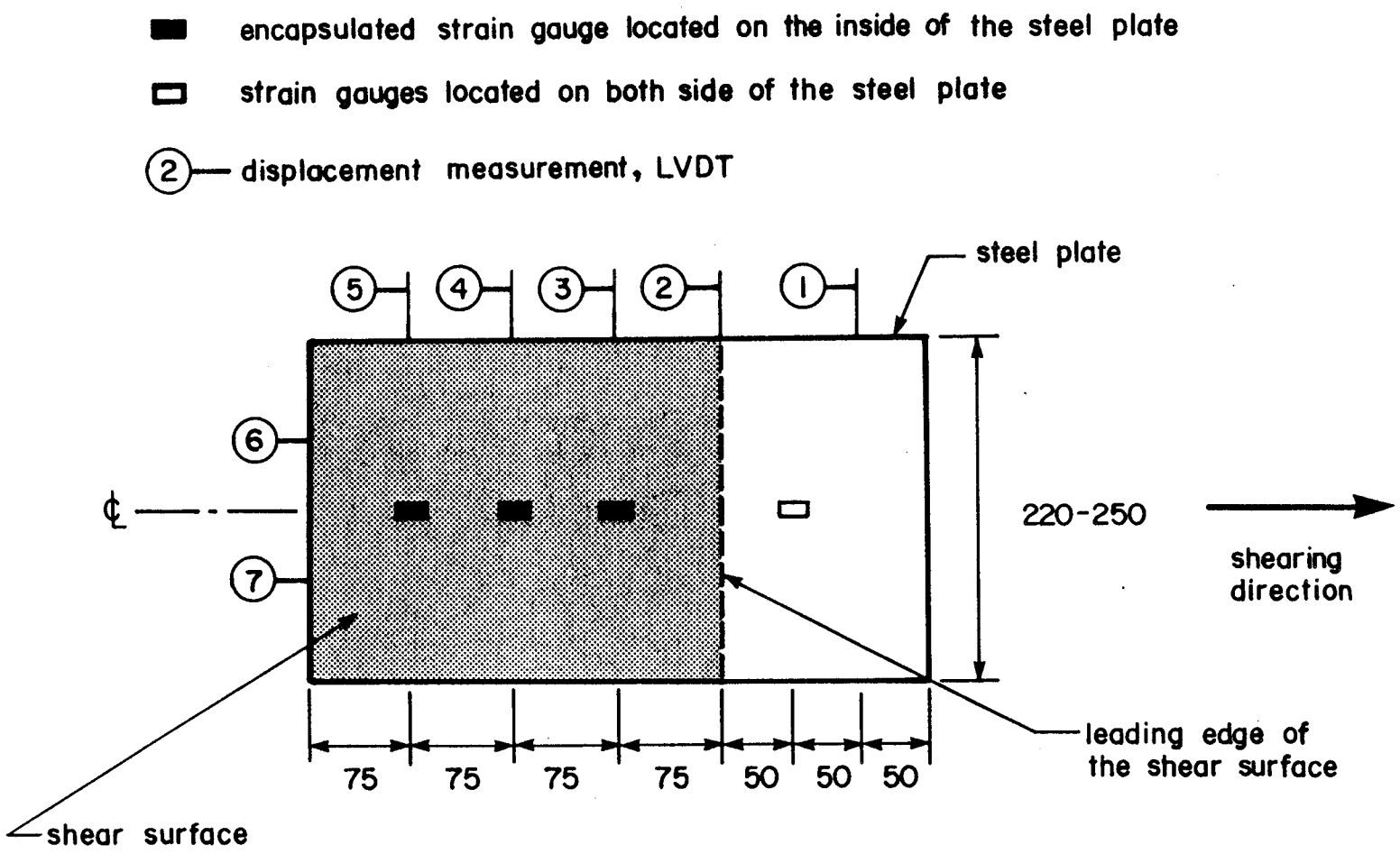

Figure 3.15 INSTRUMENTATION DIAGRAM - STEEL CONCRETE INTERFACE TEST

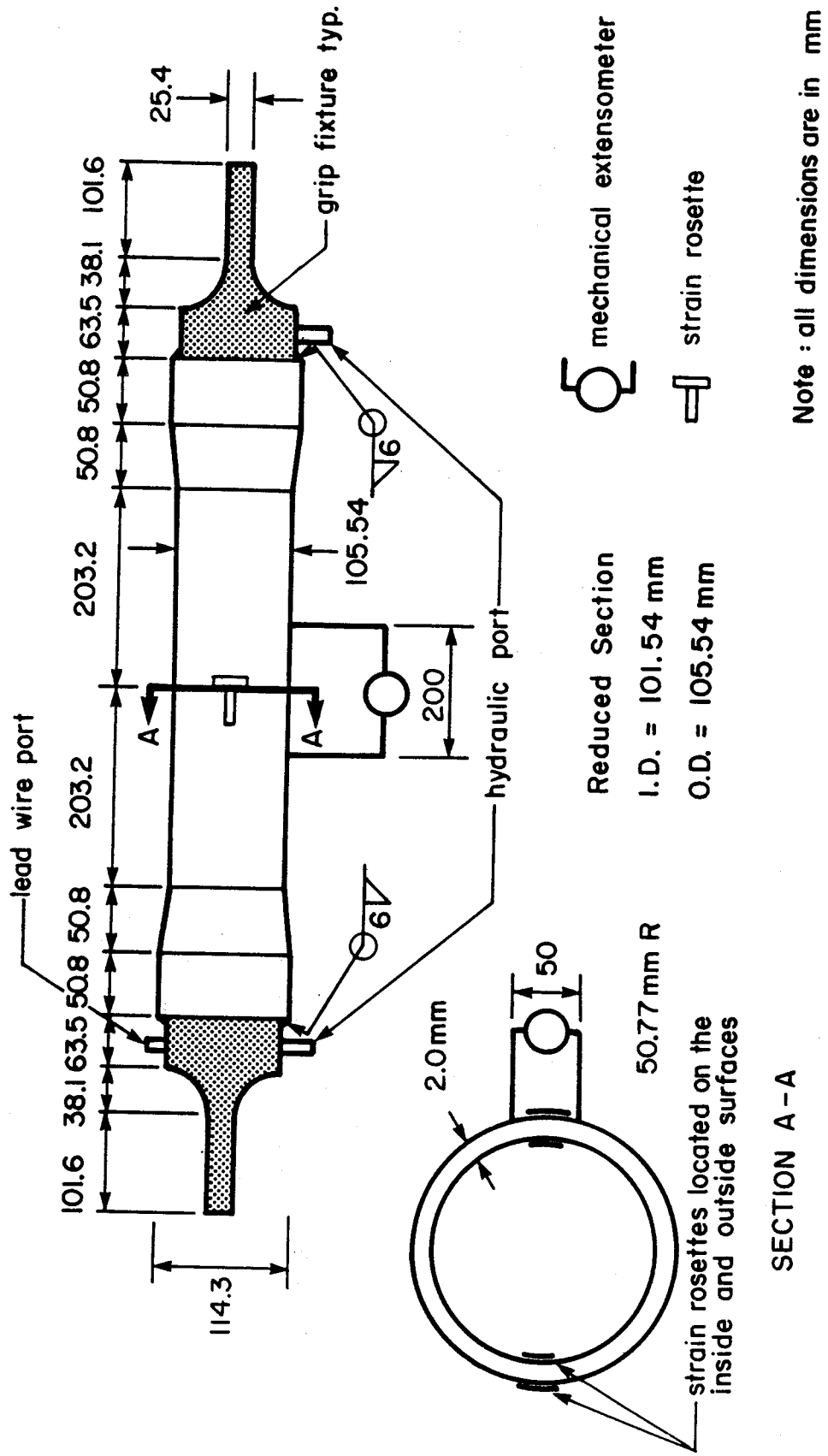

Figure 3.16 PLANE STRAIN TENSION SPECIMEN

4. MATERIAL PROPERTIES AND BEHAVIOUR

Ancillary tests were carried out on the steel plates and the concrete used in the tests to establish the uniaxial stress-strain characteristics of these materials. The internal forces and internal force distribution could then be determined from these stress-strain relationships and strains measured during the tests.

4.1 Steel Plates

4.1.1 General

Four different steel plates were used in the construction of the test specimens. With the exception of the 3.18 mm thick plate, which was non-structural steel, the chemical and mechanical properties reported on the mill certificate are given in Table 4.1 and 4.2, respectively.

The 25.4 mm thick test specimens were flame cut and the thinner plates were sheared from the parent plate such that the long direction of the specimen plate coincided with the rolling direction of the parent plate. This orientation will be referred to as the longitudinal direction. Coupons and shear test specimen plates were flame cut from the test plates in the laboratory so that the orientation of the specimens was known.

4.1.2 Stress-Strain Relationships - Uniaxial Stress

Based on the characteristic parameters of the stress-strain curves as determined from tension coupon tests and as given in Tables 4.3, 4.6, 4.9 and 4.12, a series of mathematical expressions have been developed to describe the stress-strain curves. The general expression takes the form:

$$[4.1] \quad \sigma = A + B\epsilon + C\epsilon^{1/2} + D\epsilon^{1/3} + E\epsilon^{1/4} + F\epsilon^{1/5} + G\epsilon^{1/6}$$

where: σ = Stress, MPa
ϵ = Strain, mm/mm
A,B,C,D,E,F,G = Coefficients

Some of the coefficients A to G may be zero for various ranges of strain. The strain ranges and corresponding coefficients for the 6.35 mm (1/4 inch), 4.76 mm (3/16 inch), 3.18 mm (1/8 inch), and 25.4 mm (1 inch) thick plates for both the longitudinal and transverse directions are given in Tables 4.4, 4.5, 4.7, 4.8, 4.10, 4.11, 4.13 and 4.14, respectively. The stress-strain curves given by these expressions, for both directions and for each plate, are found in Figures 4.1 and 4.2. For all practical purposes they coincide with the mean experimental curves for each direction of each plate thickness.

The elastic values for Poisson's ratio, ν, were determined experimentally for each plate and are given in Tables 4.3, 4.6, 4.9 and 4.12. Inelastic values for Poisson's ratio, based on Stang et al. (1946), are given by:

$$[4.2] \qquad \nu_p = \frac{1 - \sqrt{\frac{1 + \delta}{1 + \epsilon_x}}}{\epsilon_x} \quad \text{for } \epsilon_x > \epsilon_y$$

where: ϵ_x = Maximum principal strain, mm/mm

ϵ_y = Yield strain, mm/mm

δ = Dilatation associated with the volume change that occurs during the elastic straining

$\delta = \epsilon_y(1 - 2\nu)$

in which, ν = Elastic value for Poisson's Ratio

4.1.3 Uniaxial Stress - Plane Strain

The stress-strain curves and the characteristic material properties of the tension coupons and the cylindrical specimen tested in a state of uniaxial stress showed little variance one from the other. Therefore, the comparison of the behaviour between a steel subjected to a state of uniaxial stress and a state of plane strain was based on the data from the cylinder tests only. The data are summarized in Table 4.15. Tabulated true stress-strain data and octahedral shear stress shear strain data as derived in Section 4.1.4.2 are given. The data is shown graphically in Figure 4.3 where the octahedral shear stress is plotted versus the octahedral shear strain. The following observations were made:

1. the octahedral shear stress octahedral shear strain curves lie close together regardless of the state of stress;

2. the maximum octahedral shear stress, τ_{oct}, is an invariant of the state of stress and is approximately constant at rupture;

3. the energy of local plastic distortion per unit volume, the area under the octahedral shear stress shear strain curve, and a measure of ductility, is given by

[4.3] $$W = \int_0^{\gamma_{oct}} \tau_{oct} \, d\, \gamma_{oct}$$

where: τ_{oct} = Octahedral shear stress
γ_{oct} = Octahedral shearing strain

and decreases with an increase in the ratio of transverse to longitudinal stress. For this particular case, the ratio of W for plane strain to uniaxial stress was 0.834 and 0.761 for cylinder tests 2 and 3, respectively, with a mean value of 0.80.

4. the ratio of the true transverse to longitudinal stress given by

[4.4] $$n = \sigma_2/\sigma_1$$

was constant in the elastic region at a value of 0.29 and increased up to a value of 0.5 at rupture for the plane strain cylinder tests, as can be determined from the stress path shown in Figure 4.4. As would be expected for a plane strain condition, the slope of the stress path $d\sigma_3/d\sigma_1$ throughout the elastic range (up to the yield locus) is identically equal to Poisson's Ratio ($\sigma_z=\nu\sigma_x$). This relationship is also observed to hold true in the inelastic region with $\sigma_z=\nu_p\sigma_x$.

The first three observations confirm those made by other researchers such as Ludwik (1928), Taylor and Quinney (1931) and Davis (1945; 1948).

4.1.4 Transformation Model

Based on the above observations a transformation model was developed to transform uniaxial stress-strain curves to plane strain stress-strain curves. The transformed plane strain stress-strain curve was then used to interpret strain measurements recorded in areas of the plates where a plane strain stress state existed.

Transformation functions were defined for the elastic and plastic regions of behaviour using Hooke's Law and the von Mises-Huber-Hencky yield criterion, respectively. The elastic limit was defined as the intersection of these two theories at the transformed yield point. The plastic limit or ultimate strain was determined using a reduced strain energy for the state of plane strain in conjunction with the transformed stress-strain curve.

4.1.4.1 Elastic Region

The generalized form of Hooke's Law for a three dimensional state of stress gives equations:

$$[4.5a] \qquad \epsilon_x = \frac{1}{E}(\sigma_x - \nu\sigma_y - \nu\sigma_z)$$

$$[4.5b] \qquad \epsilon_y = \frac{1}{E}(-\nu\sigma_x + \sigma_y - \nu\sigma_z)$$

$$[4.5c] \qquad \epsilon_z = \frac{1}{E}(-\nu\sigma_x - \nu\sigma_y + \sigma_z)$$

which can be simplified to give the stress as a function of strain in the x-direction (taken to be the direction along the length of the member and parallel to the in-plane load) for both the uniaxial stress and the plane strain case. The simplification for the uniaxial stress case when σ_y and σ_z are set equal to zero and for the plane strain case when σ_y and ϵ_z are set equal to zero yields Equations 4.6 and 4.7, respectively.

$$[4.6] \qquad \sigma_{xus} = E\,\epsilon_x$$

$$[4.7] \qquad \sigma_{xps} = \frac{E\epsilon_x}{(1-\nu^2)}$$

The ratio of the normal stresses for the two cases gives

$$[4.8] \qquad \frac{\sigma_{xps}}{\sigma_{xus}} = \frac{1}{(1-\nu^2)}$$

where the transformation function for the elastic region is $1/(1-\nu^2)$ and ν is equal to the elastic value of Poisson's ratio. The stress for the plane strain condition becomes

$$[4.9] \qquad \sigma_{xps} = \frac{1}{(1-\nu^2)}\,\sigma_{xus}$$

for any given value of ϵ_x. The steel behaves as being apparently stiffer than the uniaxial stress case. This transformation function is valid up to the point of yielding.

4.1.4.2 Plastic Region

The von Mises-Huber-Hencky yield criterion, "Theory of Constant Elastic Strain Energy of Distortion", Nadai (1950),

$$[4.10] \qquad 2Y^2 = (\sigma_1-\sigma_2)^2 + (\sigma_2-\sigma_3)^2 + (\sigma_3-\sigma_1)^2$$

and shown graphically in Figure 4.4, was used to describe the relationship of principal stresses in the plastic region. The data in Figure 4.4 and the experimental evidence of Ludwik (1928), Taylor and Quinney (1931), and Davis (1945; 1948) support the use of this criterion at both the yield and ultimate stress. Although the plastic distortion per unit volume, W, given by Equation 4.3, varies with changing states of stress, the relationship between the octahedral shear stress, τ_{oct}, given by Equation 4.11, and the octahedral shear strain, γ_{oct}, given by Equation 4.12, seem to be unique and independent of the state of stress as shown in Figure 4.3.

$$[4.11] \qquad \tau_{oct} = \frac{1}{3}\sqrt{(\sigma_x-\sigma_y)^2+(\sigma_y-\sigma_z)^2+(\sigma_z-\sigma_x)^2}$$

where: σ_x, σ_y, σ_z = principal stresses

$$[4.12] \qquad \gamma_{oct} = \frac{2}{3}\sqrt{(\epsilon_x-\epsilon_y)^2+(\epsilon_y-\epsilon_z)^2+(\epsilon_z-\epsilon_x)^2}$$

where: ϵ_x, ϵ_y, ϵ_z = principal strains

The post-yield transformations require transformations for both stress and strain.

For stress, the transformation function is obtained by equating τ_{oct} expressed in terms of σ_x for uniaxial stress

$$[4.13] \qquad \tau_{oct} = \frac{\sqrt{2}}{3} \sigma_{xus}$$

with τ_{oct} expressed in terms of σ_x for the plane strain condition.

$$[4.14] \qquad \tau_{oct} = \frac{\sqrt{2}}{3} \sqrt{(1 - \nu_p + \nu_p^2)}\, \sigma_{xps}$$

The transformation becomes:

$$[4.15] \qquad \sigma_{xps} = \frac{1}{\sqrt{1 - \nu_p + \nu_p^2}} \sigma_{xus}$$

where: ν = Plastic value for Poisson's Ratio, ν_p

The values of ν_p determined from the uniaxial stress test (cylinder 1), Stang's equation (Equation 4.2), and the ratio of principal stresses σ_z/σ_x taken from the plane strain cylinder tests for strains less than 0.01 all agree closely, as shown in Figure 4.5. Stang's equation can be used to provide a smooth transition for ν_p between the elastic value and the value calculated at a strain of 0.01, where ν_p=0.455. Subsequently, Stang's equation deviates from test

values of ν_p and σ_z/σ_x, and a straight line approximation of ν_p was used for strains between 0.01 and ϵ_u to give values of ν_p between 0.455 and 0.50.

Similarly, for strain, the transformation function is obtained by equating γ_{oct} expressed in terms of ϵ_x for uniaxial stress

$$[4.16] \qquad \gamma_{oct} = \frac{2\sqrt{2}}{3} \sqrt{(1 + \nu_p^2)}\ \epsilon_{xus}$$

with γ_{oct} expressed in terms of ϵ_x for the plane strain condition.

$$[4.17] \qquad \gamma_{oct} = \frac{2\sqrt{2}}{3} \sqrt{1 - a + a^2}\ \epsilon_{xps}$$

The transformation becomes:

$$[4.18] \qquad \epsilon_{xps} = \sqrt{\frac{(1+\nu_p^2)}{(1-a+a^2)}}\ \epsilon_{xus}$$

where: $a = \frac{\epsilon_{yps}}{\epsilon_{xps}}$, the ratio of strains for a plane strain state of stress.

If the material in a plane strain state of stress is behaving elastically, the ratio of $\epsilon_{yps}/\epsilon_{xps}$, is by Hooke's Law,

$$[4.19] \qquad a = \frac{-\nu}{1 - \nu}$$

and for ν=0.29, Equation 4.19 gives a=-0.41 as found by cylinder tests 2 and 3.

For the fully plastic case of zero volume change, a=-1 and if Equation 4.19 were to be satisfied then the inelastic value of Poisson's ratio, ν_p=0.5 would have to be used. This is in agreement with Equation 4.19. Therefore, it appears reasonable to use Equation 4.18 as the transformation function with a determined from Equation 4.19 (as a function of ν_p) for the plastic region.

4.1.4.3 Yield Point

Because yielding is suppressed for plane strain, Hooke's Law can be used up to the point where the yield stress is described by the yield criterion, a transformed stress equal to $1/\sqrt{1-\nu+\nu^2}\ \sigma_y$. This corresponds to a strain of $(1-\nu^2)/\sqrt{1-\nu+\nu^2}\ \epsilon_y$ (ϵ_y - yield strain). The transformation equations developed for the plastic region can also be used to determine this point.

4.1.4.4 Reduced Ductility

The ratio of energy of local plastic distortion per unit volume for plane strain to uniaxial stress gives a measure of the reduced ductility. The maximum uniaxial strain in the x-direction at rupture for plane strain was determined such that the area under the transformed stress-strain curve was equal to the ratio of W_{ps}/W_{us} times the area under the uniaxial stress-strain curve.

4.1.5 Stress-Strain Relationships - Plane Strain

The uniaxial stress-strain curves for each of the steel plates used for the composite plate test specimens were transformed to plane strain stress-strain curves for the x-direction with the transformation model described in Section 4.1.4. The coefficients used to describe the transformed curves for the 6.35 mm (1/4 inch), 4.76 mm (3/16 inch), and 3.175 mm (1/8 inch) plates are given in Tables 4.16, 4.17 and 4.18, respectively. The uniaxial stress-strain curve and the corresponding transformed plane strain stress-strain curve described by the functions given in Tables 4.4 and 4.16, respectively, are shown in Figure 4.6 for the 6.35 mm (1/4") plate.

4.2 Concrete

4.2.1 General

Thirty MPa normal weight concrete, with five percent air entrainment, Type 10 cement, 15 mm maximum size aggregate, and a 100 mm slump was specified for the concrete mix.

The two batches of ready mix concrete required for the test specimens were supplied by Independent Transit Mix Ltd. Edmonton, and had the mix design given in Table 4.19. Cylinders 1 to 20, modulus of rupture beams marked 1 and 2, all shear specimens and bulkheads, and plate element C121T6 were cast from the first batch of concrete. Cylinders 21 to

50, modulus of rupture beams 3 to 6, and the remaining plate elements were cast from the second batch of concrete.

Slumps of 95 and 85 mm were obtained from concrete samples taken from the middle portions of batches 1 and 2, respectively. Pencil vibrators were used to consolidate the concrete in the specimens.

The schedule for testing of the concrete cylinders and modulus of rupture beams is given in Table 4.20.

The density of the concrete was determined from weight and volume measurements made on the concrete cylinders. Based on 20 cylinders from batch 1 and 30 cylinders from batch 2, the density was found to be 2300 kg/m^3 and 2275 kg/m^3, respectively.

4.2.2 Properties of Concrete in Compression

The characteristic material properties as determined from standard compression tests are given in Table 4.21.

The two least-squares-best-fit third degree polynomials were derived to express the uniaxial compressive strength of the concrete as a function of time in days,t, for concrete batches 1 and 2, are respectively.

$$[4.20] \qquad f'_c = 24.088+0.6305t-0.0065916t^2+0.000023316t^3$$

$$[4.21] \qquad f'_c = 24.276+0.8549t-0.0097186t^2+0.000038499t^3$$

These equations, along with the corresponding data, are

shown in Figure 4.7. The strengths predicted by these expressions are only valid for the age of concrete during the test period, 7 to 83 days.

Although there was some scatter in the variation of ultimate strain, as no correlation was found with strain rate or age of concrete, the mean values were used in any subsequent analysis. For batches 1 and 2 the mean values for the ultimate strain are 0.002430 and 0.002435, with coefficients of variation of 0.0683 and 0.0620, respectively. For each cylinder the stress-strain data were evaluated according to the standard CSA A23.2-9C (1977) to determine the modulus of elasticity in compression. The modulus was calculated by dividing the difference between the stress at 40% of the ultimate load and the stress at 0.005% strain by the corresponding difference in strain values. These data were fitted with expressions similar to those for the compressive strength and are given by equations 4.22 and 4.23 for batches 1 and 2, respectively.

$$[4.22] \qquad E_c = 19137.0 + 212.05t - 2.5589t^2 + 0.010647t^3$$

$$[4.23] \qquad E_c = 18918.3 + 259.06t - 3.1359t^2 + 0.0130535t^3$$

These equations along with the corresponding data are shown in Figure 4.8.

4.2.3 Properties of Concrete in Tension

Because the number of split cylinder tests and modulus of rupture tests was small and owing to the scatter of results obtained by other researchers, the maximum tensile strength was set equal to the modulus of rupture as defined by Clause 9.5.2.3 of CAN3-A23.3-M84(1984). Although conclusive statements cannot be made, experimental values are comparable with this definition of strength.

4.2.4 Stress-Strain Relationships

4.2.4.1 Compressive Stress-Strain Relationships

Based on load deformation measurements for twenty standard compression cylinder tests for batch 1 and twenty-five for batch 2, unit or dimensionless stress-strain curves for uniaxial compression were developed for the two batches and are:

$$[4.24] \quad \frac{f_c}{f'_c} = 0.0124+1.4521\left[\frac{\epsilon}{\epsilon_o}\right]-0.0844\left[\frac{\epsilon}{\epsilon_o}\right]^2-0.3769\left[\frac{\epsilon}{\epsilon_o}\right]^3$$

$$[4.25] \quad \frac{f_c}{f'_c} = 0.0108+1.3265\left[\frac{\epsilon}{\epsilon_o}\right]+0.0154\left[\frac{\epsilon}{\epsilon_o}\right]^2-0.3491\left[\frac{\epsilon}{\epsilon_o}\right]^3$$

where: f'_c = Compressive strength as described in Section 4.2.2
f_c = Stress, MPa, corresponding to a strain, ϵ
ϵ = Concrete strain, mm/mm
ϵ_o = Ultimate strain, mm/mm, corresponding to the compressive strength, f'_c

The unit uniaxial compressive stress-strain curve for batch 1 is shown in Figure 4.9. Because measurements were

not made, the descending branch of the curve is assumed to be that described by the Todeschini et al. (1964), and is of the form,

$$[4.26] \qquad \frac{f_c}{f'_c} = \frac{2\,(\epsilon/\epsilon_o)}{1 + (\epsilon/\epsilon_o)^2}$$

4.2.4.2 Modified Compressive Stress Strain Relationships

Timoshenko and MacCullough (1949) reported tests conducted by A. Föppel which showed that the compression heads of a test machine influences the behaviour, strength and failure of compression specimens. Due to the development of sliding friction between the specimen and the load surfaces (compression heads), the lateral expansion associated with the compression of the specimen is prevented or significantly reduced, resulting in an altered state of stress at the ends of the specimen. Because of the relatively small aspect ratio, d/l = 2.0 for typical cylinders, the influence of boundary restraint may affect the entire cylinder. The concrete cylinder test as it is currently conducted is not representative of true uniaxial behaviour.

Consequently, a series of cylinders were tested in compression to examine the effects of end restraint. For three cylinders the end restraint was reduced by placing a thin layer of paraffin wax between the load surfaces of the test machine and the sulphur caps of the test cylinder. Typical compressive stress-strain curves for a cylinder with

and without the paraffin wax layer are shown in Figure 4.10. There was no appreciable difference between the behaviour of the cylinder tested with Teflon plates at the ends and the cylinder without.

The failure of the cylinder tested without paraffin wax is typically described as a shear cone failure (indicative of a modified stress field), whereas the cylinder tested with paraffin failed by tensile splitting into a series of longitudinal pie shaped segments at a transverse tensile strain around 0.00025. The longitudinal cracks and regularity (relatively constant cross-sectional area) of the pie shapes suggests that the effects of end restraint were greatly reduced. This experimental evidence corroborates the statements made by Mindess and Young (1981) that failure of concrete is controlled by a limiting tensile strain. The ultimate strength of cylinders tested with paraffin wax was approximately 67% of the average of the standard test. This failure load or stress level coincides with the development of matrix cracks in the traditional cylinder.

For the uniaxial behaviour, this evidence suggests that the maximum stress be limited to a stress corresponding to a maximum tensile strain in the transverse direction. This limit is shown in Figure 4.9 as a dashed line.

4.2.4.3 Tensile Stress-Strain Relationship

Based on the theory that failure occurs at some maximum tensile strain (250 μs), a maximum tensile strength as previously defined in Section 4.2.3 by the modulus of

rupture, and assuming an elastic-brittle stress-strain relationship for concrete in tension, the modulus of elasticity in tension was calculated to be 0.64 times the corresponding modulus of elasticity in compression. There is experimental evidence that shows that the moduli are different, and that the modulus of elasticity in tension is in some fraction of the modulus of elasticity in compression, Brattland (1987). The tensile stress-strain relationship as described is shown in Figure 4.9.

Table 4.1 CHEMICAL COMPOSITION OF STRUCTURAL STEEL PLATE

PLATE	GRADE	MANUFACTURER	HEAT NO.	CHEMICAL COMPOSITION, %						
				C	Mn	S	P	Si	Nb	V
480" x 96" x 1"	G40.21-M81 300W	S.A. Forges de Clabecq, Belgium	9958	0.082	1.351	0.017	0.024	0.356	0.020	0.004
480" x 96" x 1/4"	G40.21-M81 300W	Algoma Steel Corporation, Ltd.,Canada	5265J	0.17	0.98	0.006	0.010	0.22	-	-
480" x 96" x 3/16"	G40.21-M81 300W	S.A. Forges de Clabecq, Belgium	0391	0.080	1.356	0.020	0.022	0.267	0.25	0.003

Note: 1. Nominal plate dimensions are given in inches.

Table 4.2 MECHANICAL PROPERTIES FROM MILL CERTIFICATE

PLATE[1]	YIELD POINT MPa	ULTIMATE TENSILE STRENGTH MPa	ELONGATION %
480" x 96" x 1"	381	501	30
480" x 96" x 1/4"	371	496	21
480" x 96" x 3/16"	404	511	21

Notes: 1. Elongation was measured over a 200 mm gauge length.
2. Nominal plate dimensions are given in inches.

Table 4.3 CHARACTERISTIC PARAMETERS DETERMINED FROM UNIAXIAL STRESS STRAIN CURVES FOR THE 6.35 mm (1/4 in.) PLATES IN THE LONGITUDINAL AND TRANSVERSE DIRECTIONS

COUPON NO.	E MPa	ϵ_y $\times 10^{-6}$	σ_{yu} MPa	σ_{yl} MPa	σ_{sy} MPa	ϵ_{st} $\times 10^{-6}$	E_{st} MPa	ϵ_u $\times 10^{-6}$	σ_u MPa	ϵ_f $\times 10^{-6}$	σ_f MPa
LONGITUDINAL DIRECTION											
125.1	208000	1692	353.0	353.3	348.2	26000	3070	170600	478.7	244500	402.3
125.2	210000	1738	361.3	348.5	343.2	27040	5570	181070	476.0	240100	435.5
125.3	205900	1796	349.1	346.3	340.2	29700	4200	179630	472.6	251750	404.0
125.4	204100	1848	371.6	348.2	341.4	29400	4070	182500	471.8	258300	417.4
125.5	208800	1551	348.4	343.0	333.0	27480	3440	171200	472.5	262600	414.5
$\bar{x}$	207400	1725	356.7	347.9	341.2	27920	4070	177000	474.3	251450	414.7
TRANSVERSE DIRECTION											
225.1	211100	1743	374.4	363.1	356.8	27870	3540	-[1]	-[1]	-[1]	-[1]
225.2	215100	1680	375.1	363.2	354.6	26890	3330	174500	476.5	267000	468.0
225.3	217000	1700	376.6	355.3	354.2	27800	2440	170800	489.0	257700	435.0
225.4	208500	1837	374.4	358.7	353.3	32300	3360	171000	481.0	211000	464.1
225.5	211500	1875	370.5	351.3	347.9	26600	3040	189000	477.7	256500	445.2
$\bar{x}$	212600	1767	374.2	358.3	353.4	28300	3140	176300	481.0	248000	453.1

Notes: 1. Coupon No. 225.1 may have been loaded eccentrically due to an alignment problem. It fractured from one side, therefore the data has been omitted.
2. The mean elastic values for Poisson's ratio in the longitudinal, and transverse directions are 0.293 and 0.288, respectively.

Table 4.4 COEFFICIENTS TO DESCRIBE THE UNIAXIAL STRESS STRAIN CURVE FOR THE 6.35 mm (1/4 in.) PLATE IN THE LONGITUDINAL DIRECTION

COEFFICIENTS	STRAIN RANGE $\times 10^{-6}$ mm/mm			
	0-1725	1725-27920	27920-177000	177000-262600
A	-	347.9	-	-
B	207400	-	-330107.1	3682896.9
C	-	-	7220568.0	-54796464.3
D	-	-	-47040804.1	214634409.5
E	-	-	119023817.5	-298279025.7
F	-	-	-127056475.9	134829748.1
G	-	-	48172784.3	-

Notes: 1. $\sigma = A + B\epsilon + C\epsilon^{1/2} + D\epsilon^{1/3} + E\epsilon^{1/4} + F\epsilon^{1/5} + G\epsilon^{1/6}$

2. 6.35 mm (1/4 inch) plate material - test plate elements C121T6, C152T6, C203T6.

Table 4.5 COEFFICIENTS TO DESCRIBE THE UNIAXIAL STRESS STRAIN CURVE FOR THE 6.35 mm (1/4 in.) PLATE IN THE TRANSVERSE DIRECTION

COEFFICIENTS	STRAIN RANGE $\times 10^{-6}$ mm/mm			
	0-1767	1767-28300	28300-176300	176300-248000
A	-	358.3	-	-
B	212600	-	-379875.0	-7232360.2
C	-	-	8435909.6	102864384.2
D	-	-	-55291055.0	-397303307.4
E	-	-	140359993.9	548362670.8
F	-	-	-150143901.0	-246865700.9
G	-	-	57007540.9	-

NOTE: 1. $\sigma = A + B\epsilon + C\epsilon^{1/2} + D\epsilon^{1/3} + E\epsilon^{1/4} + F\epsilon^{1/5} + G\epsilon^{1/6}$
2. 6.35 mm (1/4) inch plate material - test plate elements C121T6, C152T6, C203T6.

Table 4.6 CHARACTERISTIC PARAMETERS DETERMINED FROM UNIAXIAL STRESS STRAIN CURVES FOR THE 4.76 mm (3/16 in.) PLATES IN THE LONGITUDINAL AND TRANSVERSE DIRECTIONS

COUPON NO.	E MPa	ϵ_y x10^{-6}	σ_{yu} MPa	σ_{yl} MPa	σ_{sy} MPa	ϵ_{st} x10^{-6}	E_{st} MPa	ϵ_u x10^{-6}	σ_u MPa	ϵ_f x10^{-6}	σ_f MPa
					LONGITUDINAL DIRECTION						
11875.1	203000	1894	363.1	348.3	336.9	26600	2420	169700	462.4	243100	424.0
11875.2	202100	1948	367.4	353.7	342.1	23200	2750	185500	468.1	257500	411.3
11875.3	203900	1922	367.9	359.0	344.0	22000	3280	181700	467.5	223700	445.1
11875.4	201600	1989	378.6	361.0	345.3	25100	4400	153300	465.7	222200	429.1
11875.5	204100	2064	366.0	363.1	343.6	25700	4000	170200	467.4	225200	422.5
$\bar{x}$	202900	1974	368.6	357.0	342.4	24520	3370	172080	466.2	234340	426.4
					TRANSVERSE DIRECTION						
21875.1	207500	1856	386.9	368.9	360.4	26050	3740	190800	472.5	288600	446.0
21875.2	206800	1933	392.2	368.9	358.5	25500	2790	180000	474.1	242000	449.6
21875.3	206900	1955	403.1	372.1	361.5	25300	2000	186500	476.1	255900	435.0
21875.4	207000	1969	391.6	371.4	360.5	28100	2570	182300	478.8	250300	429.3
21875.5	208800	2003	399.3	376.7	364.8	30400	4530	183500	477.1	252000	434.9
$\bar{x}$	207400	1943	394.6	371.6	361.1	27070	3130	184620	475.7	257760	439.0

Note: 1. The mean elastic values for Poisson's ratio in the longitudinal, and transverse directions are 0.280 and 0.286, respectively.

Table 4.7 COEFFICIENTS TO DESCRIBE THE UNIAXIAL STRESS STRAIN CURVE FOR THE 4.76 mm (3/16 in.) PLATE IN THE LONGITUDINAL DIRECTION

COEFFICIENTS	STRAIN RANGE $\times 10^{-6}$ mm/mm			
	0-1974	1974-24520	24520-172080	172080-234340
A	-	357.0	-	-
B	202900	-	-91288.6	-2324415.8
C	-	-	1990686.7	31218043.3
D	-	-	-12927469.6	-118313703.7
E	-	-	32632476.4	161759923.0
F	-	-	-34776462.4	-72409452.9
G	-	-	13169596.7	-

Notes: 1. $\sigma = A + B\epsilon + C\epsilon^{1/2} + D\epsilon^{1/3} + E\epsilon^{1/4} + F\epsilon^{1/5} + G\epsilon^{1/6}$

2. 4.76 mm (3/16 inch) plate material - test plate element C152T4

Table 4.8 COEFFICIENTS TO DESCRIBE THE UNIAXIAL STRESS STRAIN CURVE FOR THE 4.76 mm (3/16 in.) PLATE IN THE TRANSVERSE DIRECTION

COEFFICIENTS	STRAIN RANGE $\times 10^{-6}$ mm/mm			
	0-1943	1943-27070	27070-184620	184620-257760
A	-	371.6	-	-
B	207400	-	-195694.8	403147.1
C	-	-	4149170.3	-7301373.9
D	-	-	-26742467.3	30209568.1
E	-	-	67298312.6	-43083660.7
F	-	-	-71606052.5	19771852.2
G	-	-	27090347.9	-

NOTE: 1. $\sigma = A + B\epsilon + C\epsilon^{1/2} + D\epsilon^{1/3} + E\epsilon^{1/4} + F\epsilon^{1/5} + G\epsilon^{1/6}$
2. 4.76 mm (3/16 inch) plate material - test plate element C152T4.

Table 4.9 CHARACTERISTIC PARAMETERS DETERMINED FROM UNIAXIAL STRESS STRAIN CURVES FOR THE 3.175 mm (1/8 in.) PLATES IN THE LONGITUDINAL AND TRANSVERSE DIRECTIONS

COUPON NO.	E MPa	ϵ_y $\times 10^{-6}$	σ_{yu} MPa	σ_{yl} MPa	σ_{sy} MPa	ϵ_{st} $\times 10^{-6}$	E_{st} MPa	ϵ_u $\times 10^{-6}$	σ_u MPa	ϵ_f $\times 10^{-6}$	σ_f MPa
LONGITUDINAL DIRECTION											
1125.1	201500	1199	239.9	225.7	214.3	17960	2270	170000	308.8	371800	288.0
1125.2	204600	1382	236.5	244.4	233.2	22800	1860	159600	321.4	357200	269.7
1125.3	203200	1293	229.7	217.3	210.9	10010	1760	163200	312.9	375900	286.1
1125.4[1]	-	-	-	-	-	-	-	-	-	-	-
1125.5	205100	1838	250.9	234.3	226.1	14150	2240	171200	317.7	350900	290.5
$\bar{x}$	203600	1428	239.3	230.4	221.1	16230	2030	166000	312.7	363950	283.6
TRANSVERSE DIRECTION											
2125.1	213600	1279	262.1	252.1	240.0	30100	3990	189400	315.5	385800	291.2
2125.2	211600	1339	253.0	243.3	230.6	21600	1860	171500	314.8	369500	286.0
2125.3	211100	1376	253.4	240.5	229.7	21500	2100	170500	312.6	379000	275.1
2125.4	203400	1380	252.7	238.9	227.7	21300	1780	158500	312.9	390500	306.2
2125.5	206700	1561	257.6	243.7	233.3	23400	2150	175400	311.3	386800	289.0
$\bar{x}$	209300	1387	255.8	243.7	232.3	23580	2380	173100	313.4	382320	289.5

Notes: 1. Coupon No. 1125.4 was omitted from the sample due to an accidental loading of that coupon.
2. The mean elastic values for Poisson's ratio in the longitudinal, and transverse direction are 0.277 and 0.285, respectively.

Table 4.10 COEFFICIENTS TO DESCRIBE THE UNIAXIAL STRESS STRAIN CURVE FOR THE 3.175 mm (1/8 in.) PLATE IN THE LONGITUDINAL DIRECTION

COEFFICIENTS	STRAIN RANGE $\times 10^{-6}$ mm/mm				
	0-1428	1428-16230	16230-166000	166000-285000	285000-363950
A	-	230.4	-	312.7	-
B	203600	-	-42990.3	-	-1109894.9
C	-	-	930016.0	-	18160809.8
D	-	-	-6010812.9	-	-73471640.1
E	-	-	15130565.0	-	103773907.9
F	-	-	-16095810.9	-	-47367185.1
G	-	-	6087996.5	-	-

Notes: 1. $\sigma = A + B\epsilon + C\epsilon^{1/2} + D\epsilon^{1/3} + E\epsilon^{1/4} + F\epsilon^{1/5} + G\epsilon^{1/6}$

2. 3.175 mm (1/8 inch) plate material - test plate element C152T3.

Table 4.11 COEFFICIENTS TO DESCRIBE THE UNIAXIAL STRESS STRAIN CURVE FOR THE 3.175 mm (1/8 in.) PLATE IN THE TRANSVERSE DIRECTION

COEFFICIENTS	STRAIN RANGE $\times 10^{-6}$ mm/mm				
	0-1387	1387-23580	23580-173100	173100-295700	295700-382320
A	-	243.7	-	313.4	-
B	209300	-	-41214.5	-	-7515437.5
C	-	-	836823.8	-	136627854.0
D	-	-	-5273653.4	-	-572787146.8
E	-	-	13095465.3	-	823665025.4
F	-	-	-13812625.4	-	-380045513.3
G	-	-	5194047.1	-	-

NOTE: 1. $\sigma = A + B\epsilon + C\epsilon^{1/2} + D\epsilon^{1/3} + E\epsilon^{1/4} + F\epsilon^{1/5} + G\epsilon^{1/6}$
2. 3.175 mm (1/8 inch) plate material - test plate element C152T3.

Table 4.12 CHARACTERISTIC PARAMETERS DETERMINED FROM UNIAXIAL STRESS STRAIN CURVES FOR THE BULKHEAD PLATES IN THE LONGITUDINAL AND TRANSVERSE DIRECTIONS

COUPON NO.	E MPa	ϵ_y x10^{-6}	σ_{yu} MPa	σ_{yl} MPa	σ_{sy} MPa	ϵ_{st} x10^{-6}	E_{st} MPa	ϵ_u x10^{-6}	σ_u MPa	ϵ_f x10^{-6}	σ_f MPa
					LONGITUDINAL DIRECTION						
1100.1	209700	1887	392.1	376.0	347.9	19800	2560	175000	494.6	287500	339.8
1100.2	209400	1858	391.6	371.7	343.8	19250	8200	167500	494.2	285000	345.5
1100.3	206500	1869	388.9	372.1	344.1	19880	7680	162500	495.1	285000	346.9
1100.4	211400	1836	390.4	372.6	343.3	19640	8010	172500	495.1	295000	334.9
1100.5	211300	2051	389.4	374.8	348.0	20940	10900	160000	495.9	287500	332.0
$\bar{x}$	209700	1900	389.4	373.4	345.4	19900	7470	167500	495.0	288000	339.8
					TRANSVERSE DIRECTION						
2100.1	214200	1811	406.7	384.1	350.6	19830	5010	152500	499.3	255000	395.4
2100.2	213800	1855	396.5	379.7	349.7	19860	6230	185000	497.2	274000	393.4
2100.3	214300	1847	393.6	377.9	346.7	20565	11540	177500	496.5	284000	383.1
2100.4	225800	1741	392.0	377.3	369.0	20550	8760	159000	497.9	286000	377.3
2100.5	212600	2032	391.1	376.5	343.3	19160	5830	169000	497.8	269000	397.4
$\bar{x}$	213700	1886	397.0	379.1	347.6	20000	7470	168600	497.7	273600	389.3

Notes: 1. Coupon No. 2100.4 was excluded from mean value evaluation because the values did not fit the group.
2. The mean elastic values for Poisson's ratio in the longitudinal, and tranverse directions are 0.285 and 0.274, respectively.

Table 4.13 COEFFICIENTS TO DESCRIBE THE UNIAXIAL STRESS STRAIN CURVE FOR THE 25.4 mm PLATE IN THE LONGITUDINAL DIRECTION

COEFFICIENTS	STRAIN RANGE $\times 10^{-6}$ mm/mm			
	0-1857	1857-19900	19900-167500	167500-288000
A	-	373.4	-	-
B	209700	-	409101.1	693361.6
C	-	-	-8479706.4	-34580240.7
D	-	-	54252824.4	287104131.0
E	-	-	-136090573.6	-817473467.0
F	-	-	144549805.6	935970418.9
G	-	-	-54625972.7	-371725785.7

Notes: 1. $\sigma = A + B\epsilon + C\epsilon^{1/2} + D\epsilon^{1/3} + E\epsilon^{1/4} + F\epsilon^{1/5} + G\epsilon^{1/6}$

2. 25.4 mm plate - bulkhead material

Table 4.14 COEFFICIENTS TO DESCRIBE THE UNIAXIAL STRESS STRAIN CURVE FOR THE 25.4 mm PLATE IN THE TRANSVERSE DIRECTION

COEFFICIENTS	STRAIN RANGE $\times 10^{-6}$ mm/mm			
	0-1858	1858-20000	20000-168600	168600-273600
A	-	379.1	-	-
B	213700	-	350769.0	-11939606.0
C	-	-	-7350250.1	42269926.0
D	-	-	47215550.4	-3267182560.0
E	-	-	-118685944.6	9024732460.0
F	-	-	126225076.2	-10106222587.0
G	-	-	-47742194.3	3993836285.0

NOTE: 1. $\sigma = A + B\epsilon + C\epsilon^{1/2} + D\epsilon^{1/3} + E\epsilon^{1/4} + F\epsilon^{1/5} + G\epsilon^{1/6}$
2. 25.4 mm plate - bulkhead material

Table 4.15 BIAXIAL STRESS, CYLINDER TEST DATA - SAE 1026 STEEL

NO.	FRACTURE DATA						MAX. SHEAR STRESS	OCTAHEDRAL SHEAR STRESS	SHEAR STRAIN	W MPa
	TRUE STRESS, MPa			TRUE STRAIN, mm/mm						
	σ_1	σ_2	σ_3	ϵ_1	ϵ_2	ϵ_3	τ_{max} MPa	τ_{oct} MPa	γ_{oct}	
1	614.3	0.0	0.0	0.072556	-0.037246	-0.037278	307.2	289.6	0.097332	26.1
2	660.6	323.7	-6.2	0.055021	0.001153	-0.053190	333.4	272.2	0.087859	21.8
3	670.2	335.7	-6.5	0.049157	0.000667	-0.047857	338.4	277.3	0.079020	19.9

Notes: 1. σ_1, ϵ_1 stress and strain along the length of the cylinder
σ_2, ϵ_1 circumferential stress and strain
σ_3, ϵ_1 average through thickness stress and strain

2. Cylinder no.1 was tested under a state of uniaxial plane stress.
3. Cylinders no. 2 and 3 were tested in a state of plane strain.

Table 4.16 COEFFICIENTS TO DESCRIBE THE PLANE STRAIN STRESS STRAIN CURVE OF THE 6.35 mm (1/4 in.) PLATE IN THE LONGITUDINAL DIRECTION

COEFFICIENTS	STRAIN RANGE $\times 10^{-6}$ mm/mm			
	0-1771	1771-9140	9140-25470	25470-119050
A	-	388.2	401.3	-
B	226900	1440.0	-	-169165.4
C	-	-	-	3672818.5
D	-	-	-	-23665153.1
E	-	-	-	59431527.3
F	-	-	-	-63114920.6
G	-	-	-	23840609.0

Notes: 1. $\sigma = A + B\epsilon + C\epsilon^{1/2} + D\epsilon^{1/3} + E\epsilon^{1/4} + F\epsilon^{1/5} + G\epsilon^{1/6}$

2. Coefficients were derived from a transformed stress-strain curve of the plane stress stress-strain curve described in Table 4.4.

Table 4.17 COEFFICIENTS TO DESCRIBE THE PLANE STRAIN STRESS STRAIN CURVE OF THE 4.76 mm (3/16 in.) PLATE IN THE LONGITUDINAL DIRECTION

COEFFICIENTS	STRAIN RANGE $\times 10^{-6}$ mm/mm			
	0-2036	2036-9140	9140-22750	22750-115500
A	-	396.1	411.6	-
B	220160	1703.3	-	-11530.4
C	-	-	-	361721.4
D	-	-	-	-2470024.1
E	-	-	-	6317041.2
F	-	-	-	-6759168.1
G	-	-	-	2563055.0

Notes: 1. $\sigma = A + B\epsilon + C\epsilon^{1/2} + D\epsilon^{1/3} + E\epsilon^{1/4} + F\epsilon^{1/5} + G\epsilon^{1/6}$

2. Coefficients were derived from a transformed stress-strain curve of the plane stress stress-strain curve described in Table 4.7.

Table 4.18 COEFFICIENTS TO DESCRIBE THE PLANE STRAIN STRESS STRAIN CURVE OF THE 3.175 mm (1/8 in.) PLATE IN THE LONGITUDINAL DIRECTION

COEFFICIENTS	STRAIN RANGE $\times 10^{-6}$ mm/mm			
	0-1474	1474-9140	9140-15000	15000-111000
A	-	256.0	265.8	-
B	220520	1070.0	-	-31417.0
C	-	-	-	684891.8
D	-	-	-	-4407688.5
E	-	-	-	11055119.3
F	-	-	-	-11729338.5
G	-	-	-	4427971.2

Notes: 1. $\sigma = A + B\epsilon + C\epsilon^{1/2} + D\epsilon^{1/3} + E\epsilon^{1/4} + F\epsilon^{1/5} + G\epsilon^{1/6}$

2. Coefficients were derived from a transformed stress-strain curve of the plane stress stress-strain curve described in Table 4.10.

Table 4.19 CONCRETE MIX DESIGN

ITEM	BATCH #1	BATCH #2
Cement, Type 10, kg/m^3	308	308
Fly Ash, kg/m^3	76	76
Coarse Aggregate, 15 mm max., kg/m^3	955	952
Fine Aggregate, kg/m^3	830	832
Water, kg/m^3	109	109
Air Entraining Agent, $m\ell/m^3$	445	445
Water Reducing Agent(HYCOL), $m\ell/m^3$	1421	1421

Notes: 1. Batch #1 - 2 m^3, Batch #2 - 2.5 m^3.
2. 116 $m\ell$ of air entraining agent per 100 kg of cementitious material, (cement and flyash).
3. 370 $m\ell$ of water reducing agent per 100 kg of cementitious material.
4. An additional 9.1 kg of water was added to batch #1 at the lab to improve its workability.

Table 4.20 CONCRETE CYLINDER AND MODULUS OF RUPTURE BEAMS TEST SCHEDULE

DATE	ELAPSED TIME, days	CONCRETE CYLINDER NO. COMPRESSIVE STRENGTH BATCH #1	BATCH #2	SPLIT 'T' BATCH #2	MODULUS OF RUPTURE BEAM NO. BATCH #1	BATCH #2
86 04 03	-					
86 04 10	7	1,2	21,22			
86 04 17	14	3,4	23,24			
86 04 24	21	5,6	25,26			
86 05 01	28	7,8	27,28			
86 05 17	44	9,10	29,30,31	32	1	
86 05 31	58	11,12	33,34,35	36	2	
86 06 07	65	13,14	57,38,39	40		3
86 06 14	72	15,16	41,43,44	42		4
86 06 21	79	17,18	45,46,47	48		5
86 06 25	83	19,20	49,50			6

Table 4.21 MATERIAL PROPERTIES DETERMINED FROM STANDARD CONCRETE TESTS

TIME, t	COMPRESSION						MODULUS OF RUPTURE		SPLIT 'T' CYLINDER
days	BATCH #1			BATCH #2			BATCH #1	BATCH #2	BATCH #2
	f'_c MPa	ϵ_o $\times 10^{-6}$	E_c MPa	f'_c MPa	ϵ_o $\times 10^{-6}$	E_c MPa	f_r MPa	f_r MPa	f_t MPa
7	27.0	2110	20300	30.2	2332	20560			
	27.9	2225	21100	29.5	2405	20640			
14	32.2	2578	20480	34.5	2529	22010			
	32.3	2751	20830	34.0	2431	21930			
21	36.5	2589	22170	37.8	2625	22120			
	33.9	2543	22320	38.9	2439	24240			
28	37.2	2571	23500	41.8	2575	23500			
	37.8	2412	23480	41.3	2545	23980			
44	40.0	2252	25340	42.4	2070	26620	4.04		2.81 (4.22)[2]
	38.4	2263	23750	43.1	2236	25770			
				43.3	2382	24390			
58	43.4	2444	24650	46.1	2226	25090	3.36		2.97 (4.46)[2]
	43.0	2494	23820	46.6	2449	26140			
				46.3	2537	24130			

Table 4.22 con't

TIME, t	COMPRESSION						MODULUS OF RUPTURE		SPLIT 'T' CYLINDER
days	BATCH #1			BATCH #2			BATCH #1	BATCH #2	BATCH #2
	f'_c MPa	ϵ_o x10^{-6}	E_c MPa	f'_c MPa	ϵ_o x10^{-6}	E_c MPa	f_r MPa	f_r MPa	f_t MPa
65	46.7	2564	24300	50.4	2513	25810		4.06	3.08 (4.62)[2]
	44.6	3425[1]	22020	48.2	2557	24680			
				49.1	2411	26670			
72	45.0	2486	24950	49.6	2338	26860		4.08	3.43 (5.15)[2]
	41.8	2252	25960	48.9	2558	25330			
				51.1	2650	26350			
79	43.7	2523	24720	50.6	2453	26060		4.06	3.70 (5.55)[2]
	44.8	2506	24950	50.6	2492	25500			
				50.7	2403	27170			
83	44.4	2241	25690	47.4	2120	27500		4.25	
	43.9	2376	26300	52.4	2613	26730			

Notes: 1. This value of ϵ_o appeared to be spurious and was excluded from the data set.

2. The flexure strength of 1/3 point loaded 6 in. x 6 in. beams = 1.35 to 1.65 (average 1.5) times the split cylinder strength. The average adjusted value is found in the brackets.

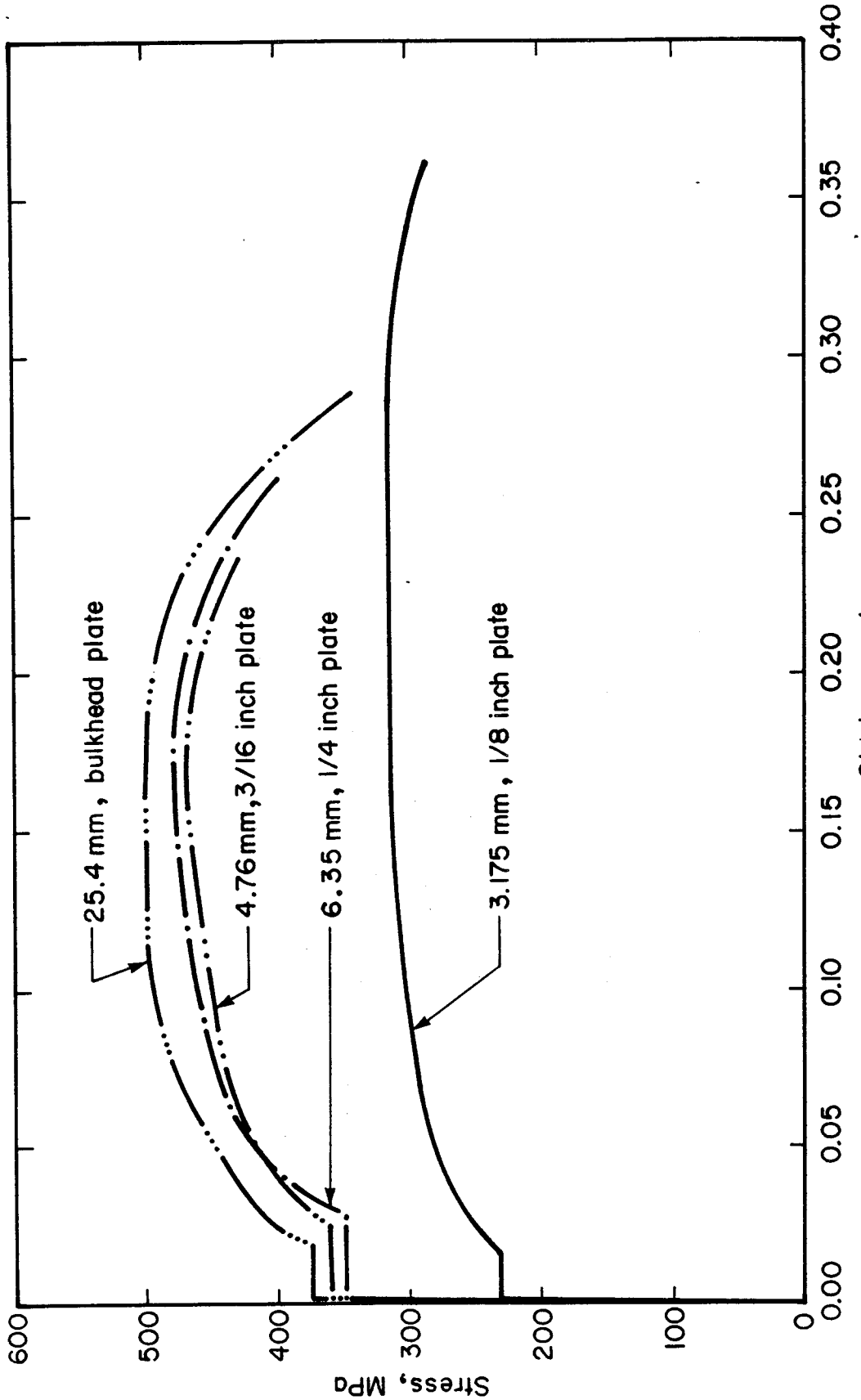

Figure 4.1 UNIAXIAL STRESS STRAIN CURVES FOR THE STEEL PLATES - LONGITUDINAL DIRECTION

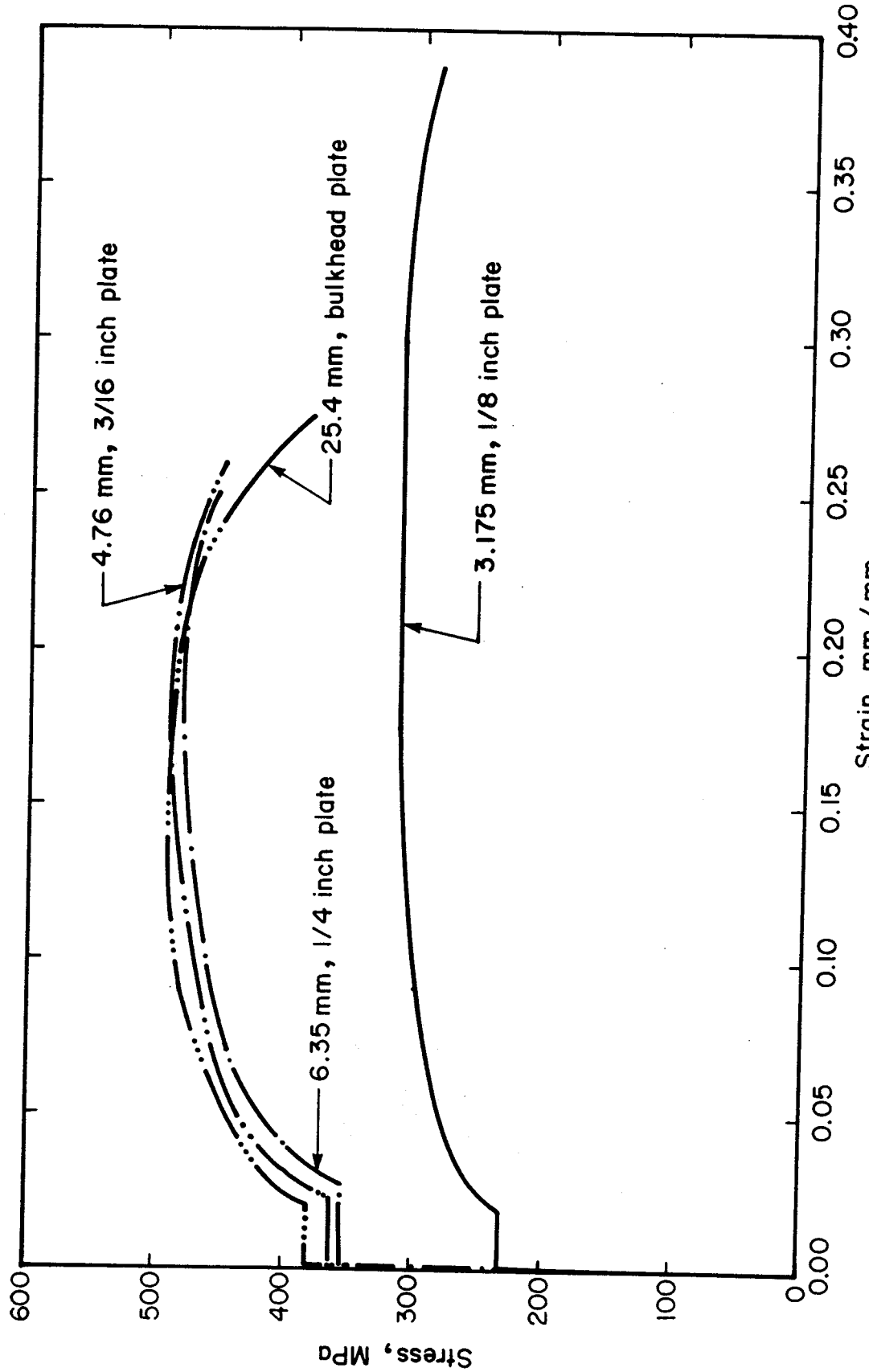

Figure 4.2 UNIAXIAL STRESS STRAIN CURVES FOR THE STEEL PLATES - TRANSVERSE DIRECTION

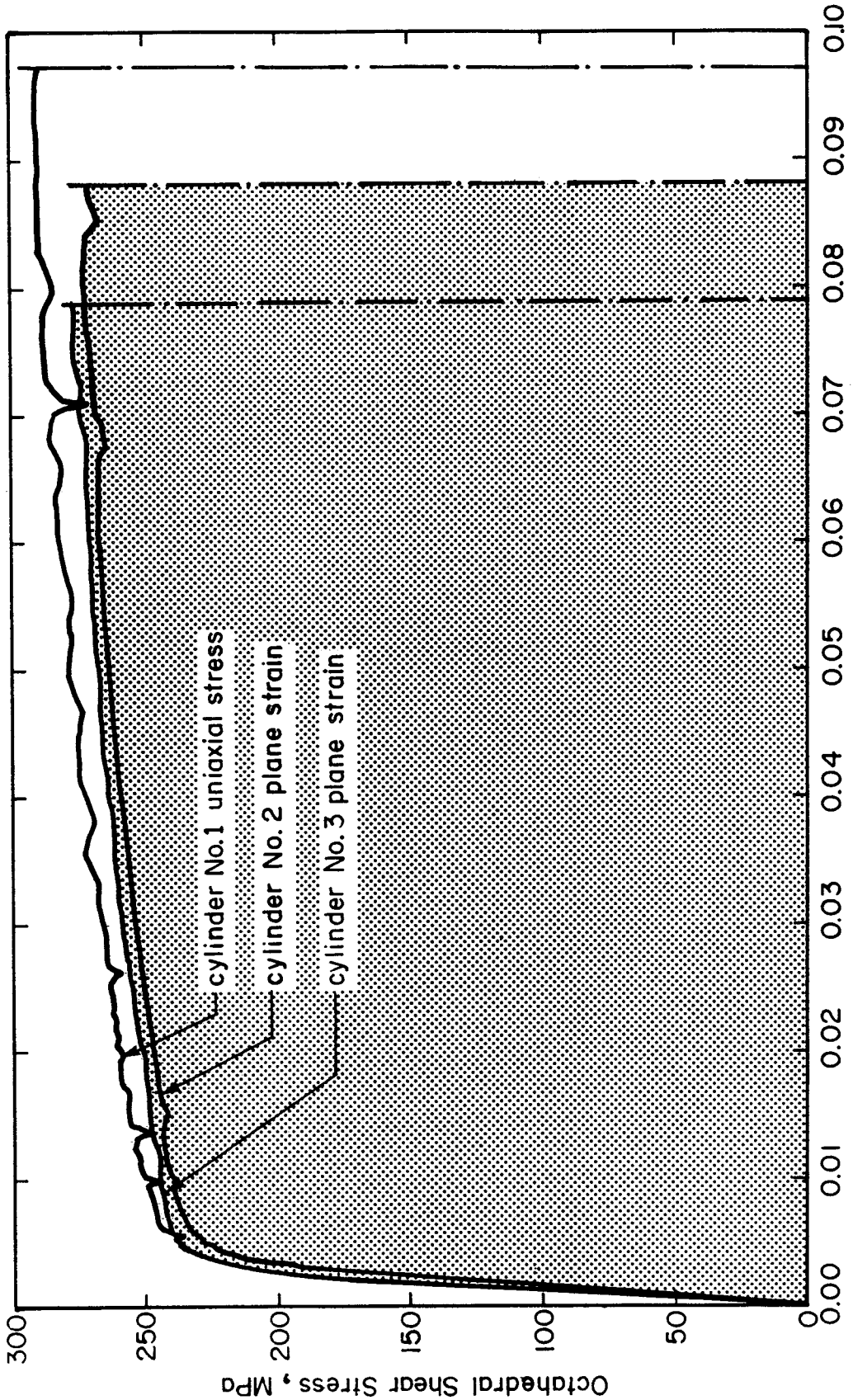

Figure 4.3 OCTAHEDRAL SHEAR STRESS SHEAR STRAIN CURVES

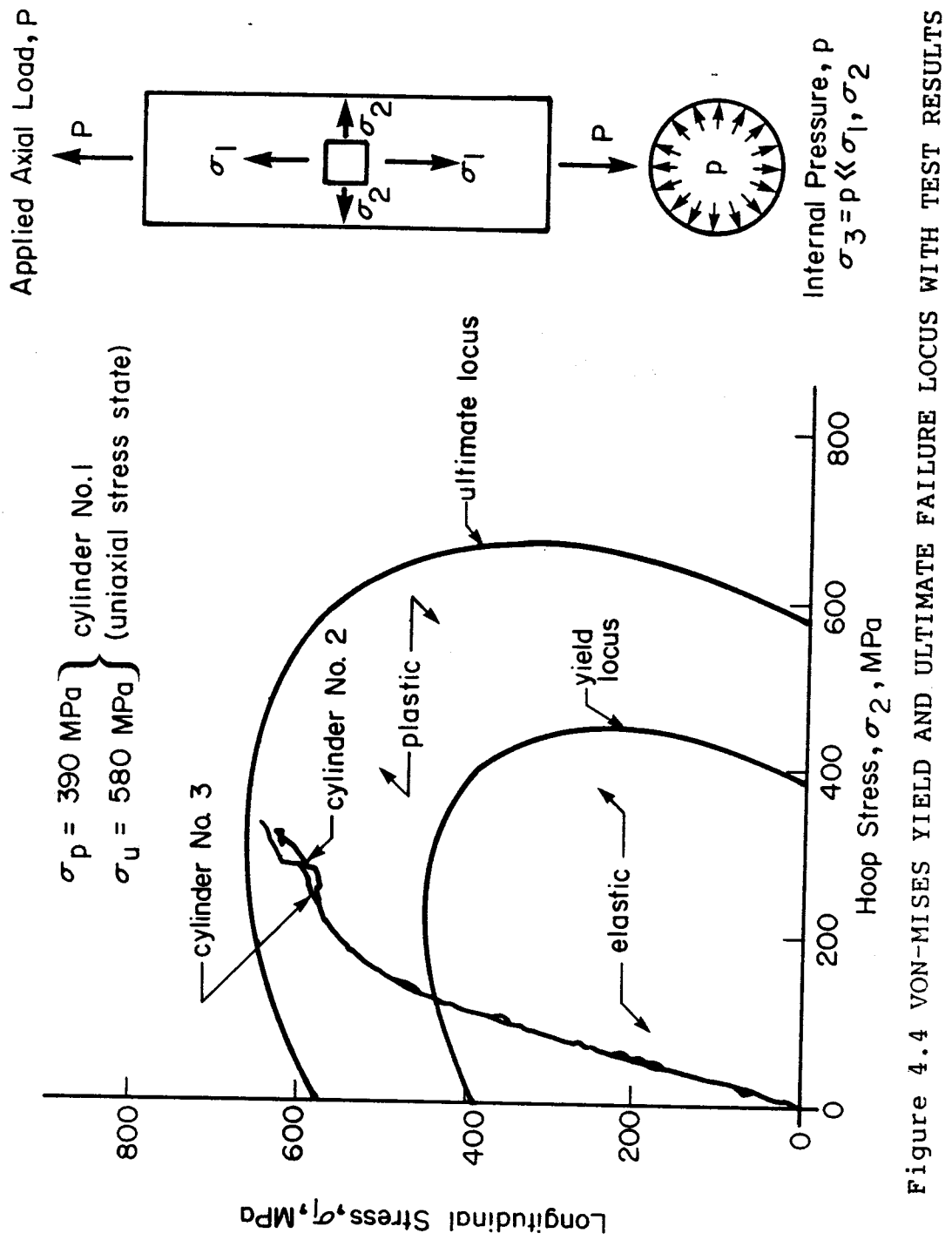

Figure 4.4 VON-MISES YIELD AND ULTIMATE FAILURE LOCUS WITH TEST RESULTS

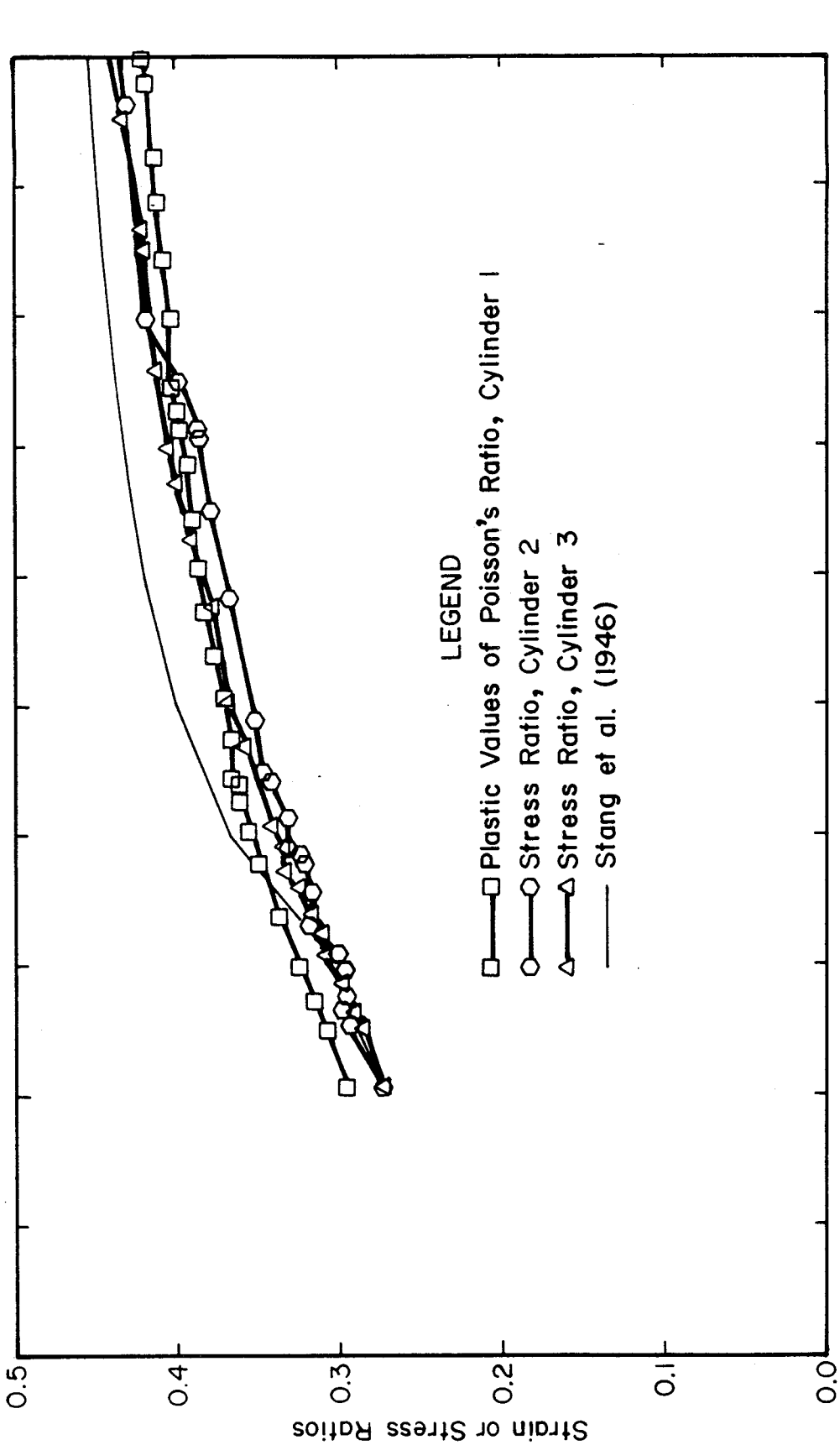

Figure 4.5 COMPARISON OF STRAIN AND STRESS RATIOS

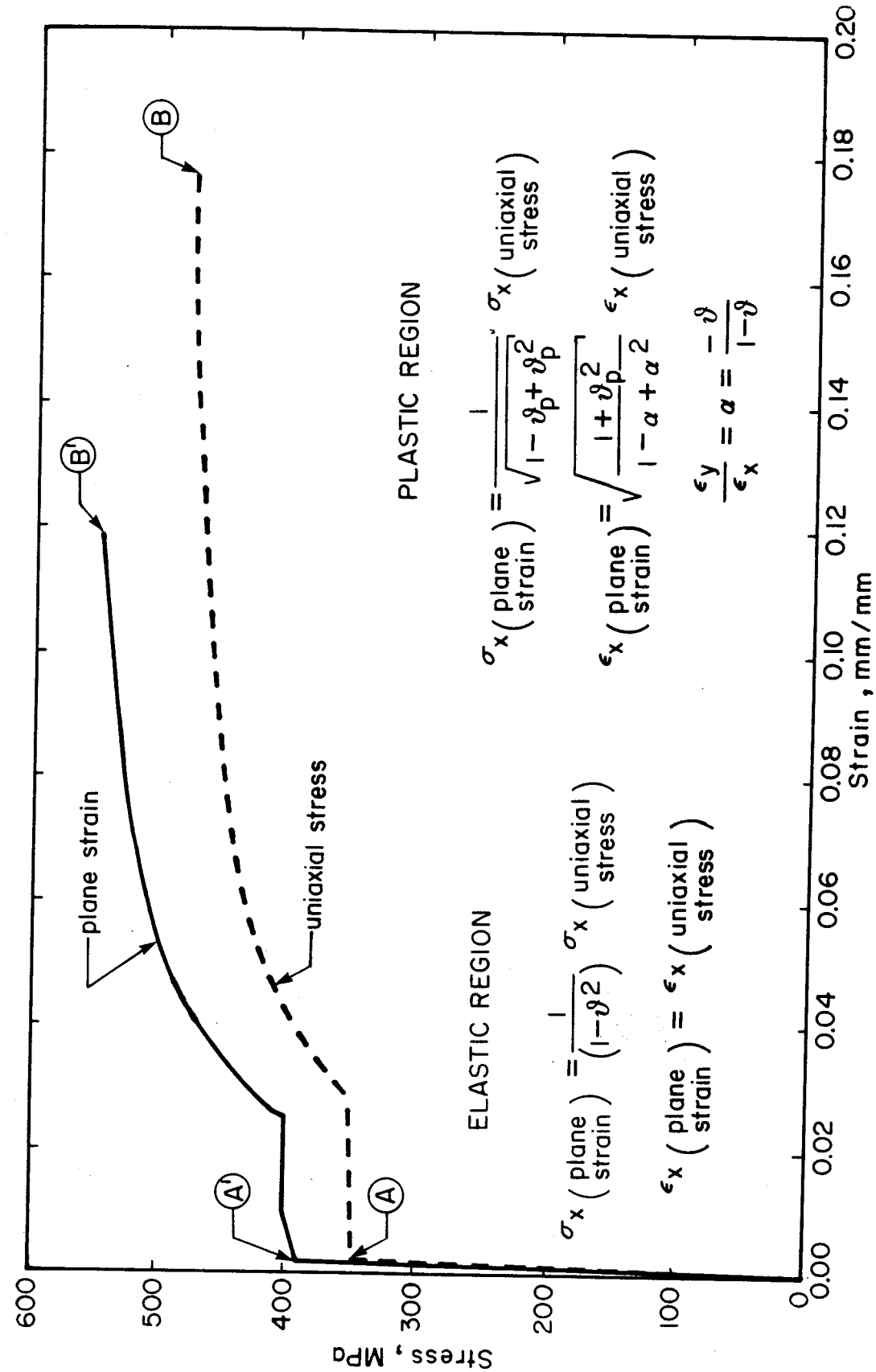

Figure 4.6 TRANSFORMED STRESS STRAIN CURVES

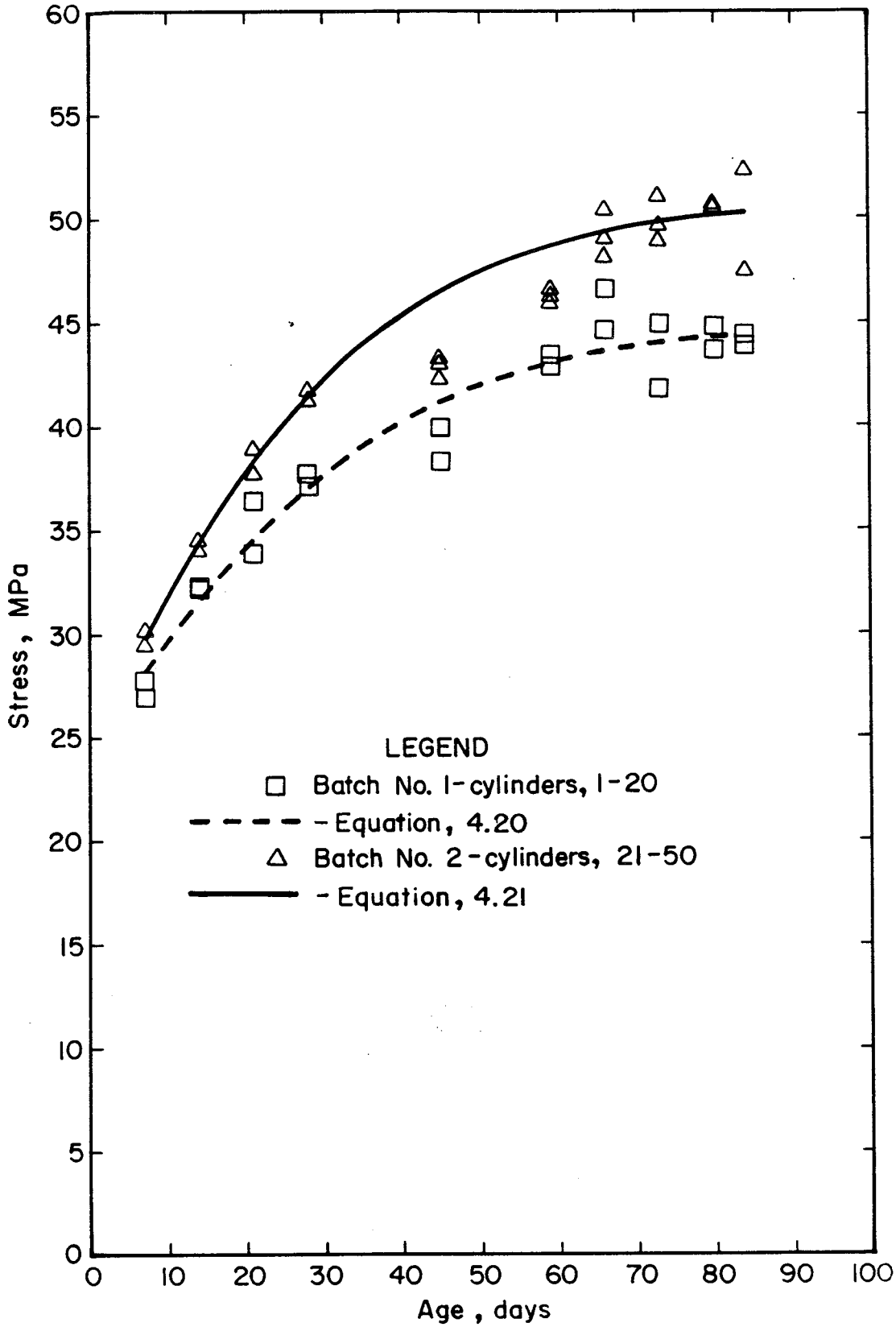

Figure 4.7 COMPRESSIVE STRENGTH TIME RELATIONSHIPS FOR CONCRETE

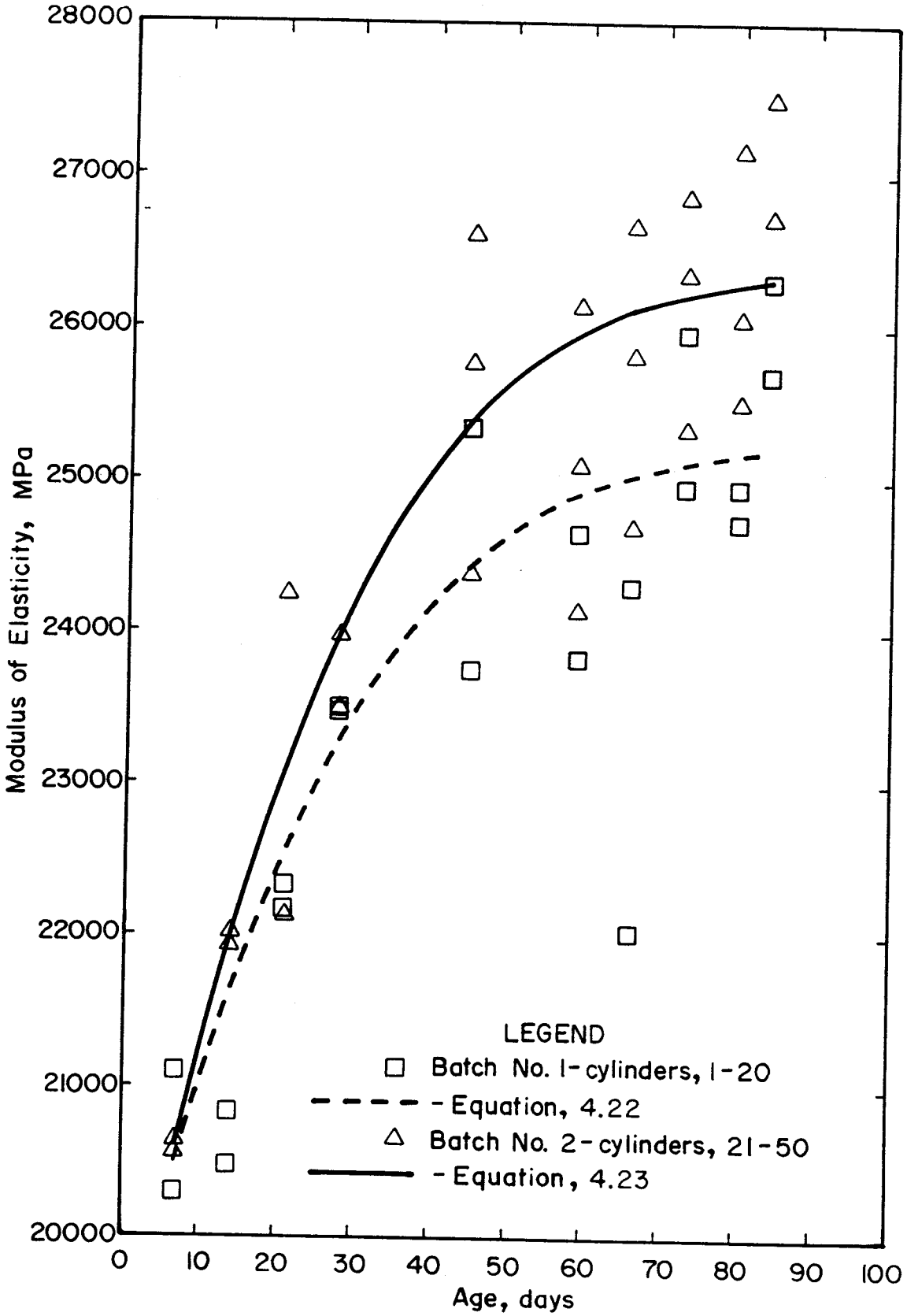

Figure 4.8 MODULUS OF ELASTICITY FOR COMPRESSION TIME RELATIONSHIPS FOR CONCRETE

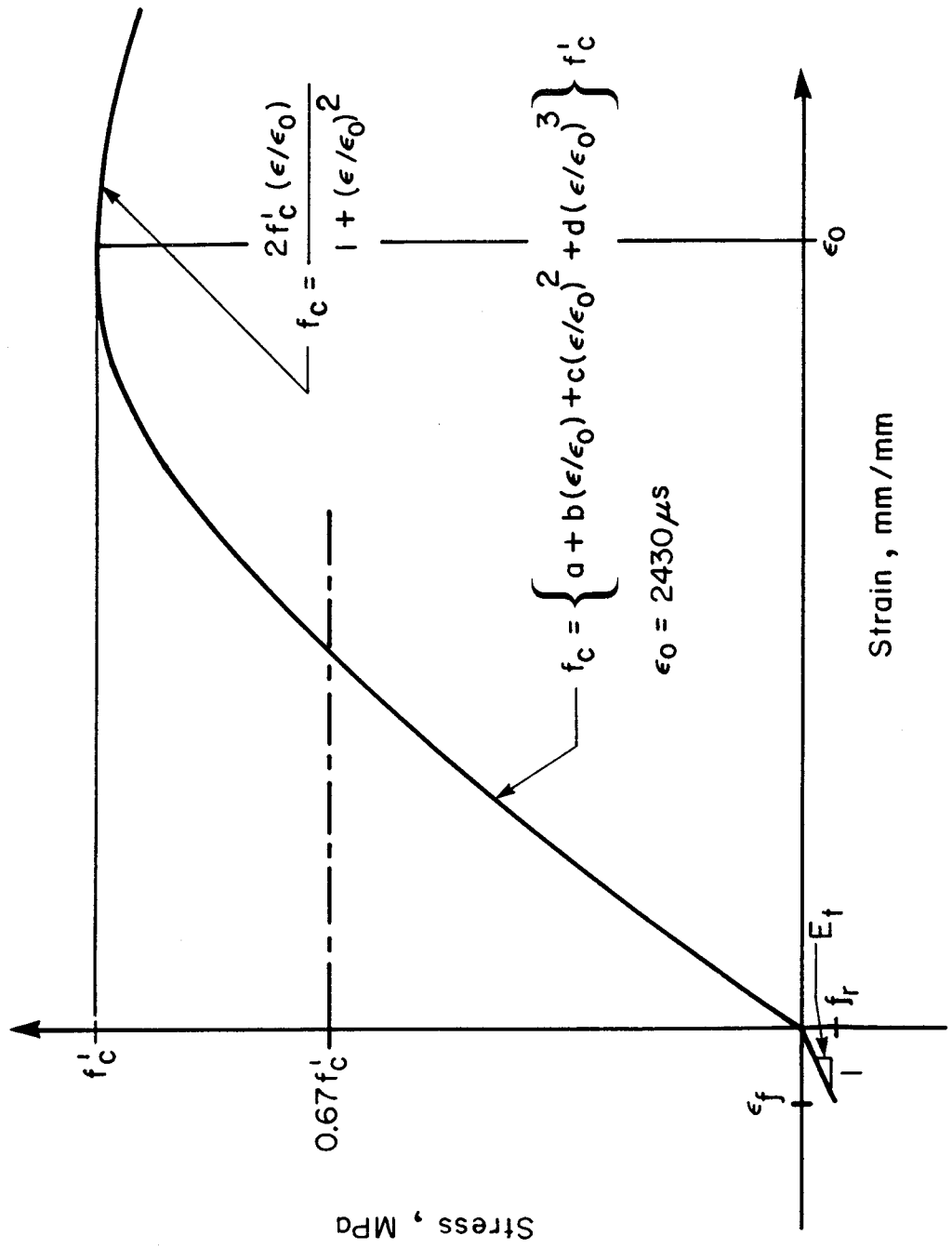

Figure 4.9 UNIAXIAL STRESS STRAIN CURVE FOR CONCRETE

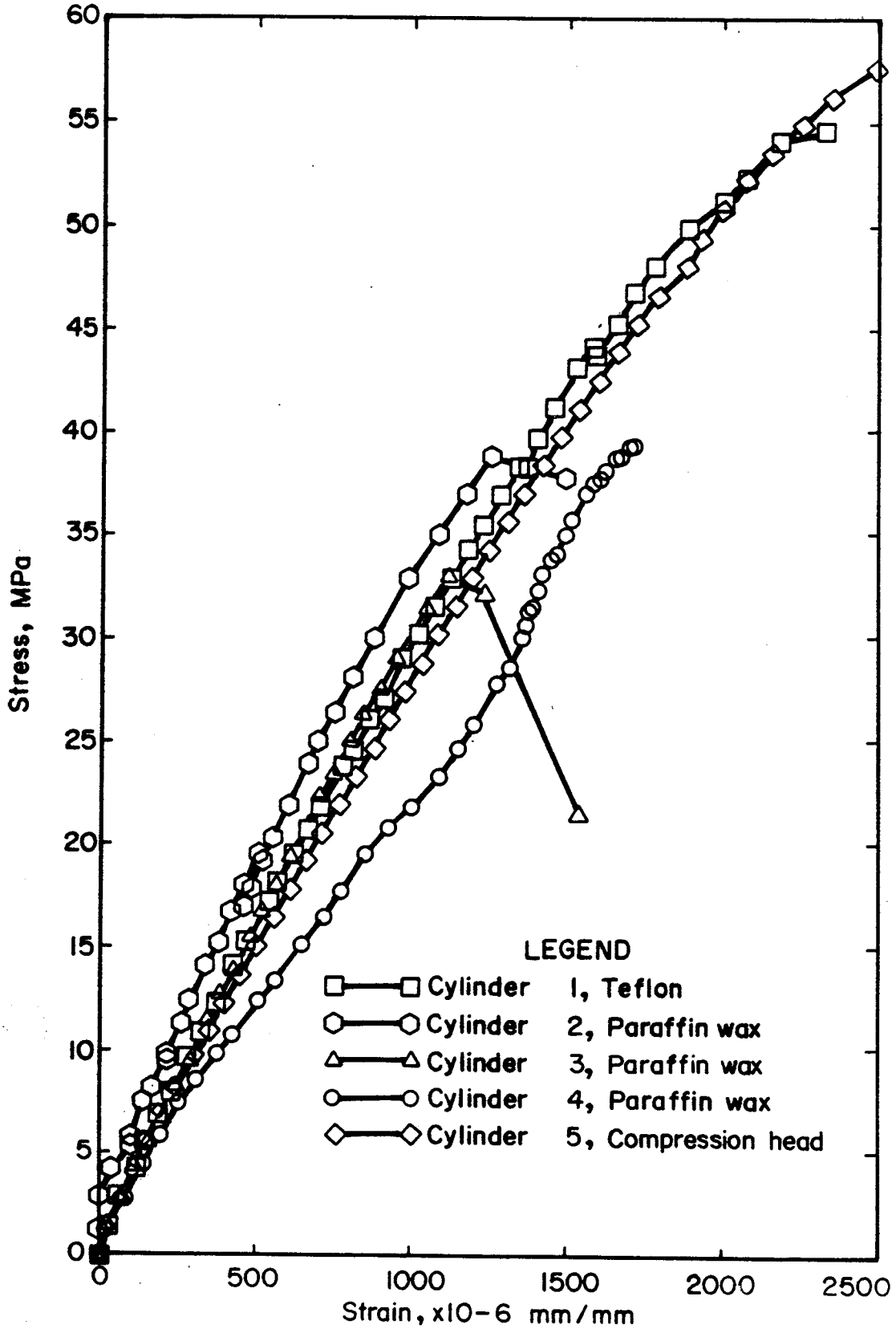

Figure 4.10 COMPRESSIVE STRESS STRAIN CURVES WITH DIFFERENT END RESTRAINT

5. STEEL CONCRETE INTERFACE TEST RESULTS

5.1 General Behaviour

Test specimen identification numbers, dimensions of the steel plate, and the corresponding yield and ultimate tensile loads as calculated from the tension coupon data are given in Table 5.1.

5.2 Shear Deformation Response

5.2.1 Test Series 1 - Virgin Response

Five test specimens of similar geometry and one nominal plate thickness were tested under different normal loads, N, varying from 0.2 P to 1.0 P, where P is the normal load required to develop a friction force, F, large enough to fracture the steel plate. The shear displacement response of these tests are shown in Figure 5.1, 5.2 and 5.3 for normal loads of 600 kN, 900 kN, and 1500 kN, respectively, where the displacement is the horizontal movement of the leading edge of the plate.

These curves exhibit several interesting features. Test ST6.04, with a normal load of 0.4 P, is a good illustration of the classical shear or frictional force deformation response for sliding friction as shown in Figure 5.1. The peak load value gives the static coefficient of friction, and the plateau gives the dynamic or kinetic friction coefficient, with the coefficient of friction defined as:

[5.1] $\mu = F/N$

in which, F = Frictional or shear force, kN

N = Normal force, kN

After the peak value was reached, release of strain energy resulted in a sudden displacement, and the frictional force decreased. Subsequently, as the horizontal (shear) loading continued, the kinetic frictional force response curve was established. This curve is relatively smooth indicating a continuous dissipation of strain energy. For normal loads of 0.4 P, 0.6 P and greater the kinetic curves are discontinuous and the slip occurs in jumps. The phenomena of sliding friction is a discontinuous process made up of a series of strain energy dissipation steps, somewhat analogous to the shear deformation response of the continental plates of the earth, known as earthquakes. With further increases in normal load, up to that causing failure of the plate, the load displacement steps are accentuated and dominate the response. The magnitude of the strain energy releases is proportional to the magnitude of the normal load. After large relative displacements the response shows the usual more or less continuous kinetic plateau. This is attributed to a change in the surface characteristics along the interface. The plateau, however, still consists of a series of smaller strain energy dissipation steps or shear deformation jumps.

Typical load strain curves for strains measured along the length of the plate are given in Figure 5.4 for test ST6.06. As expected, for any given position of the plate with respect to the concrete block, the steel strains are a maximum at the loaded edge and dissipate to zero at the other end as the frictional force is introduced into the concrete. The strain in the steel plate is constant in the region in front of the concrete where there is no frictional drag. Displacement distributions can be determined by integrating the strain along the length of the plate with a zero datum located at the free or unloaded edge of the plate as indicated in Figure 5.4.

5.2.2 Test Series 2 - Repeated Loading with Increased Normal Loads

Relative movement or slip between the steel plate and the concrete or some form of delamination may occur at small normal loads. The most accurate representation of the shear deformation response is given by the kinetic response. The kinetic response is a lower bound to the force that can be transmitted by friction across the interface.

Four test specimens of different nominal plate thicknesses were tested under repeated horizontal or shear loads with increased normal loads. Figure 5.5 illustrates the typical shear deformation response obtained for test ST6. Similar characteristics to those described previously are shown here. The only true static peak value is

associated with the virgin curve, static peak curves under increased normal loads for subsequent shear deformation curves after some displacement has occurred are generally reduced and are only slightly greater than or equal to the kinetic value for the same normal load.

5.3 Discussion

Figure 5.6 shows the relationship between the frictional force and the normal load, and Figure 5.7 shows the relationship between coefficient of friction and normal load curves, for all the tests. Figure 5.6 shows that the frictional force is proportional to the normal load up to a normal load of about 900 kN. At this load level, in addition to the compressive stresses due to the normal load, the couple produced by the shear forces on the top surface of the concrete and the reaction near the bottom start to introduce significant additional compressive stresses at the leading edge of the block. Estimates of the normal stresses indicate that matrix cracking of the concrete should occur. This is supported by observations of cracking of the concrete during the tests. The increased slope of the frictional force normal force curve at this point was attributed to the change in surface characteristics resulting from matrix cracking of the concrete.

Also shown on Figure 5.6 are the static and kinetic response values from the first series of tests. The static curve lies above the kinetic curve but approaches the

kinetic curve with increasing normal load. These values merge as a result of the change in the shear deformation response at large normal loads where there are large strain energy dissipation steps.

Apart from the values obtained from the first normal load shear deformation response curve for the second series of tests, the static and kinetic curves are essentially the same. As would be expected, there does not appear to be any significant variance between the curves regardless of loaded area or steel plate thickness.

The coefficient of friction values corresponding to the frictional forces described above were calculated using Equation 5.1 and are shown in Figure 5.7. The mean value of the coefficient of kinetic friction is 0.5 with a coefficient of variation of 0.15.

Table 5.1 GEOMETRIC PROPERTIES AND REFERENCE LOADS

TEST SPECIMEN	DATE	PLATE DIMENSIONS WIDTH, mm	THICKNESS, mm	YIELD LOAD P_y, kN	ULTIMATE LOAD P_u, kN
		SERIES 1 - VIRGIN SHEAR DEFORMATION RESPONSE			
ST6.02	86 07 10	248.2	6.82	588.9	802.9
ST6.04	86 07 11	248.5	6.90	596.5	813.3
ST6.06	86 07 14	250.1	7.24	630.0	858.8
ST6.08	86 07 15	248.3	7.12	615.1	838.5
		SERIES 2 - REPEATED LOADING WITH INCREASING NORMAL LOADS			
ST3	86 07 21	219.1	3.06	154.2	209.3
ST4	86 07 18	219.6	4.69	367.6	480.1
ST6	86 07 17	249.2	7.46	646.7	881.7
ST25	86 07 22	224.6	25.3	2122	2813

Note: 1. Test specimen identification; i.e. ST6.02, ST - shear test, 6 - approximate plate thickness in mm, .02 - fraction of (20%) normal load required to develop the frictional force to fracture the steel plate

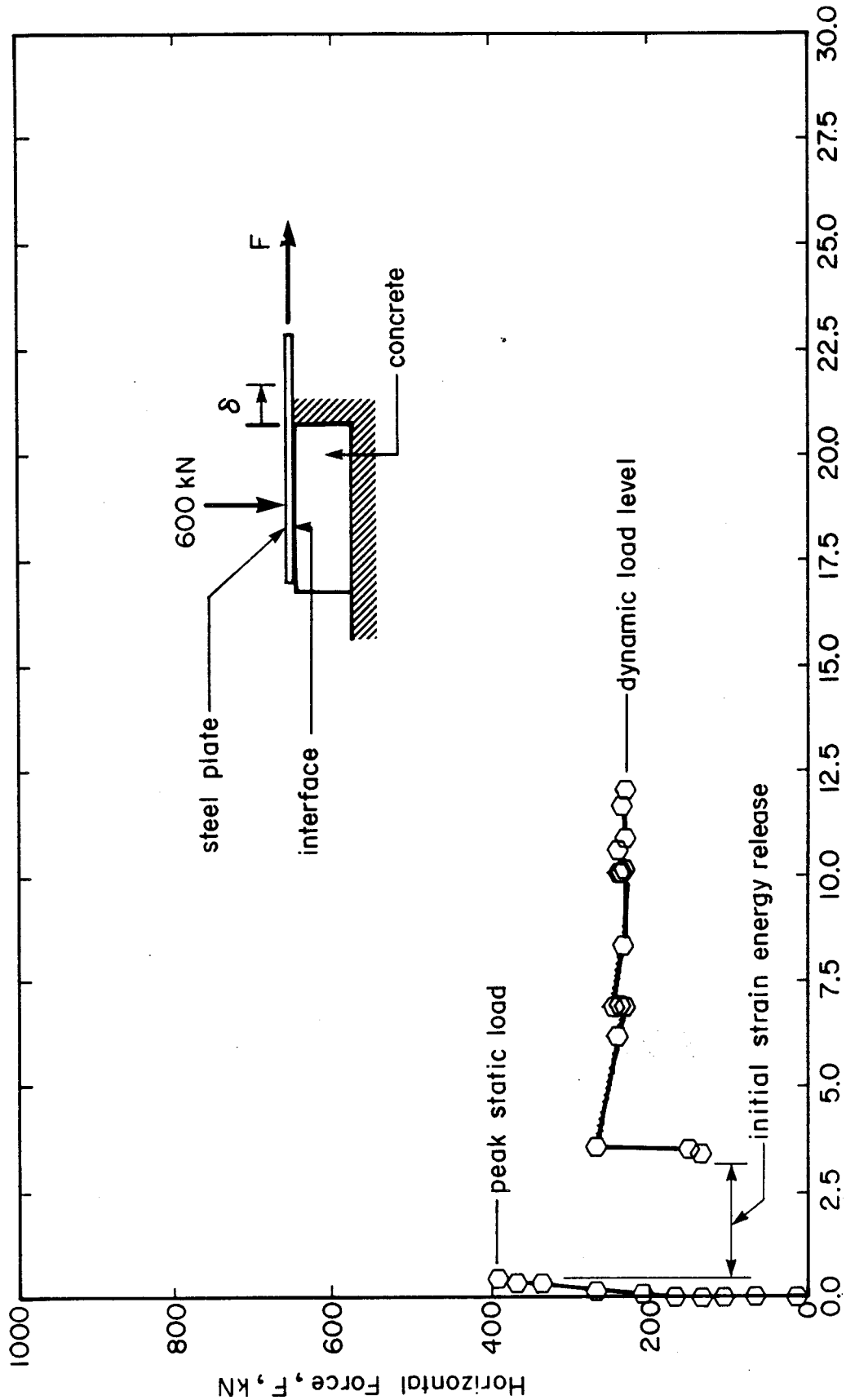

Figure 5.1 VIRGIN SHEAR DISPLACEMENT RESPONSE TEST WITH A NORMAL LOAD OF 600 kN

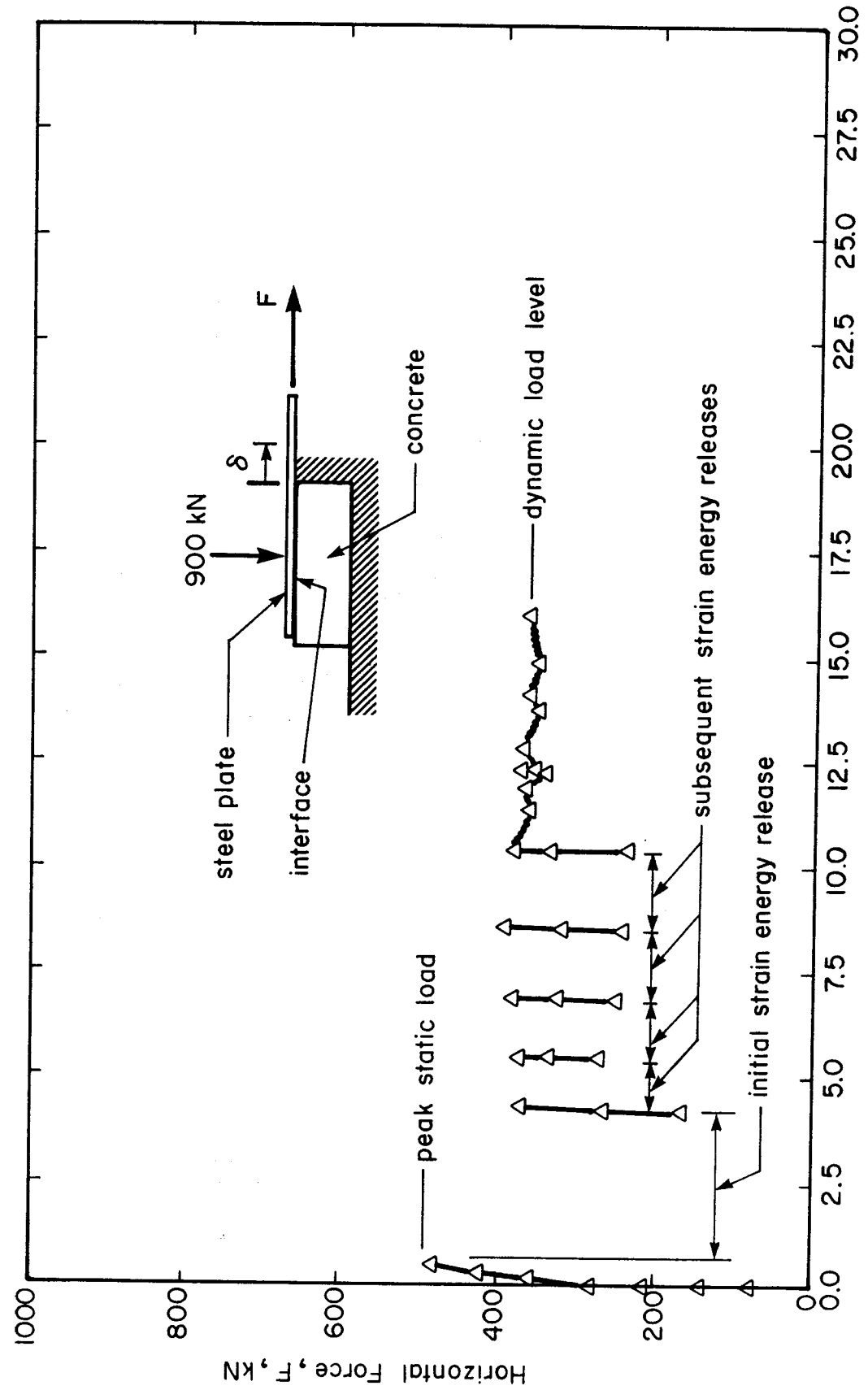

Figure 5.2 VIRGIN SHEAR DISPLACEMENT RESPONSE TEST WITH A NORMAL LOAD OF 900 kN

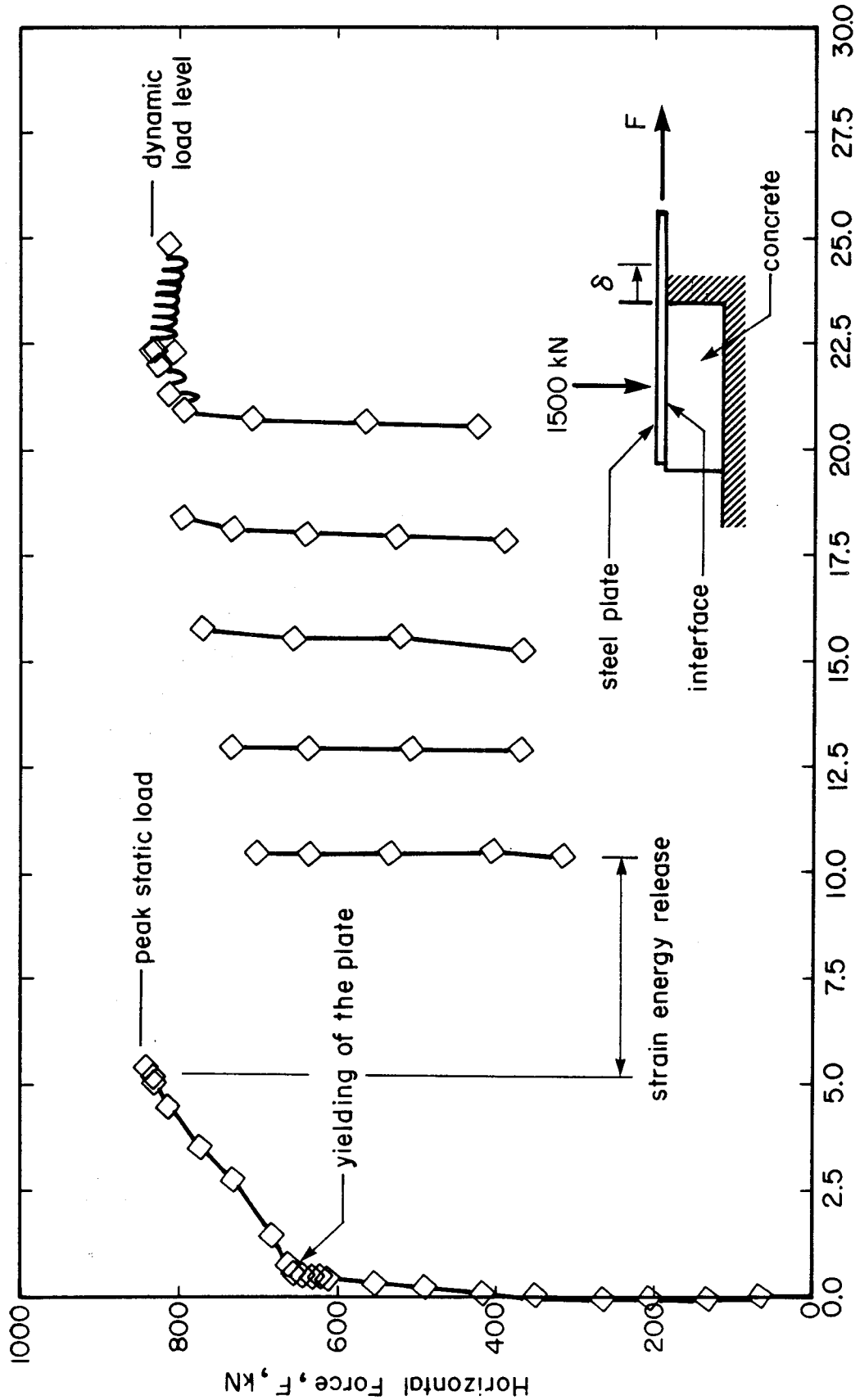

Figure 5.3 VIRGIN SHEAR DISPLACEMENT RESPONSE TEST WITH A NORMAL LOAD OF 1500 kN

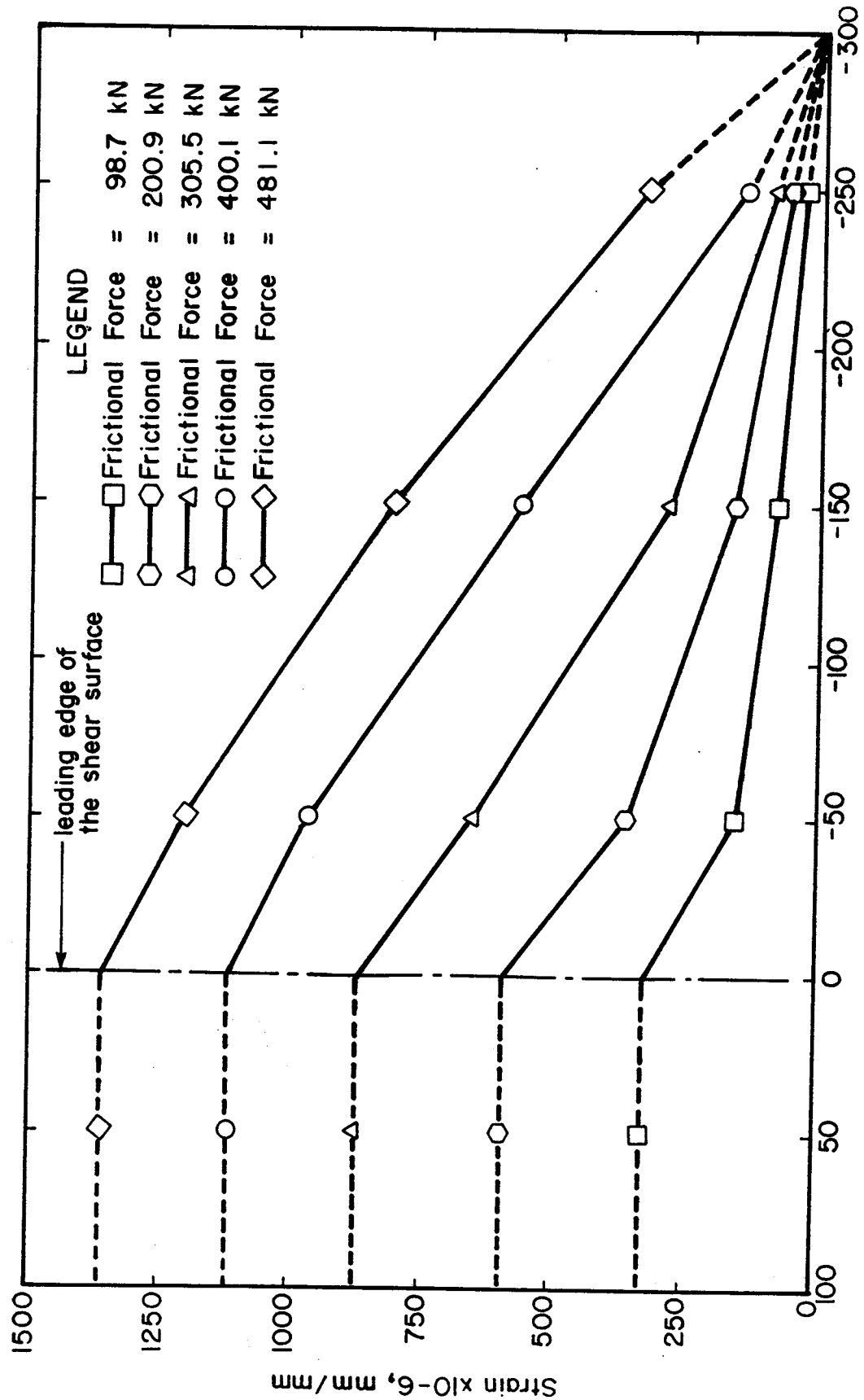

Figure 5.4 TYPICAL STRAIN DISTRIBUTIONS ALONG THE LENGTH OF THE PLATE, TEST ST6.06

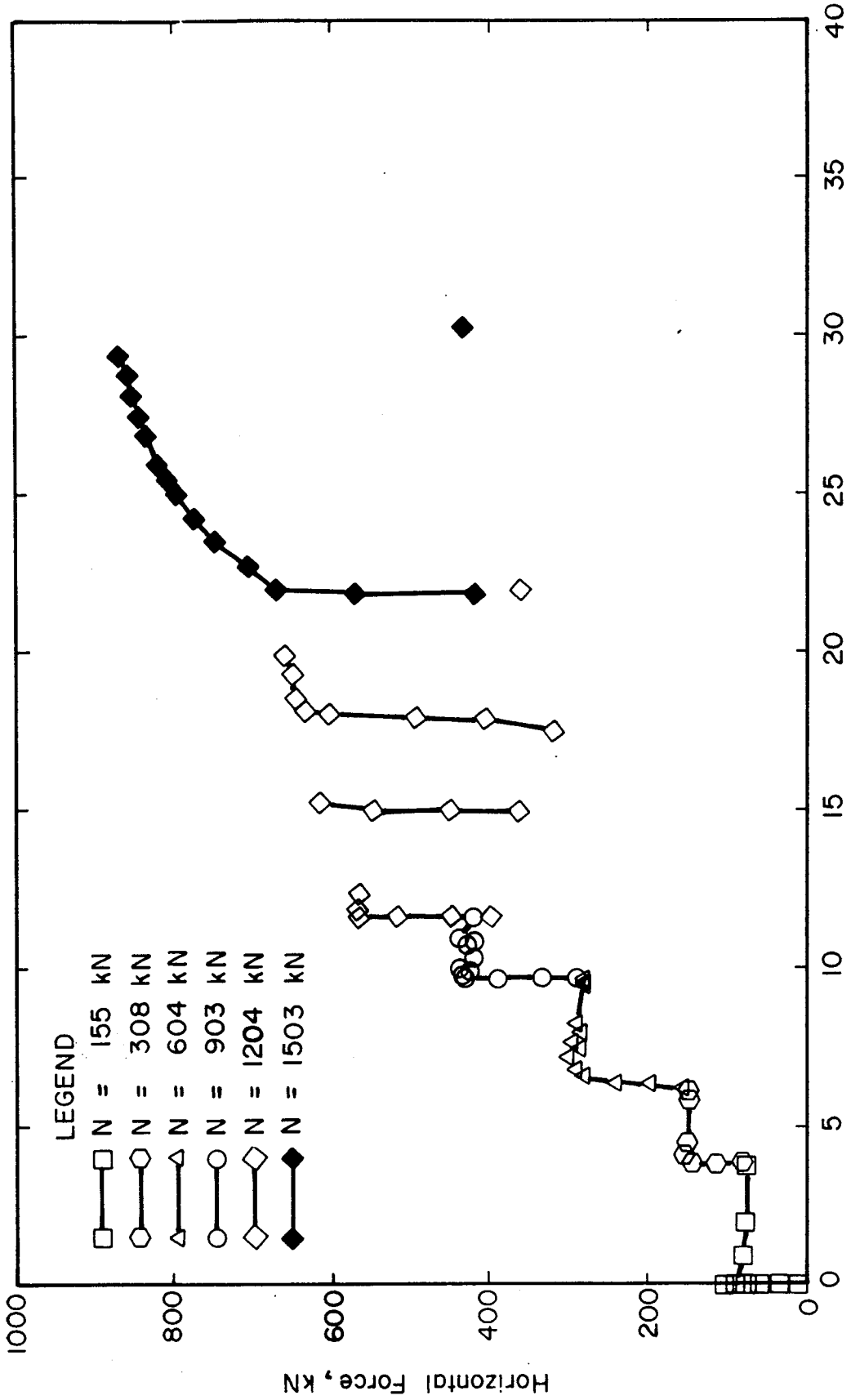

Figure 5.5 SHEAR DISPLACEMENT RESPONSE, TEST ST6

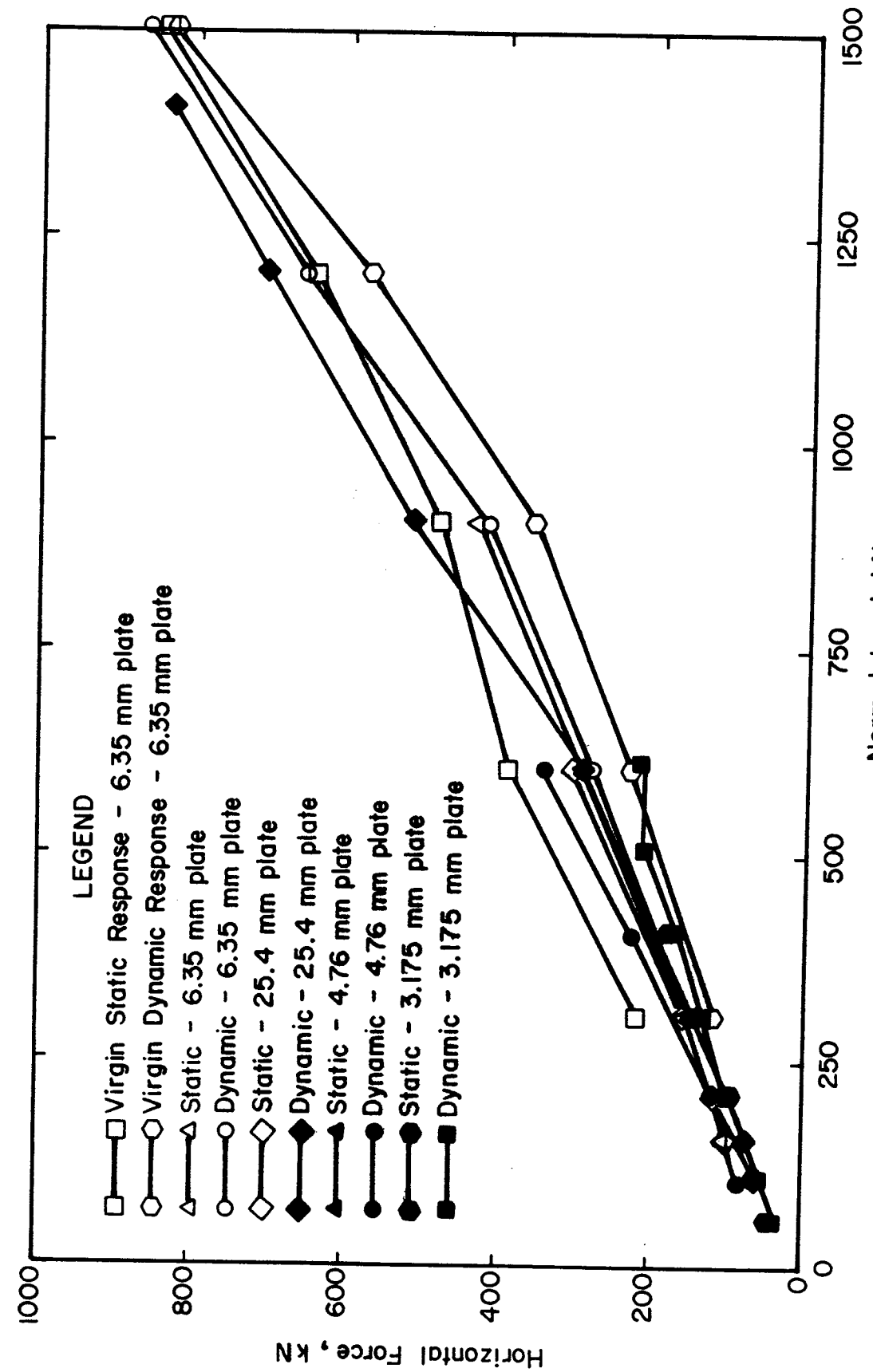

Figure 5.6 FRICTION FORCE NORMAL LOAD RELATIONSHIP

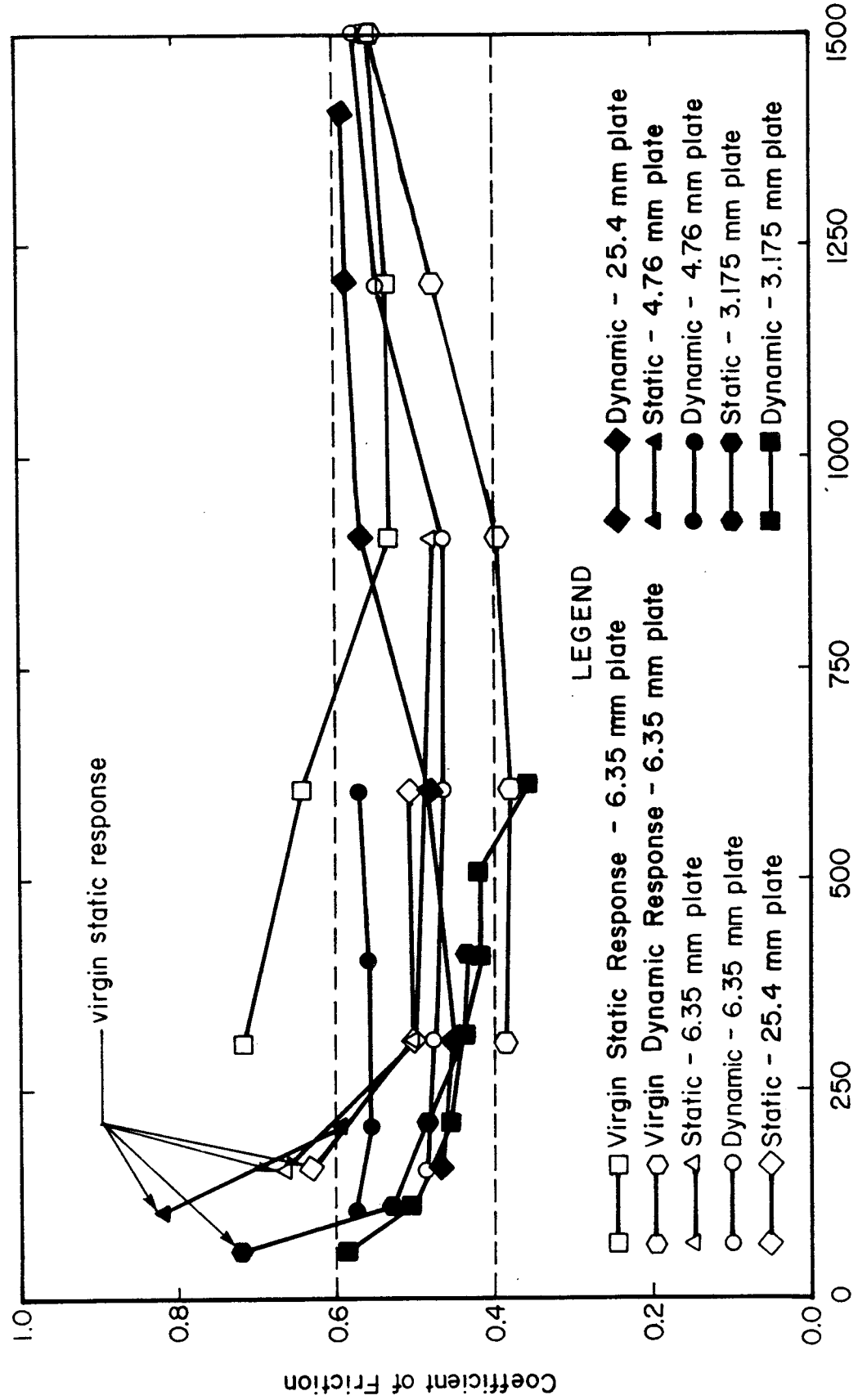

Figure 5.7 COEFFICIENT OF FRICTION RELATIONSHIP

6. RESTRAINED PLATE TEST RESULTS

6.1 General Behaviour

In Figure 6.1 are plotted the centre span deflection versus total applied load for plates of similar steel plate thicknesses and in Figure 6.2 are plotted the same curves for composite plates with constant section depth. The behaviour of the restrained plates can be divided into three quite distinct regions: flexural, flexural membrane, and membrane behaviour. Tables 6.1 to 6.6 summarizes the restrained plate tests giving dates, total load, load steps, with corresponding deflections and behaviour, and observations or events recorded during the tests.

6.1.1 Composite Plate Tests

6.1.1.1 Flexural Behaviour

For any continuous composite structure loaded symmetrically the changes in flexural stiffness are delineated by:

1. first cracking;
2. development of plastic hinges at the supports;
3. development of a plastic hinge at centre span.

These demarcation points are illustrated on the load deflection curve for test C203T6, a typical test of a composite plate, in Figure 6.3.

The flexural behaviour of these plates was dominated by the progression of cracking of the concrete in tension,

crushing of the concrete in compression and by localized yielding of the steel plate in tension at the crack locations. First cracking was characterized by the formation of a small number of flexural cracks on the tension (lower) side under the inmost load points, at centre span, and adjacent to the supports on the upper side. The deflected shape of the composite plate could be approximated closely as two straight line segments with sharp changes in slope at the crack locations.

Plastic hinges first formed at both ends of the span adjacent to the supports. These manifested themselves as zones of cracked and crushed concrete on the tension and compression sides, respectively, with parallel yield lines across the width of the steel plate over the cracks. The cracked and crushed concrete are shown in Figure 6.4(a). The widths of the flexural cracks at these points ranged between 1.8 and 4.0 mm. With further loading, the flexural cracks opened and the localized yielding of the plate associated with the crack spread. Cracks in the concrete then ranged between 7 and 10 mm in width.

Formation of the plastic hinge at centre span started with the development of a horizontal crack located 10 to 20 mm below the top plate as shown in Figure 6.4(b) for test C152T6. As discussed in Section 4.2.4.2, the formation of such cracks parallel to the direction of the principal internal compressive force is an indication that the compressive strength of the concrete has been reached. As a

result of the growth in width of the horizontal cracks, the depth of the section increases between 1.05 and 1.10 times the original depth. If adequate through-thickness reinforcement or plate interconnection were provided, the formation and propagation of the horizontal cracks would be suppressed, and the flexural capacity of the section could be increased. This load level corresponds to the maximum flexural capacity of the section at approximately 10% of the final centre span deflection. A net tensile force measured in the horizontal restraint frame corresponds to an outward movement of the bulkhead supports. This is shown in Figures 6.5 and 6.6 as the development of some initial tensile force measured from the offset position. The offset position results from the pretensioning in the plates. The measurements of restraint are further discussed in Section 6.5. There were no signs of distress or buckling of the steel plates on the compression side of the composite plate element either at the supports or at centre span.

6.1.1.2 Flexural-Membrane Behaviour

Subsequent to the formation of the last hinge, the composite plate deflects with no increase in load capacity, until the tensile force in the horizontal reaction frame is reduced to zero and the bulkhead supports have returned to their original positions. With further increased loading, the horizontal frame starts to provide the reaction to the in-plane or membrane forces being developed in the plate. Tensile forces in the plate result in compressive forces in

the frame. The compression force in the horizontal reaction frame develops at a decreasing rate and the variation of the force with applied load is typically parabolic. For test C203T6 in Figure 6.5, this action occurs between the end of the flexural behaviour and the point 'B', at a horizontal force of about 1400 kN. In this region, for this test an average of about 2.9 kN of reaction load is needed to develop 1 kN of total applied transverse load. The parabolic increase is consistent with elastic membrane action.

To accommodate the increased change in curvature along the length of the plate as the centre span deflection increases, the concrete core breaks down into a series of blocks, which conform to the load plates. The change in curvature is concentrated at the edges of the load plates in the form of flexural cracks. The formation of concrete blocks progresses from the centre of the span in each direction towards the supports as the deflections increase. The steel plates mold themselves around the concrete blocks. Existing flexural cracks simply opened up or split into a fan-like array of smaller cracks. A few of the larger flexural cracks had widths greater than 10 mm. Over the supports where there are regions of sharp curvature, the crack widths were much larger and the splintering of the concrete more severe. The horizontal crack at midspan increased in length and propagated towards the supports. While the crack pattern is difficult to discern in Figure 6.7, it can be seen that the plate consists of two more or

less straight segments.

Yielding of the top steel plate spread from the supports towards centre span and the bottom plate from the centre towards the supports. Yield lines formed across the width of the plate at an angle between 40 and 45 degrees to a line perpendicular to the long direction of the plate.

Approximately 30% of the total centre span deflection was reached at the load level corresponding to the change in behaviour from flexural membrane to membrane.

6.1.1.3 Membrane Behaviour

The major portion of the load deformation response of the composite plate was dominated by membrane behaviour of the two steel plates as shown in Figures 6.1 and 6.2.

While the overall behaviour of the composite plate is dictated by membrane action some contribution from the concrete occurs locally. This load carrying mechanism plays a minor role and diminishes as the centre span deflection increases. The decrease arises primarily because the concrete strain softens after reaching its ultimate strength.

A close examination of the steel plate test behaviour, which acted essentially as a membrane throughout, shows that the load deformation curve is bilinear, as shown in Figure 6.1 with a break at point 'A'. The increase in stiffness has been attributed, Ratzlaff and Kennedy (1986), to strain hardening of the steel plate. Evaluating the behaviour of the plate acting as a membrane and subjected to transverse

load shows this to be the case as described subsequently in Section 7.3. The change in stiffness for the composite plate tests are not as well defined due to non-uniform straining of the top and bottom plates.

Yielding of the steel plates, began when flexural behaviour was still playing a role, and continued to spread throughout the plate. The concrete continued to break down as previously described with the cracks in the concrete becoming more evenly distributed along the length of the plate in a fan-like appearance. The crack pattern is shown in Figure 6.8. The horizontal restraint force continued to increase up to failure. As can be seen for test C203T6 in Figure 6.5, the increase is relatively large from point 'B' up to point 'C' where yielding of both the top and bottom steel plates between the supports and the first load points occurred. Subsequently, the horizontal restraint force increased much more slowly.

At a typical centre span deflection of approximately 350 mm and an end rotation of the composite plate of approximately 20 degrees over the bulkhead supports, cracks began to appear at the upper edge of the bottom steel plate over the inside edge of one or both of the supports. The cracks resembled flexural cracks in concrete, initiating at the top of the bottom steel plate, where the combination of bending and axial strains are a maximum, and propagated down through the thickness. With continued loading and increasing deflections the cracks increased in width, depth and number.

At centre span deflections of between 440 and 460 mm, cracks were observed on the top steel plate. These were accompanied by necking of the steel plate both through the width and thickness. As loading continued, the cracks continued to propagate through the thickness and opened up, until separation and ultimately failure occurred, most frequently in the bottom plate. Typical cracks are shown for the top plate and bottom plate in Figure 6.9.

Failure in all cases was a shear tension failure resulting from exceeding a fracture strain of one or more of the steel plates as described in Tables 6.1 to 6.6. From an examination of the cracks and necking of the plate at the supports, it was concluded that fracture could have occurred at either end. The average angular rotation of the plates over the supports was 29.8 degrees with a coefficient of variation of 0.072. In all cases, regardless of plate thickness or section depth, the ultimate failure mode, centre span deflection, and deflected shape of the structure were about the same.

The deflected shape of composite plate test C203T6 is shown in Figure 6.10. The limits of each region of behaviour are identified.

6.1.2 Steel Plate Test

As a basis for comparison with the composite plate tests, two steel plates, one on top of the other, with no mechanical shear interconnection, were tested. From this

test the contribution of the steel plates alone can be determined. The load centre span deflection curve for this test is shown in Figure 6.1.

Because the span to depth ratio for this plate was large, L/d=205.6, the general behaviour of the plate from the initial stages of loading to ultimate was dominated by membrane behaviour. No flexural behaviour was discernable. Observations during the test support the hypothesis that a cable analysis based on consistent deformations is valid for determining the deformed shape, strain distribution and internal force distribution. The observations were:

1. under transverse load the plate deformed to the shape of the load plates, forming a series of straight line segments with concentrated curvature located at the inside edge of the supports and the edges of the load plates;
2. yield pattern, sequence of loading and propagation of yielding
    a. yield lines parallel to and over the inside edge of the support
    b. parallel yield lines at locations of concentrated curvature
    c. yield lines at 40 - 45 degrees propagating from the support towards the adjacent load point, one end then the other
    d. continuing yielding towards the interior load points
    e. yielding of the centre segment of the plate

f. yield lines at 40 - 45 degrees formed as the section of the plate between the support and the horizontal reaction frame (anchor span), one side then the other.

Straining in any given segment was quite uniform at all load levels.

Although cracks were not observed during the test, an examination of the plates after the test showed that cracks and the associated localized necking existed not only at the support, but also in a less developed stage at several of the locations where the curvature was concentrated. Failure occurred as for the composite plates and as described in the previous section.

6.2 Steel Strain Distributions

Electrical resistance strain gauges located at discrete points along the length of the plates as discussed in Section 3.2.3.6 were used to measure strains up to 25 000 μs. Strains greater than this value were calculated from measurements of the deformed shape of the plate assuming uniform straining over any given segment. Final strains were determined from before and after measurements of the plate dimensions.

Representative steel strain distributions are shown for the top and bottom plates at three load levels, for the steel plate test, C121T6 and C203T6 in Figures 6.11, 6.12 and 6.13, respectively. The first load level corresponds to

the upper limit of the elastic membrane behaviour for the steel plate test and the attainment of the maximum flexural load for the composite plate tests. The second level corresponds to general yielding or strain hardening of the steel plates with increased straining greater than strain hardening of the plate segments between the bulkheads and the first load points. The third level corresponds to fully developed membrane behaviour for all the tests.

For the composite tests, the strains at the maximum flexural load were relatively small. The strains for the top plate were tensile and maximum over the supports and decreased in magnitude to a small tensile or even a compressive strain at centre span. The strains for the bottom plate were tensile and maximum at centre span and decreased to a small tensile value at the supports. The strains for the steel plate test at the first load level were generally equal to or just less than the yield strain along the length of the plate, except for the plate segments between the bulkheads and the first load points where strain hardening existed.

At the second load level, general yielding or strain hardening of the steel plates and increased straining greater than strain hardening for both plates in the steel plate test and for the top plate in the composite test for the plate segment between the supports and the first load point occurred. For all cases at load level three, the strains over the inside edges of the supports, for both the

top and bottom plates, were extremely large (125 000 μs). At midspan the strains dropped down to strain hardening strain or less. Steel strain measurements were compared to the strains calculated from the behavioural models described in Chapter 7.

6.3 Concrete Strain Distributions

Concrete strains were measured at the locations shown in Figure 3.13 at the load levels corresponding to the ultimate flexural capacity of the composite plates. These measurements have marginal utility for two reasons: (i) the exact state of stress is not known and therefore the transformation of strains to stresses and hence internal forces is questionable; and (ii) the strains were measured over a finite gauge length which encompassed regions containing cracked or crushed concrete, non-uniform straining makes the interpretation of the data difficult. Because of this, measurements were made only once. However, qualitative information about the interaction between the steel plates and the concrete core can be deduced from the measurements as can the relative magnitude of the load carried by the concrete and whether or not the concrete was in tension or compression. Concrete and steel strains corresponding to the flexural capacity of the composite plate, for test C152T4, are shown in Figure 6.14 and 6.15, respectively.

Figure 6.14 suggests that the concrete will be cracked in tension in the upper fibres over the support and in the bottom fibres near midspan where large crack widths would be expected. The upper concrete fibres at midspan are heavily strained in compression as are the bottom fibres at the supports. From Figure 6.15 the steel strains of the bottom plate are always tensile while the top plate has compressive strains in the positive moment region.

Because these strains were determined using a mechanical extensometer, they represent the average strain over the gauge length. For tensile strains in the concrete exceeding 250 μs (the fracture strain suggested in Section 4.2.4.3), the corresponding changes in length (deformations) between gauge points have been calculated and are shown in brackets in Figure 6.14. The deformations are generally concentrated at single cracks and are good indications of the crack widths.

6.4 Slip Distributions

Slip or differential displacement of two materials along an interface results from the rigid body displacements (sliding) of one body with respect to the other and/or the accumulation of differential in-plane straining, of the materials. For the case when local slip is due to accumulated differential in-plane straining defined as the total difference in elongation of the two materials, then

[6.1] $$\omega_x = \int_0^x (\epsilon_{sx} - \epsilon_{cx})dx$$

where: ω_x = Local slip, mm
ϵ_{sx} = Longitudinal in-plane strain in the steel at a distance "x" from a point of zero slip, mm/mm
ϵ_{cx} = Longitudinal in-plane strain in the concrete at a distance "x" from a point of zero slip, mm/mm

Slips were measured along the length of the plate when the ultimate flexural capacity was reached. Typical slip distributions, corresponding to the concrete and steel strains described in Section 6.3, are shown for test C152T4 in Figure 6.16. These distributions were corroborated by additional measurements of the relative movements of the Demec points. There are several interesting features:

1. essentially zero slip occurred at the point of symmetry, centre span, and at the ends of the plate element;
2. the slip distributions are symmetric about the centre line of the test span; and
3. the direction of slip, the relative movement of the steel plate with respect to the concrete core, for the top plate and bottom plate within the span are opposite.

The first two features are a function of the load pattern and boundary conditions while the last is a result of the large deformation behaviour and fracture of the concrete core. To accommodate large curvature changes, the concrete core fractured into wedge shape pieces and formed a series of straight line segments with the angle changes concentrated at crack locations. The steel plates, like

flexible skins, stretched over and contained the concrete. As the curvature increased, the in-plane force of the steel plate acting on the concrete caused the wedge to splinter, resulting in a fan like array of cracks and a more gradual change in slope. This action depends upon the thickness of the steel plate and the depth of the concrete core.

Because the steel plate was not mechanically interconnected to the concrete it was able to slip on it. For the left hand half of the composite plate, as wedges formed and cracks opened, the top plate slipped to the left relative to the concrete. Although the steel plate was straining in tension (large strains), the rigid body movement of the wedge adjacent to the top plate exceeded the total extension of the steel plate. This combined slip action is shown in Figure 6.17. The extension of the bottom steel plate exceeded the combined straining and rigid body movement of the concrete, resulting in a relative slip of the steel to the right.

If slip and/or splintering was not allowed to occur in regions of tension, then large crack openings in the concrete will cause localized straining of the steel plate, which may be sufficiently large to cause rupture and premature failure of the plate element.

6.5 Restraint Measurements

6.5.1 Horizontal Restraint Frame

The response of the horizontal restraint frame to the test plates under load is shown in Figures 6.5 and 6.6 for tests of constant plate thickness and tests of constant section depth, respectively. While a compressive load in the frame is equivalent to a tensile load in the test plate, some of the tension within the test span is taken out as shear in the bulkheads.

The curves can best be described by first examining the behaviour in the steel plate test. The zero offset, exhibited in all tests, but marked for the steel plate test, corresponds to the load induced in the specimen due to weld shrinkage. Upon applying a transverse load, a load is introduced into the frame at an approximate rate of 2.5 kN per kilonewton of applied load. The slightly nonlinear response is a function of the small deflections, the boundary movements and the resulting geometry of the deformed membrane. At an applied load of 830 kN, there is a sharp change in the slope of the curve due to yielding of the plate segment between the bulkheads and the first load points. Deflections increased rapidly with significant changes in geometry. Subsequent yielding of the other segments of the test span had little effect on the force in the horizontal restraint frame. Another discrete change in slope occurs when yielding and strain hardening of the

anchor spans adjacent to the test span takes place. Near failure the curve flattens as a result of large deformations with the steep slope of the membrane transferring the transverse load more effectively into the bulkheads.

The curves for the composite plate tests are similar to that of the steel plate test with two major differences:

1. the increase in length of the composite plate in flexure resulted in an outward movement of the bulkheads and a decrease in load in the external frame. The initial compression in the restraint due to weld shrinkage decreased. Not until the flexural capacity of the section was reached did the frame start to restrain the test plates as described in Section 6.1.1 (point 'B' on the curve for test C203T6);
2. the rate at which the load in the restraint frame developed decreased sooner and less rapidly as a result of non-uniform straining, yielding and strain hardening.

Both effects become more pronounced with increasing section depth. For tests of different plate thickness, the curves exhibit the same characteristics, but in different proportions.

6.5.2 Vertical End Restraint

Measurements were made of the vertical end restraining force required to maintain the anchor (adjacent) spans in an horizontal orientation. This load, in addition to the rotational restraint generated by the bulkheads, provided

the reaction necessary to develop the negative moment capacity of the plate. The maximum force was reached when the test plate reached its flexural capacity. Subsequently, the restraining force decreased slightly and then remained essentially constant throughout the remainder of the test.

6.5.3 Lateral Confinement Devices

The passive lateral confinement devices were provided to simulate the lateral confinement of surrounding concrete in a real structure. The loads measured in the load rods of the lateral confinement devices were extremely small. Calculated values of pressure developed by the passive confinement devices did not exceed a maximum pressure of 2 MPa with an average of only 0.2 MPa. Maximum pressures occurred during flexural behaviour, just prior to compression failure of the concrete. The pressures then diminished with increasing deflection of the plate. The transverse pressures across the width did not develop as anticipated because the concrete simply expanded through the thickness in the direction of least resistance. This is supported by measurements which indicated an overall increase in thickness of the composite plate. The state of stress in the concrete was therefore essentially uniaxial.

6.6 Final Strain Measurements

Prior to testing and after failure, the steel plate thicknesses and widths were measured at a number of locations along the length of the member, as shown in Figure 6.18. Based on these measurements, strains across the width, through the thickness and along the length were calculated using Equations 6.2, 6.3, and 6.4, respectively.

$$[6.2] \qquad \epsilon_w = \ln\left(\frac{w_f}{w_o}\right)$$

where:
- ϵ_w = True strain across the width of the steel plate, mm/mm
- w_f = Width of the steel plate after failure, mm
- w_o = Original width of the steel plate, mm

$$[6.3] \qquad \epsilon_t = \ln\left(\frac{t_f}{t_o}\right)$$

where:
- ϵ_t = True through-thickness strain in the steel plate, mm/mm
- t_f = Thickness of the steel plate after failure, mm
- t_o = Original thickness of the steel plate, mm

$$[6.4] \qquad \epsilon_\ell = \ln\left(\frac{A_f}{A_o}\right)$$

where:
- ϵ_ℓ = True longitudinal strain in the steel plate, mm/mm
- A_f = Area of the steel plate after failure, mm^2
- A_o = Original area of the steel plate, mm^2

Strain distributions and strain ratio distributions (ϵ_w/ϵ_ℓ, ϵ_t/ϵ_ℓ) are shown for a typical test, C121T6, for the top and bottom plates in Figures 6.19 to 6.22. The strains and strain ratios are plotted as absolute values.

The strain distributions shown in Figure 6.19 and 6.21 exhibit several interesting features. The distributions are symmetric about centre span and parallel which indicates symmetrical loading conditions and excellent repeatability. The parallelism of the curves suggest a strong correlation between strains across the width, through the thickness and along the length. "Spikes" in the strain distributions are the result of local necking or thinning of the plate at locations where significant angle changes occurred. The largest of these spikes are at the edge of the span adjacent to the bulkheads. In general, the strains across the width are considerably less than the through-thickness strains, which are an appreciable fraction of the longitudinal strains.

The strain ratio distributions, shown in Figure 6.20 and 6.22, indicate that the state of stress imposed on the plate was between that of uniaxial stress and plane strain. Based on the assumption of zero volume change for plastic straining, the ratio of strains ϵ_w/ϵ_ℓ and ϵ_t/ϵ_ℓ for a state of uniaxial stress are 0.5. For a state of plane strain the strain across the width is zero and the through-thickness strain is ϵ_ℓ. Thus the strain ratio ϵ_w/ϵ_ℓ is zero and the absolute value of the strain ratio ϵ_t/ϵ_ℓ is 1.00. Figures 6.22 and 6.23 show that the strain ratio ϵ_w/ϵ_ℓ lies between zero and 0.5 as suggested and the strain ratio ϵ_t/ϵ_ℓ lies between 0.5 and 1.00. For the bottom plate at the supports, the strain ratios of zero and one indicate a plane strain

condition there.

Table 6.1 HISTORY OF STEEL PLATE TEST

DATE	OBSERVATION AND/OR EVENT	BEHAVIOUR	LOAD STEPS	LOAD RANGE[1] kN	DEFLECTION RANGE[2] mm
86 05 06	•Initial sag removed by tightening load transfer plates to the horizontal restraint frame	flexural	1 - 2	0	0.0 to 9.2
	•Remaining portion of the initial load sequence	membrane	3 - 9	0 - 24	9.1 to 18.4
86 05 07	•Continued loading	membrane	10 - 17	24 - 72	18.4 to 44.4
86 05 08	•Continued loading	membrane	18 - 40	72 - 532	44.4 to 124.6
	•Unloaded	membrane	41 - 46	532 - 98	124.6 to 71.3
	•Increased stiffness of box plate elements by providing additional stiffness at column locations				
86 05 09	•Continued loading	membrane	47 - 94	98 -1672	71.3 to 295.1
86 05 10	•Adjusted jacks				
	•Continued loading	membrane	59 - 93	1672 - 3127	250.4 to 490.2
	•Shear failure, bottom plate south end				

Notes: 1. The load given is the sum of the loads acting on the span between the bulkhead supports.
2. The Deflection is given at centre span and is positive downwards.

Table 6.2 HISTORY OF COMPOSITE TEST C121T6

DATE	OBSERVATION AND/OR EVENT	BEHAVIOUR	LOAD STEPS	LOAD RANGE kN	DEFLECTION RANGE mm
	d = 121.0 mm, t = 6.35 mm, L/r = 25				
86 05 24	•Initial load sequence	flexural	1 - 12	0 - 39	0.0 to 13.2
	•Continued loading	flexural	13 - 20	39 - 139	13.2 to 50.3
		flexural membrane	21 - 27	139 - 180	50.3 to 80.1
86 05 25	•Continued loading	flexural membrane	27 - 41	180 - 625	80.1 to 140.1
		membrane	42 - 58	625 - 1285	140.1 to 250.4
86 05 26	•Adjusted jacks •Continued loading •shear failure, bottom plate, south end	membrane	59 - 93	1285 - 3021	250.4 to 490.2 ≅494.6

Notes: 1. The load given is the sum of the loads acting on the span between the bulkhead supports.
2. The Deflection is given at centre span and is positive downwards.

Table 6.3 HISTORY OF COMPOSITE TEST C152T6

DATE	OBSERVATION AND/OR EVENT	BEHAVIOUR	LOAD STEPS	LOAD RANGE kN	DEFLECTION RANGE mm
	d = 152.4 mm, t = 6.35 mm, L/r=20				
86 06 01	•Initial load sequence	flexural	1 - 10	0 - 50	0.0 to 10.1
	•Continued loading	flexural	11 - 16	51 - 196	10.1 to 40.2
		flexural membrane	17 - 31	196 - 295	40.2 to 100.1
86 06 02	•Continued loading	flexural membrane	32 - 40	295 - 600	100.1 to 140.1
		membrane	41 - 60	600 - 1515	140.1 to 300.2
	•Adjusted jacks •Continued loading	membrane	61 - 76	1515 - 2252	300.2 to 400.2
86 06 03	•Continued loading	membrane	77 - 121	2252 - 3468	400.2 to 555.2
	•Shear failure, bottom plate north end				≅560

Notes: 1. The load given is the sum of the loads acting on the span between the bulkhead supports.
2. The Deflection is given at centre span and is positive downwards.

Table 6.4 HISTORY OF COMPOSITE TEST C152T4

DATE	OBSERVATION AND/OR EVENT	BEHAVIOUR	LOAD STEPS	LOAD RANGE kN	DEFLECTION RANGE mm
	d = 152.4 mm, t = 4.76 mm, L/r = 20				
86 06 08	•Initial load sequence	flexural	1 - 12	0 - 47	0.0 to 10.1
	•Continued loading	flexural	13 - 18	47 - 179	10.1 to 40.5
		flexural membrane	19 - 38	179 - 484	40.5 to 130.2
86 06 09	•Adjusted jacks •Continued loading(19 load steps of data on fluke lost)	membrane	60 - 87	1076 - 2003	280.2 to 460.2
	•Knife edge plates slipped		88 - 89		≅464
	•Relocated knife edge plates and made necessary corrections				
86 06 10	•Continued loading •Shear failure, both plates south end	membrane	90 - 101	2003 - 2263	460.0 to 515.2

Notes: 1. The load given is the sum of the loads acting on the span between the bulkhead supports.
2. The Deflection is given at centre span and is positive downwards.

Table 6.5 HISTORY OF COMPOSITE TEST C152T3

DATE	OBSERVATION AND/OR EVENT	BEHAVIOUR	LOAD STEPS	LOAD RANGE kN	DEFLECTION RANGE mm
	d = 152.4 mm, t = 3.175 mm, L/r = 20				
86 06 15	•Initial load sequence	flexural	1 - 10	0 - 37	0.0 to 13.3
	•Continued loading	flexural	11 - 16	37 - 110	13.3 to 35.1
		flexural membrane	16 - 31	110 - 157	35.1 to 100.1
86 06 16	•Continued loading	flexural membrane	32 - 40	152 - 196	100.1 to 135.2
	•Adjusted jacks	membrane	41 - 60	195 - 475	135.2 to 300.1
	•Continued loading	membrane	61 - 73	475 - 723	300.1 to 400.1
86 06 17	•Continued loading	membrane	74 - 104	723 - 974	400.1 to 530.2
	•shear failure, bottom plate, south end				≅533.4

Notes: 1. The load given is the sum of the loads acting on the span between the bulkhead supports.
2. The Deflection is given at centre span and is positive downwards.

Table 6.6 HISTORY OF COMPOSITE TEST C203T6

DATE	OBSERVATION AND/OR EVENT	BEHAVIOUR	LOAD STEPS	LOAD RANGE kN	DEFLECTION RANGE mm
		d = 203.2 mm, t = 6.35 mm, L/r = 15			
86 06 22	•Initial load sequence	flexural	1 - 9	0 33.1	0.0 to 3.3
	•Continued loading	flexural	10 - 16	33 - 303	3.3 to 30.5
		flexural membrane	17 - 32	303 - 450	30.5 to 100.2
86 06 23	•Continued loading	flexural membrane	33 - 42	450 - 695	100.2 to 140.2
		membrane	43 - 64	695 - 1511	140.2 to 300.2
	•Adjusted jacks •Continued loading	membrane	65 - 80	1511 - 2334	300.2 to 400.1
86 06 24	•Continued loading	membrane	81 - 115	2334 - 3316	400.1 to 525.1
	•Shear failure, bottom plate, south end				≅528.2

Notes: 1. The load given is the sum of the loads acting on the span between the bulkhead supports.
2. The Deflection is given at centre span and is positive downwards.

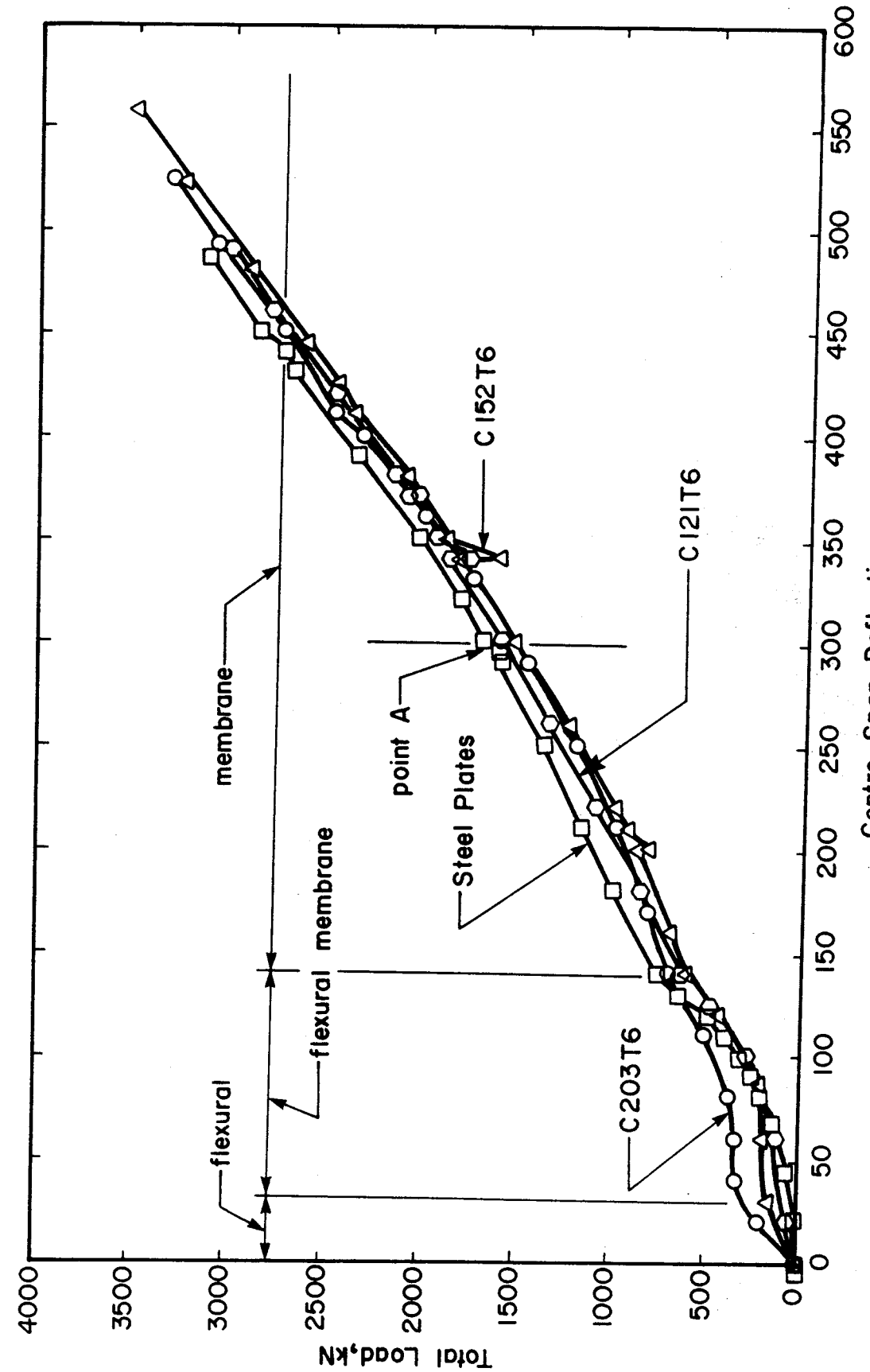

Figure 6.1 LOAD DEFLECTION BEHAVIOUR - CONSTANT STEEL PLATE THICKNESS

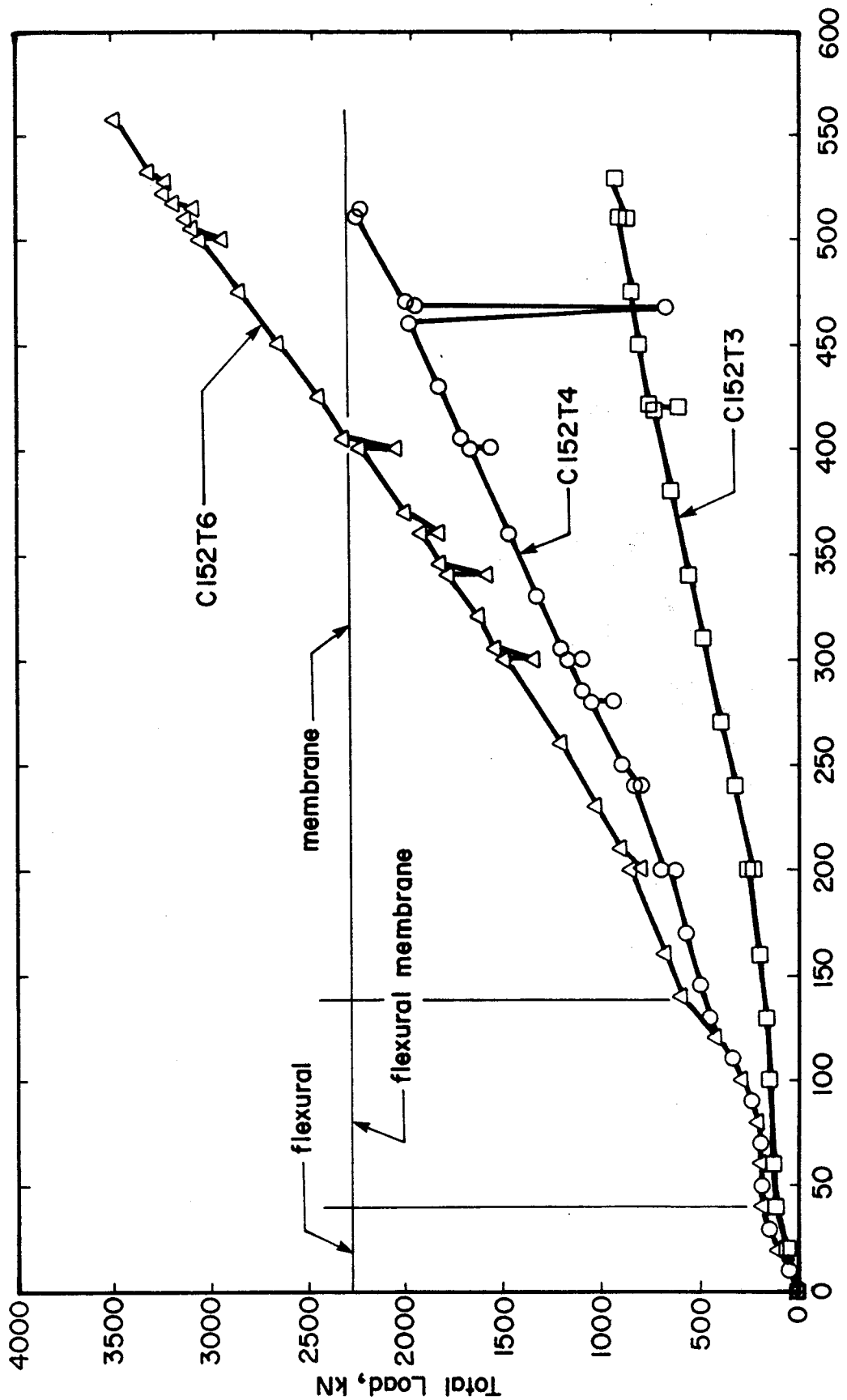

Figure 6.2 LOAD DEFLECTION BEHAVIOUR - CONSTANT SECTION DEPTH

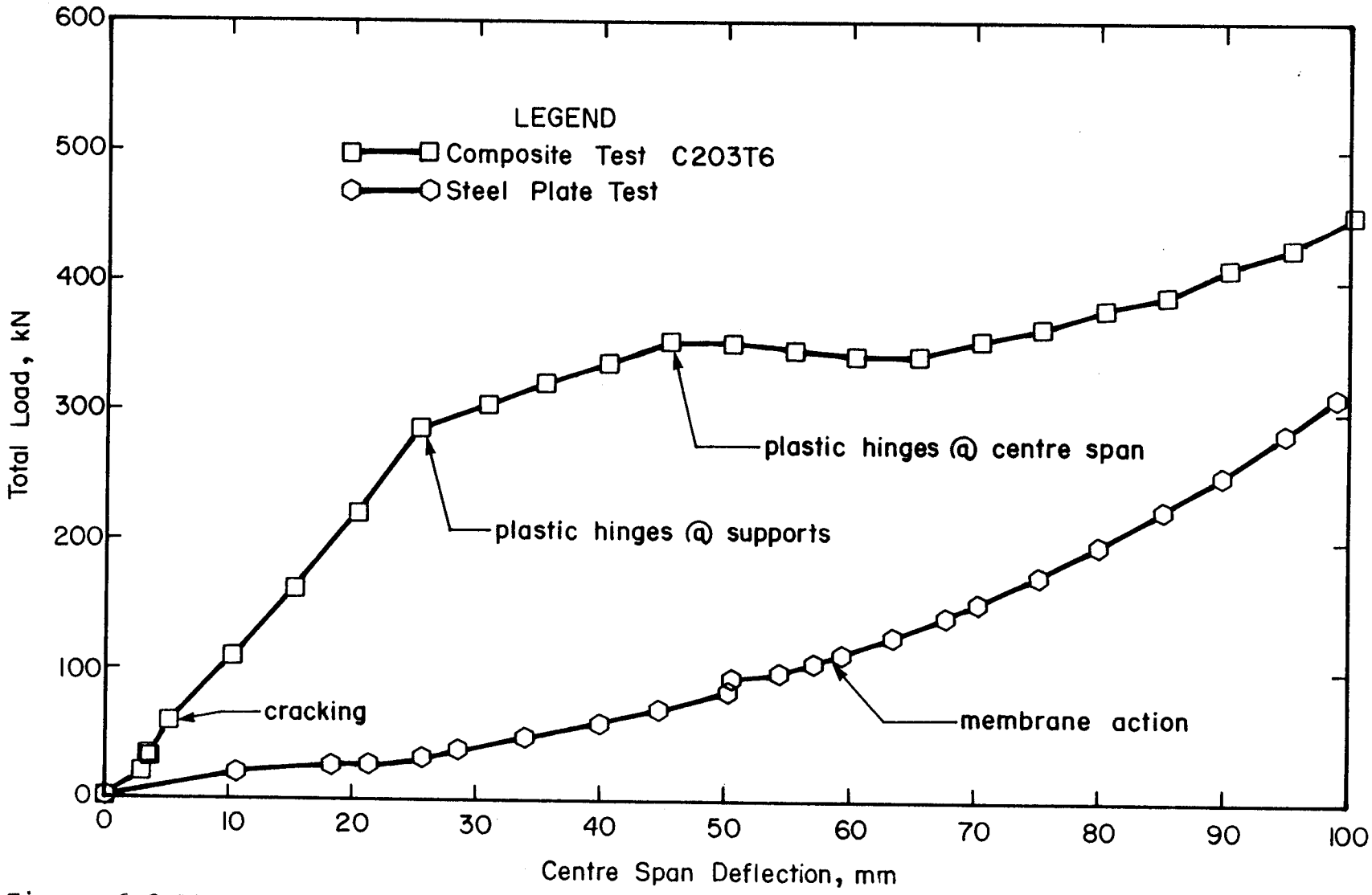

Figure 6.3 FLEXURAL BEHAVIOUR, TEST C203T6, COMPARED TO MEMBRANE BEHAVIOUR, STEEL PLATE TEST

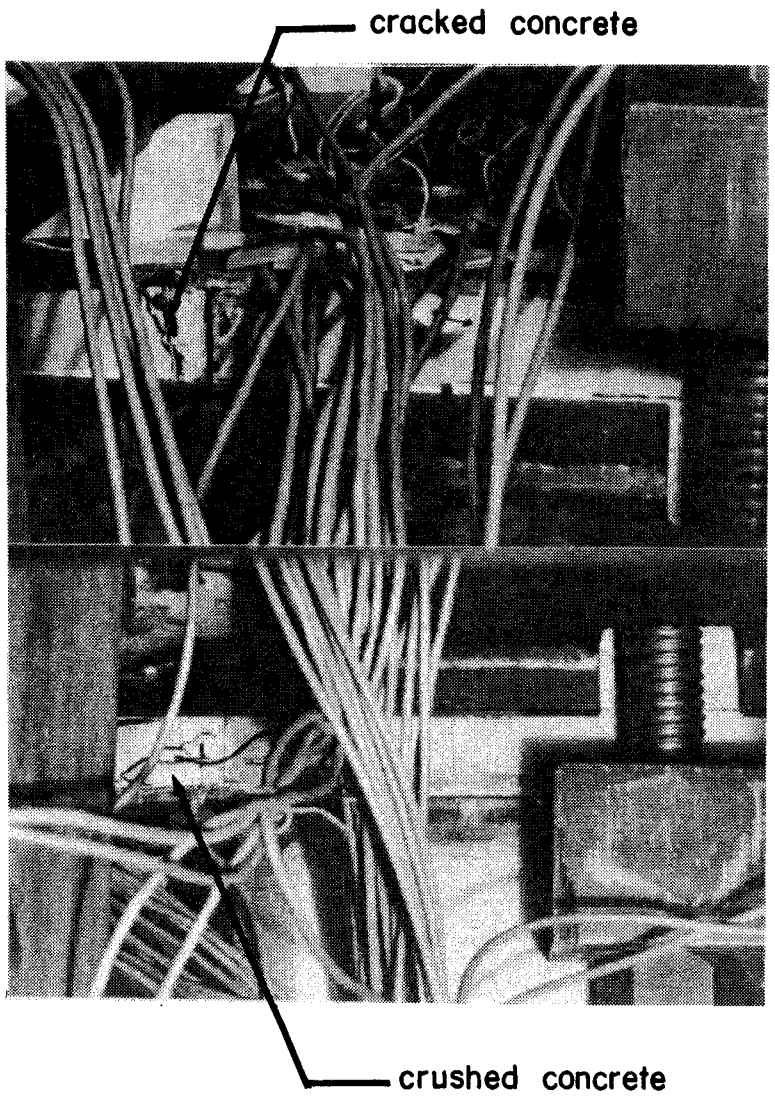

(a) Plastic hinge at the support

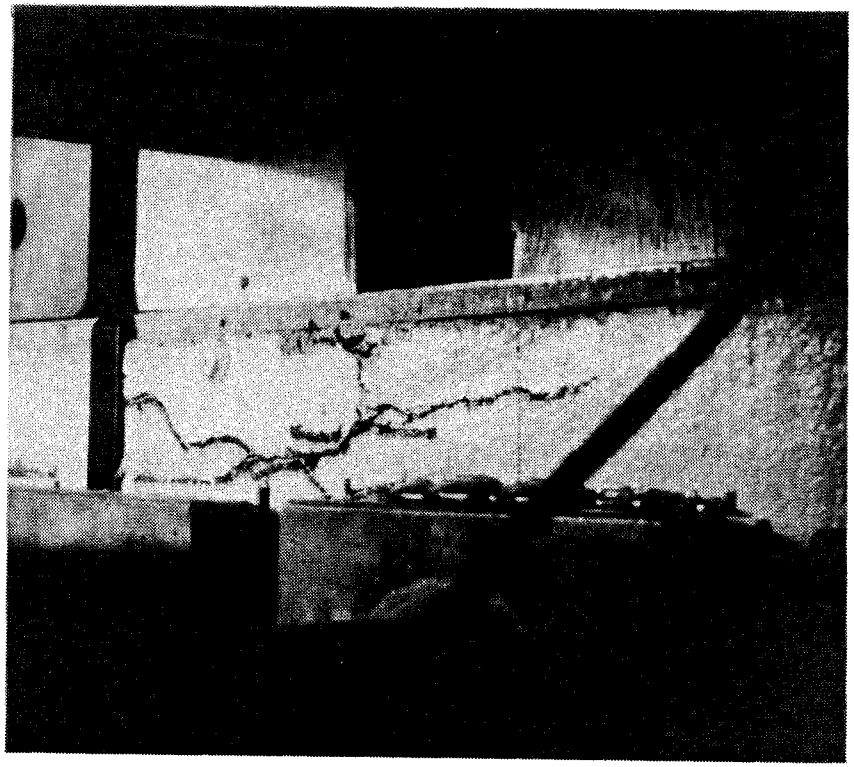

(b) Compression failure at midspan

Figure 6.4 CRACK PATTERNS, FLEXURAL BEHAVIOUR

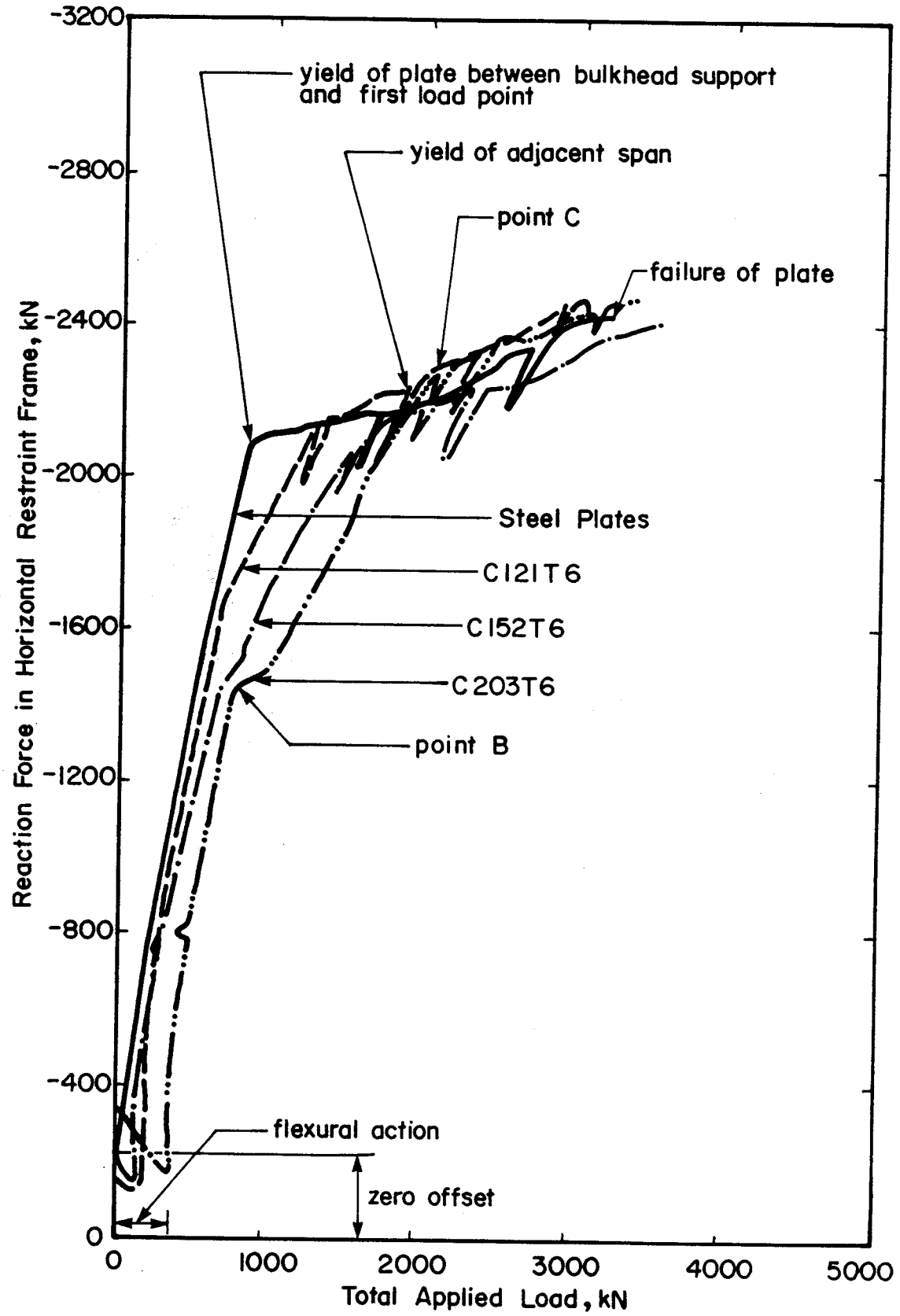

Figure 6.5 HORIZONTAL RESTRAINT - CONSTANT PLATE THICKNESS

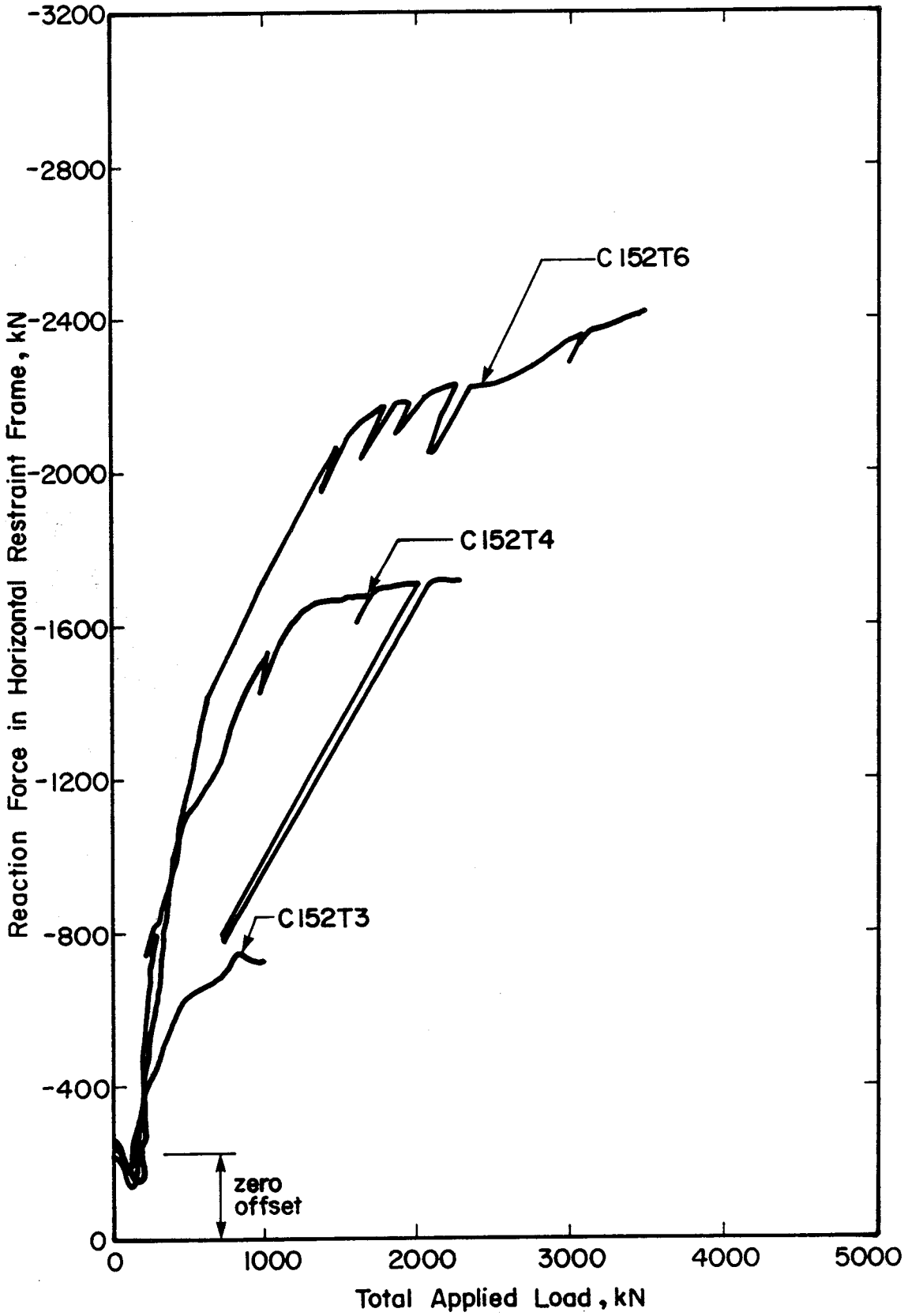

Figure 6.6 HORIZONTAL RESTRAINT - CONSTANT SECTION DEPTH

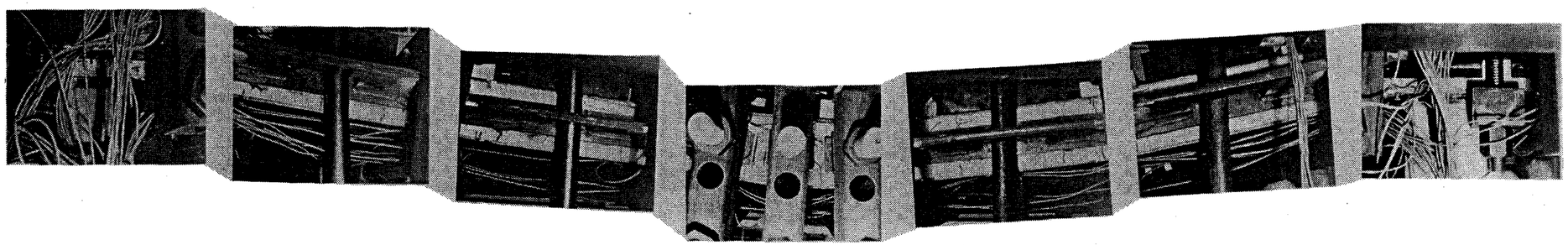

Figure 6.7 CRACK PATTERN, FLEXURAL MEMBRANE BEHAVIOUR

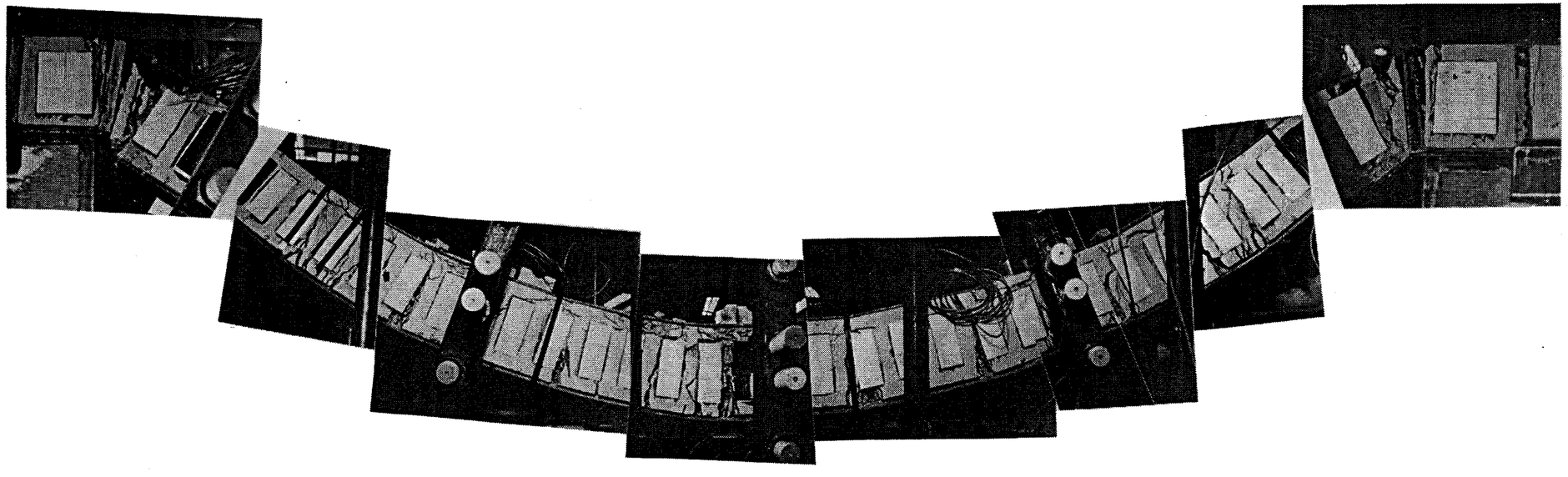

Figure 6.8 CRACK PATTERN, MEMBRANE BEHAVIOUR

(a) Test C152T3, top plate - south end

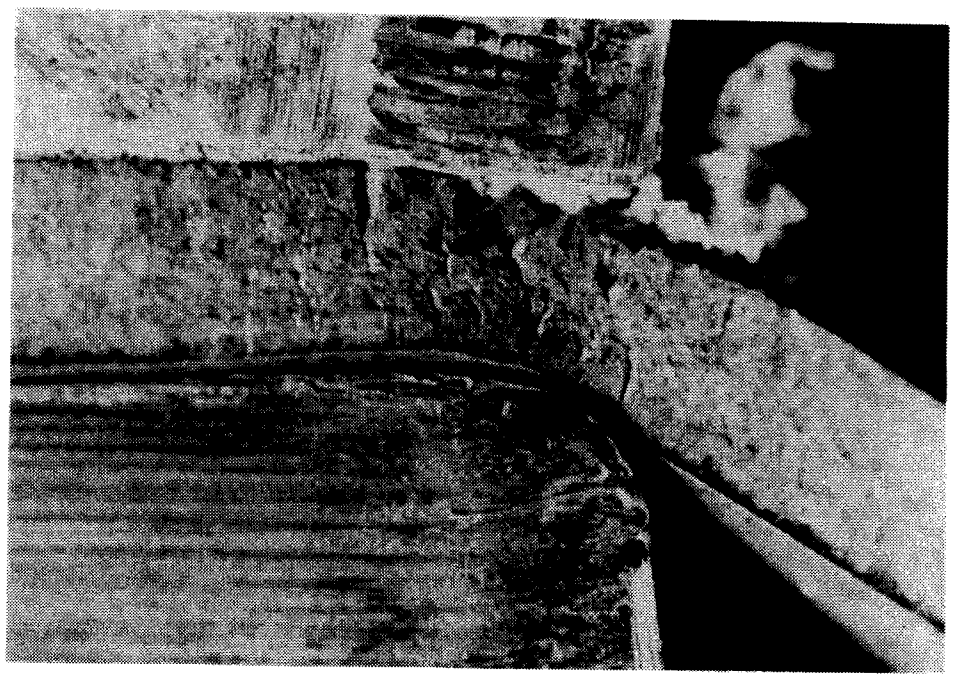

(b) Test C203T6, bottom plate - north end

Figure 6.9 FRACTURE CRACKS IN THE STEEL PLATE

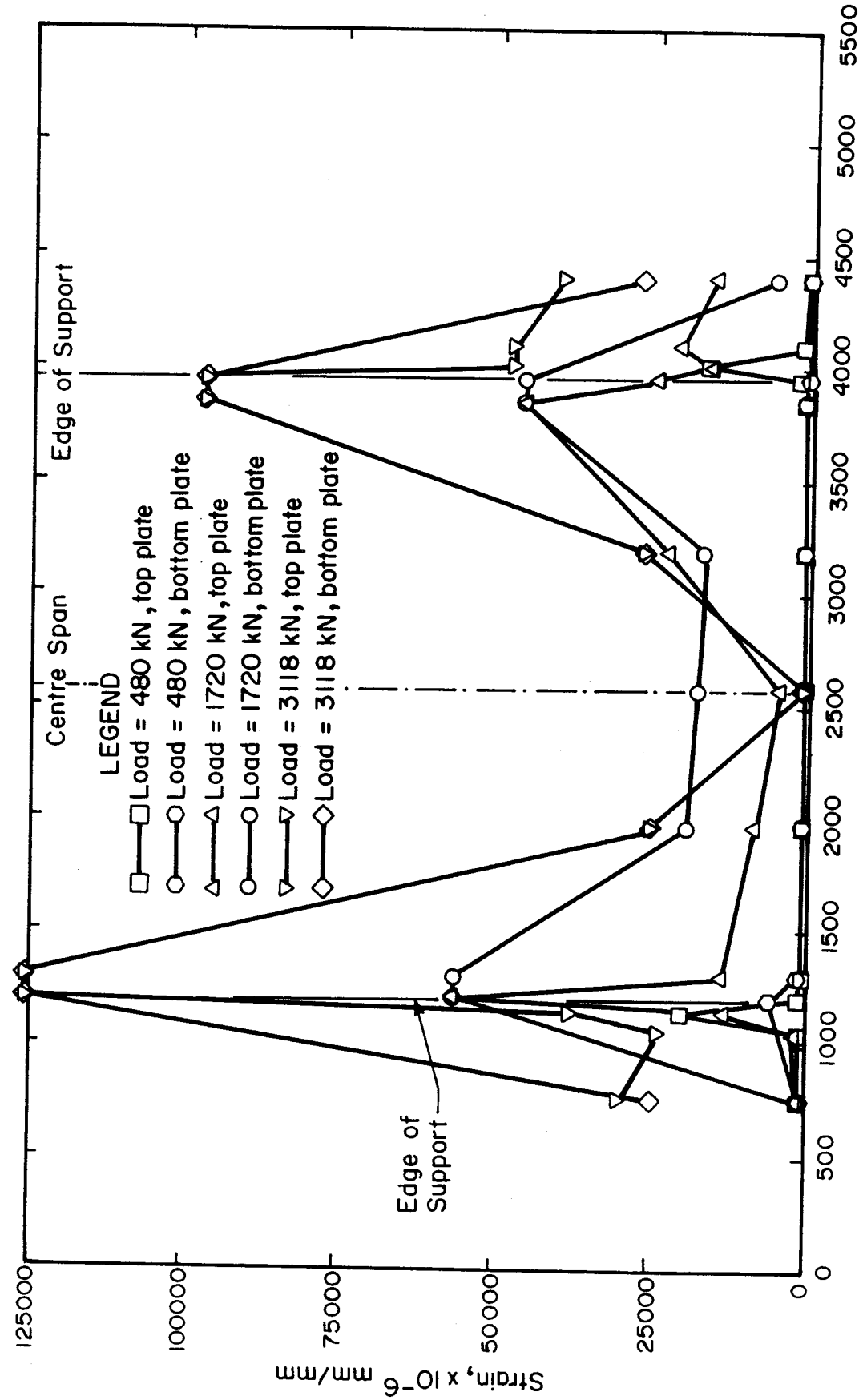

Figure 6.11 STEEL STRAIN DISTRIBUTIONS - STEEL PLATE TEST

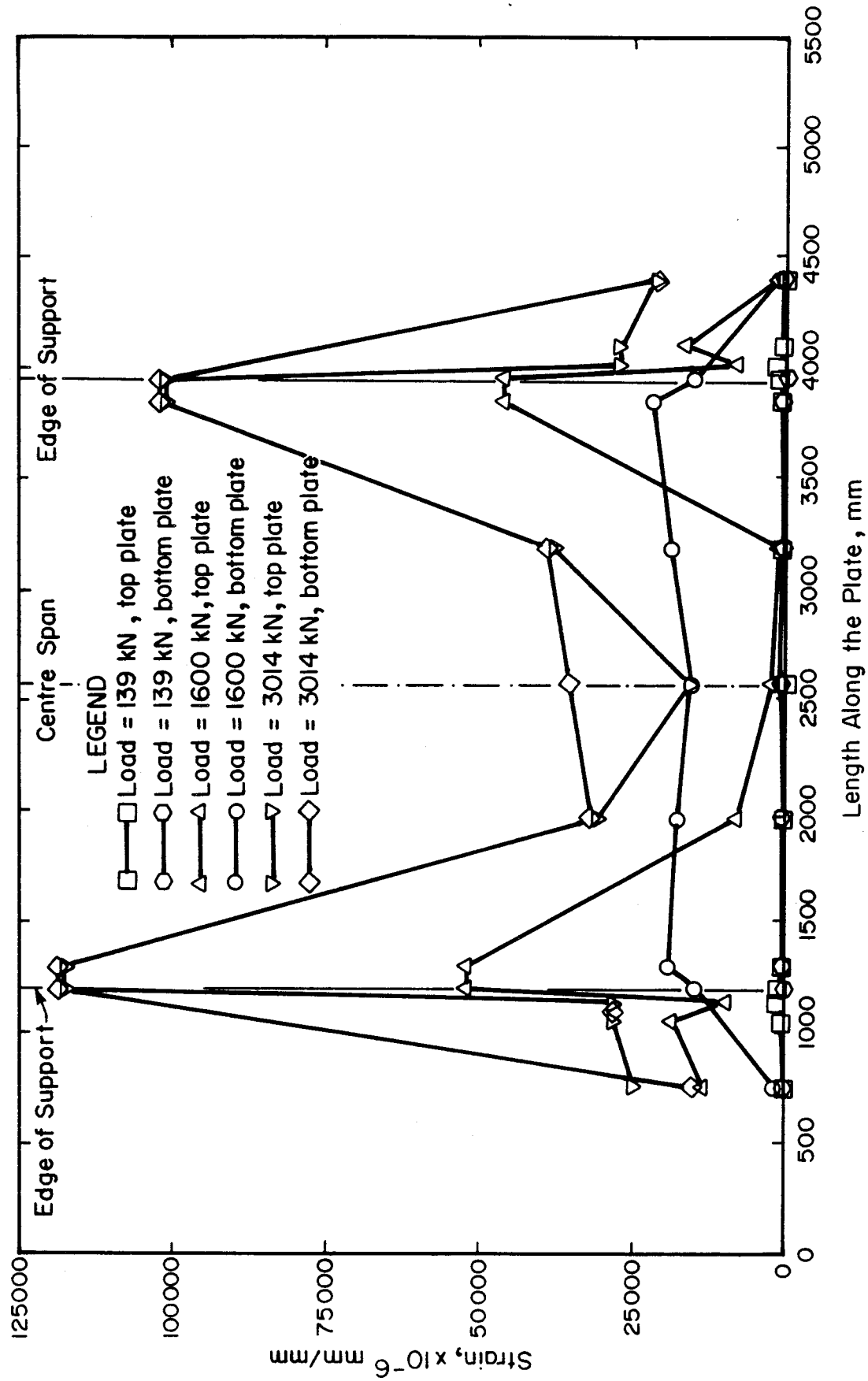

Figure 6.12 STEEL STRAIN DISTRIBUTIONS - TEST C121T6

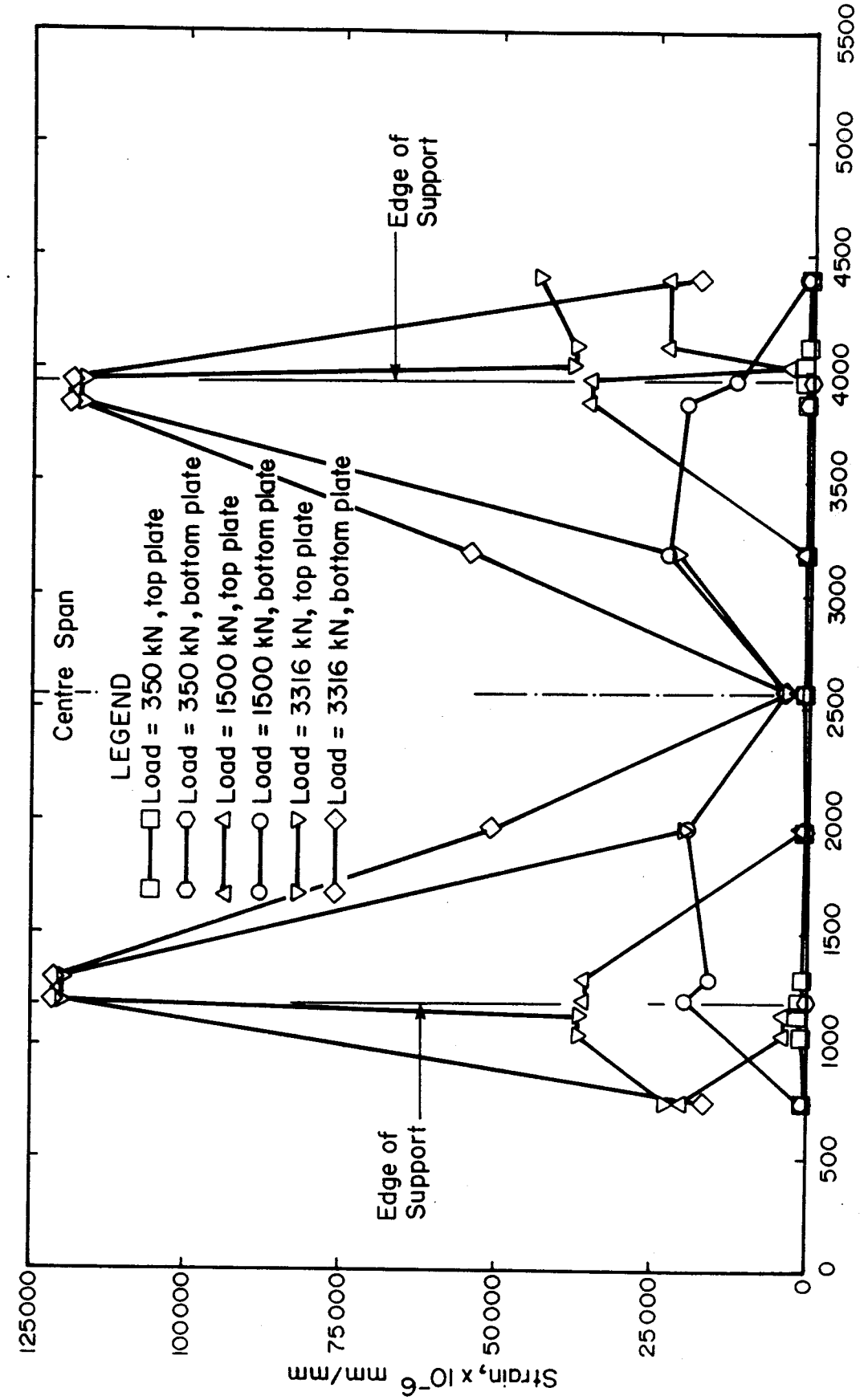

Figure 6.13 STEEL STRAIN DISTRIBUTIONS - TEST C203T6

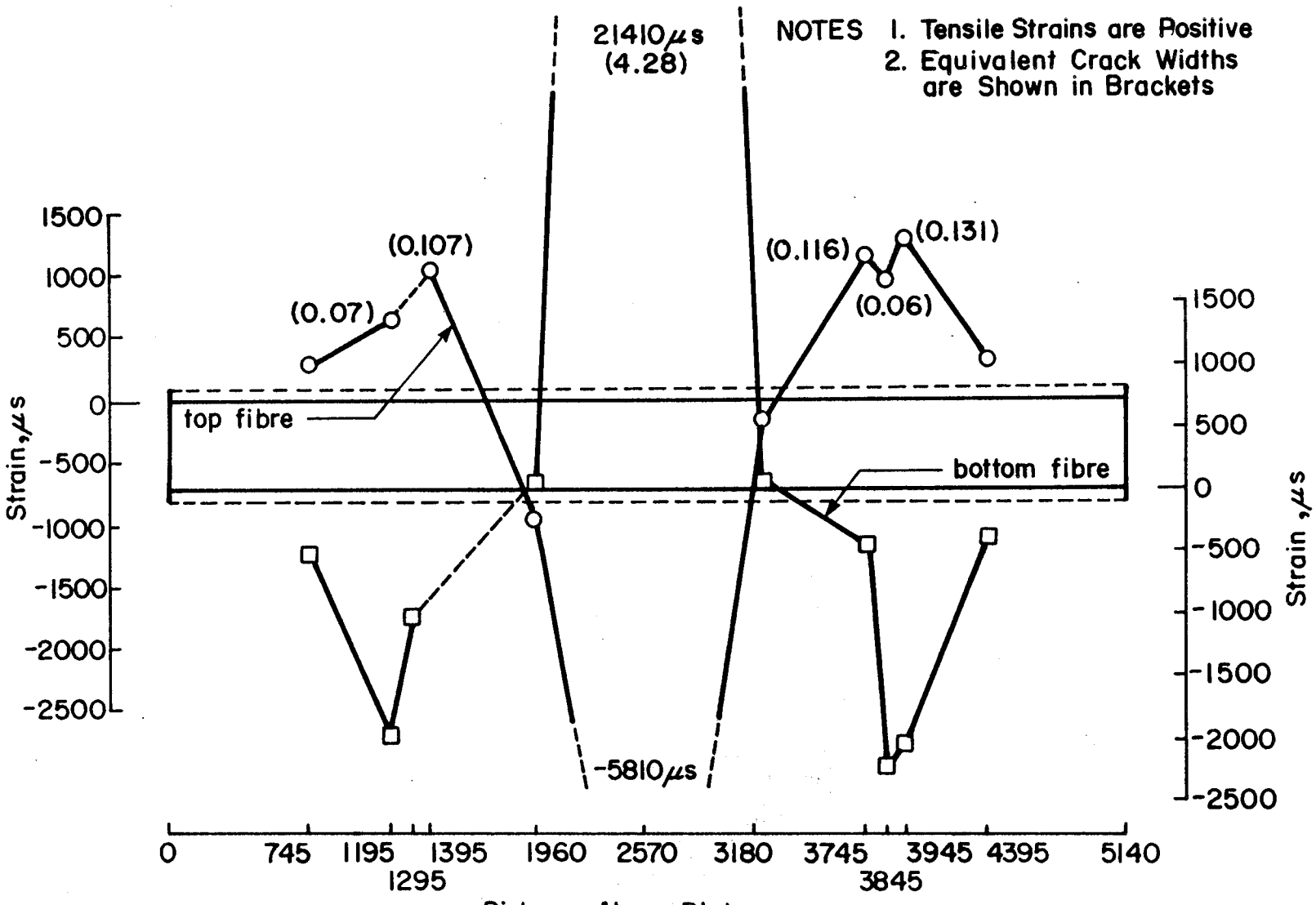

Figure 6.14 CONCRETE STRAINS, TEST C152T4

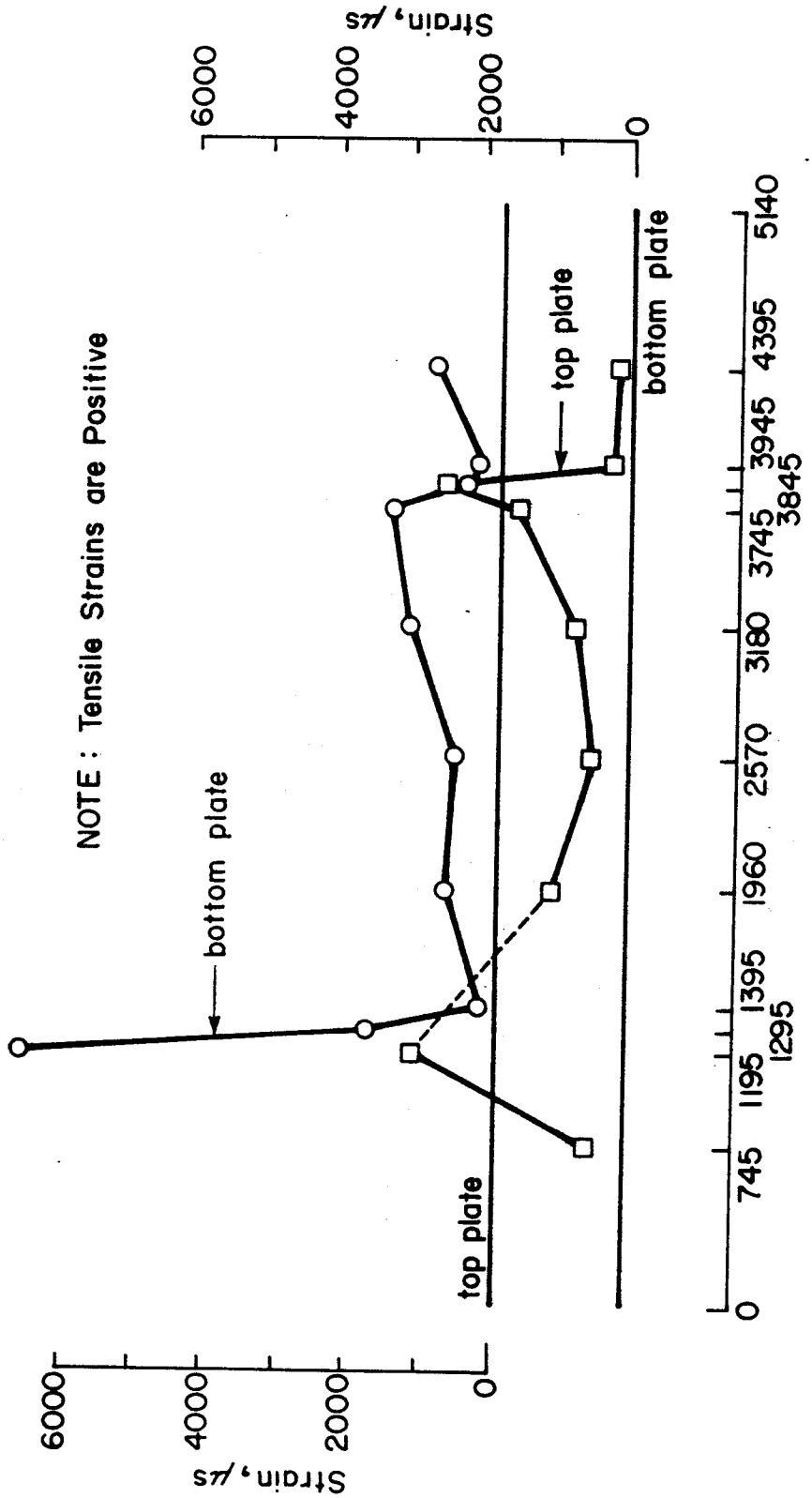

Figure 6.15 STEEL STRAINS, TEST C152T4

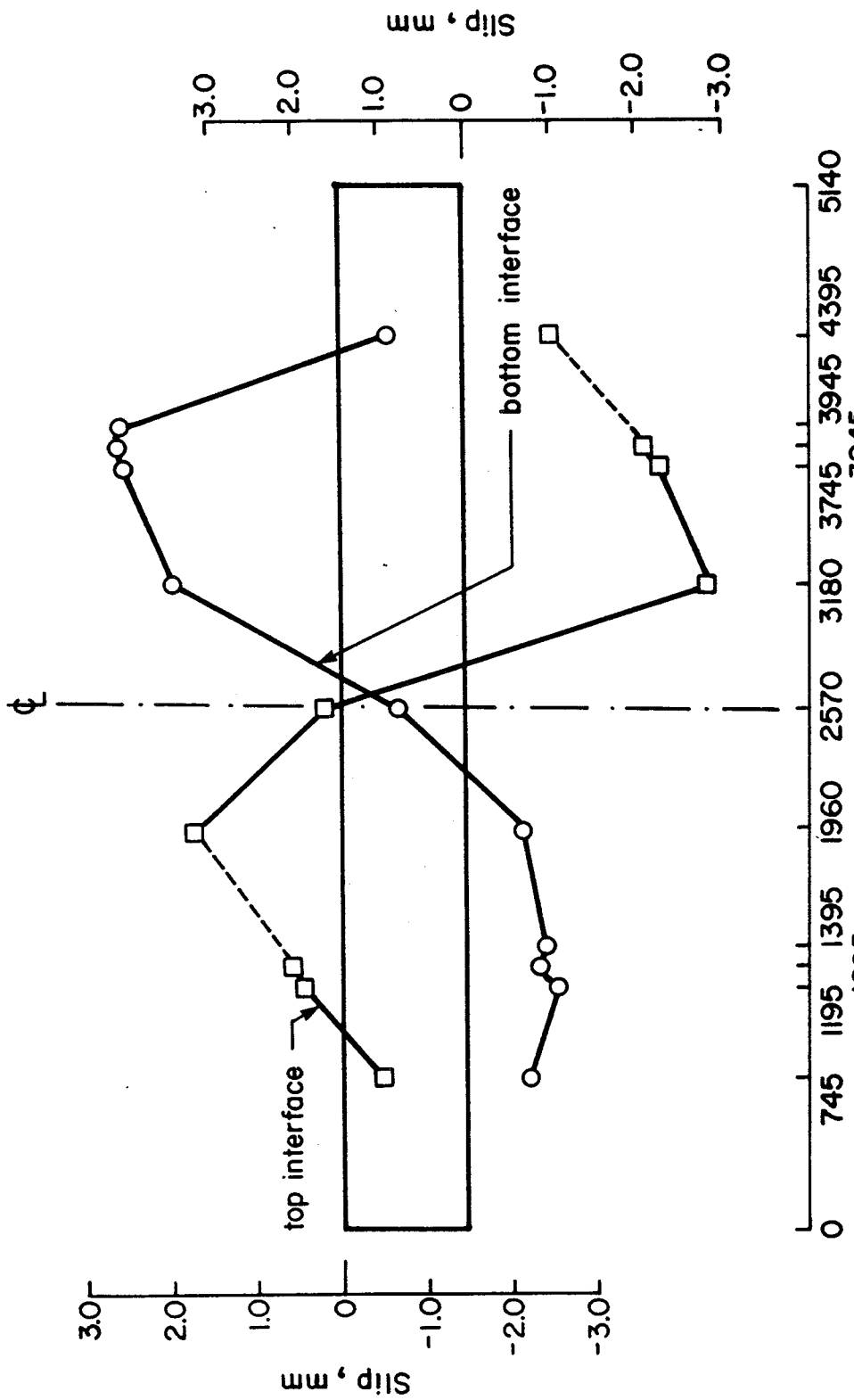

Figure 6.16 SLIP DISTRIBUTIONS, C152T4

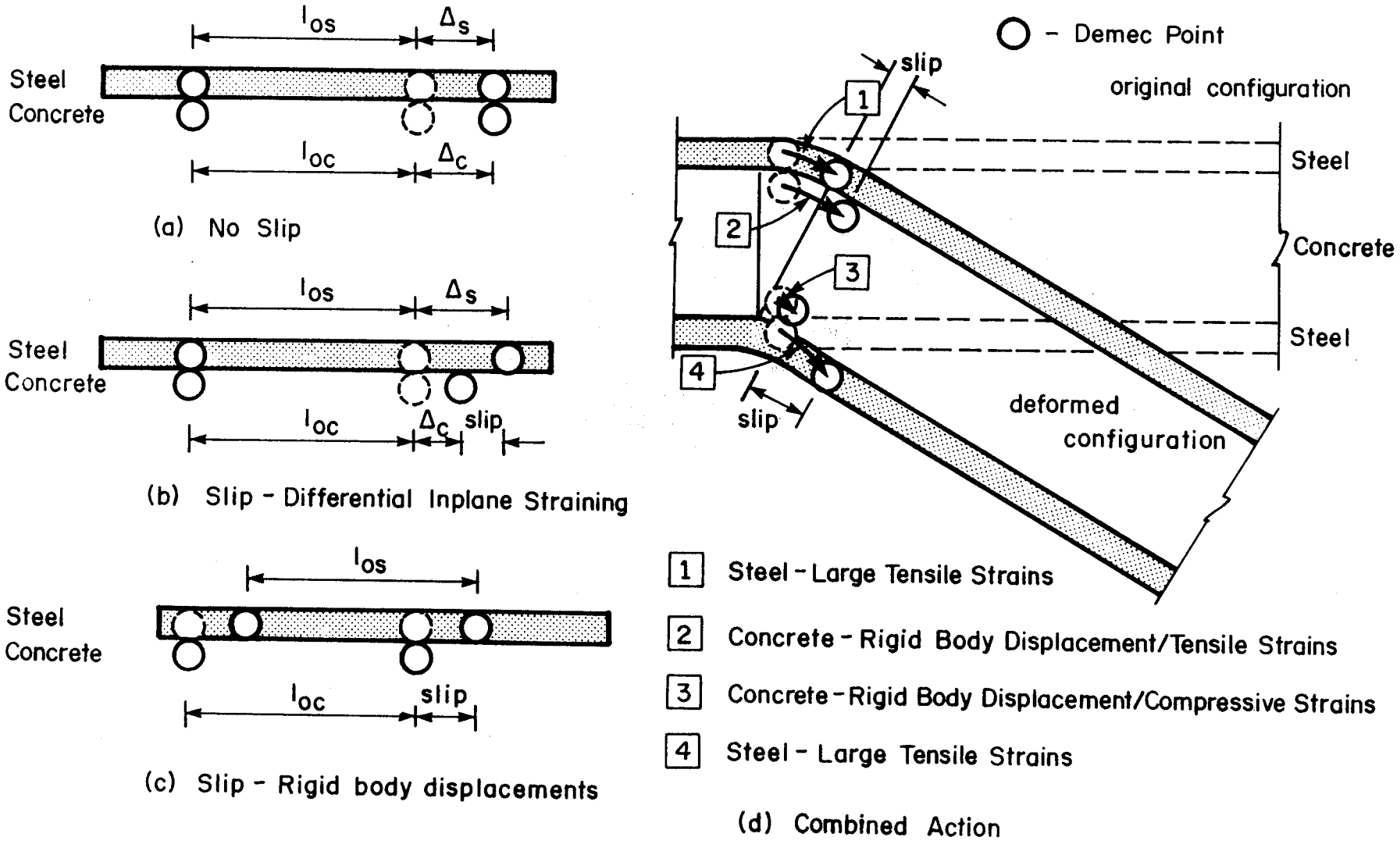

Figure 6.17 MECHANISMS OF SLIP

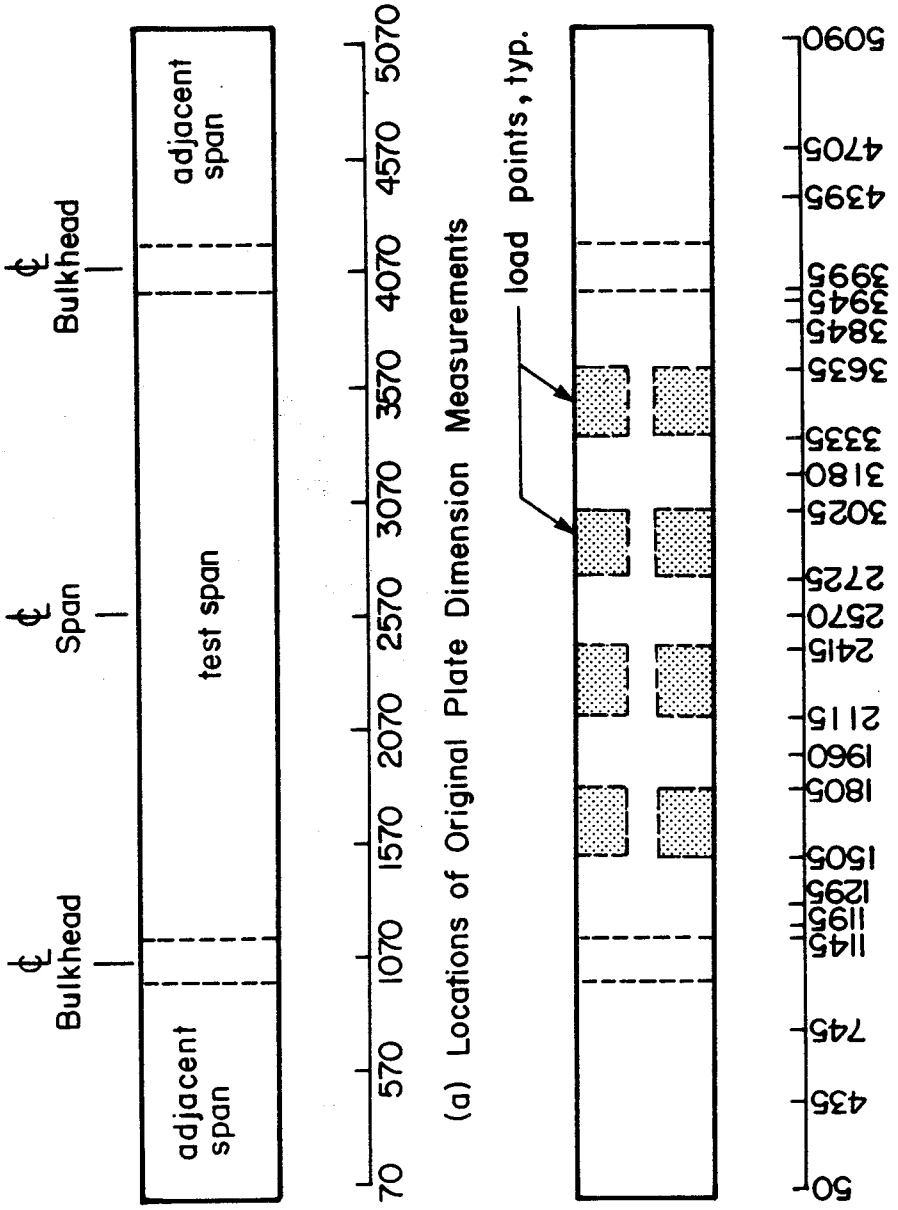

Figure 6.18 LOCATION OF PLATE DIMENSION MEASUREMENTS

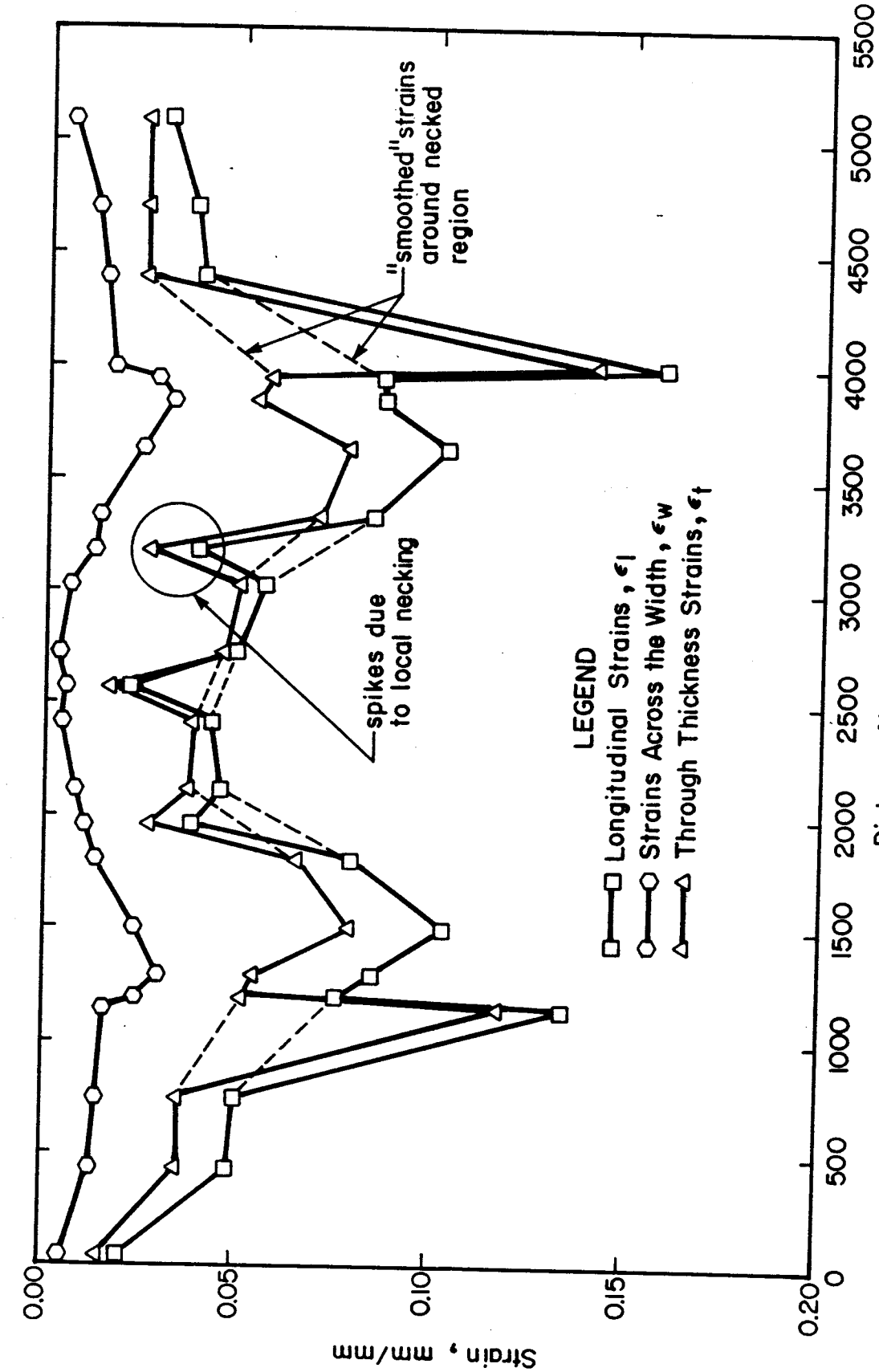

Figure 6.19 STRAIN DISTRIBUTION, TOP PLATE - TEST C121T6

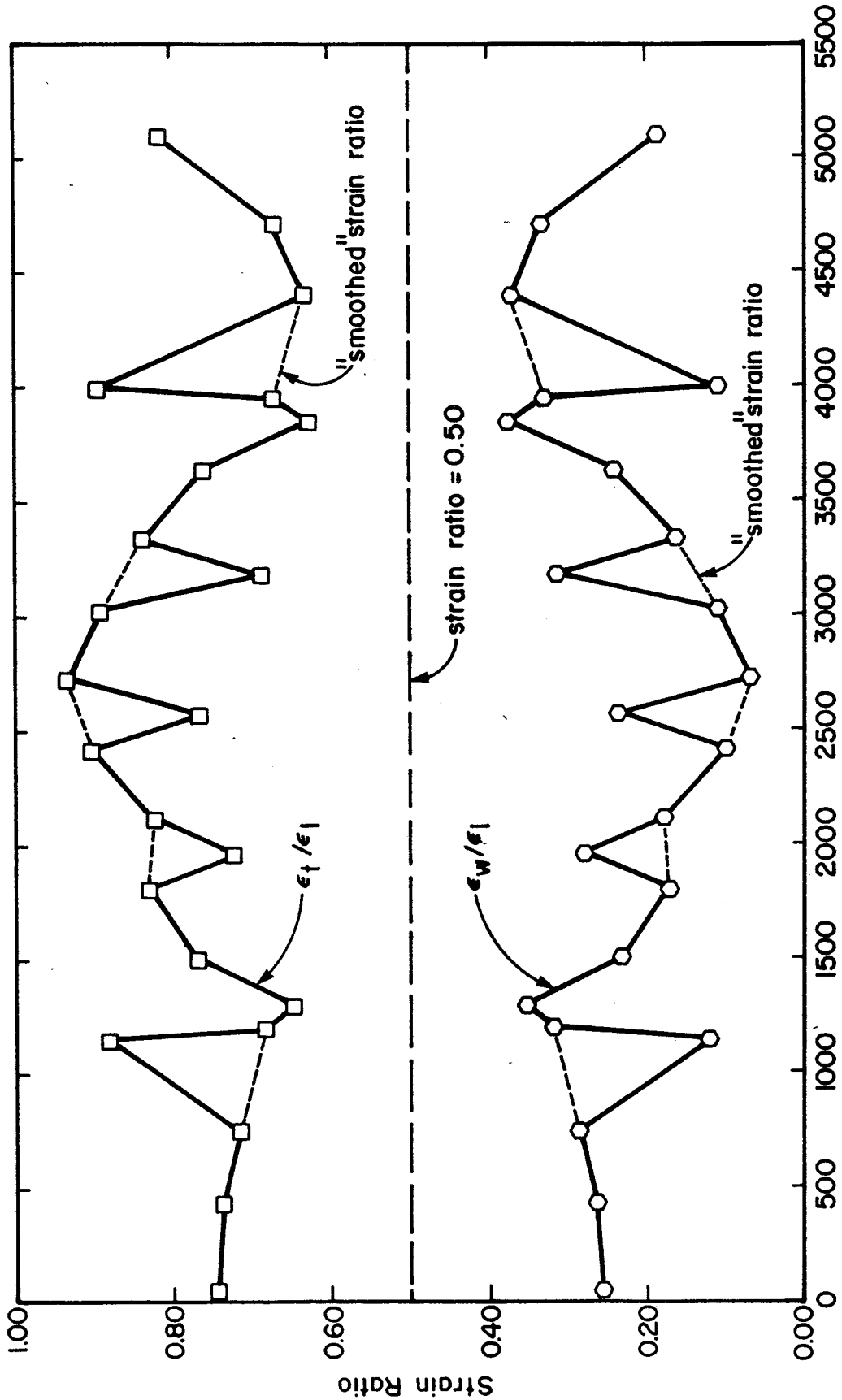

Figure 6.20 STRAIN RATIO DISTRIBUTION, TOP PLATE - TEST C121T6

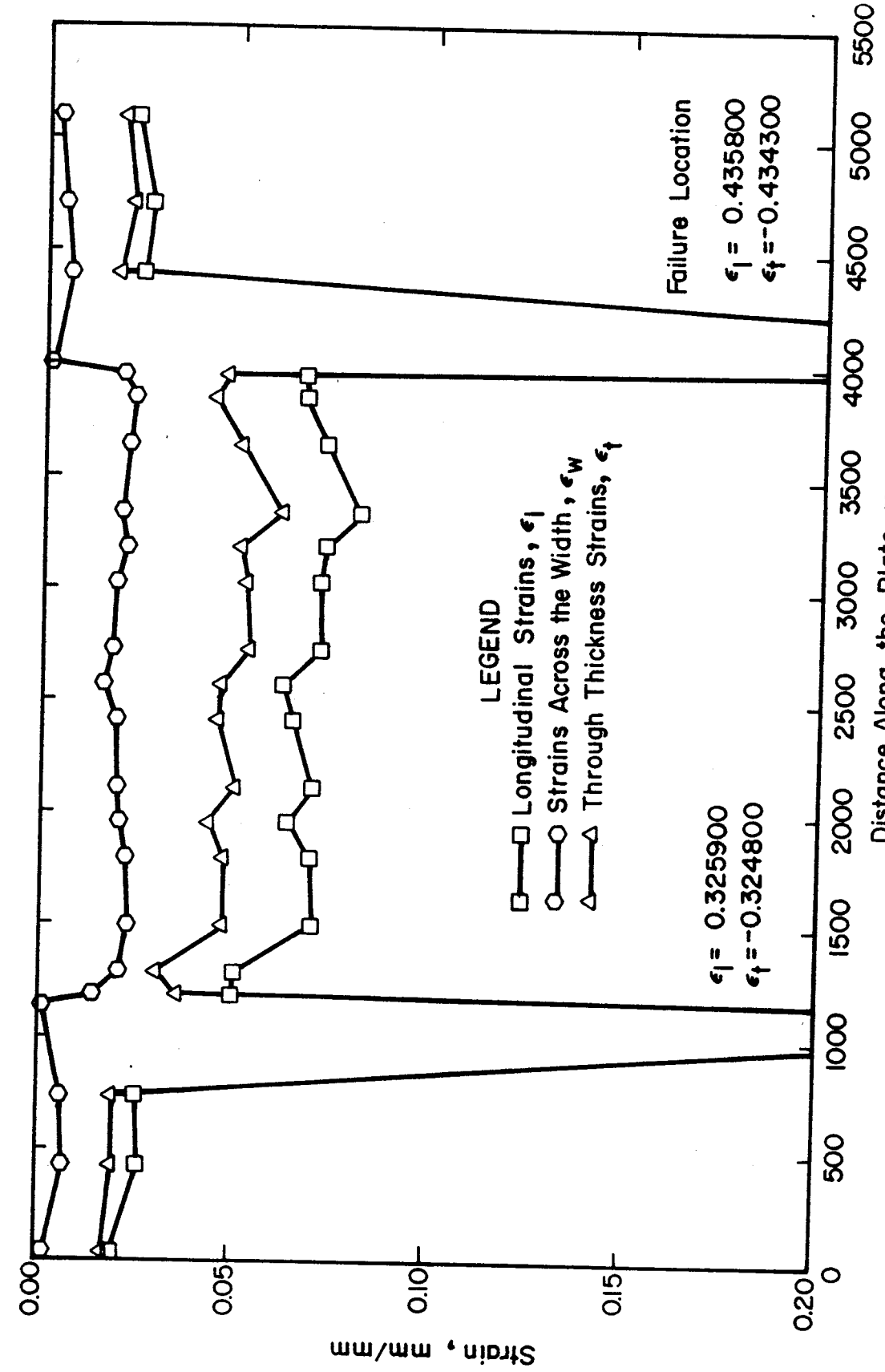

Figure 6.21 STRAIN DISTRIBUTION, BOTTOM PLATE - TEST C121T6

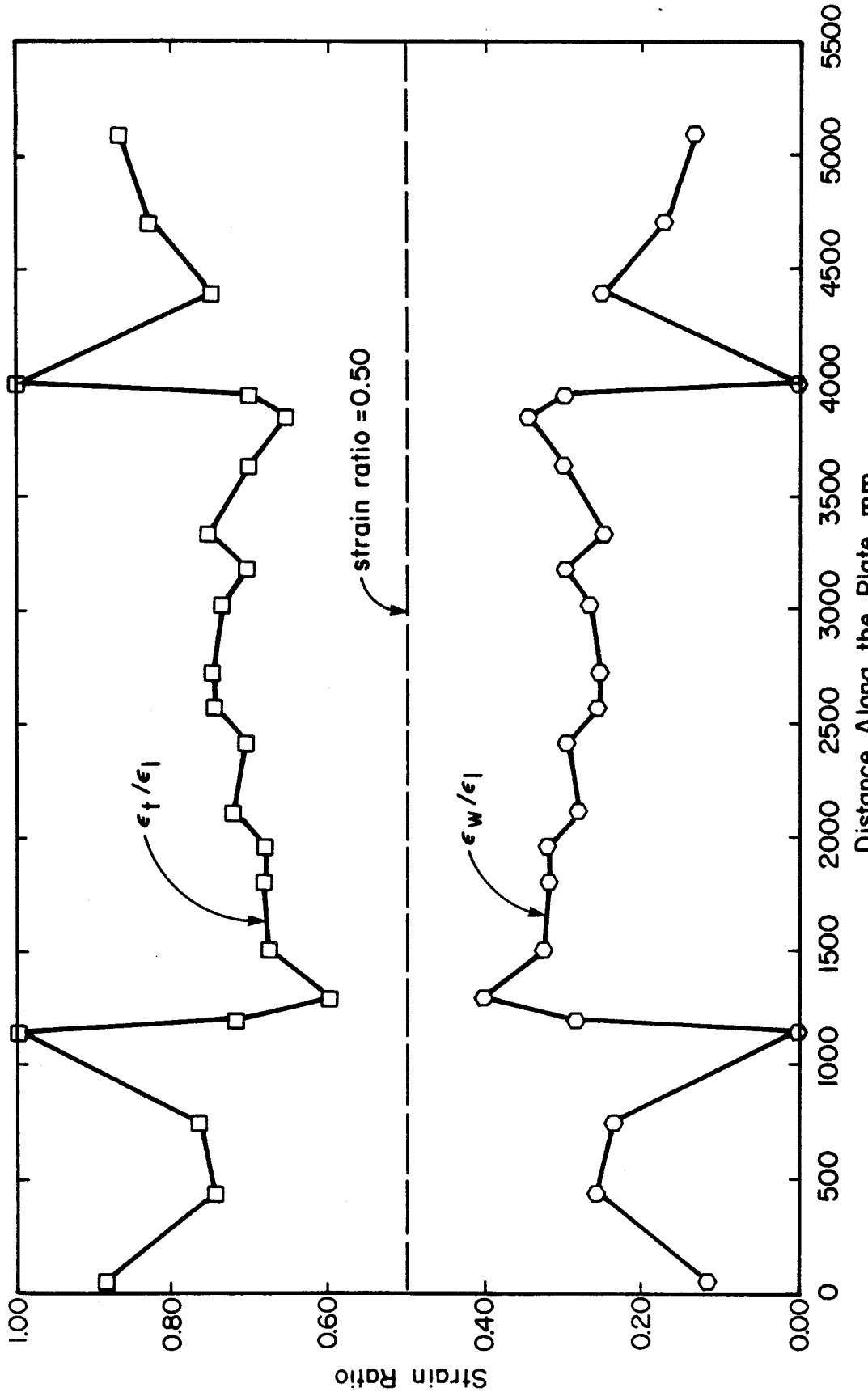

Figure 6.22 STRAIN RATIO DISTRIBUTION, BOTTOM PLATE - TEST C121T6

7. ANALYSES

7.1 General

Two behavioural models have been developed to describe the basic modes of behaviour exhibited by the composite plates. The methods of analysis, features and limitations of the flexural and membrane models are presented in Sections 7.2 and 7.3, respectively. Predictions of the load deflection behaviour and failure modes are verified by comparison with the test data. The models are used to establish the effect of varying key parameters on the behaviour of the plates. An ultimate strength model, based on an extension of the von Mises-Huber-Hencky yield criterion to ultimate condition, is presented. The overall behaviour is presented in Section 7.5.

7.2 Flexural Model

7.2.1 Description and Limits of Behaviour

A flexural model has been developed to describe the load deflection behaviour of steel-concrete composite plates without mechanical shear interconnectors. The load and corresponding deflections were determined from a nonlinear incremental analysis based on an assumed displaced shape, equilibrium of forces on the deformed element (defined by a probable load carrying mechanism), and compatible deformations of the element with the boundaries.

Load is carried primarily by the element behaving as a tied arch as shown schematically in Figure 7.1. The arch consists of seven compression struts, four extending from the supports to the load points and three horizontal struts bridging between the load points, and the bottom plate acting as a tension tie. Additional load is carried by the top plate in tension as a result of load transfer by friction from the compression struts at the load points and from membrane action. These have been incorporated into the analysis. A detailed description of the forces acting on one half of the plate element shown in the displaced configuration is given in Figure 7.2 and Figure 7.3.

Although the model is for a particular load pattern and load distribution, the analysis could be applied equally well to other load cases by simply selecting the appropriate load paths, by determining the internal forces (based on equilibrium of the deformed shape), and by identifying the critical section. For slender plate elements this becomes the location of maximum moment.

The limits of the analysis are defined for over-reinforced members by compression failure of the concrete at midspan, and for under-reinforced members, by yielding of the bottom plate in tension. Limits of the applicability of this analysis for determining flexural capacity of composite plates, in terms of maximum and minimum slenderness limits, L/d, have yet to be defined. With a large L/d, membrane behaviour dominates from the

start and the flexural model is not applicable. With a small L/d, the critical concrete element may change from the horizontal compression strut at midspan to an inclined strut from the load point to the support. A modified model would need to be developed. The analysis does not include the post-flexural failure behaviour described by the continued degradation of the concrete and composite action, nor the development of full membrane action.

7.2.2 Features

The following parameters have been included as variables in the analysis:

1. nonlinear material models, as shown in Figure 7.4;
2. material properties: f'_c, E_c, f_r, E, ϵ_y, σ_y, ϵ_{st}, E_{st}, σ_u;
3. geometric properties: thickness of the top and bottom plates - t_t and t_b, and the depth and width of the composite section - d and w;
4. coefficient of sliding friction between the steel and the concrete, μ=0.5;
5. boundary stiffness as determined from the stiffness of the surrounding structure;
6. pretension forces in the steel plates.

7.2.3 Method of Analysis

For any applied load, the following steps are used to determine the corresponding centre span deflection:

1. a small value of centre span deflection, y, is assumed;

2. based on the centre span deflection, the assumed displaced shape and the distribution of loads, the internal forces are calculated by statics;
3. the deformation of the top and bottom plates is calculated;
4. the load carried by the top plate in membrane action is calculated and subtracted from the applied load. The internal forces, taking the membrane contribution of the top plate into consideration, are re-evaluated and steps 2 to 4 were repeated until satisfactory convergence of the top plate deformations is achieved;
5. if the deflection satisfies the deformation convergence criterion, then another load is assumed and the analysis continues until failure is predicted to occur or the limits of the analysis are exceeded. Otherwise the assumed centre span deflection, y, is incremented until the deflection and corresponding internal deformations satisfy the deformation convergence criterion.

7.2.4 Deformation Convergence Criterion

Because the flexural behaviour of the composite plate was dominated by the behaviour of the concrete, the convergence criterion was based on compatibility of the internal deformations of the critical strut element path with the external deformations required to achieve compatibility with the boundaries.

The external deformation that has to be imposed on the element to make it conform to its boundaries is equal to a length 'a', shown in Figure 7.5, which results from a rigid body rotation of a rectangular concrete block one-half the length of the span. The length 'a' is given by:

$$[7.1] \qquad a = \frac{\ell}{2}(\cos\theta - 1) + d_c \sin\theta$$

where: a = external deformation, mm
ℓ = span length, mm
d_c = depth of the concrete core, mm
θ = angle of rotation

$$\theta = \tan^{-1}\left(\frac{2y}{\ell}\right),$$

where y equals the centre span deflection, mm

The deformation "a" is shared between the supports and the centreline.

The corresponding internal deformations were determined over the same section. The critical length is defined as the prime load carrying path which extends from the support to the inmost load point and then to centre span as shown in Figure 7.5. This length is divided into five segments: two nodal struts, a combined load strut, the remainder of compression strut no. 2, and the remainder of the centre horizontal strut. To calculate the deformation, the loads, lengths, areas and corresponding stiffnesses for each of these segments were determined.

The loads for each of the struts were obtained by statics from the analysis described in Section 7.2.1.

The area of the struts was assumed to be constant throughout with the dimensions defined by the width of the plate and the depth as a function of the bearing length, z, as determined from the displaced shape, and given by:

$$[7.2] \quad z = b + c$$

where:

$$b = \frac{a \sin\theta}{\cos\theta}$$

$$c = \frac{a \cos\theta}{\sin\theta}$$

The bearing length, z, is the total bearing length of both contact sides; one at the support and the other at midspan. The depth of contact on either side is z/2. The protruded shape defined by z/2 and a/2, is a triangle with the length c much greater than b. Enforcing compatibility of deformation here implies the formation of a triangular strain distribution, which is approximated, for small strains and an elastic stress strain curve, with a rectangular stress block of 1/2 the depth z/2, i.e. z/4.

Although the internal forces and the corresponding depth of the compression struts are likely to be different at the supports and at midspan, the depth of the compression struts was idealized as an average value, approximated as z/4.

The lengths for the nodal struts are defined as one-half the depth of the compression strut. Based on the geometry of the truss, the length of the region of overlap

of the combined strut, segment 2 in Figure 7.5 (a), was approximated as the depth of the concrete core and the length of the other segments were determined accordingly.

Table 7.1 lists the parameters used to calculate the internal deformations.

The bilinear stress-strain curve given in Figure 7.4 (a) was used for all segments except the nodal segments. Because of the concentrated angle changes in the nodal segments, the compressive stresses are exceedingly large and therefore the stiffness of these segments was taken arbitrarily to be a small non-zero number, 0.03 E_c. It was assumed that when either the combined strut or compression strut no. 2 reached the reduced stiffness load level, corresponding to a stress of 0.67 f'_c, that the other would also assume this stiffness. The increased load capacity after this point is attributed to some confinement given to these struts by the surrounding concrete. The horizontal segment stiffness is dictated by the first portion of the stress-strain curve. Further increase in capacity, beyond 0.67 f'_c, is not possible because the concrete at that critical section is in a state of uniaxial stress with little or no transverse confinement.

When the total deformation over the span length, as determined from the deformations of each segment, equals the deformations required for external compatibility, convergence is achieved.

7.2.5 Results

The load deflection curves predicted by the flexural model and those from the corresponding tests are shown in Figures 7.6, 7.7 and 7.8, for test plates of constant steel plate thickness, constant section depth, and for test C152T3, respectively.

The test curves exhibited the following characteristics:

1. the tests generally experienced some initial deflection without any significant load increase. This is attributed to initial set of the system;
2. the load deflection response was essentially linear to the point where plastic hinges developed at the supports, after which there was a substantial decrease in stiffness. The flexural stiffnesses before and after hinge formation were related to the depth of the concrete core and not to the thickness of the steel plates;
3. after flexural failure, although there was a slight decrease in capacity, the composite plates recovered this capacity and then carried increasing load with increasing deflections because of the membrane action.

The flexural model identifies the failure mode and the portion of the load deflection curve attributed to flexural behaviour. A summary of the failure modes predicted by the model, and the test to predicted ratios for failure load are given in Table 7.2.

In Figure 7.6, all predicted curves are in reasonable agreement with the test curves as they are in Figure 7.7, with the exception of test C152T3. Excepting C152T3, the mean value of the test to predicted flexural failure load from Table 7.2 is 1.07 with a coefficient of variation of 0.088. Test C121T6 in this set gives the largest test to predicted ratio of 1.21. The variance increases with increasing slenderness ratios, L/d, and is attributed to the relatively greater contribution of the membrane action to the total load carrying capacity.

The model also underestimates the strength of specimen C152T3, this time by 1.41 times. Yielding of the bottom plate is predicted at a load of 95 kN, at which load yielding did occur. With subsequent strain hardening, the test specimen formed plastic hinges and carried more load flexurally. The model as presently developed does not extend beyond yielding of the bottom plates.

It is of special interest that the model predicts the load deformation behaviour quite well, within its limitations, when the initial set of the test plates is taken into account. This prediction recognizes the reduced strength of the concrete under uniaxial stress conditions and does not require any "adjustment coefficients".

The model was used to make a parametric study of the influence on the flexural behaviour of the composite plate of varying the section depth and the bottom plate thickness. Test C203T6 was used as the base case. In the study, the

section depth was varied from 204.2 mm to 400.0 mm while keeping the plate thickness constant at t_b=6.91 mm; and while the bottom plate thickness was varied from 6.91 mm to 15.0 mm keeping the section depth constant, d=400.0 mm. The results of this study are shown in Figure 7.9. Test C203T6 had a depth of 204.2 mm and a bottom plate thickness of 6.91 mm.

By increasing the section depth, curves 1, 2, 3 and 4, the following occurred:

1. the behaviour changed from that of an over-reinforced member to that of an under-reinforced member. The "failure" mode changed from a compression failure of the concrete at midspan to yielding of the bottom plate;
2. the initial stiffness increased from 11.3 kN/mm for d=204.2 mm, curve 1, to 69.3 kN/mm for d=400.0 mm, curve 4, an increase of 6.1 times with an increase in depth of 2.02 times;
3. the ultimate flexural capacity increased from 350 kN to 1300 kN, an increase of 3.7 times.

The argument for increasing the bottom plate thickness is that it provides the tie for the tied arch action and therefore should result in increased capacity. Curves 5, 6 and 7 of Figure 7.9 show that varying the bottom plate thickness does not change the initial flexural stiffness appreciably. Curves 5 and 6 are shown as one because the behaviour was essentially identical. This is corroborated by the results of tests, C152T6, C152T4 and C152T3 in Figure

7.7, which have about the same initial slope. The failure mode changes from an under-reinforced to an over over-reinforced member with increasing plate thickness, as would be expected. In this particular example at least, the proportion of the steel and concrete shows that, for balanced or for over-reinforced conditions, the ultimate flexural capacity and behaviour remains relatively unchanged. For less than balanced reinforcing (curve 4 as compared to curve 5) there is a decrease in flexural capacity as was the case for test C152T3.

Curves 5 and 6 with bottom plate thicknesses of 9 and 10 mm had virtually identical load deflection curves. They fall on either side of the balance point, with one failing by yielding of the bottom plate, and the other by compression of the concrete. Curve 7, for a member with a bottom plate thickness of 15 mm, is below curve 6 for a member with a 10 mm thick plate. As the total section depth is the same, this appears to be due to the reduction in the concrete thickness. This was also the prediction of test C152T6 as compared with the prediction of test C152T4.

The flexural model allows the designer to proportion the section to achieve the required flexural stiffness, capacity and failure mode.

7.3 Membrane Model

7.3.1 Description and Limits of Behaviour

A membrane model has been developed to describe the load deflection behaviour of steel plates of finite width. The load and corresponding deflections are determined using a nonlinear incremental analysis based on equilibrium of forces on the deformed shape and on compatible deformations of the steel plate with flexible boundaries. Flexural and flexural membrane behaviour are not included in this analysis.

The half span model of the plate consists of five segments extending from the support to the edges of each load plate and then to centre span as shown in Figure 7.10. A series of five spring elements, one in parallel with a series of four, represent the boundary stiffness. These represent the boundary conditions of the test set-up as do the five segments and four loads. Other loadings and boundary conditions could be readily modelled. All spring elements were modelled as linear elastic elements, except the anchor span, which had the same nonlinear stiffness (material) model as the plate.

The upper limit to the load carrying capacity of the plates was set at the load which produces a critical state of stress in the plate given by the ultimate stress on the von Mises failure surface as described subsequently in Section 7.4.

Although the model was developed for this particular problem, the method of analysis can be applied to any load and restraint system. It may also be possible to extend the solution to a double membrane separated by links which maintain the spacing between the plates without influencing the behaviour of either membrane.

7.3.2 Features

The following parameters have been included as variables in the analysis:

1. nonlinear material model for the steel, shown in Figure 7.4;
2. Material properties: E, ϵ_y, σ_y, ϵ_{st}, E_{st}, σ_u;
3. Geometric properties: plate thickness and width;
4. Boundary stiffnesses.

7.3.3 Method of Analysis

For any applied load, the following steps are used to determine the corresponding centre span deflection:

1. a small value of centre span deflection, y, is assumed;
2. based on the distribution of loads the horizontal force, H, is calculated;
3. the internal forces, corresponding strains (based on linearized stress strain curves, Figure 7.4) and extensions of each segment are calculated;
4. the horizontal projection of each extended segment is calculated;

5. the sum of these projections is compared to the original length between the flexible boundary (support) and centre span. If the projected length of the membrane is greater than the original length, the centre span deflection, y, is increased and steps 2 to 4 are repeated until the lengths are in close agreement;
6. the resulting horizontal force, H, is applied to the boundary and the corresponding x-displacement is determined;
7. if the x-displacement of the boundary due to the load, H, is greater than the displaced position of the boundary, then the boundary is displaced by an amount Δ_x, and a new length between the boundary and centre span is calculated;
8. steps 1 to 7 are repeated until the x-displacement of the boundary due to the horizontal load is in agreement with the displaced boundary position;
9. another load is assumed and the analysis continued until failure, defined as rupture of the steel plates, occurs.

7.3.4 Results

The load deflection curves predicted by the membrane model and those from the corresponding tests are shown in Figures 7.11 and 7.12 for steel plate test and composite plates of constant steel plate thickness, and for composite plates of constant section depth, respectively. The predictions for horizontal restraint forces are shown in

Figure 7.13 together with some test results. The plate thicknesses given are the nominal plate thicknesses for each steel plate.

Apart from the flexural behaviour, for which the membrane model is not applicable, the predicted curves are in reasonable agreement with the test results. Some variations exist because of initial set and a difference in straining of the top and bottom plates for the composite tests. This results in slightly softer test response as shown in the figures. The model accurately predicts:

1. the influence of boundary movements on the load deflection behaviour of the plate;
2. the occurrence and progression of yielding and strain hardening for the steel plate test;
3. The magnitude of the reaction force required to develop the membrane force as shown in Figure 7.13 for the case of the two 6.35 mm plates with yielding anchor spans.

Failure loads are discussed subsequently in Section 7.4.

Based on this model a parametric study was conducted to study the influence of boundary stiffness, material behaviour and plate thickness. The results of this study are illustrated in Figures 7.13 and 7.14, for load horizontal restraint and for load deflection of the plate, respectively.

The effect of changing the boundary stiffness is apparent in Figures 7.13 and 7.14. Decreasing the boundary stiffness from an infinite stiffness to the test value, and

then to 1/10th of the test value, increased the centre span deflection corresponding to the end of the elastic membrane response, from 71 mm to 128 mm, and 361 mm, respectively, as seen in Figure 7.14. Reducing the boundary stiffness decreased the area under the load deflection curve hence the energy absorption capacity of the element. For this particular problem, the 90% reduction in boundary stiffness represents a 20% decrease in energy absorption capacity. Conversely, there is little energy absorption capacity to gain by increasing the stiffness to a large amount. Figure 7.13 shows in curves 1, 2 and 3 that the maximum horizontal force required to develop the membrane remains virtually unchanged when the boundary stiffness is changed.

Changes in plate thickness or material behaviour alter the magnitude of load for a given deflection, but not the basic behaviour. The magnitude of load is directly proportional to the plate thickness and to the stress level corresponding to that particular deflection. The maximum horizontal force required to develop the ultimate membrane strength is equal to the yield load of the plate element times $1/\cos\theta$, where θ is the angle of the critical plate segment with respect to the horizontal at failure.

This analysis allows the design engineer to determine both the strength and stiffness of the boundary so that the desired energy absorption capacity is achieved.

7.4 Failure Criterion

Ultimate failure of the composite plate occurred with rupture of one or both of the steel plates. Rupture occurs when the state of stress in the material on a critical section exceeds a limiting value. The limiting value is defined here by an extension of the von Mises-Huber-Hencky yield criterion to ultimate. In the general form, for any state of stress, this criterion gives:

$$[7.3] \quad (\sigma_x-\sigma_y)^2+(\sigma_y-\sigma_z)^2+(\sigma_z-\sigma_x)^2+6(\tau_{xy}^2+\tau_{yz}^2+\tau_{zx}^2) = 2U^2$$

where: σ_x, σ_y, σ_z = normal stresses in the x, y, z coordinate system
τ_{xy}, τ_{yz}, τ_{zx} = shear stresses in the x, y, z coordinate system
U = ultimate stress for uniaxial stress, σ_u

The critical section for the plate element occurs at the support where the plate is in a state of plane strain and σ_y (through-thickness stress), τ_{yz} and τ_{zx} are all equal to zero, and the transverse stress, σ_z, is $\nu\sigma_x$, Poisson's ratio times the longitudinal stress. Simplifying the general formulation for the particular problem gives:

$$[7.4] \quad (1 - \nu + \nu^2)\ \sigma_x^2 + 3\tau_{xy}^2 = U^2$$

From an examination of the free body diagram in Figure 7.15, it can be seen that the critical section is subjected to a combination of normal and shear forces acting on the

original cross-sectional area, A_o. The average normal stress, σ_x, acting over the critical cross section is

$$[7.5] \qquad \sigma_x = \frac{P}{A_o}$$

where: P = horizontal component of the membrane force, S

Similarly, the average shear stress is

$$[7.6] \qquad \tau_{xy} = \frac{V}{A_o}$$

where: V = vertical component of the membrane force, S

Stresses computed from the test loads are compared to the limiting stresses given by equation 7.4 at ultimate conditions, with Poisson's ratio equal to ν_p, as previously discussed. The results are summarized in Table 7.3. The mean test to predicted value is 1.128 with a coefficient of variation of 0.037. This value is less than 1.0 because stresses have been assumed to be constant over the entire cross-section. This is not likely to be the case, even with significant ductility.

Equation 7.4 can be rewritten to form a strength interaction equation in terms of loads. Letting the ultimate force that can be developed on the critical cross section be Y, where:

$$[7.7] \qquad Y = U A_o$$

and substituting Equations 7.5, 7.6 and 7.7 into Equation 7.4 and dividing by the U^2 term gives:

$$[7.8] \qquad \beta \left(\frac{P}{Y}\right)^2 + 3 \left(\frac{V}{Y}\right)^2 = 1.0$$

where: $\beta = (1-\nu+\nu^2) = 0.75$ for $\nu=0.5$

This interaction equation is shown in Figure 7.15, where the test values are also plotted. Compared to the interaction diagram these test values would, of course, give the same test to predicted ratios as given in Table 7.3. The test points are clustered because, only one span was used in the tests and the members all failed at about the same angle, θ.

Based on this interaction equation the design engineer can determine the ultimate failure load for any combination of shear or axial load at the plate edge.

7.5 Overall Behaviour

The overall behaviour of the test specimen ranges from flexural to membrane behaviour and within the ranges of applicability of the models developed for flexural and membrane behaviour there is good agreement with the test data. The solutions are not additive.

The transition between the two models is a combination of flexural and membrane behaviour, which occurs subsequent to reaching the flexural capacity of the system and is characterized by increasing deformation without reduction in load carrying capacity. This indicates that the increasing

strength due to membrane action replaces the lost flexural strength until membrane action only exists.

The limiting strength of the system is given by the failure criterion which is based on a combined stress state and an extension of the von Mises-Huber-Hencky yield criterion to ultimate. The mean test to predicted value for the ultimate load was 1.128 with a coefficient of variation of 0.037.

Table 7.1 FLEXURAL MODEL - PARAMETERS TO CALCULATE INTERNAL DEFORMATIONS

SEGMENT	DESCRIPTION	LOAD P, kN	LENGTH L, mm	AREA$_2$ A, mm^2	MODULUS E, MPa
1	nodal strut	$CS_1 + CS_2$	z/8	zw/4	$.03E_c$
2	combined load strut	$CS_1 + CS_2$	d_c	zw/4	bilinear, see Figure 7.3
3	compression strut no. 2	CS_2	$\ell_2 - d_c - z/8$	zw/4	bilinear, see Figure 7.3
4	centre horizontal strut	$C_1 + C_2$	$\ell_h - z/8$	zw/4	bilinear, see Figure 7.3
5	nodal strut	$C_1 + C_2$	z/8	zw/4	$.03E_c$

Notes: 1. Segments are defined in Figure 7.5.
2. The total internal deformation is equal to the sum of each segment given by equation 7.3.

Table 7.2 FLEXURAL BEHAVIOUR - FAILURE LOADS

TEST SPECIMEN	TEST LOAD kN	FLEXURE MODEL kN	TEST / PREDICTED	FAILURE MODE (PREDICTED)
C121T6	139.6	115.0	1.21	compression failure of the concrete at midspan
C152T6	195.5	185.0	1.06	compression failure of the concrete at midspan
C152T4	192.1	190.0	1.01	compression failure of the concrete at midspan
C152T3[1]	134.2	95.0	1.41	yielding of the bottom plate
C203T6	352.6	350.0	1.01	compression failure of the concrete at midspan

NOTES: 1. The test load is the total applied load at which a compression failure occurred in the concrete at midspan.
2. The behaviour of this test specimen lies outside the limits of the flexural model. Yielding of the bottom plate occurred at 95.0 kN. Therefore the mean test to predicted ratio does not include this test.
3. The mean test to predicted ratio is 1.07 with a coefficient of variation of 0.088.

Table 7.3 ULTIMATE FAILURE LOADS

TEST SPECIMEN	LOADS AT SUPPORT		STRESSES AT SUPPORT		VON MISES FAILURE STRESS, MPa		TEST / PREDICTED
	AXIAL P, kN	SHEAR V, kN	AXIAL σ_x, MPa	SHEAR τ_{xy}, MPa	TEST[1]	PREDICTED[2]	
STEEL	2690	1567	387.9	226.0	515.8	474.3	1.088
C121T6	2682	1511	391.6	220.6	510.9	474.3	1.077
C152T6	2714	1734	401.2	256.3	563.7	474.3	1.189
C152T4	1886	1132	386.7	232.1	523.2	466.3	1.122
C152T3	867	487	275.8	154.9	359.2	312.7	1.149
C203T6	2704	1658	394.9	242.2	541.2	474.3	1.141

NOTES: 1. Test value calculated from von Mises formulation for plane strain,

$\sqrt{\sigma_x^2 (1 - \nu + \nu^2) + 3\tau_{xy}^2}$ where, $\nu = \nu_p = 0.5$.

2. Predicted value is the ultimate strength, σ_u, of the plane stress stress strain curve.
3. The mean test to predicted ratio is 1.128 with a coefficient of variation of 0.037.

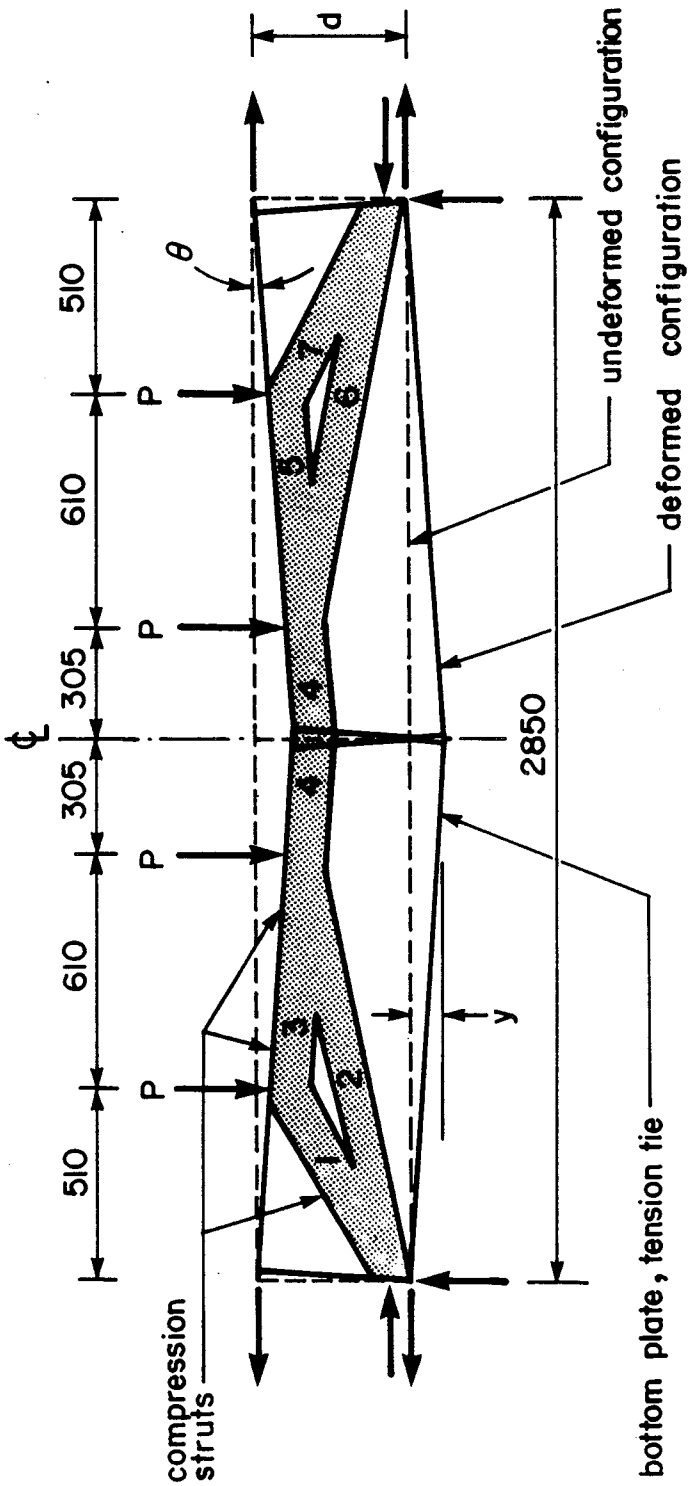

Figure 7.1 TIED ARCH ANALOGY

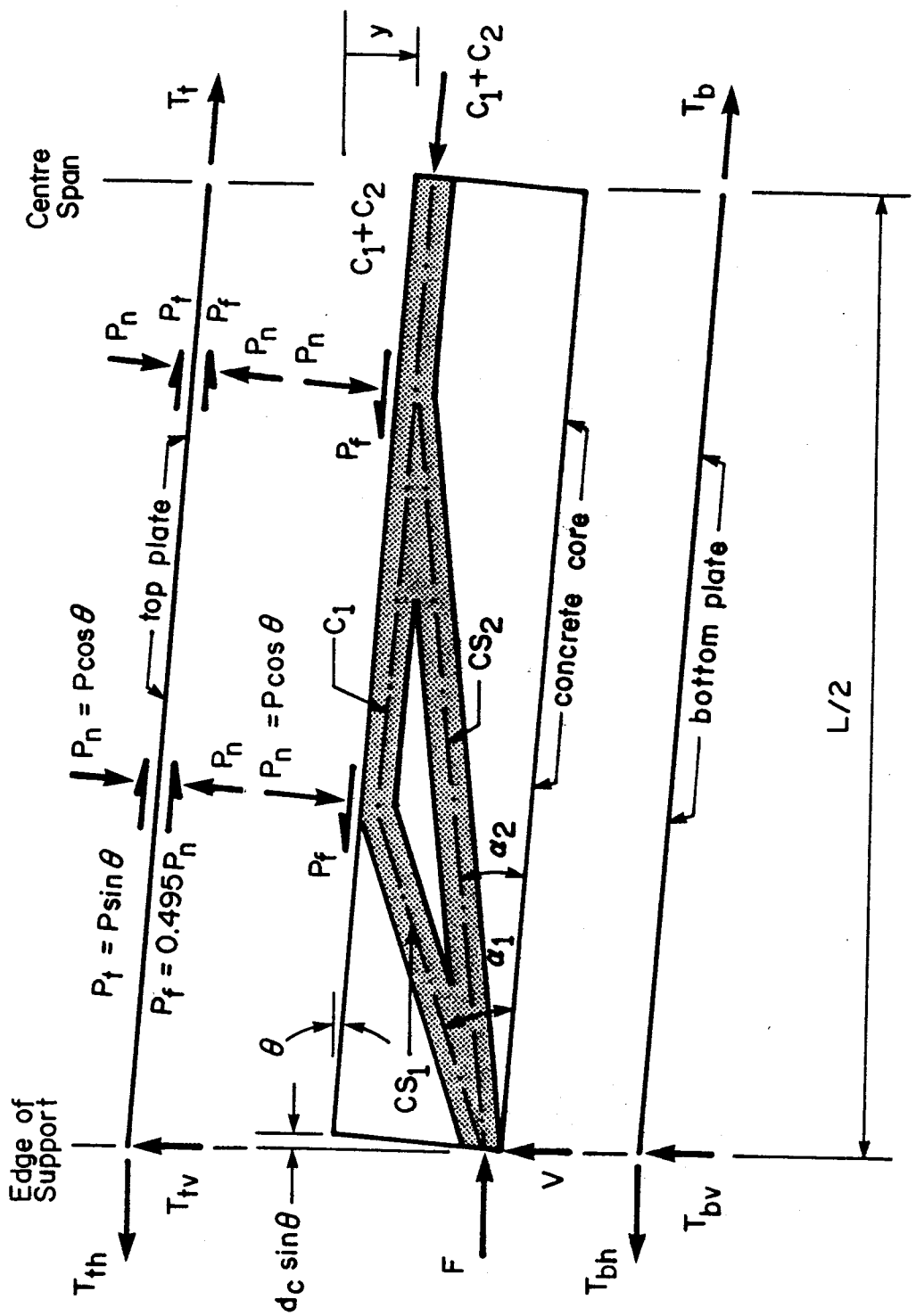

Figure 7.2 FREE BODY DIAGRAM

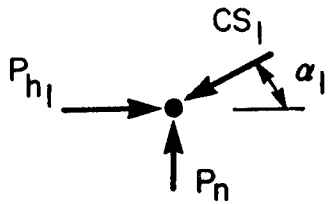

$P_{h_1} = P_n / \tan \alpha_1$

(a) Compression Strut – 1

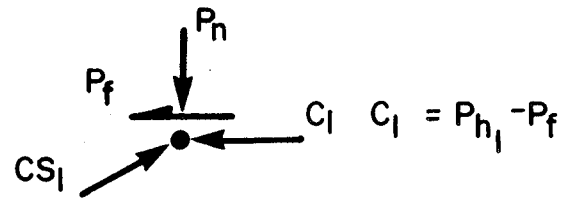

$C_1 = P_{h_1} - P_f$

(b) Horizontal Compression Strut – 1

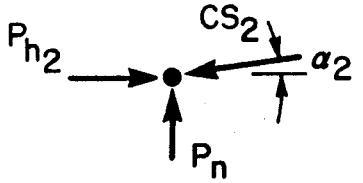

$P_{h_2} = P_n / \tan \alpha_2$

(c) Compression Strut – 2

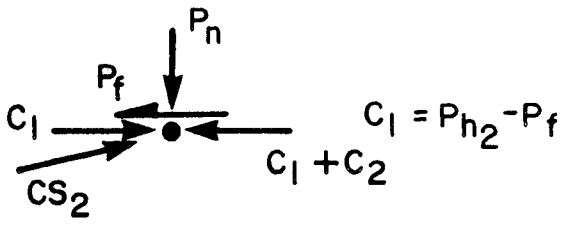

$C_1 = P_{h_2} - P_f$

(d) Horizontal Compression Strut – 2

$T_{th} = 2(P_t + P_f) \cos\theta + T_f / 2.0$

$T_{tv} = 2(P_t + P_f) \sin\theta$

T = Net Force in Top Plate at Centre Span

$T_{bh} = (C_1 + C_2) \cos\theta + T_f / 2.0$

$T_{bv} = (C_1 + C_2) \sin\theta$

$T_b = C_1 + C_2 + T_f / 2.0 \cos\theta$

T_f = Pretension Force

$F = (P_{h_1} + P_{h_2}) \cos\theta - 2P_n \sin\theta$

$V = (P_{h_1} + P_{h_2}) \sin\theta + 2P_h \cos\theta$

Figure 7.3 FORCE DEFINITIONS

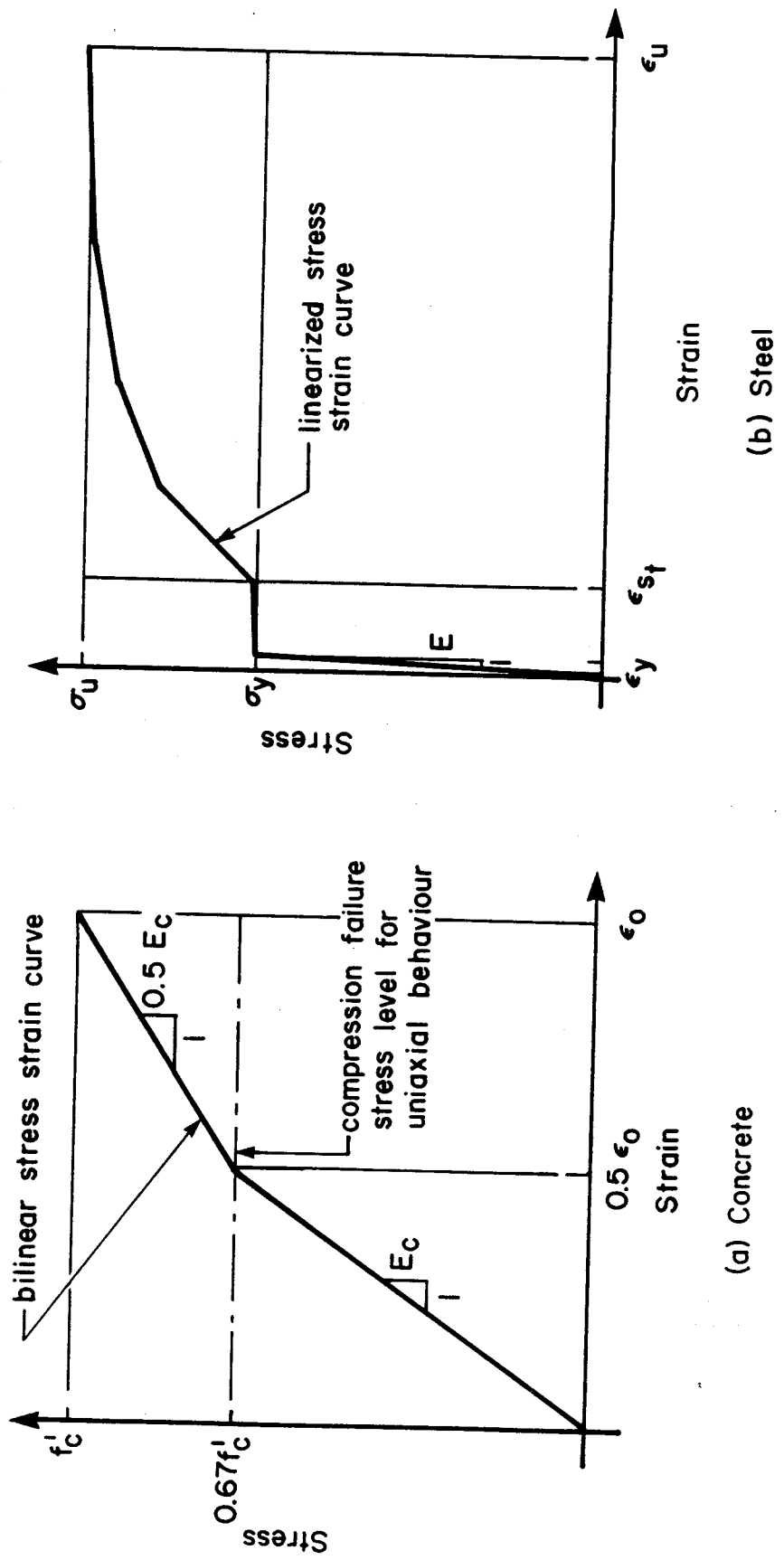

Figure 7.4 NON-LINEAR MATERIAL MODELS

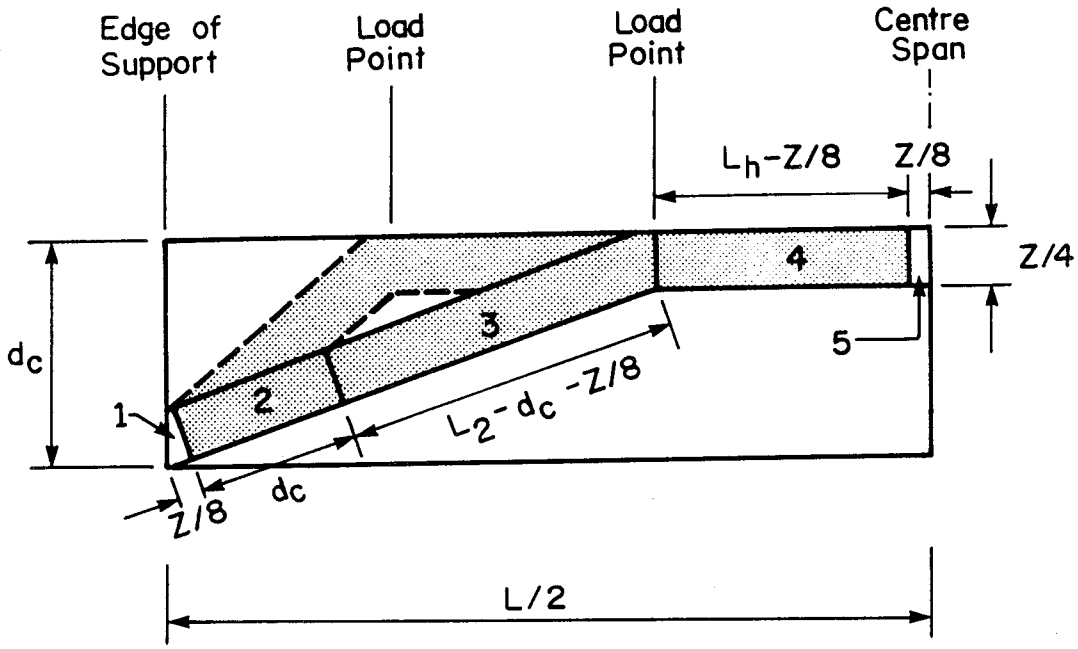

(a) Internal Deformations - Segment Definitions

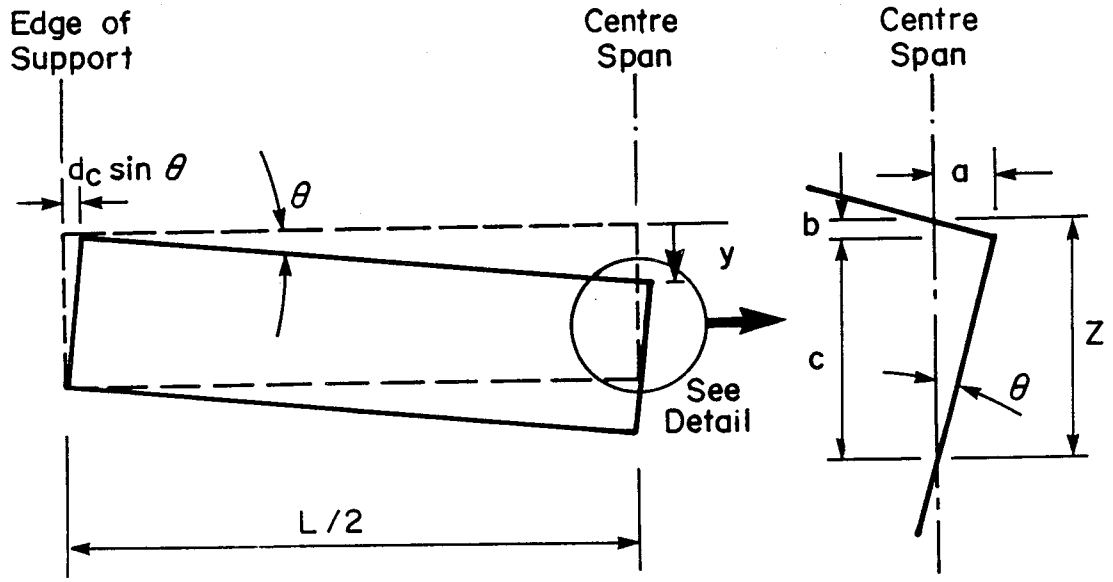

Rigid Body Displacement of Concrete Core Detail

(b) External Deformations - Rigid Body Displacements

Figure 7.5 DEFORMATION CONVERGENCE CRITERION

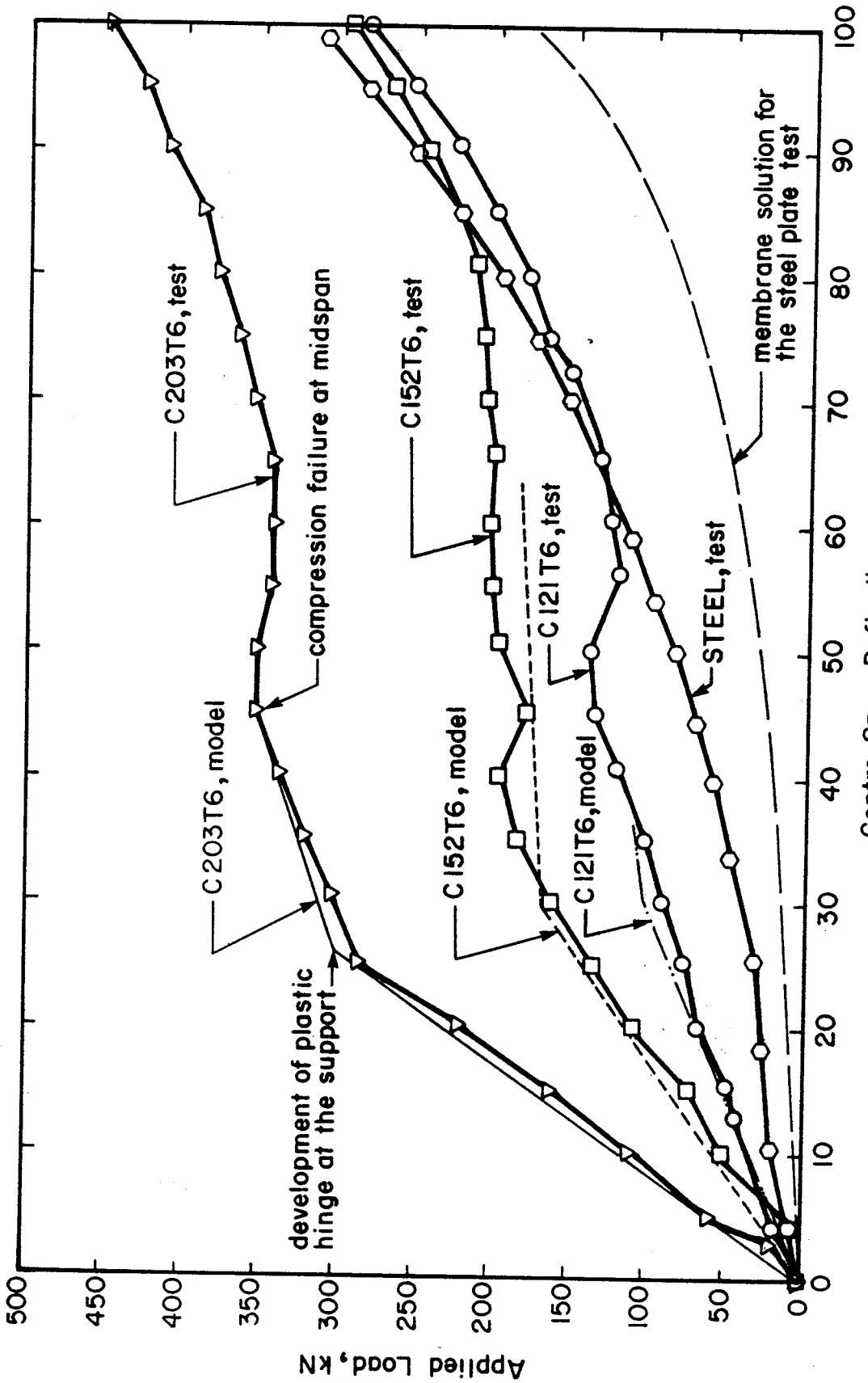

Figure 7.6 TEST AND PREDICTED LOAD DEFLECTION CURVES - CONSTANT PLATE THICKNESS

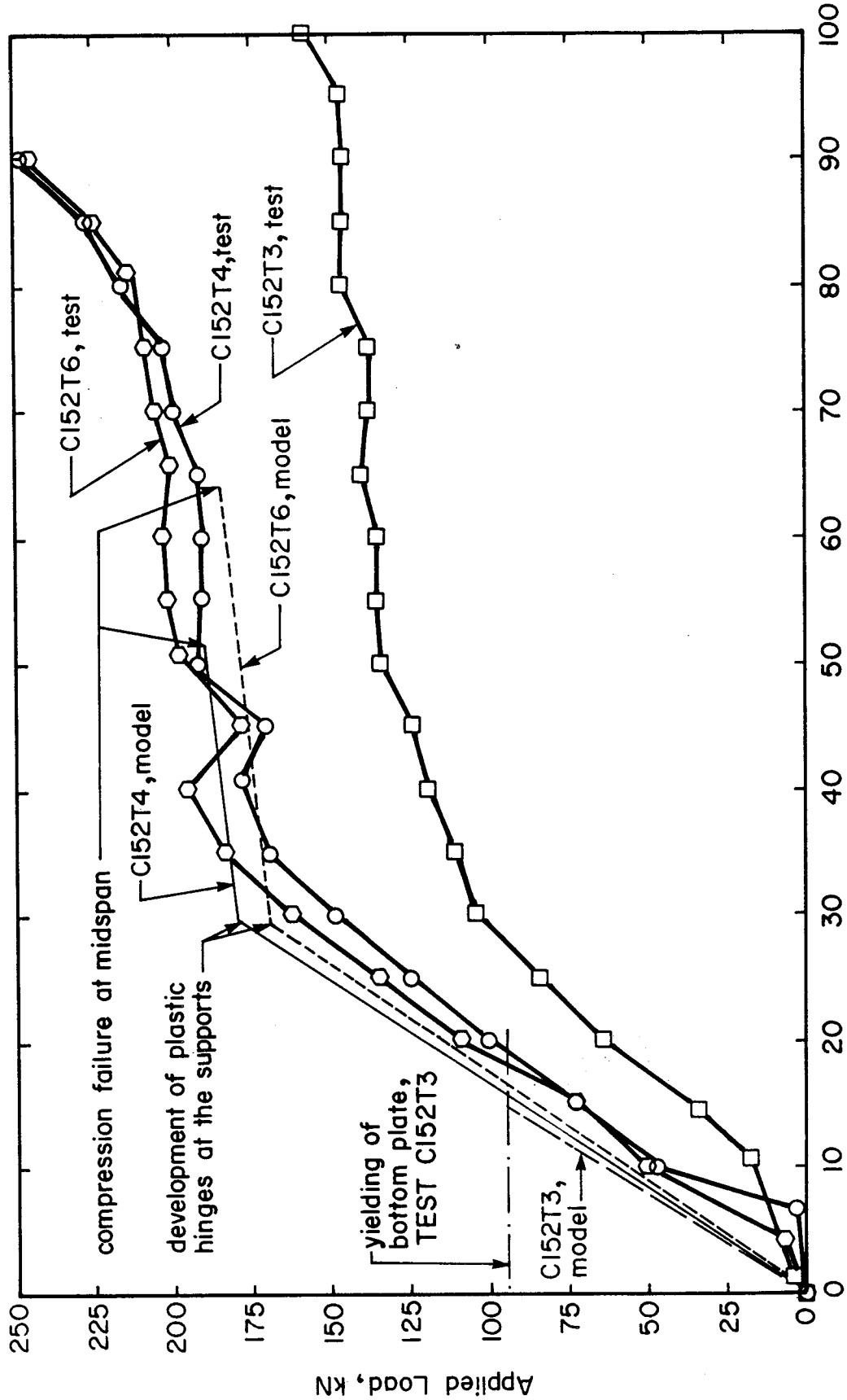

Figure 7.7 TEST AND PREDICTED LOAD DEFLECTION CURVES - CONSTANT SECTION DEPTH

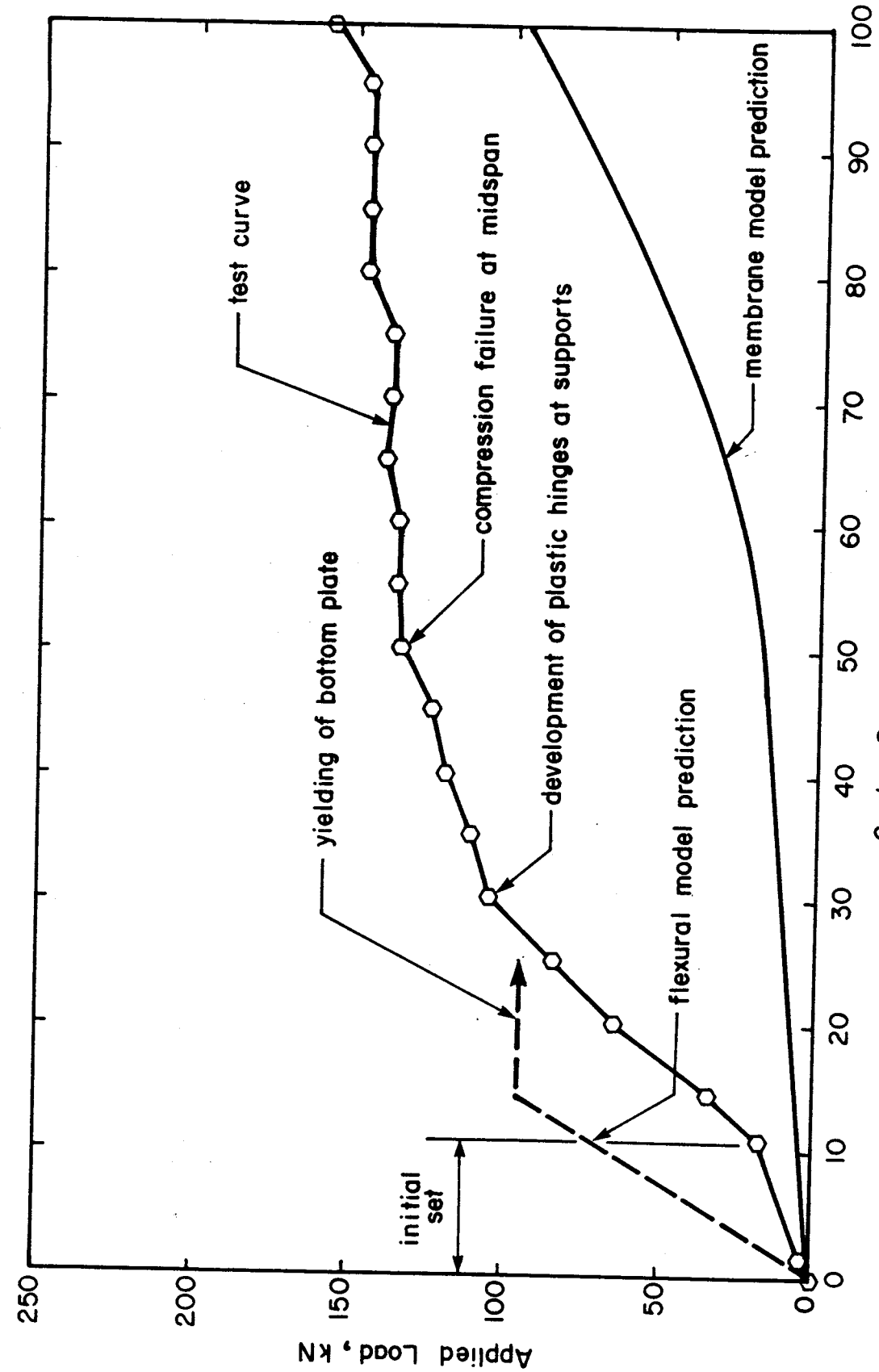

Figure 7.8 TEST AND PREDICTED LOAD DEFLECTION CURVES - TEST C152T3

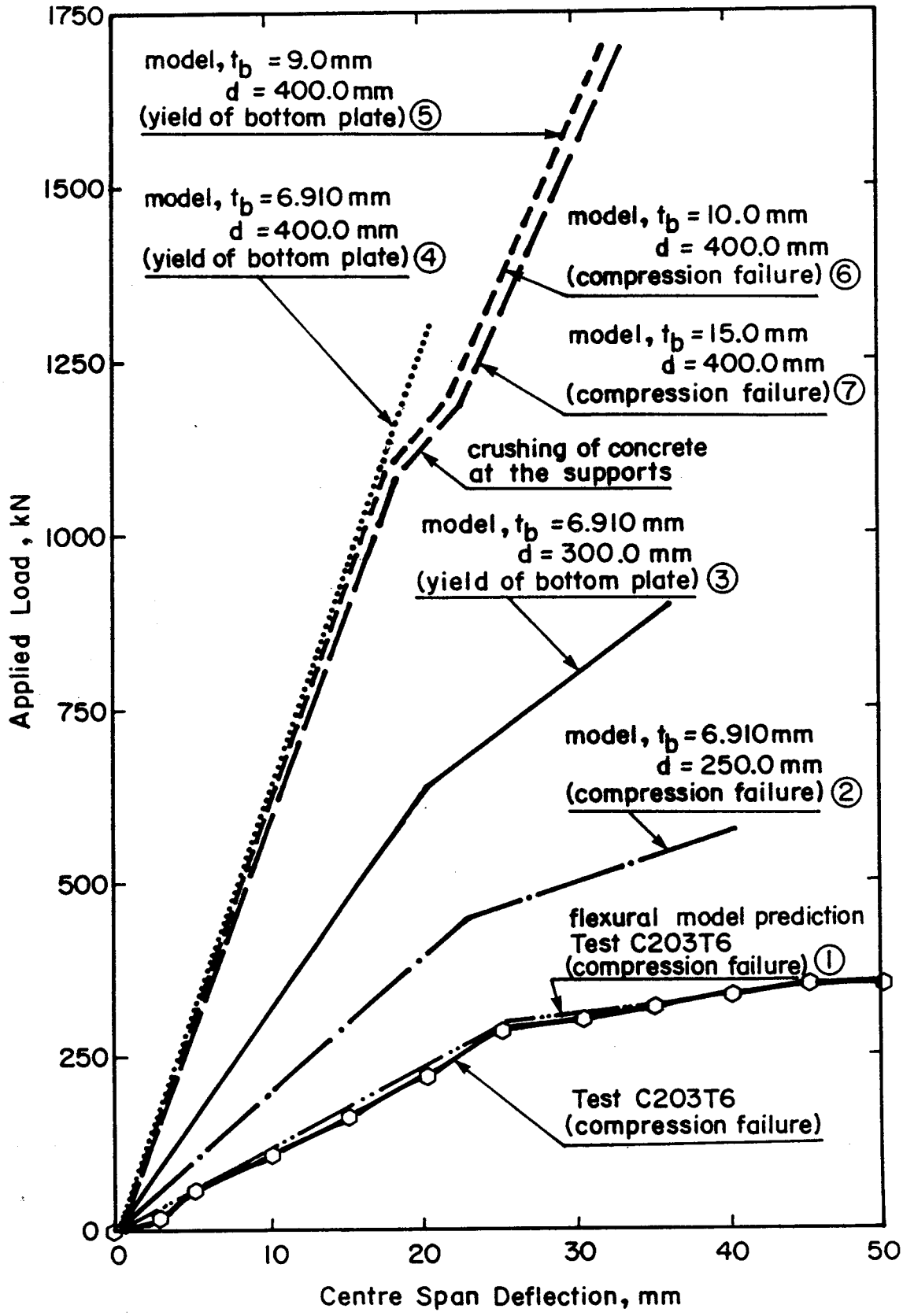

Figure 7.9 FLEXURAL MODEL - PARAMETRIC STUDY

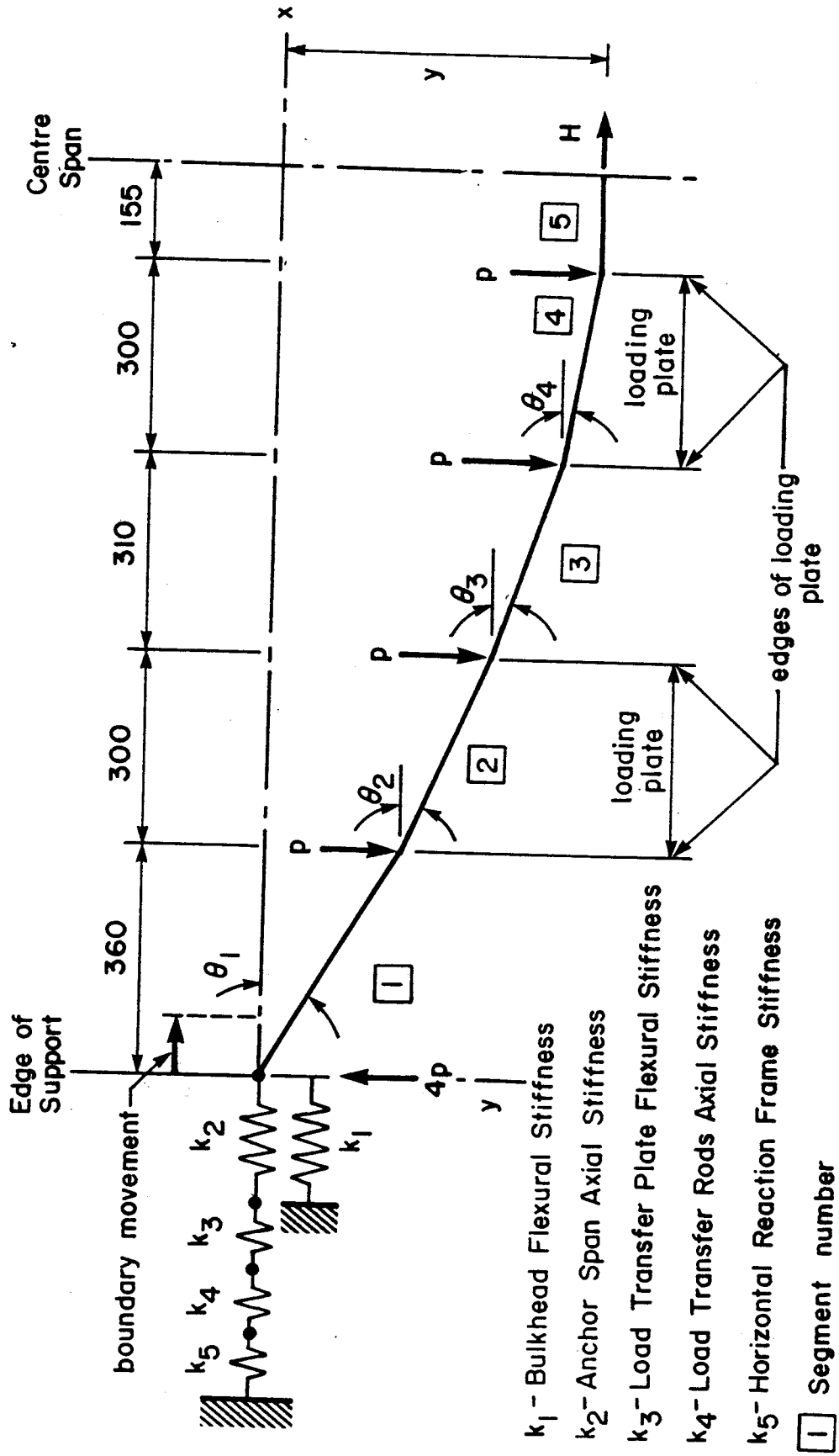

Figure 7.10 MEMBRANE MODEL

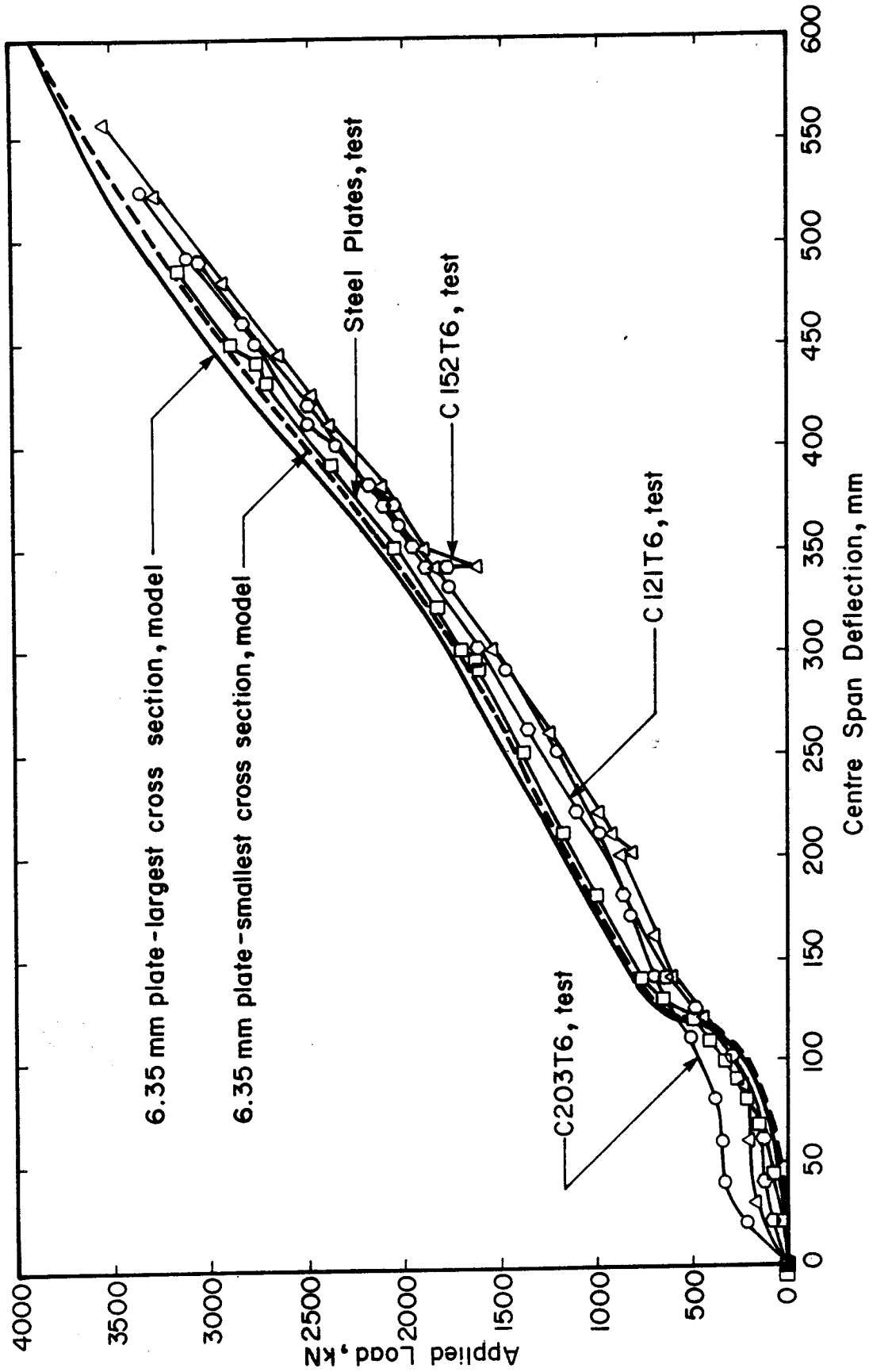

Figure 7.11 TEST AND PREDICTED LOAD DEFLECTION CURVES - CONSTANT PLATE THICKNESS

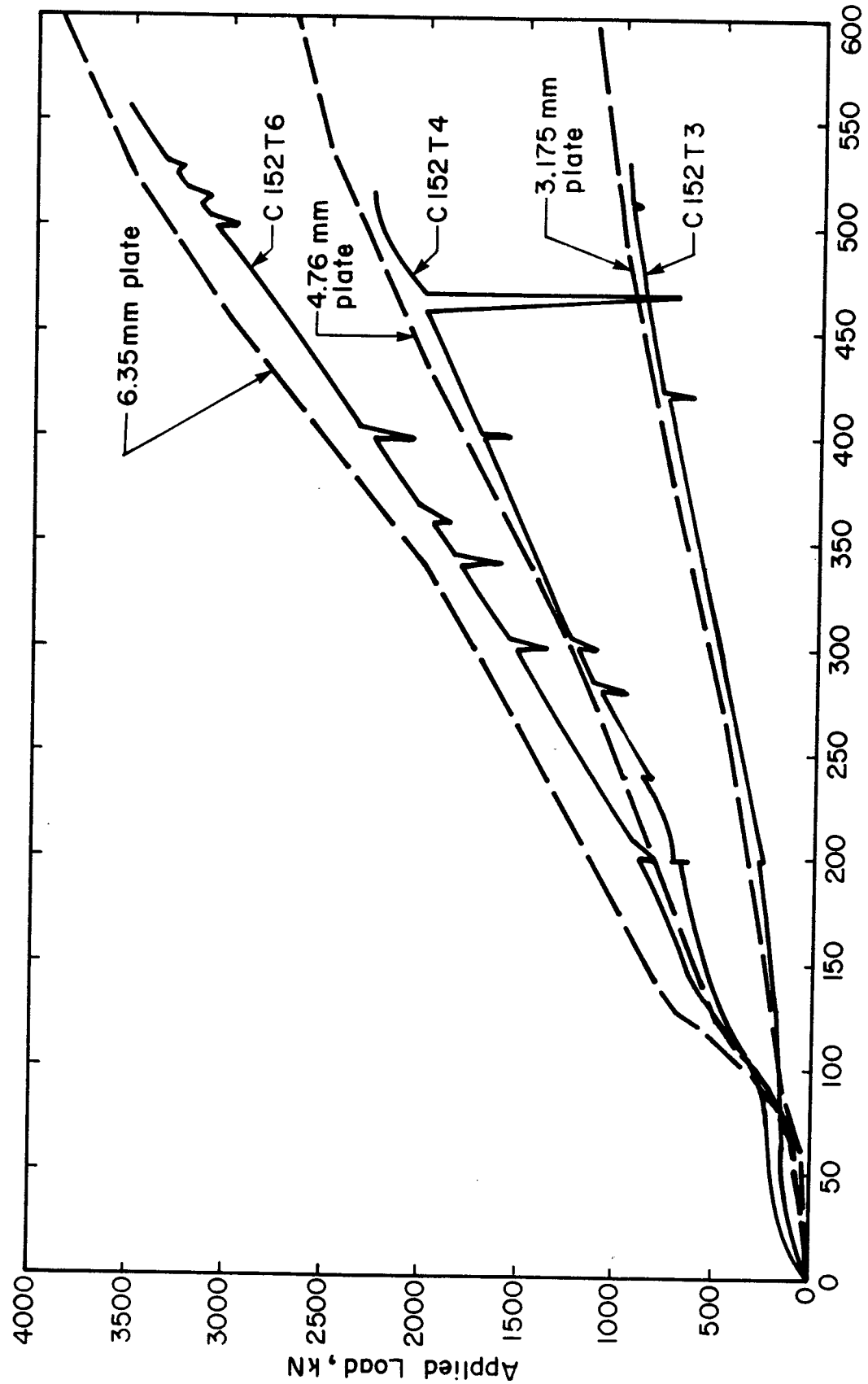

Figure 7.12 TEST AND PREDICTED LOAD DEFLECTION CURVES - CONSTANT SECTION DEPTH

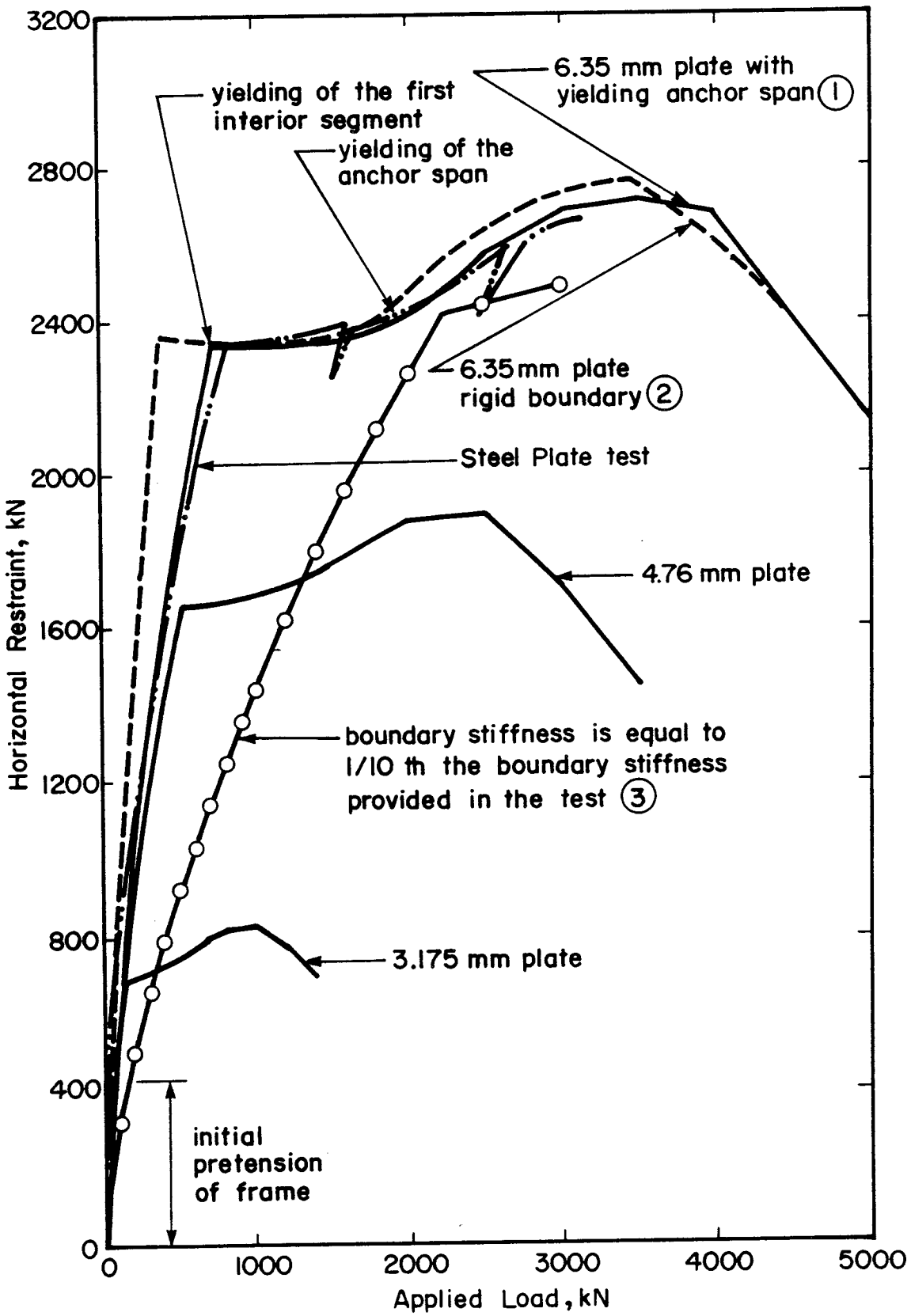

Figure 7.13 TEST AND PREDICTED HORIZONTAL RESTRAINT

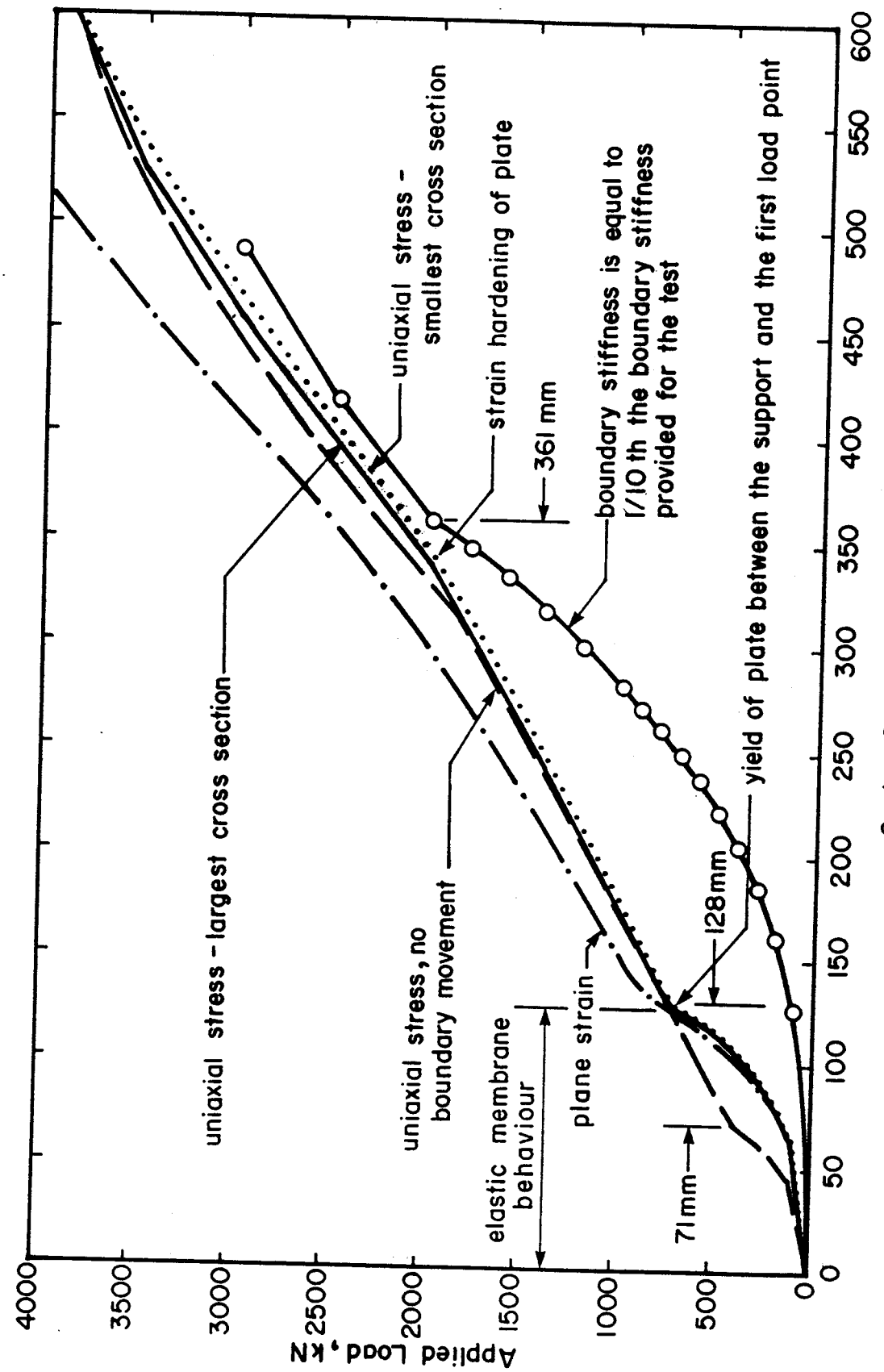

Figure 7.14 LOAD DEFLECTION CURVES - PARAMETRIC STUDY

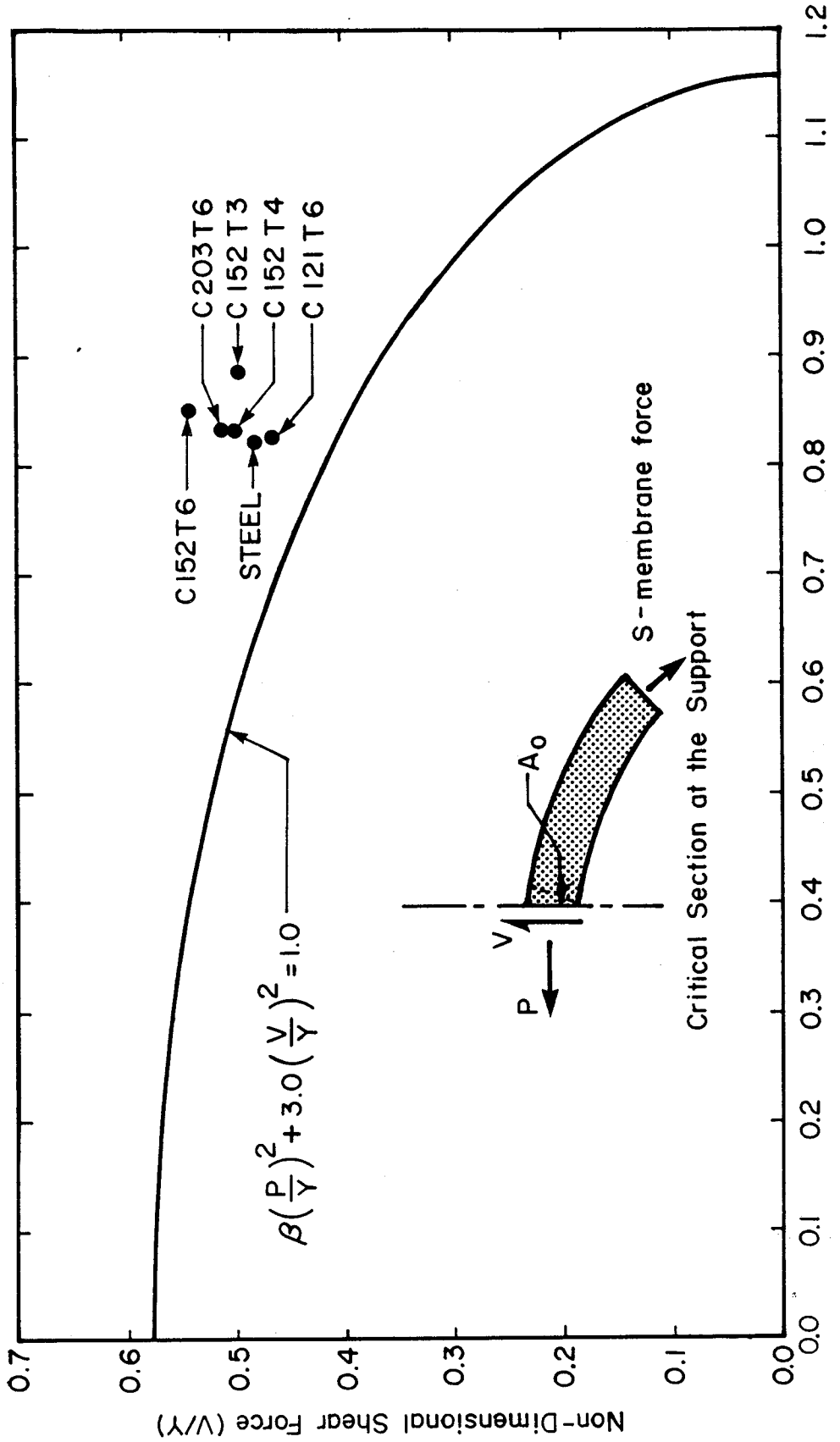

Figure 7.15 FAILURE SURFACE

8. DESIGN APPLICATIONS

8.1 General

A flexural and a membrane model have been developed to describe the load deflection response of steel-concrete composite plates without mechanical shear interconnection. The loads and corresponding deflections were determined by a nonlinear incremental analysis based on measured geometric and material properties, an assumed displaced shape, equilibrium of forces and compatibility of deformations of the composite plate with the boundaries. The analyses have a wide range of applicability and are not limited by plate thicknesses, stress-strain characteristics, section depth, boundary stiffness, nor to the coefficient of friction between steel and concrete. Although the analyses were developed for this particular load configuration, they can be modified to apply equally well to other configurations.

The models, together with the failure criterion, allow the design engineer to:

1. proportion the section to achieve the required flexural stiffness, capacity and failure mode;
2. determine the strength and stiffness of the boundary system so that the desired strength and energy absorption capability of the plate can be achieved;
3. select the appropriate plate sizes to resist the maximum equivalent static load.

Having developed the general configuration for the structure

and having determined the environmental loads, the designer would select the relative proportions of the section by trial and error to provide the required response as predicted by the flexural and membrane models.

8.2 Specific Aspects of Design

8.2.1 Construction

Because of the simplicity of the element, no stiffeners, no shear connectors, fewer pieces and less welding are required, making construction and placement of the concrete easier. Elimination of these pieces also reduces the weight of steel in the structure offering significant cost savings.

8.2.2 Fracture Toughness

The total thickness of steel in the top and bottom plates can be distributed arbitrarily except that the bottom (or inside) plate must be proportioned for flexure. By making the inside plate thicker, thereby satisfying the flexural requirements, the overall fracture toughness of the assembly is improved because:

1. the temperature gradient through the thickness of the wall exposes the thick plate to temperatures much less than the climatic temperatures, lessening fracture toughness requirements and fracture susceptability of the plate. The thinner tougher plate is placed on the

outside;

2. the thicker main load carrying plate is subjected to less severe loading rates. The concrete core and the outside plate dampen the impact.

8.2.3 Energy Absorption

Based on the load deflection response of the plates, it can be seen that a great amount of energy can be absorbed through plastic deformation. When the membrane behaviour of the composite plates is recognized, utilized and properly designed, the plates can receive a significant number of impacts and absorb energy through accumulated plastic deformation before rupture occurs. If the accumulated deformation of a section became excessive, replacement may be necessary, but this could be anticipated.

8.2.4 Punching Failure

Concrete infill in sandwich plate construction has been recognized to spread or distribute the load over a large area lessening load intensities and the chance of punching failure.

Stiff elements tend to absorb energy through local plastic deformations, which are generally small when compared to the plastic deformation energy of larger more flexible elements. For an impact load this may lead to a premature failure as a result of punching through, as shown by several tests reported in Chapter 2. Flexible elements

such as the one proposed are more desirable from this point of view.

8.2.5 Fatigue

Based on experimental evidence from fatigue tests of composite plate elements by Matsuishi et al.(1980), fatigue of these elements in the elastic or plastic regions of behaviour did not seem to be an issue as long as proper detailing was ensured. Fitzpatrick (1987) repeats that fatigue has not been a problem for caisson type structures currently operating in the Arctic.

8.3 Other Applications

With an increasing knowledge and understanding of the behaviour of steel-concrete composite plates, also comes increased and diversified usage of the element.

A variation has been considered for the legs of offshore structures, to replace the heavily stiffened steel large diameter tubes with a composite sandwich annulus. More than 100 small scale tests were conducted by Goode(1980) and Montague(1985; 1986) to obtain experimental evidence about the performance of these elements. Models such as the flexural or membrane model developed here could be combined and modified to describe the behaviour of such a system.

Other uses may extend to other engineering applications such as shear walls or prefabricated bridge deck panels.

9. SUMMARY, CONCLUSIONS AND RECOMMENDATIONS

9.1 Summary

An experimental and analytical program was undertaken to determine:

1. the strength and behaviour of steel-concrete composite plates without mechanical shear interconnection and subjected to transverse loads;
2. the shear deformation response of the steel-concrete interface under varying normal loads;
3. the effects of boundary restraint and the problems of implementing such restraint.

A series of six one-span steel-concrete composite plate elements, with a main span of 3050 mm centre-to-centre of supports, axially restrained and made continuous, were tested with a four point load system. The primary variables were the steel plate thickness, which varied from 3.18 to 6.35 mm, and the section depth, which gave span to depth ratios from 15 to 25.

Material properties and behaviour were established from a series of ancillary tests which included shear interface tests, tension coupons, biaxial stress plane strain tension coupons, concrete cylinders and concrete prisms.

The literature review presents the relevant research on the steel-concrete composite plate behaviour and on steel plate membrane behaviour.

The analyses included basic data reduction and the development of:

1. a transformation model to convert the longitudinal stress strain curve of a conventional uniaxial coupon test to an equivalent one for plane strain so that strain data from the tests could be interpreted;
2. a flexural model to describe the load deflection behaviour of steel-concrete composite plates without mechanical shear interconnectors;
3. a membrane model to describe the load deflection behaviour of steel plates of finite width and flexible boundaries (a description of boundary forces is also given);
4. a failure criterion to describe rupture of the steel plates at the supports.

A comparison was made between the models and test data.

9.2 Conclusions and Recommendations

1. The focus of current and past experimental and analytical work has been on the flexural capacity of steel-concrete composite beams where the influence of in-plane restraint provided to the beam element by the rest of the structure has been ignored.
2. The function relating the octahedral shear strain, γ_{oct}, to the octahedral shear stress, τ_{oct}, is independent of the state of stress, and the maximum octahedral shear stress is approximately constant at rupture.

3. The energy of local plastic distortion per unit volume, a measure of ductility, given by the area under the octahedral shear strain shear stress curve, W, decreases with an increase in the ratio of transverse to longitudinal stress. For the particular case tested, the ratio of W for plane strain to uniaxial stress was 0.8.
4. The transformation model developed for converting the longitudinal stress-strain curves of a conventional uniaxial tension test to one for plane strain yielded results which were in excellent agreement with the test results from the plane strain and the uniaxial stress tests.
5. The influence of altering the state of stress for the material from uniaxial stress to plane strain is to strengthen and stiffen the longitudinal stress-strain curve. The apparent ductility of the material is reduced by as much as 40%. Necking of the material at ultimate becomes highly localized.
6. By reducing the effect of end restraint on the behaviour of a standard concrete cylinder test, only 67% of the compressive resistance, f'_c, can be mobilized. It is speculated that the compressive resistance of the concrete is related to the maximum tensile strain that can be developed. These tests indicate that the value is around 250 μs.
7. The mean value for the kinetic coefficient of sliding friction between the steel and concrete was 0.5 with a

coefficient of variation of 0.15.

8. The composite plates exhibit two distinct types of behaviour, flexural and membrane with a transition from one to the other.
9. The flexural stiffness of steel-concrete composite plates is chiefly a function of depth of the concrete core.
10. The ultimate load carrying capacity of the plate was unaffected by the prior flexural behaviour.
11. The ultimate load carrying capacity is a function of the steel plate thickness, support conditions and the load distribution.
12. In all tests, a shear tension failure occurred when a fracture strain or an ultimate stress of one or more of the plates at the support was exceeded.
13. In all tests, the ultimate failure mode, the centre span deflection and the deflected shape of the structure were about the same, regardless of plate thickness or section depth.
14. The average maximum centre span deflection at failure was 1 in 5.46 of the span length and the average maximum angular rotation at the support was 29.8 degrees.
15. Apparent slip between the concrete core and the steel plates was the result of one or both of the following mechanisms:
    a. accumulated differential straining
    b. rigid body displacements

16. The vertical end restraint maintained the geometry of the system and provided the necessary reaction to develop the full negative moment capacity of the section over the support.
17. Lateral confinement of the concrete core proved to have little or no effect on the behaviour because the concrete simply expanded through the thickness in the direction of least restraint.
18. Measurements of plate dimensions before and after the test showed that the critical section of the plate, where rupture occurred, was in a state of plane strain.
19. A flexural model was developed to describe the load deflection behaviour of steel-concrete composite plates without mechanical shear interconnectors. The model gives loads and deflections which are in good agreement with the test results.
20. The flexural model provides a general analysis technique which can be used for other load configurations to proportion the section to achieve the required flexural stiffness, load capacity and flexural failure mode.
21. A membrane model was developed to describe the load deflection behaviour of steel plates of finite width. The model is in close agreement with the test results. The model is general and can be applied to other load configurations and boundary stiffnesses and can be used to determine the energy absorption capacity of the plate and the strength and stiffness of the restraint system

so that the required behaviour could be achieved.

22. If full membrane capacity is required, then the in-plane restraint mechanism must be able to develop a load equal to the yield load of the plate element divided by the cosine of the angle that the critical plate segment makes with the non-deformed position.
23. Variations in boundary stiffness alter the extent of the elastic membrane behaviour region. The less stiff the boundary system, the greater the extent of this region.
24. A failure criterion, based on the combined stress state at the critical region and on an extension of the von Mises-Huber-Hencky yield criterion to ultimate, gives a mean test to predicted value of 1.128, for the membrane failures, with a coefficient of variation of 0.037. This criterion is also presented as a strength interaction equation in terms of the normal and shear loads on the plate cross section.
25. The innate characteristics of the steel-concrete composite plate include flexural strength, membrane strength, fracture toughness, energy absorption capability, and favorable fatigue life. These along with the flexural and membrane analyses allow the design engineer to proportion the section to achieve a wide range of favourable responses.

9.3 Future Work

Further research and development in the following areas would be of interest:

1. analytical work to develop a complete model to describe more fully the interaction of flexural and membrane behaviour. The following features could be incorporated:
   a. post bottom-plate yield behaviour
   b. varying load patterns and intensities
   c. double membrane analysis to account for variation in plate loads between the top and bottom plates
   d. multispan model
   e. variations in stress-strain models to account for different strain rate response of impact loads
   f. flexible bulkhead supports (axial stiffness)
   g. calculations of plastic deformation energy;
2. analytical and experimental studies to determine the influence of different combinations of axial and shear forces, restraint across the width and mandrel radii on the failure of the plates at the supports. From this investigation a comprehensive strain rupture criterion could be developed;
3. a small number of composite plates could be tested to verify the extension from two dimensional to three dimensional behaviour;
4. the experimental work could be continued on plates with a broader range of flexural behaviour, boundary stiffnesses and plate thicknesses (including different

bottom and top plate thicknesses), to provide the necessary data to verify the models presented in Chapter 7. Subsequently, this could be extended to investigate the influence on strength and behaviour by:

a. welding the plates to the supports
b. interconnecting the plates together at locations other than at the supports
c. adding shear connectors
d. varying support condition details
e. variable loads, patterns and sequencing of loads

5. Because this work investigated only the static behaviour of composite plates, further analytical and experimental work is required to determine the material and member behaviour under dynamic and impact loads which simulate ice loads in the Arctic.

REFERENCES

ABAM Engineers Inc. 1983. Proposal - Development Design and Testing of Composite Ice Wall Structures for Arctic Platforms. No. 28, December.

ABAM Engineers Inc. 1985. Composite Ice Wall Structures Design and Test - Program Phase II. A Proposal to Perform Developmental Design and Testing of Composite Ice Wall Structures for Arctic Platforms.

Akiyama, H., Koseki, K., Taira, K. and Sasaki, M. 1986. Strength of Steel/Concrete Composite Sandwich Members. Transactions of the Japan Concrete Institute, Vol. 8, III-16-A, December, pp. 337-344.

American Society for Testing and Material (ASTM). 1977. Standard Methods and Definitions for Mechanical Testing of Steel Products. ASTM A370-77, Philadelphia, Pennsylvania.

American Society for Testing and Material (ASTM). 1985. Standard Methods of Tension Testing of Metallic Materials. ASTM E8-85a, Philadelphia, Pennyslvania.

Brattland, A. 1987. Shrinkage and Flexural Tests of two Full Scale Composite Trusses, Master of Science Thesis, University of Alberta.

Bruce, J. C. and Roggensack, W. D. 1984. Second Generation Arctic Platforms Lessons from First Generation Design Experience. Offshore Technology Conference, Houston, Texas, May 7-9, Paper 4798.

Canadian Standards Association (CSA). 1977. Methods of Test for Concrete. National Standard of Canada CAN3-A23.2-M77, Canadian Standards Association, Rexdale, Ontario.

Canadian Standards Association (CSA). 1984. Design of Concrete Structures for Buildings. National Standard of Canada CAN3-A23.3-M84, Canadian Standards Association, Rexdale, Ontario.

Carstens, T., ed. 1980. Working Group on Ice Forces on Structures. U. S. Army Cold Regions Research and Engineering Laboratory, Special Report 80-26, June, 153 p.

Centre for Frontier Engineering Research. 1987. Private communication, Edmonton, Alberta.

Chang, P. Y., Seibold, F. and Thasanatorn, C. 1980. A Rational Methodology for the Prediction of Structural Response Due to Collisions of Ships. Society of Naval Architects and Marine Engineers Transactions, Vol. 88, pp. 173-193.

Chiu, R., Haciski, E. and Hirsimaki, P. 1981. Application of Plastic Analysis to U. S. Coast Guard Icebreaker Shell Plating. Society of Naval Architects and Marine Engineers Transactions, Vol. 89, pp. 249-274.

Clarkson, J. 1963. Tests on Flat Plated Grillages Under Uniform Pressure. Royal Institution of Naval Architects, Transactions, Vol. 105, pp. 467-484.

Clarkson, J. 1956. A New Approach to the Design of Plates to Withstand Lateral Pressure. Transactions of the Institution of Naval Architecture, Vol. 98, pp. 443-463.

Croasdale, K. R. 1983. The Present State and Future Development of Arctic Offshore Structures. 7th International Conference on Port and Ocean Engineering under Arctic Conditions, Helsinki, Finland, April 5-9, Vol. 4, pp. 489-518.

Croasdale, K. R. and Marcellus, R. W. 1981. Ice Forces on Large Marine Structures. IAHR, International Symposium on Ice, Quebec, July 27-31, pp. 755-770.

Davis, E. A. 1948. The Effect of Size and Stored Energy on the Fracture of Tubular Specimens. Journal of Applied Mechanics, Vol. 15, September, pp. 216-221.

Davis, E. A. 1945. Yielding and Fracture of Medium-Carbon Steel Under Combined Stress. Journal of Applied Mechanics, Vol. 12, March, pp. A13 - A24.

Davis, E. A. 1943. Increase of Stress with Permanent Strain and Stress-Strain Relations in the Plastic State for Copper Under Comnbined Stresses. Journal of Applied Mechanics, Vol. 10, December, pp. A187-A196.

Davis, H. E. 1948. Behaviour of Steel Under Biaxial Stress as Determined by Tests on Tubes. Journal of Applied Mechanics, Vol. 15, September, pp. 201-215.

Drucker, D. C. 1957. Plastic Design Methods - Advantages and Limitations. Society of Naval Architects and Marine Engineers Transactions, Vol. 65, pp. 172-196.

Fitzpatrick, J. 1987. Private Communication.

Fitzpatrick, J. 1983. The Single Steel Drilling Caisson: A Novel Approach to Bottom-Founded Structures in Arctic Water. 58th Annual Technical Conference and Exhibition of the Society of Petroleum Engineers of AIME, Paper 11999.

Fraenkel, S. J. 1948. Experimental Studies of Biaxially Stressed Mild Steel in the Plastic Range. Journal of Applied Mechanics. Vol. 15, September, pp. 193-200.

Gerwick Jr., B. C. and Jahns, H. O. 1979. Conceptual Design of Floating Drilling Production and Storage Caisson for Arctic Waters. 5th International Conference on Port and Ocean Engineering under Arctic Conditions, Trondheim, Norway, August 13-18, Vol. 2, pp. 1173-1189.

Gerwick Jr., B. C. and Karp, L. B. 1979. Icebreaker Experience as a Guide to Sea Ice Forces on Structures. Conference on Civil Engineering in the Oceans IV, San Franscisco, September 10-12, Proceedings Vol. 2, pp. 622-637.

Hattori, Y., Ishihama, T., Yamamoto, T., Matsuishi, M. and Iwata, S. 1985. On the Strength of Composite Steel Concrete Structure. 8th International Conference on Port and Ocean Engineering under Arctic Conditions, Narssarssuaq, Greenland, September 7-14, Vol. 2, pp. 445-454.

Hooke, R. and Rawlings, B. 1969. An Experimental Investigation on the Behaviour of Clamped, Rectangular, Mild Steel Plates Subjected to Uniform Transverse Pressure. Proceedings of the Institution of Civil Engineers, Vol. 42, pp. 75-103.

Hooke, R. 1970. Post-Elastic Deflection Prediction of Plates. Journal of the Structural Division, ASCE, Vol. 96 (ST4), pp.757-771.

Hosford, W. E. and Cadelle, R. M. 1983. Metal Forming, Mechanics and Metallurgy. Prentice Hall Inc., Inglewood Cliffs, N. J., 330 pp.

Hughes, O. F. 1983. Ship Structure Design, A Rationally - Based, Computer Aided Optimization Approach. John Wiley and Sons Inc., New York, N. Y.

Hughes, O. F. 1983. Design of Lateral Loaded Plating - Concentrated Loads. Journal of Ship Research, Vol. 27, No. 4, December, pp.252-264.

Hughes, O. F. 1981. Design of Laterally Loaded Plating - Uniform Pressure Loads. Journal of Ship Research, Vol. 25, No.2, June, pp.77-89.

Ludwik, P. 1928. Bruchgefahr und Materialprüfung, Schweiz. Verband Materialprüfung. Tech. Ber. 13, Zürich, November.

Matsuishi, M. and Iwata, S. 1983. Composite Prestressed Concrete/Steel Structural Modules - 2. Statical Strength Hitachi Zösen Technical Review, Vol. 43, No. 3, September, pp. 140-150.

Matsuishi, M. and Iwata, S. 1983. Composite Prestressed Concrete/Steel Structural Modules - 1. Stresses and Deformation During Prestressing. Hitachi Zösen Technical Review, Vol. 43, No. 2, June, pp. 27-32.

Matsuishi, M. and Iwata, S. 1982. On the Composite Prestressed Concrete/Steel Structural Module Naval Architecture and Ocean Engineering, Vol. 20, pp. 120-133.

Matsuishi, M., Nishimaki, H., Iwata, S. and Suhara, T. 1980. On the Strength of Composite Steel - Concrete Structures of a Sandwich System (4th Report) - Effect of Girder Web Hitachi Zösen Technical Review, Vol. 41, No. 4, December, 6 p.

Matsuishi, M., Nishimaki, H., Iwata, S. and Suhara, T. 1980. On the Strength of Composite Steel - Concrete Structures of a Sandwich System (3rd Report) - Effect of Repeated Loadings. Hitachi Zösen Technical Review, Vol. 41, No. 1, March, pp. 8-12.

Matsuishi, M., Nishimaki, H., Takeshita, H., Iwata, S. and Suhara, T. 1978. On the Strength of Composite Steel - Concrete Structures of a Sandwich System (2nd Report) - Nonlinear Analysis using the Finite Element Method. Hitachi Zösen Technical Review, Vol. 39, No. 1, March, pp. 26-35.

Matsuishi, M., Nishimaki, H., Takeshita, H., Iwata, S., Zösen, H. and Subara, T. 1978. On the New Composite Steel - Prestressed Concrete Structural Module for Offshore Structures. Offshore Technology Conference, Houston, Texas, Paper 3158, pp. 949-956.

Matsuishi, M., Nishimaki, K., Takeshita, H., Iwata, S. and Suhara, T. 1977. On the Strength of Composite Concrete/Steel Structure of a Sandwich System (1st Report) - Experiment of Statical Strength and Ultimate Strength Analysis. Hitachi Zösen Technical Review, Vol. 39, No. 3, September, pp. 11-20.

Matsuishi, M., Nishimaki, H., Takeshita, H., Iwata, S. and Suhara, T . 1977. On the Strength of New Composite Steel - Concrete Material for Offshore Structures. Offshore Technology Conferenece, Houston, Texas, Paper 2804, pp.589 -594.

McDermott, J. F., Kline, R. G., Jones, E. L., Manier, N. M. and Chiang, W. P. 1974. Tanker Structural Analysis for Minor Collisions. Society of Naval Architects and Marine Engineers Transactions, Vol. 82, pp.382-414.

Mindess, S. and Young, J. F. 1981. Concrete. Prentice Hall Inc., Englewood Cliffs, N.J.

Montague, P. 1986. Composite Vessels for Deepwater Operation; The Influence of Shell Length and Severe Damage. Proceedings of the Institution of Civil Engineers, Paper 8972, Vol. 81, June, pp. 175-219.

Montague, P., Goode, C.D., El-din Shukry, M. 1985. Tests on Composite Cylinders under External Pressure at Manchester University 1976-1985. Simon Engineering Laboratories, University of Manchester, England, November.

Nadai, A. 1950. Theory of Flow and Fracture Solids. Vol. 1, Second Edition, McGraw-Hill Book Company, Inc. Toronto.

Nojiri, Y. and Koseki, K. 1986. Structural Behaviour and Design Method of Steel/Concrete Composite Ice Walls for Arctic Offshore Structures. Offshore Technology Conference, Houston, Texas, May 5-8, Paper No. 5292, 8p.

O'Flynn, B. 1987. Composite Ice-Resisting Walls. Ph.D. Thesis, University of Alberta.

Osgood, W. R. 1947. Combined-Stress Tests on 245-T Aluminum-Alloy Tubes. Journal of Applied Mechanics, Vol. 14, June, pp. A147-A153.

Ozawa, K., Tanaka, Y. and Ueda, T. 1986. Shear Resisting Mechanism of a Composite Member with Steel and Concrete. Transactions of the Japan Concrete Institute, Vol. 8, III-10-A, December, pp. 295-302.

Ratzlaff, K. P. and Kennedy, D. J. L. 1986. Behaviour and Ultimate strength of Continuous Steel Plates Subjected to Uniform Transverse Loads. Canadian Journal of Civil Engineering, Vol. 13, No.1, pp.76-85.

Ratzlaff, K. P. and Kennedy, D. J. L. 1985. Analysis of Continuous Steel Plates Subjected to Uniform Transverse Loads. Canadian Journal of Civil Engineering, Vol. 12, No.3, pp. 685-699.

Ratzlaff, K. P. and Kennedy, D. J. L. 1985. Behaviour and Ultimate Strength of Transversely Loaded Continuous Steel Plates. Structural Engineering Report No. 130, University of Alberta, November, 114 p.

Ratzlaff, K. P. and Kennedy, D. J. L. 1984. Design of Steel Plates to Resist Transverse Ice Loads. Proceedings: Cold Regions Engineering Specialty Conference; Canadian Society of Civil Engineering, held at Edmonton, Alberta, April 4-6, pp. 769-793.

Shioya, T., Matsumoto, G., Okada, T., and Ota, T. 1986. Development of Composite Members for Arctic Offshore Structures. PolarTech '86, International Offshore and Navigation Conference and Exhibition, Vol. 2, pp. 660-677.

Stang, A. H., Greenspan, M. and Newman, S. B. 1946. Poisson's Ratio of Some Structural Alloys for Large Strains. Research Paper RP 1742, Journal of Research of the National Bureau of Standards, 37, October, pp. 211-221.

Suhara, T., Nishimaki, K., Matsuishi, M. and Iwata, S. 1982. On the Strength of Composite Concrete Structures of a Sandwich System. Naval Architecture and Ocean Engineering, Vol. 18, pp.132-145.

Taylor, G. I. and Quinney, H. 1931. The Plastic Distortion of Metals. Transactions, Royal Society of London, Series A, Vol. 230, pp. 323-362.

Timoshenko, S., and MacCullough, G.H. 1949. Elements of Strength of Materials. 3rd Ed., D. Van Nostrand Company, Inc., Toronto, pp. 353-354.

Timoshenko, S. 1940. Theory of Plates and Shells. 1st Ed., McGraw-Hill Book Company, London.

Todeschini, C. E., Biunchini, A. C. and Kesler, C. E. 1964. Behavior of Concrete Columns Reinforced with High Strength Steels. American Concrete Institute Journal, Vol. 61, June, pp. 701-716.

Young, A. G. 1959. Ship Plating Loaded Beyond the Elastic Limit. Transactions of the Institution of Naval Architecture, Vol. 101, pp. 143-165.